

STRUCTURAL MASS SPECTROMETRY STRATEGIES FOR SYSTEMS BIOLOGY

By

Jeffrey Richard Enders

Dissertation

Submitted to the Faculty of the

Graduate School of Vanderbilt University

in partial fulfillment of the requirements

for the degree of

DOCTOR OF PHILOSOPHY

In

Chemistry

December, 2012

Nashville, Tennessee

Approved:

Brian O. Bachmann

David E. Cliffl

John A. McLean

John P. Wikswo

Copyright © 2012 by Jeffrey Richard Enders
All Rights Reserved

To my wife, Carly, for her emotional and moral support
and
to my parents, Richard and Deborah Enders, and my sister Allyson Kern
for their emotional, moral, and financial support

ACKNOWLEDGEMENTS

First and foremost, I would like to thank Dr. John A. McLean for his valuable mentorship and continuous stream of support and guidance throughout this arduous project. It is also important to acknowledge my fellow group members Jody May, Cody Goodwin, Jay Forsythe, Seth Byers, Kelly Hines, Sarah Stow, Nichole Lareau, and Rafael Montenegro for creating a lab dynamic that was accommodating to long hours of work, and sometimes fun. Dr. Christina Marasco's contribution to this project has been indispensable. The work would certainly not have come together as nicely (if at all) were it not for her efforts.

My committee, consisting of Dr. David Cliffler, Dr. Brian Bachmann, and Dr. John Wikswa, has been instrumental in preparing me for this process. Meetings with them always generated numerous potential new angles and approaches to any difficulties I was experiencing. I appreciate all the time they devoted to guiding me throughout this process.

A number of teachers and professors have helped me tremendously throughout my life. My grade school teacher, Mrs. Jackie Gordon, taught me that school didn't always have to be boring and that I needed to always try to challenge myself in academics. In high school, Mrs. Sheila Gavin, was very influential in my academic development and in my appreciation of the written and spoken word. My undergraduate research advisor, Dr. Kevin Owens deserves much credit for ionizing my neutral interest in mass spectrometry and encouraging me to apply to Vanderbilt University.

Most of the work in the thesis could not have been completed without the frequent and strictly work related talks in the BME coffee room with Cody and Jody. Thanks to them for all of their valuable insight.

I would also like to acknowledge the financial support for this work which came from the NIH (R01GM092218 and RC2DA028981), the US Defense Threat Reduction Agency (HDTRA-09-1-0013), the Vanderbilt University College of Arts and Sciences, the Vanderbilt Institute of Chemical Biology, and the Vanderbilt Institute for Integrative Biosystems Research and Education. Special thanks go to Allison Price as well, for her helpful editorial insight on a number of manuscripts and proposals.

TABLE OF CONTENTS

	Page
DEDICATION	iii
ACKNOWLEDGEMENTS	iv
LIST OF TABLES	ix
LIST OF FIGURES	x
LIST OF ABBREVIATIONS	xiii
 Chapter	
I. INTRODUCTION	1
1. Ion mobility-mass spectrometry as a tool for performing systems biology measurements	1
2. Overview and theory of ion mobility separations	2
3. Transforming drift time to collision cross section	5
4. Data interpretation in conformation space	8
5. Peptide and protein analysis using ion mobility-mass spectrometry techniques	13
A. Characterizing and interpreting peptide and protein structure	14
(i). Applications of IM-MS to peptide and protein characterization	14
(ii). Computational methods for peptide and protein structural interpretation	24
B. The future of proteomics IM-MS studies	30
6. Instrumentation Overview	31
A. Drift tube ion mobility	32
B. Traveling wave ion mobility	33
C. High-field asymmetric waveform ion mobility spectrometry	34
D. Instrumental arrangements for fragmentation studies by ion mobility–MS/MS	36
E. Ionization source consideration	36
7. Dimensions for expansion	38
A. Spatial	39
B. Temporal	45
Statement of Dissertation	48
II. SYSTEMS BIOLOGY MEASUREMENTS USING ION MOBILITY-MASS SPECTROMETRY.....	49
1. Introduction	49
A. The multitrapp nanophysiometer	51
B. Ion mobility as a tool for measuring temporally dynamic living biological systems	53

C. Multidimensional data handling	57
D. Combining IM-MS with microfluidics for cellular culture effluent analysis	58
2. Methods	60
3. Results and discussion	62
A. Preliminary studies	62
B. <i>Saccharomyces cerevisiae</i>	63
C. Jurkat cells	66
4. Conclusions	66
III. ONLINE SOLID PHASE EXTRACTION AS A MEANS OF OVERCOMING NON-VOLATILE INORGANIC ION MASS SPECTROMETRY SIGNAL SUPPRESSION	70
1. The history of charged droplet formation for purposes of analytical chemistry	70
2. Fundamentals of electrospray formation	74
3. Fundamentals of electrospray suppression	81
4. A dual-column solid phase extraction strategy for online collection and preparation of continuously flowing effluent streams for mass spectrometry	83
5. Experimental	87
6. Results and discussion	90
A. Metrics and design criteria	90
B. Method validation	94
7. Conclusions	103
IV. REAL-TIME CELLULAR EXOMETABOLOME ANALYSIS WITH A MICROFLUIDIC-MASS SPECTROMETRY PLATFORM	106
1. Introduction	106
2. Methods	112
A. Microfluidic bioreactor design and fabrication	112
B. Cell culture and “in-culture” cocaine exposure	114
C. Metabolomics sample preparation and UPLC-ESI-IM-MS analysis	116
D. Online cell loading and experimentation	117
E. Solid phase extraction desalter	117
F. Online cell effluent desalting and mass spectrometry analysis	118
G. Data processing and multivariate statistical analysis	120
3. Results	121
A. Platform integration and evaluation	121
B. PDMS surface passivation for increased signal-to-noise ratio	124
C. Comparison of UPLC-ESI-IM-MS to MTNP-SPE-nESI-IM-MS	127
D. Cocaine metabolism in naïve and experienced T cell	128
E. In-culture cellular analysis	134
4. Conclusions	134
A. Platform capabilities and shortcomings	134
B. Cellular memory of cocaine experience	136
V. CONCLUSIONS AND FUTURE DIRECTIONS	138

Appendix

A.	ADAPTED REFERENCES	144
B.	IMAGING MS PROTOCOL	146
C.	PLATFORM TROUBLESHOOTING GUIDE	151
	REFERENCES	187
	CURRICULUM VITAE	222

LIST OF TABLES

Table	Page
1.1	Recent techniques for performing systems biology measurements 3
1.2	Listing of biophysical studies of model peptides and proteins 16
1.3	Topical listing of IM-MS studies related to instrumentation, proteome profiling, and medicinal research 19
1.4	Listing of IM studies of protein complexes 25
3.1	Surface tension and vapor pressure values for some common ESI solvents 76
3.2	Typical relative figures of merit for methods commonly used for the removal of salt from biological samples 91
3.3	Quantitative data demonstrating the limits of detection for the dual-column online solid phase extraction desalter 98
C.1	Parameters for MassLynx MS Tune DDA method file 194

LIST OF FIGURES

1.1	The basics of ion mobility instrumentation and theory	6
1.2	Illustrative representation of collision cross section and ion-molecule collisions	9
1.3	A 2D IM-MS conformation space plot for several lipid and oligonucleotide standards	11
1.4	A plot of IM-MS conformation space for different molecular classes based on different gas-phase packing efficiencies	12
1.5	Modeling protocol used to interpret peptide and protein structure	27
1.6	Schematics of an Ionwerks IM-MS and a commercial Waters Synapt G2	35
1.7	ESI-IM-MS/MS of bradykinin, illustrating the two modes of IM-MS/MS	37
1.8	Various examples of IM-MS when used for imaging applications	41
1.9	IM-MS applications for brain and kidney molecular detection	42
1.10	ESI-TWIM-MS/MS of the carbohydrate, lacto-N-fucopentaose 1 (LNFP1)	44
2.1	A comparison of the orthogonality of LC-MS and IM-MS	54
2.2	A three-dimensional scatter plot of an LC-ESI-IM-MS spectrum displaying plasma from whole rat blood	56
2.3	A schematic diagram for the online ESI-IM-MS analyses of the cellular exometabolome	59
2.4	Demonstration of precise molecular control over the microenvironment inside a microfluidic device	64
2.5	Temporal analysis of yeast exometabolome	65
2.6	Biomolecular analysis of Jurkat cell culture using IM-MS	67
3.1	Drawings and the first published photographs of a Taylor cone	71
3.2	Spectra demonstrating the first use of ESI for analyzing high mass molecules	72
3.3	Depictions and photographs of electrospray droplets in flight and suspended	78
3.4	A depiction of the various effects of salt on electrospray analysis	82
3.5	Examples of salt clustering and ion suppression	84
3.6	Absorbance spectra of hematin standards to quantitate recovery	89

3.7	Diagrams and step table of the online dual-column SPE desalter	95
3.8	Experimental scheme with valve timing and sample elution for the online apparatus	97
3.9	TICs and XICs for a variable analyte concentration experiment, showing perfusion of different analytes	100
3.10	Demonstration of desalting capabilities of the dual-column SPE apparatus when used to assess an online dynamically fluctuating flow stream	102
3.11	Data from a microfluidically-cultured population of insulinoma (Rin-m5f) cells	104
4.1	Experimental scheme showing the potential cell fates	111
4.2	PDMS silanization scheme	113
4.3	Cocaine exposure scheme for both in culture and online cell experiments	115
4.4	Solid phase extraction desalter setup	119
4.5	MTNP-SPE-nESI-IM-MS platform scheme	122
4.6	Channel silanization data demonstrating decrease in adsorption	126
4.7	Walking principal component analysis of exometabolomic profiles of naïve and cocaine-experienced Jurkat T cells for online analysis	129
4.8	Benzoylcegonine time course and fragmentation data	131
4.9	Cocaine metabolism tree	132
4.10	Additional metabolite time course data	133
4.11	Walking principal component analysis of exometabolomic profiles of naïve and cocaine-experienced Jurkat T cells for in-culture analysis	135
5.1	Robot scientist schematic	140
5.2	Proposed microfluidic device for cellular communication analysis	142
C.1	A table detailing all the different types of threading used	153
C.2	Photolithography and replica molding diagram	156
C.3	PDMS silanization procedure	159
C.4	Cell loading diagram	163
C.5	Wiring and connection diagram for VICI/Valco/Cheminert actuated valves	167
C.6	Valve arrangement 1	171
C.7	Stepwise depiction of the 6-step desalting method using valve arrangement 1	172

C.8	Example of how valve arrangement 1 may be used in conjunction with automated varying flow	173
C.9	Valve arrangement 2	175
C.10	Stepwise depiction of the 2-step desalting method using valve arrangement 2	176
C.11	Valve arrangement 3	177
C.12	Valve cycle steps for valve arrangement 3	178
C.13	Depiction of the solvent composition scheme for valve arrangement 3	179
C.14	A valve arrangement incorporating 6 columns	180
C.15	The nESI source	182

LIST OF ABBREVIATIONS

Å	Angstrom
APCI	Atmospheric pressure chemical ionization
ATD	Arrival time distribution
CCS	Collision cross section
CE	Capillary electrophoresis
CID	Collision induced dissociation
CRM	Charge residue model
Da	Dalton
DESI	Desorption electrospray ionization
DFT	Density functional theory
DTIM	Drift tube ion mobility
E	Electric field strength
E/N	Gas number density
ESI	Electrospray ionization
FAIMS	High-field asymmetric waveform ion mobility spectrometry
H/D	Hydrogen/deuterium
ID/OD	Inner diameter/outer diameter
IEM	Ion evaporation model
IM	ion mobility
K	Mobility proportionality constant
K^+	Potassium ion
K_0	Reduced mobility proportionality constant
k_B	Boltzmann's constant
L	Length

LC	Liquid chromatography
Li ⁺	Lithium ion
LOC	Lab-on-a-chip
m/z	Mass to charge ratio
MALDI	Matrix assisted laser desorption/ionization
MD	Molecular dynamics
MDa	Mega Dalton
m_i	Ion mass
m_n	Neutral mass
MRM	Multiple reaction monitoring
MS	Mass spectrometry
MTNP	Multitrap Nanophysiometer
N_0	Number density of the drift gas at standard temperature and pressure
Na ⁺	Sodium ion
NaCl	Sodium chloride
nESI	Nanoelectrospray ionization
NH ₄ ⁺	Ammonium ion
NMR	Nuclear magnetic resonance
p	Pressure
PCA	Principal component analysis
PDMS	poly(dimethylsiloxane)
PEEK	Polyether ether ketone
PLS-DA	Partial least squares-discriminant analysis
RPMI	Roswell Park Memorial Institute
SID	Surface induced dissociation

SPE	Solid phase extraction
STP	Standard temperature and pressure
T	Temperature
t_0	Ion start signal time
t_{atd}	Arrival time distribution
t_d	Drift time
t_{drc}	Drift time correction factor
TIC	Total ion chromatogram
TOF	Time-of-flight
TWIM	Traveling wave ion mobility
UPLC	Ultra performance liquid chromatography
V	Volt
v_d	Ion drift velocity
XIC	Extracted ion chromatogram
Ω	Collision cross section

CHAPTER I

INTRODUCTION

1. Ion mobility-mass spectrometry as a tool for performing systems biology measurements

Following the mapping of the human genome in the early 2000's, biological research has experienced a significant shift in philosophy. Genetics research has followed a very successful practice of isolated and compartmentalized studies where a single particular gene is perturbed and then a single or suite of specific effects is monitored. These methods paved the way for the maturation of molecular biology and led to a wealth of information on many genes and gene clusters. However, an organism is not a collection of genes and proteins, but something much more; something that functions holistically and symbiotically, with all portions working in unison. Kitano described protein/gene network diagrams as being “analogous to a static roadmap, whereas what we really seek to know are the traffic patterns, why such traffic patterns emerge, and how we can control them”.¹ This ideology of treating and analyzing organisms as a whole as opposed to their isolated parts has become the basis of systems biology.

Systems biology seeks to describe the function of a biological system using a holistic, multiscale approach. This approach encompasses the analyses of molecular classes such as the genome, transcriptome, proteome, and metabolome (among others) of a biological system. Systems biology asserts that while understanding genes and proteins is important, the most important aspects going forward are more closely related to the system's network structure and network dynamics.¹ Researchers of systems biology have adopted a hybrid discovery-driven/hypothesis-driven approach to meet these challenges. The first step of this proposed

approach is to define all of the components in the system. Then, by systematically perturbing this system, while monitoring all of these components, one is able to use computational biological methods to generate a network structure model of what is observed. This model will define all components of the system in terms of their mathematical relationship with all other components. With this model in hand the researcher/computational method generates a new perturbation that best tests that network structure model. From here, subsequently more refined models are produced until all perturbation reactions can be justified by the model.²

This type of experiment can be translated into many bioanalytical fields and techniques (Table 1.1). Some fields (*e.g.*, genomics) have defined their entire component set, while others are well on their way (*e.g.*, proteomics), or are in the early stages (*e.g.*, metabolomics). Crucial to this endeavor has been the establishment of internet-based databases.³ Moving forward additional techniques are required to sample the dynamics of cellular events and make systems biology measurements. Ideally this measurement should monitor as many analytes as possible and as frequently as possible in order to garner the most complete picture of the organism as a whole. It is the goal of this work to show that ion mobility and mass spectrometry are uniquely qualified to make these fast and broad measurements.

2. Overview and theory of ion mobility separations

A recent advance in mass spectrometry (MS) instrumentation is the incorporation of post-ionization separations on the basis of ion mobility (IM) combined with subsequent MS analysis (IM-MS). Importantly, IM-MS adds an additional dimension of separations on the basis of analyte structure to facilitate interpretation of MS spectra directly from complex biological samples. Typically, separations in the IM dimension are completed in hundreds of microseconds to milliseconds and yield direct structural information (ion–neutral collision cross sections, or

Table 1.1. A table of some of the more popular/recent techniques for performing systems biology measurements. Also listed are some general capabilities and limitations associated with each technique. Representative references for each technique are noted in brackets.

DNA sequencers/ DNA microarrays [4-6]

Capabilities

- Genomes can generally be fully mapped
- High-throughput
- Genomes are largely static

Limitations

- No direct indication of phenotype
- Gene network associations must be inferred, limiting disease prediction abilities

MS-based proteomics [7-10]

Capabilities

- More descriptive than genome
- High-throughput

Limitations

- Reproducibility can be problematic
- Post translational modifications can be difficult to observe

MS-based metabolomics [11-14]

Capabilities

- Potentially most indicative of phenotype
- Provides ability to infer metabolism all the way up to genotype

Limitations

- Most transient/difficult to measure
- Metabolite databases are largely incomplete

Yeast two-hybrid (Y2H) [15,16]

Capabilities

- No protein manipulation required
- Simple and inexpensive
- Scalable and amenable to automation

Limitations

- Intrinsic caveats related to yeast expression and nuclear localization
- High false positive/false negative rates

Protein-protein immunoprecipitation-mass spectrometry (IP-MS) [17,18]

Capabilities

- Gold standard of protein-protein interactions
- Tagging strategies negate need for specific antibodies

Limitations

- Only applicable to suspected interaction partners
- Not high-throughput
- High false positive/false negative rates

apparent ion surface area in \AA^2) for analytes. These characteristics make IM-MS a unique fit for exploring the temporal and spatial biomolecular complexities of biological systems, ranging from single cell measurements to groups of cells in culture to entire organisms.

Although gas-phase IM separations have existed for well over a century¹⁹ and coupling IM-MS has existed since the early 1960s,^{20,21} the utility of IM-MS for biomolecular separations was not fully realized until combined with soft ionization techniques, such as electrospray ionization (ESI) and matrix-assisted laser desorption/ionization (MALDI).²²⁻²⁶ Following these pioneering studies, research recently has extended IM-MS techniques to the study of various biological fields, such as small molecule analyses,²⁷⁻³² proteomics,³³⁻³⁹ viral assembly studies,⁴⁰⁻⁴² non-covalent complexes,⁴³⁻⁴⁵ or directly from thin tissue sections.^{46,47} Despite this recent expansion, IM-MS was only introduced commercially in 2006. Before that time, this technology was only available to those who could build the instruments themselves or get access to a custom built instrument.

Ion mobility-mass spectrometers are composed of an ion source, a mobility separation cell, a mass analyzer, and a detector as depicted in Fig. 1.1(a). There are many variations to the general design such as different ion sources (*i.e.*, ESI, MALDI) and types of ion mobility separation cells used (*i.e.*, whether the ions are dispersed in space or time). For imaging IM-MS applications typically time-of-flight (TOF) mass analyzers are used for timescale considerations as described below. This work focuses on temporal ion dispersion through the use of drift tube ion mobility or traveling wave ion mobility (DTIM and TWIM, respectively). In contrast with high-energy ion-neutral gas-phase collisions used in collision-induced dissociation (CID), both DTIM and TWIM separations utilize low-energy gas-phase collisions to separate ions on the basis of predominantly molecular surface areas. Briefly, gas-phase ions are injected into a drift tube filled with a neutral drift gas and migrate under the influence of a weak electrostatic field

gradient (Fig. 1.1(b)). This field is electrostatic for drift tube and electrodynamic for traveling wave separations, respectively. The migration of these ions is impeded by collisions with the neutral drift gas to a degree that is proportional to apparent surface area or collision cross section. To a first approximation, these collisions are assumed to be completely elastic and the conditions of the cell (*i.e.*, electric field, temperature, and gas number density) are tuned such that the collisions are of sufficiently low energy to avoid inducing any structural or chemical changes. Thus, the elution order of ions is based upon their gas-phase packing density (*i.e.*, the physical density to which the individual molecule is folded and packed) in the gas-phase. Thus, larger ions have a lower mobility than smaller ions which result in longer drift times versus shorter drift times, respectively. Although the experimental parameter obtained from IM separations is the ion arrival time distribution (t_{atd}) or the time between ion injection and ion detection, it can be converted to collision cross section or apparent surface area as illustrated in Fig. 1.1(c).

3. Transforming drift time to collision cross section

This section details how arrival time distributions may be converted to collision cross sections based on the kinetic theory of gases for drift tube separations. Derivations of the ion–neutral collision cross section theory can be found in several excellent texts and reviews.⁴⁸⁻⁵⁰ Procedures to estimate collision cross section using traveling wave IM are described elsewhere.^{31,51-59}

The separation of ions in a weak electrostatic field (E) is measured as the ion drift velocity (v_d) and is related by the proportionality constant, K , which is the mobility of the ion in a particular neutral gas:

$$v_d = KE[1]$$

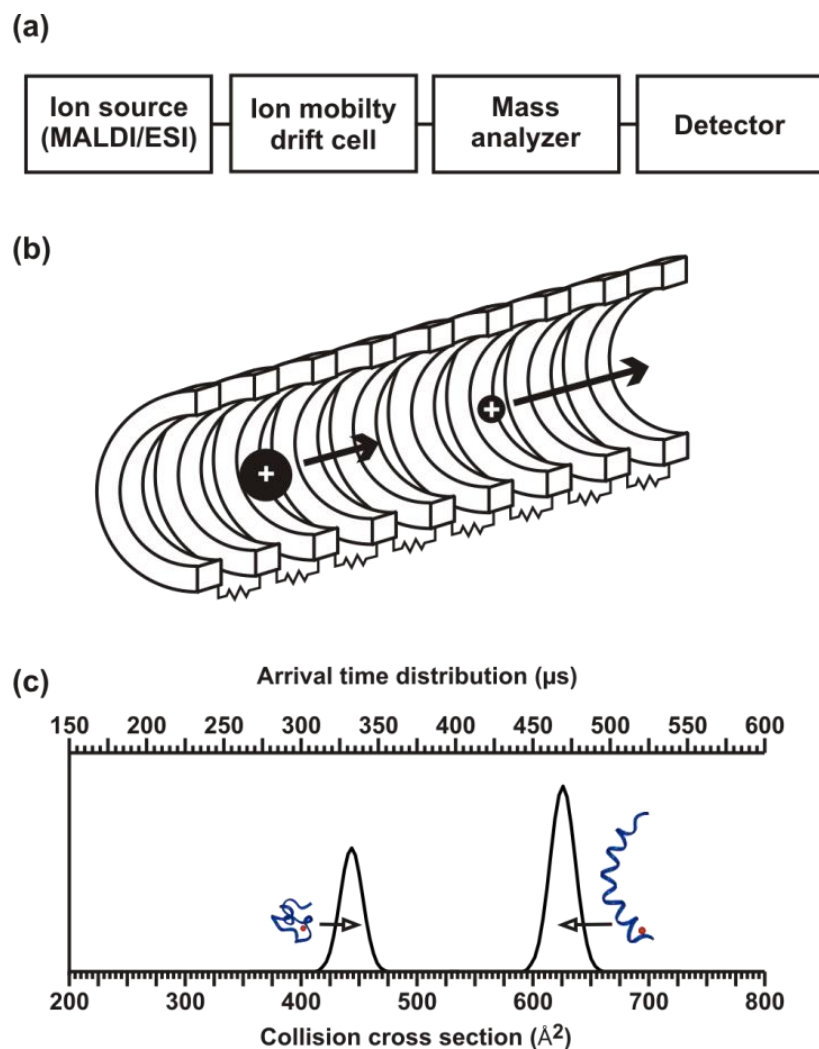


Figure 1.1. (a) A block diagram of the primary components of biological IM-MS instrumentation. (b) A conceptual depiction of an IM drift cell. A stack of ring electrodes are connected via resistors in series to form a voltage divider, which is typically designed to generate a relatively uniform electrostatic field along the axis of ion propagation. Ions of larger apparent surface area experience more collisions with the neutral drift gas and therefore elute slower than ions of smaller apparent surface area. (c) A hypothetical IM separation for peptide ions exhibiting two distinct structural sub-populations corresponding to globular (left) and to helical (right) conformations. The arrival time distribution data (top axis), or what is measured, can be transformed to a collision cross section profile (bottom axis) via equation [4]. Reprinted from reference 60.

The drift cell is of a fixed length (L), and the velocity of the ion packet is determined by measuring the drift time (t_d) of the packet across the drift cell. In evaluating K , the drift velocity of the ion packet depends not only on the electrostatic field strength but also on the pressure (p , Torr) of the neutral drift gas and the temperature (T , kelvin) of separation. Therefore, it is conventional practice to report K as the standard or reduced mobility (K_0), which normalizes the results to standard temperature and pressure conditions (*i.e.*, 0° C and 760 Torr):

$$K_0 = K \frac{p}{760} \frac{273}{T} \quad [2]$$

For applications where IM is used to obtain structural information about the ion, such as those in structural proteomics and biophysics, the IM separations are performed using weak electrostatic fields (*ca.* 20–30 V cm⁻¹ Torr⁻¹). Provided the field strength is sufficiently weak, or under so-called low-field conditions, a closed equation for the ion–neutral collision cross section can be expressed from the kinetic theory of gases. For electrostatic fields higher than the low field limit, the ion velocity distribution depends less strongly on the temperature of the separation and the mean ion energy increases as it traverses the drift region. Consequently, K is no longer constant and depends on the specific ratio of the electrostatic-field to the gas number density (E/N) (See Ref. ⁵⁰ for a derivation of calculating the low field limit for a particular analyte.). When the IM separations are performed in low-field conditions, (*i.e.*, constant K) the mobility is related to the collision cross section of the ion–neutral pair:

$$K_0 = \frac{(18\pi)^{1/2}}{16} \frac{ze}{(k_B T)^{1/2}} \left[\frac{1}{m_i} + \frac{1}{m_n} \right]^{1/2} \frac{760}{p} \frac{T}{273} \frac{1}{N_0} \frac{1}{\Omega} \quad [3]$$

where these parameters include the charge of the ion (ze), the number density of the drift gas at STP (N_0 , 2.69×10¹⁹ cm⁻³), the reduced mass of the ion–neutral collision pair (ion and neutral

masses of m_i and m_n , respectively), Boltzmann's constant (k_B), and the ion–neutral collision cross section (Ω). Inspection of equation [3] shows that the mobility of an ion is inversely related to its collision cross section or apparent surface area. Substituting for K_0 in equation [3] and rearranging to solve for the collision cross section yields:

$$\Omega = \frac{(18\pi)^{1/2}}{16} \frac{ze}{(k_B T)^{1/2}} \left[\frac{1}{m_i} + \frac{1}{m_n} \right]^{1/2} \frac{t_d E}{L} \frac{760}{p} \frac{T}{273} \frac{1}{N_0} \quad [4]$$

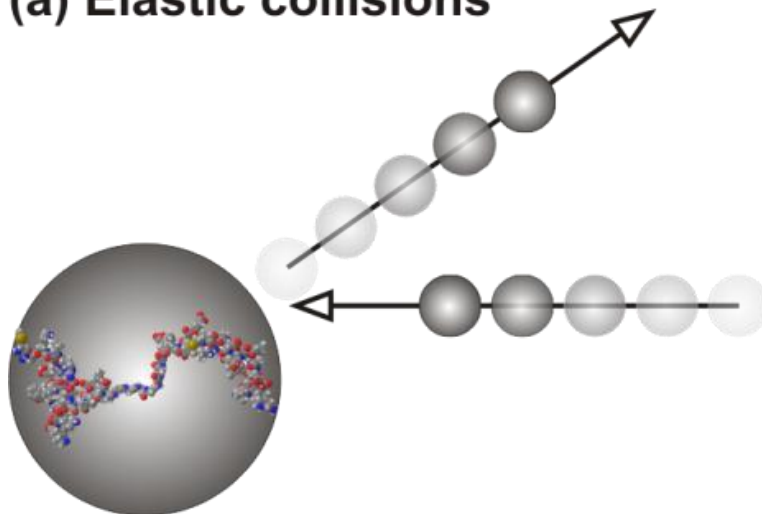
which is the typical functional form of the equation used to solve for collision cross sections from IM data. Conceptually, the ion–neutral collision cross section can be thought of as the radius of the orientationally averaged projection of the ion in combination with the drift gas, *i.e.*, $\Omega = \pi (r_i + r_{\text{He}})^2$, as depicted in Fig. 1.2(a).⁴⁹

In equations [3] and [4], the collisions of ions with neutrals are considered to be a completely elastic process (Fig. 1.2(a), (b)). Thus, the collision cross section obtained is termed the hard-sphere collision cross section. When compared to molecular simulations, these collision cross section measurements can provide detailed structural information about the analyte.⁶¹⁻⁶⁴

4. Data interpretation in conformation space

Typical data for a 2D IM-MS separation are presented in Fig. 1.3 for the separation of lipids and oligonucleotides. Conformation space data (Fig. 1.3(a)) are termed such because they represent biomolecular conformation, or structure, as a function of m/z . Presentation of 3D conformation space data (IM arrival time distribution, m/z , and signal intensity) is typically projected with false coloring or grey scale representing signal intensity. An integrated mass spectrum over all arrival time distributions, which is what would be observed in the absence of

(a) Elastic collisions



(b) Inelastic collisions

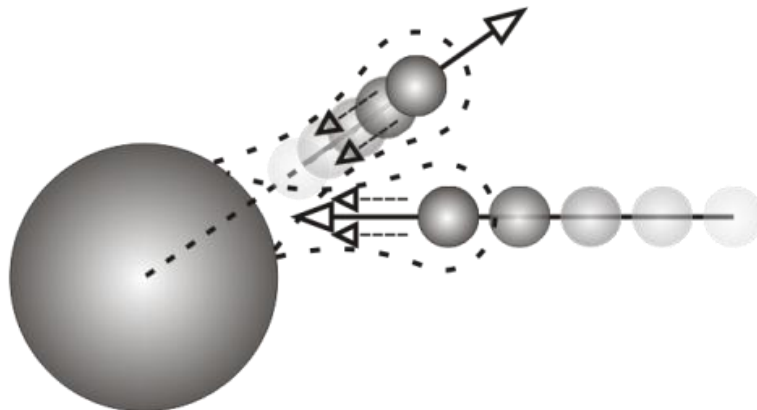


Figure 1.2. (a) Illustrative representation of the ion-neutral collision cross section. Also depicted is an example of an elastic collision where the total kinetic energy of the neutral gas molecule (small sphere) and the analyte ion (large sphere) prior to collision is equal to their kinetic energy following the collision. (b) Representation of an inelastic collision, where some amount of kinetic energy is lost through the collision process.

IM is shown in Fig. 1.3(b). An integrated IM arrival time distribution is illustrated by the white curve of Fig. 1.3(c). This would be obtained by placing the detector directly after the IM drift cell. By plotting the data in 2D conformation space two distinct correlations are observed, one for lipids and one for oligonucleotides. Note that either extracted mass spectra or arrival time distributions can be derived from conformation space data. For example, an extracted arrival time distribution over the m/z range of 860–870 is represented by the gray curve in Fig. 1.3(c). This extracted arrival time distribution region illustrates the baseline resolution achieved for a sodium coordinated lipid (sphingomyelin 44:1, $m/z = 866.7$ Da) and a protonated oligonucleotide (CGT, $m/z = 860.2$ Da) of nearly the same m/z . One of the main challenges in the analysis of complex biological samples is the large diversity of molecular species with the high probability for isobaric molecules at a particular m/z . Structural separations on the basis of ion mobility allow isobaric species belonging to different biomolecular classes to be easily resolved (Fig. 1.4), resulting in more confident peak assignments. Although biomolecules are generally composed of a limited combination of elements (*e.g.*, C, H, O, N, P, and S), different biomolecular classes preferentially adopt structures at a given m/z correspondent to the prevailing intermolecular folding forces for that class. A hypothetical plot delineating regions of conformation space for which different biomolecular classes (*e.g.*, nucleotides, carbohydrates, peptides, and lipids) are predicted to occur is presented in Fig. 1.4(a). This is a result of different average densities for different molecular classes (nucleotides > carbohydrates > peptides > lipids⁶⁵). Although more pronounced for an m/z range over 2,000, at lower ranges as that depicted in Fig. 1.4(b) separations are still feasible but the correlations begin to overlap.

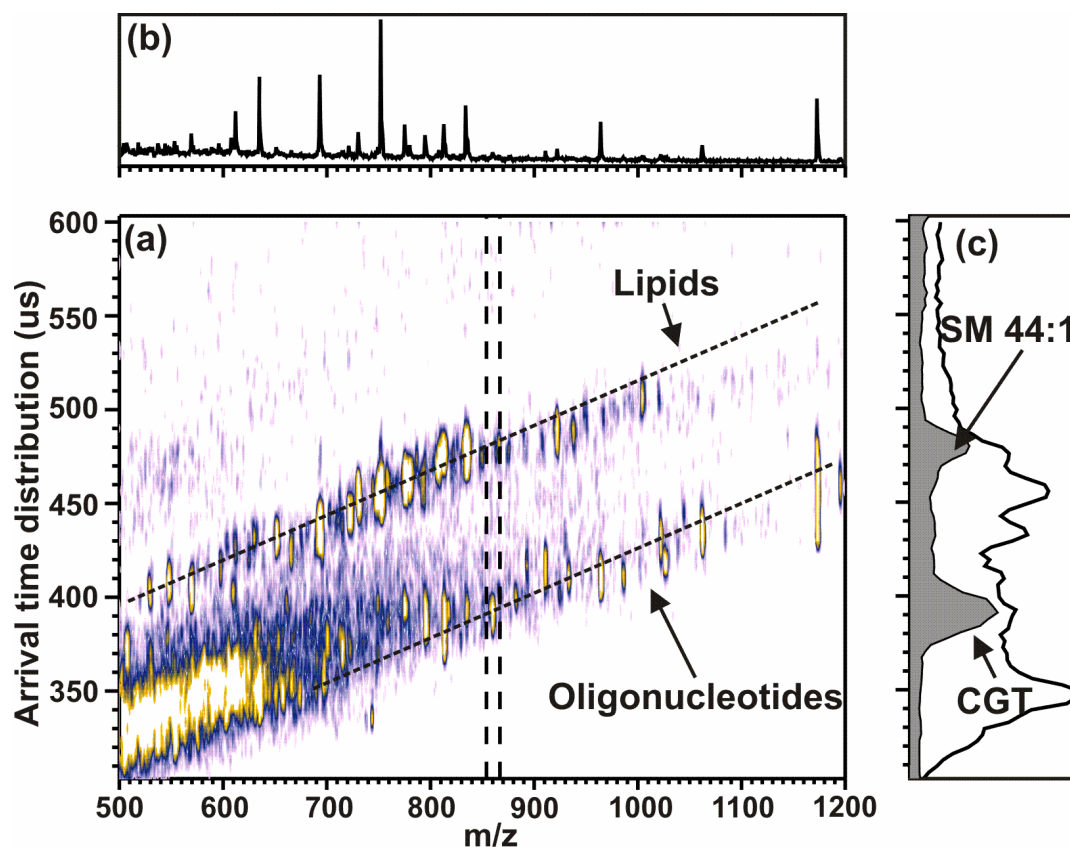


Figure 1.3. (a) A 2D IM-MS conformation space plot for several lipid and oligonucleotide standards. This data illustrates the variation of gas-phase packing efficiencies for different types of biomolecules. (b) An integrated mass spectrum over all arrival time distributions. (c) The white curve represents the integrated arrival time distribution over the mass range of 500-1200 m/z , whereas the grey curve represents an extracted arrival time distribution over the mass range of 860-870 m/z . The latter illustrates baseline resolution of two peaks with similar masses but different mobilities (lipid- [sphingomyelin 44:1+Na]⁺, m/z = 866.7 Da; oligonucleotide- [CGT+H]¹, m/z = 860.2 Da). Figure reprinted from reference 60.

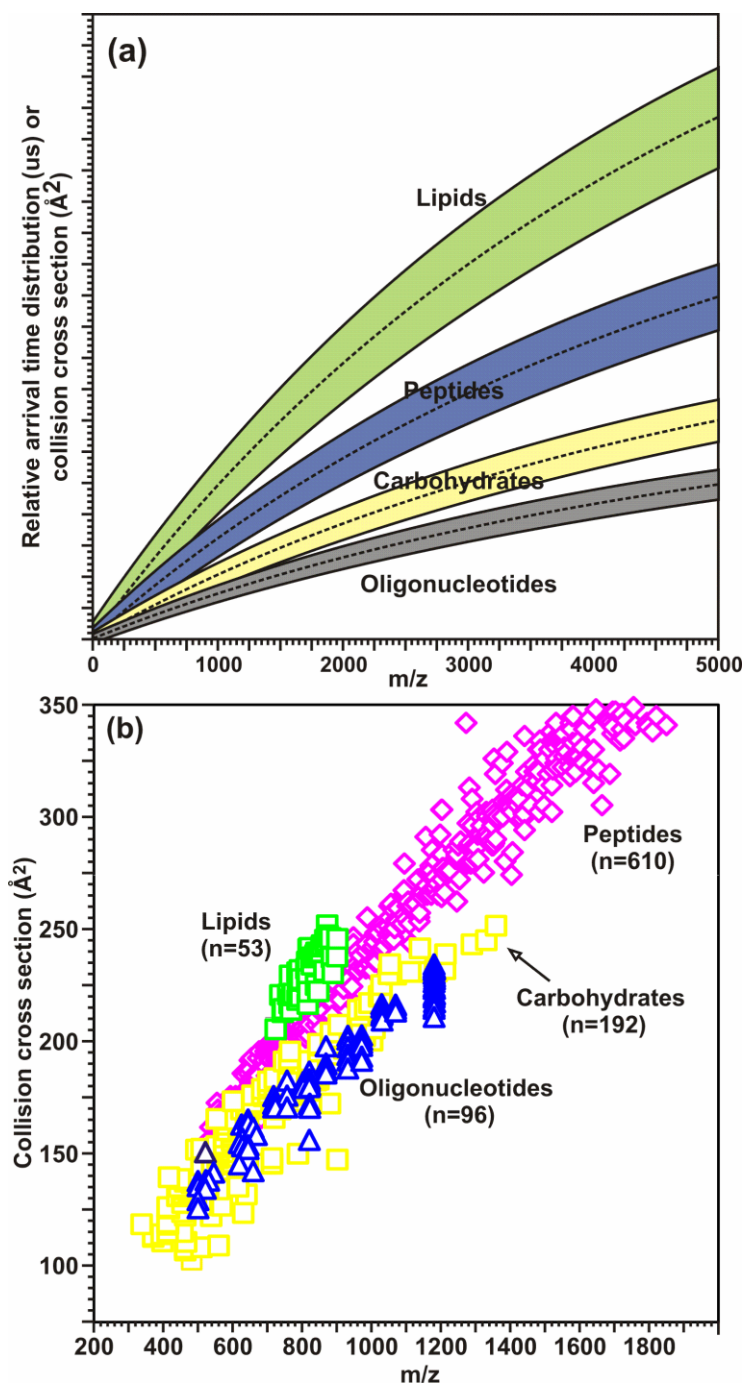


Figure 1.4. (a) A hypothetical plot illustrating the differences in IM-MS conformation space for different molecular classes based on different gas-phase packing efficiencies. (b) A plot of collision cross section as a function of m/z for different biologically-relevant molecular classes, including: oligonucleotides ($n = 96$), carbohydrates ($n = 192$), peptides ($n = 610$), and lipids ($n = 53$). All species correspond to singly-charged ions generated by using MALDI, where error $\pm 1\sigma$ is generally within the data point. Values for peptides species are from Ref. ⁶⁶. Reprinted from reference 60.

5. Peptide and protein analysis using ion mobility-mass spectrometry techniques

One of the main applications of IM-MS to bioanalytical fields has been to study peptides and proteins. Contemporary proteomics research generally involves either structural/functional proteomics or comprehensive protein identification from complex biological samples.^{65,67-70}

The native-state structures of large proteins and other biological molecules adopt conformations that regulate biological function. Detailed geometries of native state structures are typically obtained by using nuclear magnetic resonance⁷¹⁻⁷³ and X-ray crystallography.⁷⁴⁻⁷⁷ Although these are considered the gold standards for structure elucidation they both have attendant limitations. Structural elucidation by nuclear magnetic resonance (NMR) generally requires highly purified samples and is generally applicable only to proteins of moderate size. X-ray crystallography requires that the protein can be crystalized, which can be exceptionally challenging for membrane-bound and highly flexible proteins. The conformational changes associated with macromolecules in solution-phase, or in gas-phase, are due to transitions between native and denatured states, sometimes through thermodynamically stable intermediates. Some conformational changes associated with large biological molecules in solution are retained in the gas-phase.⁷⁸⁻⁸⁰ Thus, advances in gas-phase structural determinations may provide a unique means for performing structural proteomics directly from complex samples.

Rapid peptide and protein identification is facilitated by advances in liquid chromatography (LC) combined with electrospray ionization (ESI); this combination has resulted in reliable interfaces necessary for quantitative bioanalyses using LC-MS and LC-MS/MS. Although LC-MS/MS, combined with bioinformatics, is the work-horse in contemporary MS-based proteomics research, there remain several significant challenges, including: (i) long analysis times, (ii) limited concentration dynamic range, (iii) poor detection of low abundance

species (*e.g.*, post-translationally modified proteins), and (iv) simultaneous detection of proteins with widely varying physical properties (*e.g.*, hydrophobicity, pI).

Gas-phase IM-MS separations combined with LC-IM-MS and LC-IM-MS/MS can now address, in part, several of these challenges.^{34,35,37,81-86} By performing separations in the gas-phase, rather than the liquid-phase, IM separation speed is on the timescale of milliseconds. This is well suited for coupling with MS, whereby hundreds of mass spectra can be acquired across the IM elution profile and then subsequently stitched together to provide a 2D plot of IM vs. mass spectra. For example, a single plasma profiling experiment using 2D LC coupled with IM-MS can be completed in *ca.* 3 h, which is nearly an order of magnitude faster than is required for conventional LC-MS/MS.⁸⁷

A. Characterizing and interpreting peptide and protein structure

An increasing amount of research is focused on utilizing IM-MS for the determination and characterization of peptide and protein structure in support of structural proteomics, and these advances will be important in drug discovery. In this context absolute collision cross sections (CCS) are obtained using DTIM instruments and are then interpreted utilizing quantum mechanical and molecular dynamics calculations.

(i). Applications of IM-MS to peptide and protein characterization

IM-MS studies can now be used to structurally characterize peptide systems consisting of a few to many amino acids. Further, the approach can be even extended to massive protein complexes in structural biology. When combined with LC approaches, IM-MS can be used to detect trace level proteins that are present in complex samples such as human urinary and plasma samples.^{34,37,84} A survey of studies using IM-MS to investigate the structural biophysics of

model peptides and proteins is presented in Table 1.2. A summary of studies aimed at instrumentation for the study of peptides and proteins, proteome profiling, and medicinal research is presented in Table 1.3.

IM-MS can be used to examine the detailed structures of amino acids, as illustrated by the work of Bowers group in their gas-phase studies of cationized glycine. This work showed that these molecular ions mostly exhibit charge-solvation structures.⁸⁸ Small alkali ions (*e.g.*, sodium) bind to both the N- and the C-terminus whereas larger alkali ions (*e.g.*, rubidium and cesium) bind preferentially to the C-terminus.⁸⁸ The stabilization of the charge-solvation structure compared to that of the salt bridge is larger for GlyCs⁺ than for GlyNa⁺. The approach is to use a high pressure drift cell with ESI introduction and augment with molecular dynamics calculations.⁸⁹ The outcome shows that solvating water molecules primarily bind to the ionic functional groups present in peptides. Density functional theory (DFT) calculations for dipeptide ions ([Gly-Gly + H⁺]⁺, [Gly-Ala + H⁺]⁺, [Ala-Gly + H⁺]⁺, [Ala-Ala + H⁺]⁺, [Pro-Gly + H⁺]⁺ and [Gly-Trp + H⁺]⁺)⁹⁰ show that the dominant water adsorption process involves a significant conformational change to accommodate the bridging water molecule. Molecular modeling and DFT calculations of deprotonated dimers of alanine and glycine⁹¹ indicate that the charge is poorly shielded and readily available for non-covalent interaction with other molecules.

High-resolution IM measurements and molecular dynamics simulations of larger systems, namely protonated polyglycine and polyalanine (Gly_nH⁺ and AlanH⁺, where, n = 3 - 20) in the gas-phase, can also be done, as illustrated by the Jarrold group.⁹² They found that the measured CCS for both the polyglycine and the polyalanine peptides are consistent with a self-solvated globule conformation. Here the change in conformation is due to the peptide chain wrapping around the charge located on the terminal amine. The conformations of unsolvated leucine-based peptides form helices more readily than alanine, but less readily than valine (Val >

Table 1.2. Listing of biophysical studies of model peptides and proteins. Table reprinted from reference 93.

Model Systems – Peptides/Proteins	Type of Study	References
Alanine, Glycine, Arginine, mod AA	gas-phase conformations noncovalent or cation/peptide interaction	88,89,94
Ala, Gly, Pro, Trp based dipeptides, poly (Ala)	folding, gas-phase conformations, helices and sheets	89-91,95,96
Modified pentapeptides	hydration and folding	90,92,97-112
poly (Gly) and modified poly (Gly)	gas-phase conformations, helices and sheets	92,100,105,106,110,111,113,114
poly (Pro)	anhydrous helices/globules	115
poly (TrpGly)	gas-phase conformations	116
modified poly (Leu), poly (Val)	helices and sheets	100
di-AA clusters	gas-phase conformations, noncovalent interactions	95
Serine clusters	noncovalent or cation/peptide interaction	117-119
Proline clusters	gas-phase conformations	120,121
Amyloid beta protein	gas-phase conformations, noncovalent interactions	89,94
Angiotensin II	noncovalent or cation/peptide interaction	122
Apomyoglobin	gas-phase conformations	123,124

Table 1.2, continued

BPTI (bovine pancreatic trypsin inhibitor)	hydration and folding	26,125-127
Bradykinin	H/D exchange, noncovalent interaction	25,89,98,122,128,129
Bradykinin fragment 1-5 (RPPGF)	H/D exchange	130
Cytochrome C	gas-phase conformations	26,124,126,131-135
Defensins (beta-def., P-defensin DEFB107)	gas-phase conformations, hydration and folding	136,137
Dynorphin fragments	noncovalent or cation/peptide interaction	122,138
mini Gastrin I peptide	noncovalent or cation/peptide interaction	138
Gonadotropin-releasing hormone	gas-phase conformations, hydration and folding	136
Gramicidin S	gas-phase conformations	122,139
Hemoglobin	gas-phase conformations, HD exchange	140
oxidized Insulin chain A (ICA)	noncovalent or cation/peptide interaction	98,141
Kempide	noncovalent or cation/peptide interaction	122
LHRH (leutenizing hormone releasing hormone)	hydration and folding	89
Lysozyme	gas-phase conformations, hydration and folding	66
Beta(2)-microglobulin (beta(2)m)	gas-phase conformations, folding, aggregates	142

Table 1.2, continued

Myoglobin	gas-phase conformations, hydration and folding	89
Neurotensin	gas-phase conformations, hydration and folding	89,94,96
Oxytocin	cation/peptide interaction	143,144
Alpha Synuclein	noncovalent interaction	145,146
Ubiquitin	gas-phase conformations, hydration and folding	147-154
Mobility and CCS database of ESI peptides	gas-phase conformations	155-157
CCS database of MALDI (singly charged) peptides	gas-phase conformations	66

Table 1.3. Topical listing of IM-MS studies related to instrumentation, proteome profiling, and medicinal research. Table reprinted from reference 93.

Topics	References
<i>Proteomics</i>	
Collision Induced Activation	158-161
Combinatorial studies	162
Conserved solution-phase structure	148,163-165
H/D exchange/labeling structure study	107,137,166-169
IM-(CID, SID)/MS	35-38,84-86,161,167,170-185
IM-MS resolution/separation power	70,81-85,95,156-159,161,163,167,169,171-174,180,181,183-197
IM-MS enhanced detection	157,190,192
Instrumental advances	35,84,85,157,160,161,170-174
<i>Ionization type:</i>	
ESI studies	34-38,81-87,95,137,156-160,162,167,170,171,173-188,197
MALDI studies	70,163,169,172,189-196

Table 1.3, continued

Peak Capacity of IM-MS approach	185,194,195
Peptide libraries	82,83,95,174,181,183,186-190,193,195
Peptide aggregation in gas-phase	95,98,137,198-200
Peptide Mobility/CCS Prediction Algorithm	155,201-207
Phosphorylated Peptides	186,191,193
 <i>Proteome profiling</i>	
Drosophila	35,85,86,175-179
Human urinary proteome	84
Human plasma proteome	34,37
 <i>Medicinal research</i>	
Alzheimer's disease	94,198-200,208-211
Parkinson's disease	145,146,176-179
Huntington's disease	38

Table 1.3, continued

Other	37,84,137,144,197,212,213
Shift Reagents	188

Leu > Ala).¹⁰⁰ Interestingly, the side-chain entropy is not the determining factor in helix formation when dealing with unsolvated peptides.

IM-MS methods combined with molecular modeling calculations can be used to examine the conformations and charge states of polyproline peptides, $[\text{Pro}^n + z\text{H}]^{z+}$ (where $n = 3-56$; and $z = 1-6$), as was demonstrated by Clemmer and coworkers.¹¹⁵ Their investigations show that all proline residues are in the cis configuration, and protonation at the N-terminus allows hydrogen bonds to be formed with backbone carbonyl groups of the second and third proline residues in each polyproline chain. Protonation at the N-terminus also stabilizes the helix macrodipole. Singly charged ions formed from aqueous solutions favor globular and hairpin-like conformers that contain both cis- and trans-proline residues, whereas higher charge state ions ($z = 3-6$) formed from aqueous solutions favor relatively extended conformations. With the increase in the number of proline residues, however, higher charge state ions became more compact. Similar studies can be performed on serine clusters¹¹⁸ by using a sonic-spray ionization method in an IM-MS instrument. Experimentally derived cross sections with values calculated for trial geometries indicate that large clusters favored tightly packed, roughly spherical geometries.

The collision cross section values of several cationized forms of bradykinin ($[\text{BK} + \text{H}]^+$, $[\text{BK} + \text{Na}]^+$, and $[\text{BK} - \text{H} + 2\text{Na}]^+$), introduced by MALDI, were calculated by Bowers and coworkers. All three species had very similar cross sections of $245 \pm 3 \text{ \AA}^2$, and these cross sections were independent of temperature from 300 to 600 K. This particular property of bradykinin makes it the standard calibrant peptide of choice for many IM studies.

Ion mobility measurements can be used to characterize the conformations of various charge states of proteins. An example is the +4 to +22 charge states of apomyoglobin.¹²³ When collisionally heated, the higher ($> +7$) charge states undergo proton stripping to produce +4 to

+7 charge states. This results in spontaneous collapse into partially folded conformations. Only extended conformations exist for the high (> +10) charge states in the gas-phase, and they become more extended as the number of charges increases, whereas the lower charge states (< +7) adopt a slightly more compact structure than the native protein in solution. This study also shows that the CCS per residue for the conformations of apomyoglobin and cytochrome c is similar.^{26,123} An important result from these studies is that different proteins share common structural motifs in the gas-phase, as they do in solution.^{26,131,132} One can use desorption electrospray ionization (DESI) assisted by IM-MS analysis as shown for solid-phase horse heart cytochrome c and lysozyme from chicken egg; the outcome shows, that charge state distributions are comparable to those produced by ESI.¹⁶⁵ Elongated structures of these two proteins are formed when the DESI solvent is mixed with a small amount (~2%) of acetic acid.¹⁶⁵

A peptide library containing 4000 different peptides having the general form: NH₂-Xxx-Xxx-Xxx-CO₂H, NH₂-Ala-Xxx-Xxx-Xxx-CO₂H, NH₂-Ser-Ala-Xxx-Xxx-Xxx-CO₂H, and NH₂-Leu-Ser-Ala-Xxx-Xxx-Xxx-CO₂H (where Xxx represents Ala, Arg, Asp, Glu, Gly, Leu, Lys, Phe, Ser, or Val) is now available from LC measurements combined with IM-MS.¹⁵⁷ By LC-IM-MS approximately 82% of the 4000 library components can be resolved.¹⁵⁷ There is also available a CCS database of 420 singly charged and 240 doubly charged peptide ions introduced by utilizing an ESI source followed by IM-MS.¹⁵⁵ A similar database of ion-neutral collision cross sections for 607 singly-charged peptide ions introduced with a MALDI source is available from Russell and co-workers.⁶⁶

Protein complexes are large aggregates of often two or more proteins that are non-covalently bound. These intact complexes are able to perform intricate chemical processes and are often the biological machinery at work behind many of the most important physiological functions in the body. Understanding their properties will likely be important in drug discovery and development. Electrospray ionization-ion mobility measurements of these large protein

complexes is now at the forefront of structural biology research following a number of studies throughout the 1990's and 2000's that showed that predominant secondary, tertiary, and quaternary structures were largely conserved during the transition from liquid- to gas-phase.²¹⁴ The ability of IM-MS for characterizing molecular structure makes it well suited for gaining insights in such structural biology studies.

Most IM protein complex studies are aimed at probing gas-phase structure as a reliable representation of the solution counterpart.^{215,216} Many of these studies attempt to justify the results elicited from ion mobility by comparing them to electron microscopy, X-ray crystallography, and NMR data through the use of sources such as the protein data bank.^{216,217} Work has progressed to larger and larger species, culminating in the successful ionization and structural investigation of the MVP vault protein complex at *ca.* 9.4 MDa.²¹⁸ A summary of studies using IM-MS to characterize protein complexes is provided in Table 1.4.

Computational methods have also been used to study these systems.^{43,45,51} Although current computational techniques are not able to handle the large complexes as of yet, approximations and coarse-grained models can now be used in these studies, and this work does provide significant insight into the experimental ion mobility measurements observed.

(ii). Computational methods for peptide and protein structural interpretation

Empirically determined collision cross section values can be used to probe structural motifs of various biomolecular ions including peptides/proteins^{109,131,144} and protein complexes.^{43,51} This is accomplished by augmenting IM CCS measurements with computational modeling strategies. For structural interpretation, the CCS is used as a size constraint that can be used to discriminate and interpret a subset of structures from a large pool of computationally generated conformers. Structural populations can be expected to consist of structurally similar

Table 1.4. Listing of IM studies of protein complexes. Table reprinted from reference 93.

Protein Complexes	Type of Study/Comments	References
20S proteasome from <i>Methanosarcina thermophila</i>	analysis of the binding and stoichiometry, conservation of structure in the gas-phase	216
Trp RNA binding protein (TRAP)	stability of complex, effect of Trp, RNA binding	43
Plasma protein complex 56kDa tetrameric transthyretin (TTR)	study of stable collision activated protein unfolded structures over ms time scales	45
Wheat heat shock protein TaHSP16.9	stability of dodecamers in solution and gas-phases	51
Protein kinase G (PKG)	investigation of global conformational changes of intact 152kDa dimeric PKG; structural changes upon cGMP-binding	219,220
Hepatitis B Virus (HBV) capsid protein	preservation of solution-phase structure in vacuo; study of viral capsid assembly	221
Bacteriophage P22 portal protein	structure of P22 portal protein; conformational changes upon its association with tail factor gp4	222
Acr1 Mycobacterium tuberculosis heat shock protein	collision induced activation of Acr 1, shock protein a 12 subunit 197kDa dodecameric protein	223

ions that either undergo thermally accessible structural/conformational isomerization/interconversion or, depending on intramolecular forces and atomic arrangement, may even remain in relatively fixed conformations on the time scale of the IM-MS experiment.¹⁵¹ Therefore, each IM-MS unique signal, ideally corresponding to identical ions with different conformations, has its own unique structural signature determined by the average shape of the populations of ions that create it. This structural signature is the basis for biomolecular separations observed in IM-MS (lipids from peptides, peptides from oligonucleotides and carbohydrates).^{65,196,224} It is also the explanation for the observed difference in average IM vs. m/z trendline variability (spread, structural richness) of the different biomolecular classes observed by IM-MS.^{189,224} For example, peptide mobility vs. m/z IM-MS spectra can be expected to contain predictable variability due to PTMs^{186,191,193} amino acid content, sequence,^{81,156,197} and type of cationizing agent.

Following the experimental determination of CCS, computational modeling is performed in the following general sequence: (i) the structure of the molecular ion is built by using one of the available structure-building software packages, (ii) the atomic charge parameters for the built structure are determined by using quantum chemical calculations, and point charge derivation, and (iii) molecular dynamics is performed to create a large number of structural conformers whose CCS can be computationally determined to allow experimental CCS based clustering analysis. A schematic of the workflow for combining the measured CCS with computational interpretation is illustrated in Fig. 1.5.

Currently, there are several software packages well suited for structure building of peptides and proteins, some proprietary (*e.g.*, Molecular Operating Environment, Chemical Computing Group, Montreal, Canada), and some freely available (*e.g.*, SIRIUS, University of California, San Diego). One should be aware of online structure databases and search for already

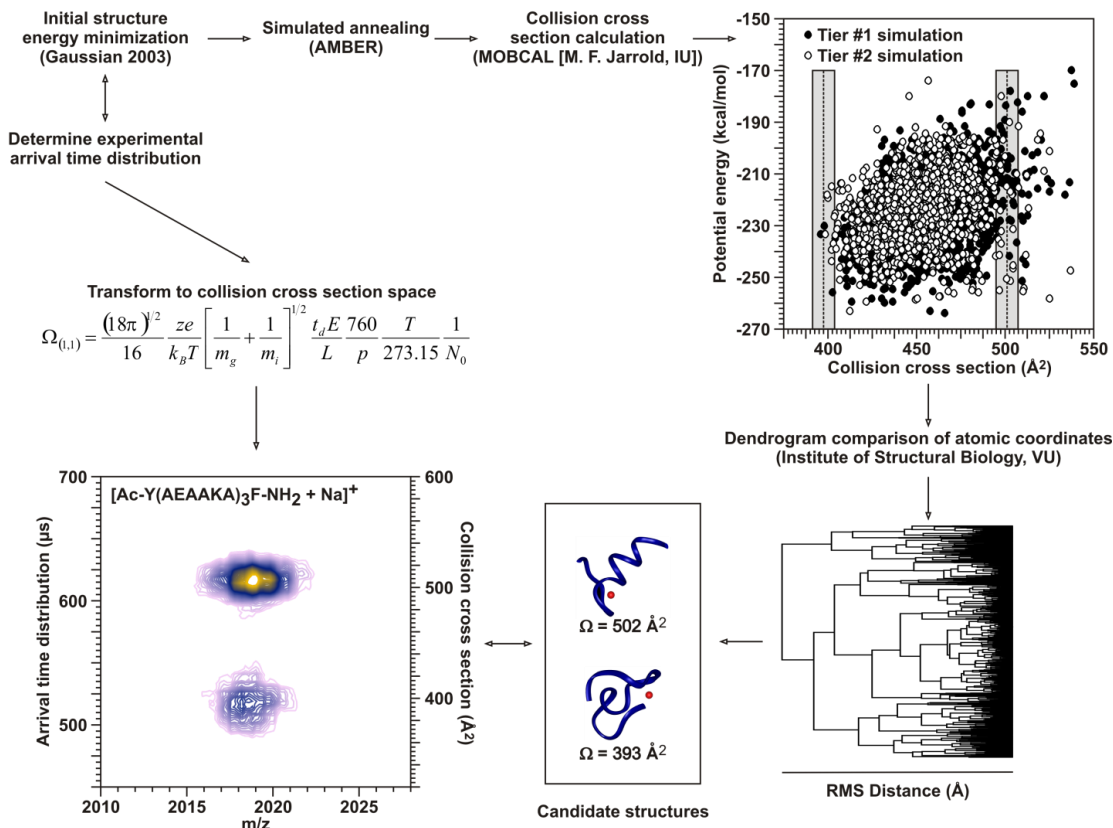


Figure 1.5. Modeling protocol used to interpret peptide and protein structure based on the absolute collision cross section measurements acquired from IM-MS data. Figure reprinted from reference 93.

available structures in publicly accessible databases such as the Research Collaboratory for Structural Bioinformatics Protein Data Bank (RCSB PDB, University of California, San Diego) and the Protein Databank (European Bioinformatics Institute, United Kingdom), which are both closely associated with the worldwide Protein Databank (wwPDB) project. Although computer processing speed has increased exponentially over several decades, computation still puts a limit on how large a system can be realistically studied by using the protocol described here. Quantum chemical minimization and electrostatic potential calculations in charge parameter development at intermediate level of quantum theory on the most powerful desktop workstations give reasonable 24 h results on systems of 20 atoms. Calculations, however, scale up exponentially not only with the level of theory and number of atoms, but also with mass of included elements. For example, studies of proteins containing metal ions may require additional specialized basis sets and time. Therefore, quantum charge parameterization of larger systems has to be done on properly capped fragments, which are later connected for molecular dynamics sampling.

There are many free and proprietary quantum mechanical software packages capable of performing the needed minimization and electrostatic potential calculations (*e.g.*, Cerius, Jaguar, Gaussian, Spartan) at basic to intermediate levels of theory. Recently DFT methods have made inroads into quantum minimization specifically for their ability to efficiently handle electron distribution of higher mass elements. However, the accuracy of DFT is still being studied and molecular dynamics parameterization lags behind these in parameter development for higher mass elements.

The last step of the computational protocol is the conformational MD sampling coupled with computational clustering analysis based on the comparison of the computed CCS values for the generated structural conformers with the experimental CCS value. Once the charge

parameters for each atom in the built structure are determined, one of the available molecular dynamics packages (*e.g.*, Amber,²²⁵ CHARMM, ACCELRY) can be used to perform conformational sampling. Conformational sampling is a molecular dynamics calculation that yields a large number of structural conformers of the studied peptide/protein ion. Two primary challenges of MD-based conformational sampling methods are the use and development of reliable MD parameters that assure chemically and structurally relevant results and of temperature protocols that lead to a completely randomized pool of final structures. Aforementioned MD software packages typically contain reliable MD parameters for standard amino acids, carbohydrates and nucleotides.

Fully randomized sampling without any bias toward one or several conformations can normally be guaranteed by selecting a temperature scheme (heating and cooling algorithm) for the MD calculation in which the studied peptide/protein structure is heated to a temperature at which it can access all reasonably expected conformational states and then cooled slowly to relax into a low-energy structural conformer. An important output result of the MD calculation is the relative potential energy value of each conformer within the pool of generated structures. The computational collision cross section value for each conformer is then calculated by using one of two currently available codes, Mobcal²²⁶ or Sigma.^{62,227,228} Once both the relative potential energy and collision cross section values are computed for each member of the computationally generated ensemble of structures, a plot of energy vs. computed CCS is generated and visually inspected. Typically the lowest energy conformers with a computed CCS that matches the experimental value range are selected for further computational analysis (*e.g.*, analysis of selected average distances, or clustering on the basis of atomic positions). Following cluster analysis, general structural motifs are obtained that are consistent with the measurement, while other structural motifs can be ruled out.

B. The future of proteomics IM-MS studies

Any drug-based treatment (both prophylactic and therapeutic) has its own limitations due to the efficacy of the drug and induced side effects that vary from one individual to another. Identification of biomarker signatures of individual patients allows for diagnosis of the disease at a very early stage and improved treatment strategies with fewer side-effects. Biomarkers can be identified by a variety of standard laboratory techniques including common blood tests, immunohistochemistry,^{229,230} and flow cytometry,²³¹ or more recent omics methods such as genomics,²³² transcriptomics,²³² proteomics,^{10,70,233} peptidomics,²³⁴ glycomics,^{82,235,236} lipidomics²³⁷ and metabolomics.²⁷ Linking the individual patients' condition with the correct drug based on clinical biomarkers opens the door for personalized medicine. Even though the instrumentation is now expensive and complex, personalized medicine may become widely accessible with advances in high-throughput and routine instrumentation. Advances in IM-MS technology over the past few decades have enhanced its ability to analyze samples collected from a large number of individuals in a reasonable amount of time; these discoveries may contribute to the discovery of biomarkers and play an important role in the field of personalized medicine.

Like any other technique, progress in the field of IM-MS is governed not only by the areas to which it is applied but also by the development of new technologies. An example is the work of Russell's group. Advancing upon initial studies,^{67,238} they recently developed a variable temperature IM-TOFMS²³⁹ for studying the structural differences between isomers. At low temperatures, a number of favorable changes occur, (i) there are more collisions between the ion and the drift gas as the mean free path is shortened, (ii) the internal energy of the ion is lowered, and (iii) long-range ion-neutral gas interactions become more pronounced. Therefore, low temperature IM-MS offers high mobility resolution, an important advantage for structural

separation of isomers having very similar cross section values. Future directions of variable temperature IM-MS will likely focus on further eliciting the folding kinetics of peptides, proteins, protein complexes, and drug/protein receptor interactions.

A second goal in instrumentation development is to increase the peak capacity of the measurement to facilitate even more comprehensive characterization of complex samples. There exist two paths to increasing peak capacity: (i) through combining separation techniques, so called 'hyphenated methods' (e.g. LC-IM-MS, and IM/IM-MS), and (ii) improvements to current designs that lead to increased mobility resolution. The introduction of the 'combing' technique by Clemmer and colleagues¹⁶⁰ is an example of hyphenated strategy to increase peak capacity. Recent experiments on a circular drift tube by Clemmer and colleagues^{240,241} will further lead to increased resolution and peak capacity in IM separations.

In summary, the ability of IM to function as a compartmentalized tool that combines well with different types of mass spectrometers and different ionization sources has led to a wide variety of applications in peptide and protein science. Ion mobility has been demonstrated to be highly useful in the characterization of samples ranging from small peptides to large protein complexes, both as a structural characterization tool and as a means for characterizing complex biological samples.

6. Instrumentation overview

The two time-dispersive methods of IM separation are DTIM and TWIM. Drift tube IM facilitates absolute collision cross section calculations.^{27,66,191,242} This data can then be compared to molecular simulation results to interpret analyte structural and conformational details. Traveling wave IM utilizes electrodynamic fields, which only provides estimated collision cross sections when measurements are compared to internal standards with previously measured

DTIM absolute collision cross sections.^{51,52} This is because gas-phase theory is insufficiently developed for the fundamental physical processes in TWIM separations, although recent efforts in this regard have been reported.^{31,51-59} Nevertheless, both DTIM and TWIM instrumentation are increasingly used for biological IM-MS applications. The most common space-dispersive ion mobility technique is High-Field Asymmetric Waveform Ion Mobility Spectrometry (FAIMS). This technique will be mentioned briefly in the sections to come but was not used in any studies in this work.

A. Drift tube ion mobility

The first ion mobility instruments were developed on a drift tube design.²⁴³ Drift tube ion mobility instruments use a static uniform field to cause progression of ions down a (typically) stacked ring drift cell. Importantly, because this ion progression is carried out in a static and uniform manner, previously developed gas-phase theory can be used to directly assess the collision cross section of these ions.^{49,50,244} This makes DTIM a popular choice of instrumentation for structural mass spectrometry applications. Drift cell instruments have been constructed with reduced pressure and atmospheric pressure drift cells, each with its own inherent benefits and challenges.²⁴⁵ Atmospheric pressure drift cells typically separate ions on a timescale of 10's of ms,²⁴⁶ whereas reduced pressure drift cells can provide separations in <1 ms for relatively short drift cells (*ca.* 10 cm⁷⁰). This is significant in certain applications where separation speed becomes important. For example, in MALDI imaging experiments⁶⁰, this separation speed is crucial because it dictates the fastest rate at which the MALDI laser can be operated without losing time correlation in signals arising from different MALDI events (*i.e.*, 10 Hz for 100 ms versus 1,000 Hz for 1 ms drift times, respectively¹⁹²). Drift tube IM resolution typically ranges

from 30 to 50 ($r=t/\Delta t$ at FWHM), whereas longer, cryogenically cooled, or higher pressure drift tubes have been reported with resolutions exceeding 100.^{241,247,248}

B. Traveling wave ion mobility

The recent commercial availability of traveling wave ion mobility (TWIM) instrumentation (Waters Corp.) has made IM-MS accessible to a large number of users. Similar to drift tube instruments, TWIM separates ions by time dispersion through collisions with a background buffer gas, but in contrast, it uses electrodynamic fields rather than electrostatic fields.^{65,249} This is accomplished by transmitting voltage pulses sequentially across a stack of ring electrodes (similar to Fig. 1.1(b)), which creates the so-called traveling wave.²⁵⁰ Conceptually, TWIM separations are performed based on the susceptibility of different ions to the influence of the specific wave characteristics and have been described as the ability of ions to “surf” on waves.²⁴⁹ Adjustable wave parameters include traveling wave pulse height, wave velocity, and ramping either of these variables. The commercial platforms (Synapt, Synapt G2, and Synapt G2-S) are comprised of a MALDI (200-Hz pulse repetition rate) or ESI source, a mass-resolving quadrupole, a trapping region for injecting pulses of ions into the TWIM, the TWIM drift cell, an ion transfer region, and an orthogonal TOFMS ($r=m/\Delta m$ at FWHM of >17,500). CID can be performed in the regions before and after the TWIM drift cell. In principle, the Synapt has sufficient activation/dissociation regions to perform up to MS⁵, although typically up to MS³ is practically feasible. Generally resolution in the TWIM is <15, but this is sufficient for the separation of many molecular classes of interest (*e.g.*, isobaric peptides from lipids). For example, TWIM has been used to separate biomolecular signals from complex samples²⁵¹ and to study the structure of peptides following CID in the trapping region.¹⁸⁴ Although protocols have

been proposed to approximate collision cross section values using TWIM experimental data, the calculations still rely on absolute values obtained using drift tube instruments (Fig. 1.6).^{31,51-59}

C. High-field asymmetric waveform ion mobility spectrometry

FAIMS separations were first documented in the early 1990s by Buryakov et al.^{252,253} FAIMS separations are performed on the basis of the nonlinear dependence of the mobility coefficient (K) in strongly varying electric fields. Unlike previously mentioned methods of IM separation, FAIMS performs separation in a space-dispersive manner rather than a time-dispersive manner. In FAIMS devices, ions are subjected to both positive and negative electric fields, which occur perpendicular to the direction of ion movement known as a high-frequency asymmetric waveform. By sending ions between two parallel plates in a separation cell using a longitudinal (or axial) gas flow and directing this waveform perpendicularly across them, ions that do not meet the exact criteria to traverse the cell will strike either the lower or upper plate. Only ions with particular mobility characteristics pass through the cell. The use of compensation voltage in FAIMS to achieve a mobility-based selection is roughly similar to the use of radio frequencies in quadrupole mass analyzers to achieve mass selection. Although other IM separation methods display data as intensity versus arrival time distribution (ATD), FAIMS data are displayed as intensity versus the scanned compensation voltage. However, one shortcoming to FAIMS is that although mass is an independent, easily calculable variable, mobility in a varying electric field is not easily predicted and depends on several variables including composition and chemical functionality, among others. Thus, it is presently not possible to make direct predictions or calculations of surface area using raw FAIMS data without first running standards and determining which compensation voltage is required for each structural representation of a particular isobaric set of ions.²⁵⁴⁻²⁵⁷

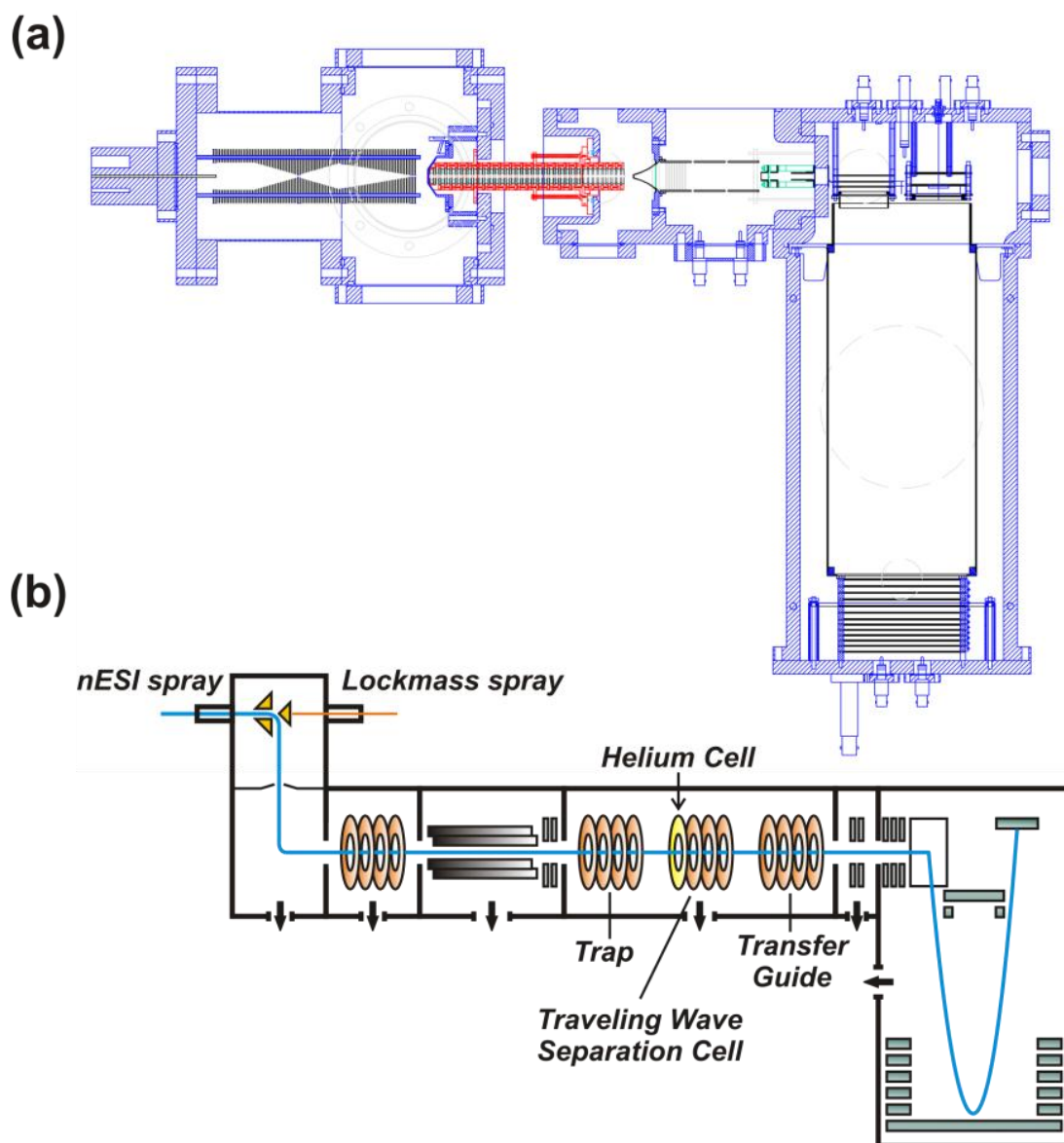


Figure 1.6. (a) A CAD rendering of a drift tube ion mobility spectrometer (Ionwerks Inc.) in ESI mode (adapted from reference 258, courtesy of Jody May). (b) A conceptual drawing of traveling wave ion mobility mass spectrometer produced by Waters Corporation also in ESI mode.

D. Instrumental arrangements for fragmentation studies by ion mobility–MS/MS

An additional advantage of IM-MS separations is the ability to obtain mobility-correlated fragmentation information by placing a region of ion activation such as CID,²⁵⁹ or surface induced dissociation (SID)^{172,260,261} between the drift tube and mass analyzer (*i.e.*, IM-MS/MS). When ion activation is performed following mobility separation, product ions that result from fragmentation can be correlated to precursor ions based upon their elution time from the IM dimension. This differs from insource fragmentation, which is not mobility aligned, because this fragmentation occurs before the mobility cell (Figure 1.7). In contemporary LC–MS approaches, ions of a particular m/z are selected and subsequently activated for fragmentation. In untargeted approaches, such as Waters' MS^E, there is no m/z selection; rather, each LC increment is subjected to activation of all masses. If the LC separation produces coeluted peaks, fragment ion spectra can be difficult to assign because they contain fragment ions arising from multiple precursor species. However, with the added IM dimension these fragmentation spectra are correlated to the precursor based on mobility, and thus enable assignment of the fragment ions to respective precursors. It is advantageous in complex biological samples where analyte amount may be limited, or when interfering species can suppress or isobarically mask the ion of interest.²⁶² Furthermore, additional stages of IM, MS, MS/MS, or IM/IM can be performed depending on the specific goals of the experiment.¹⁵⁹

E. Ionization source consideration

It is important to recognize that the two dominant MS ion sources for biomolecular species, namely electrospray ionization (ESI) and matrix assisted laser desorption/ionization (MALDI) offer complementary capabilities in spite of the fact that there are three primary differences when considering which ion source to use for specific experiments. First, MALDI

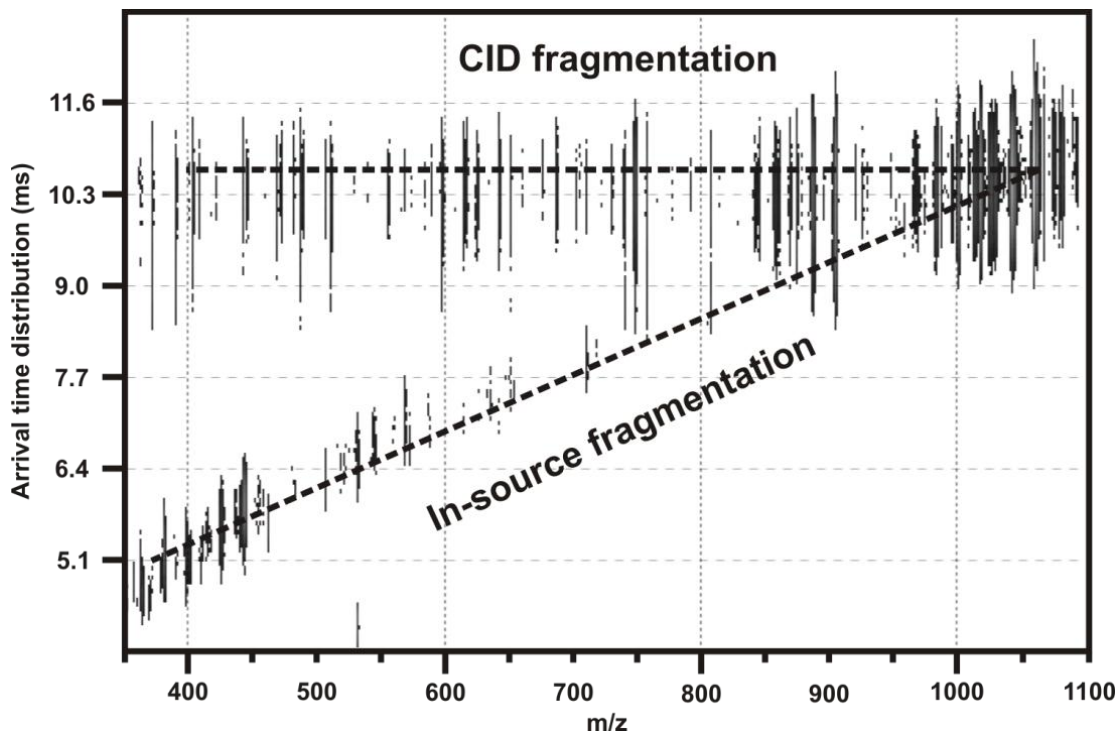


Figure 1.7. ESI-TWIM-MS/MS of the peptide, bradykinin (RPPGFSPFR), illustrating the two modes of IM-MS/MS. In-source decay fragmentation of bradykinin yields the diagonal line of peaks in the conformation space plot. Collision induced dissociation following TWIM separation for this same analyte yields fragmentation ions that share the same arrival time distribution as the parent and so shows up as a horizontal line starting at the parent at the top right and extending to the left. Reprinted from reference 93.

generally produces singly charged ions of the form $[M+H]^+$, $[M+Na]^+$, $[M+K]^+$, etc., where M is the intact molecular parent ion, while ESI produces singly charged ions for small molecules and typically multiply charged ions of the form $[M+nH]^{n+}$ for larger biomolecules such as peptides and proteins. In the analysis of complex mixtures, singly charged ions can result in less spectral complexity, while multiply charged ions better facilitate fragmentation studies using tandem MS strategies, in which the fragments of an MS-separated molecule are themselves separated by a second MS step. Second, owing to the fundamental principles of ion generation, MALDI is more tolerant of salts than ESI, but requires empirical selection of appropriate matrices. Third, MALDI and ESI generate ions in pulsed and continuous modes, respectively. Thus the choice of MALDI or ESI can have pragmatic implications regarding the integration of the biological experiment, the ion source, and the selected mass analyzer. Nevertheless, we view these ionization techniques as highly complementary. One pertinent point to consider with systems biology studies is that ESI is able to utilize a continuous liquid sample. This could provide a clear advantage if one is tracking a dynamic biological system. MALDI, on the other hand, must analyze solid sample substrates. This means that any samples collected from the system must be discretized and solidified on a MALDI target plate. In the end the solid sample will only represent the system at the time the effluent was deposited, such that a time-series analysis requires a series of MALDI samples similar to that reported by Chen et al.²⁶³ This idea is synonymous with watching a movie of what is occurring versus viewing a series of snapshots.

7. Dimensions for expansion

Ion mobility-mass spectrometry naturally excels at a number of aspects central to the study of systems biology. For example, as shown above, IM is able to simultaneously analyze multiple biomolecular classes. In addition, MS has the distinct advantages of sensitivity,

accuracy, and a wide detection dynamic range which is an important feature when trying to analyze biomolecular species.²⁶⁴ Through the use of MALDI and ESI there is the potential to analyze both solid and liquid biological matrices. There are, however, a number of areas where IM-MS can be improved to expand its prospects for systems biology research. Through the use of MALDI imaging, IM-MS would be an ideal candidate for research on spatial measurements of biological systems. For example, IM-MS could be used to not only measure multiple biomolecular classes simultaneously but with the help of MALDI imaging, one could measure multiple intact sections of an organism in the same analysis. In a separate way, ESI-IM-MS has the potential to measure network dynamics from organisms.

A. Spatial

Imaging ion mobility-mass spectrometry is based upon the principles of traditional imaging mass spectrometry²⁶⁵⁻²⁶⁷ but with the incorporation of a gas-phase ion mobility separation added to increase peak capacity and aid in molecular identification. The first examples in the literature of imaging IM-MS was performed using DTIM and demonstrated two important advantages over imaging MS strategies, namely (i) the ability to separate isobaric species on the basis of structure and m/z and (ii) enhanced signal-to-noise ratios by the separation of chemical noise.^{46,47} The former is demonstrated through the selective differentiation of nominally isobaric peptide and lipid species as illustrated in Fig. 1.8(a). In proof-of-concept experiments, both the lipid and the peptide were spotted onto a thin tissue section of mouse liver (12 μm) using a reagent spotter in either a “\” direction for the peptide or a “/” direction for the lipid (Fig. 1.8(a), top left). In the 2D IM-MS plot (Fig. 1.8(a), top right), the signal for the protonated forms of the lipid, phosphatidylcholine 34:2, and the peptide, RPPGFSP, overlaps in the m/z spectrum, but is baseline resolved in the IM arrival time

distribution with the peptide and lipid centered at 449 and 504 μs , respectively. In Fig. 1.8(a) bottom, the \times represents what would be obtained using conventional imaging MS in the absence of IM, which is a convolution of both the peptide and lipid signals. The right two images are for the same 1 Da mass range (759 – 760 m/z), but selectively for structures corresponding to putative peptides “\” and lipids “/,” respectively.⁴⁷ Thus, structurally selective imaging on the basis of molecular class results in more accurate images in contrast with conventional imaging MS alone. In Fig. 1.8(b), imaging IM-MS is demonstrated for a coronal rat brain section (16 μm) where the image to the right corresponds structurally to lipids and specifically to the sodium-coordinated cerebroside 24:0 OH ($m/z = 850.7$ Da). This results in enhanced signal to noise for species of interest through the separation of chemical noise and contaminants with IM.⁴⁶ More recently, imaging IM-MS using a TWIM drift cell has been demonstrated.²⁶⁸ Although the IM resolution is more limited using TWIM, it is sufficient for the separation of lipids from peptides as illustrated for a coronal thin tissue rat brain section (Fig. 1.9(i)). The utility of imaging TWIM-MS for mapping the distribution of a drug, vinblastine, in a kidney from a whole body section is shown in Fig. 1.9(ii), (b). The accuracy of the obtained image is increased through the addition of TWIM due to the removal of isobaric interferences common in highly complex biological samples, such as tissue. Since commercial TWIM instrumentation equipped for imaging applications was released in 2008, the present number of reports is rather limited but expected to increase substantially in the near future.

When performing imaging experiments, additional confirmation of an unidentified peak is often required. A common practice for increasing confidence in peak assignments is to image in a selected reaction monitoring mode for a fragmentation channel characteristic of the analyte of interest (*e.g.*, using CID²⁵⁹). Similar to traditional MS/MS explained previously, the coupled arrangement of IM and MS in imaging experiments yields the ability to obtain structure

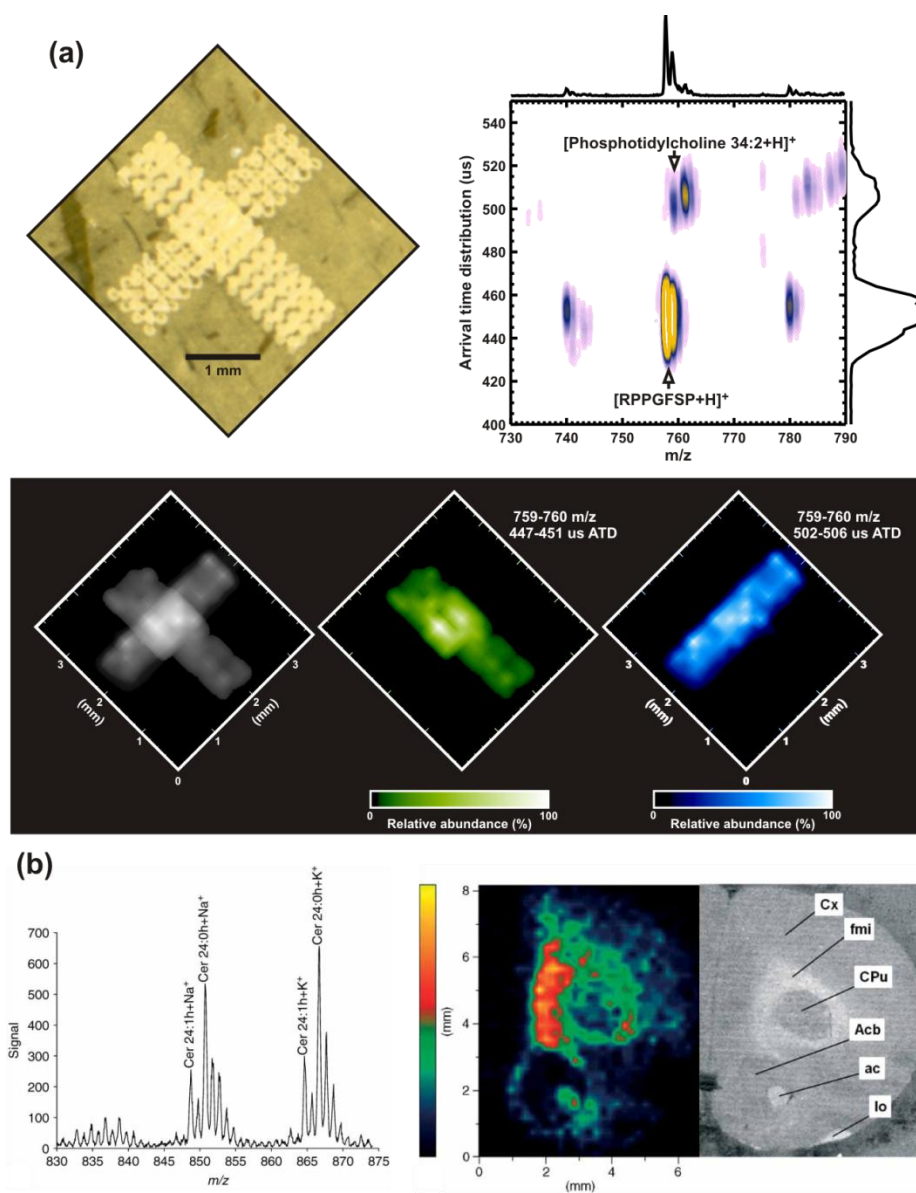


Figure 1.8. (a) Imaging DTIM-MS of a nominally isobaric peptide (RPPGFSP) and lipid (PC 34:2) deposited onto a mouse liver thin tissue section (12 μm) in the pattern of an "X". The "\/" line is RPPGFSP, while the "/" line is a phosphatidylcholine extract, respectively. (top left) An optical image of the patterned matrix/analyte spots deposited on the tissue section. (top right) A zoomed view in the region of PC 34:2 and RPPGFSP for a representative 2D IM-MS conformation space plot of a mixture of the two analytes. IM-MS signal intensity is indicated by false coloring, where purple and yellow corresponds to the least and most intense signals, respectively. (bottom left) An extracted ion intensity map over the mass range of 759-760 Da representing what would be obtained using conventional imaging MALDI-MS. (bottom middle and right) Extracted ion intensity maps for imaging DTIM-MS of the peptide and lipid over the mass range of 759-760 Da and DTIM drift times of 447-451 μs and 502-506 μs , respectively. (b, left) An integrated mass spectrum of cerebrosides directly from rat brain tissue. (b, right) Imaging DTIM-MS of the sodium-coordinated cerebroside 24:0 OH ($m/z = 850.7$). (b, far right) An optical image of an adjacent rat brain section. Histological abbreviations are: Cx - cortex; fmi - forceps minor of the corpus callosum; Cpu - caudate putamen (striatum); Acb - nucleus accumbens; ac - anterior commissure; lo - lateral olfactory tract. Reprinted from reference 60.

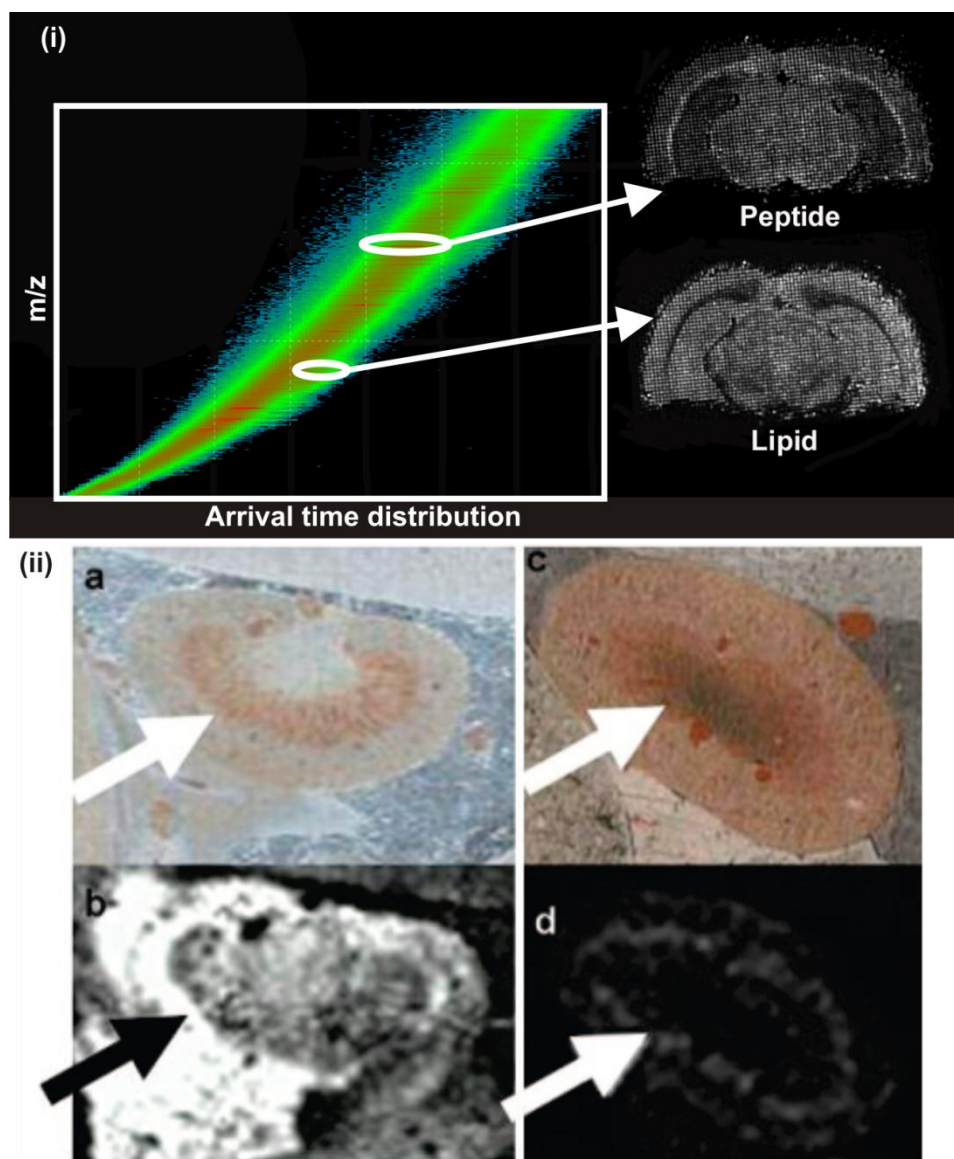


Figure 1.9. (i) Imaging TWIM-MS data of a rat brain thin tissue section illustrating selective imaging of peptides and lipids on the basis of structure. (ii) Imaging TWIM-MS data obtained in the analysis of a small drug molecule, common name vinblastine, in thin tissue kidney sections of vinblastine dosed rats. (a) An optical image of the kidney from the whole body section dosed at 6 mg kg⁻¹ IV vinblastine before matrix application. (b) The same tissue section as shown in (a) but imaged by TWIM-MS showing the distribution of vinblastine within the kidney, with the highest intensity (white) showing a broken ring of intensity between the cortex and the medulla. (c) Optical image of the kidney within the whole body section dosed with 3H vinblastine. (d) Whole body autoradiography of the tissue section shown in (c), indicated is the broken ring of slightly higher intensity (white) between the cortex and the medulla. Reprinted from reference 60.

information in the MS dimension by performing IM-MS/MS. In IM-MS/MS mode, MS¹ can be accomplished in two ways: (i) time dispersion in the drift tube can perform parent ion selection⁷⁰ or (ii) a mass analyzer can be used.²⁵⁰ By placing an ion activation region between the drift tube and mass analyzer ions may be selected for fragmentation according to drift time. Performing the ion selection in this manner provides a multiplex advantage in that all fragment ions will possess the same drift time as the parent ion. This is significant in imaging applications, because the sample is limited to the spatial coordinates of a particular pixel. In imaging IM-MS/MS experiments, multiple parent ions can be fragmented whereby fragment ions are correlated to their respective parent ions by drift time. A demonstration of the potential utility of IM-MS/MS is illustrated in Fig. 1.10 for a carbohydrate, lacto-N-fucopentaose 1 (LNFP1). In-source decay fragmentation for this carbohydrate is illustrated in Fig. 1.10(a) where fragment ions occur at different times in the IM separation. Correlated fragmentation spectra can also be obtained as illustrated in Fig. 1.10(b) by using both in-source fragmentation and post-IM CID. The CID fragmentation results in ions correlated to the drift time of the parent. Importantly, this results in redundancy of the fragment ions that are observed for higher confidence that particular fragment ions arise from the parent ion of interest. For example, the integrated mass spectra for in-source and CID fragmentation (*i.e.*, pre- and post-IM separation) are illustrated in Fig. 1.10(c), (d), respectively. When applied to multiple ions, this operation allows for multiple reaction monitoring (MRM) in a single scan. This application is a highly promising yet virtually untapped resource for biomolecular imaging MS, where limited sample exists at each pixel location. For an example of a typical MALDI-IM-MS imaging protocol, see Appendix B.

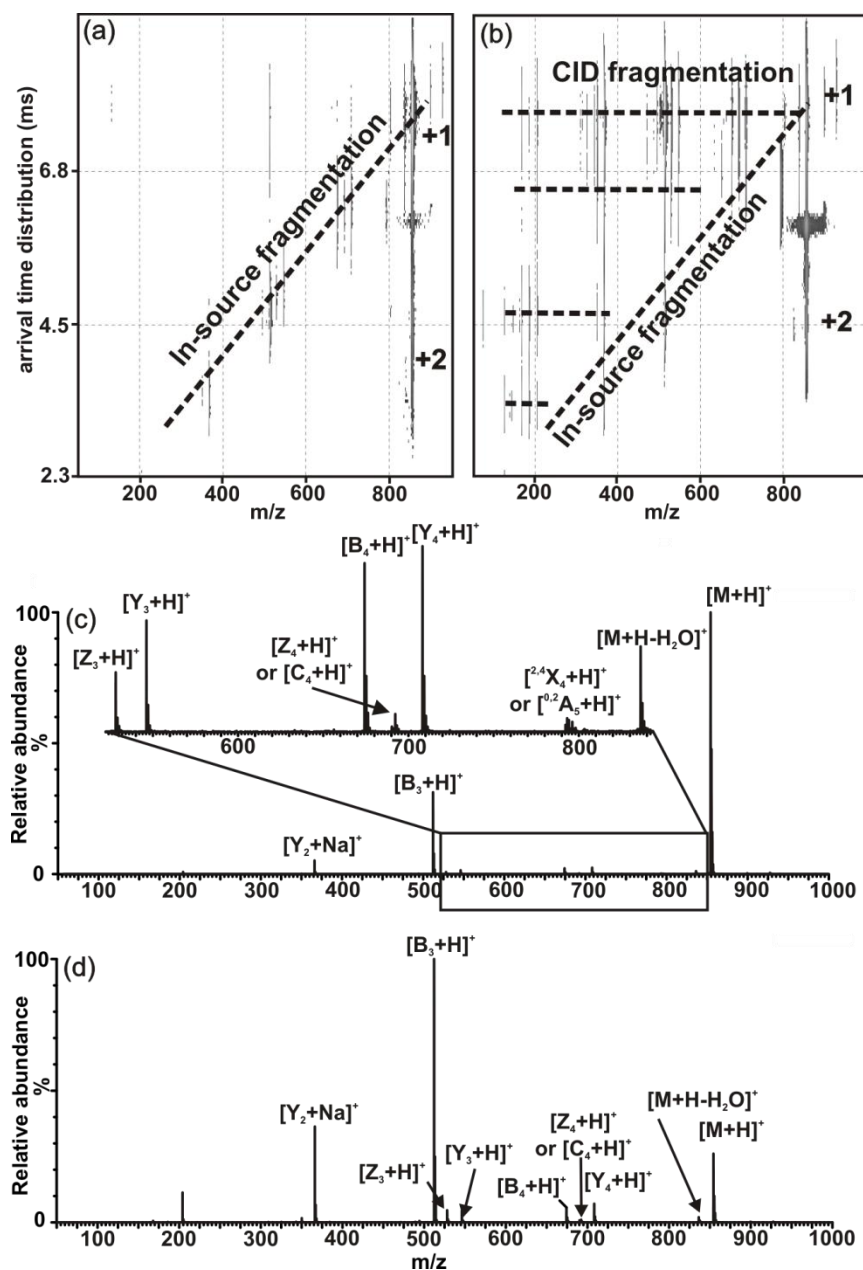


Figure 1.10. ESI-TWIM-MS/MS of the carbohydrate, lacto-N-fucopentaose 1 (LNFP1), illustrating two modes of IM-MS/MS. (a) In-source decay fragmentation of LNFP1 followed by TWIM analysis of the fragment ions. (b) In-source decay prior to TWIM separation and collision induced dissociation following TWIM separation for LNFP1. The latter results in fragment ions to be observed at the same drift time as the parent leading to the possibility for simultaneous CID for various ions at the same time. In both CID and ISD, cross-ring cleavages were seen, but glycosidic bond cleavages were the most abundant type of fragmentation. (c) In-source decay fragmentation spectrum that was extracted from the IM-MS plot above. Along with a zoom in view of the region from ~ 500 -850 Da. Nomenclature for the fragmentation pattern of carbohydrates was first used by Doman and Costello (54). All in-source fragmentation and collision-induced dissociation peaks are labeled utilizing this nomenclature. (d) CID spectrum of the top dotted line for LNFP1 extracted from (b). (c) and (d) can be compared to examine the difference between the two different means for fragmenting carbohydrates. Dotted lines are for illustration purposes of the fragmentation peaks. Reprinted from reference 60.

B. Temporal

Most modern biological approaches choose to either rapidly sample a single aspect (*e.g.*, the electrochemical detection of glucose and the use of green fluorescent protein as a means of monitoring translation) or infrequently sample a more comprehensive set of data (*e.g.*, proteomics). Intermittent sampling results in a fractional snapshot of the system, upon which biological inferences must be placed. When considering the turnover rate of certain enzymatically catalyzed reactions (*e.g.*, millimolar per second rates for ATP, ADP, and cytosolic glucose) or the rate of ribosomal translation (*i.e.*, six to nine amino acids per second for a eukaryotic cell), for example, single minute sampling resolution is considered coarse.²⁶⁹⁻²⁷¹ System dynamics is considered to be one of the key properties of systems biology¹ and for this reason, systems biology measurements are of most benefit if they are acquired with a very high temporal frequency. If likened to a video of a jogger on a treadmill, the need for rapid sampling rates in systems biology studies can be explained as follows. If one wishes to use a video to analyze how the jogger moves and how the body's joints and structure work in unison to produce forward propulsion, then a video with a very low sampling/frame rate would not be very useful. For example, if studying the jogger's motion through a 1 frame-per-second (fps) motion video the jogger may appear to be moving quite slowly and disjointedly, or perhaps may appear to not be moving at all. For this study a standard 30 fps (or faster) video would be of most use. This example draws many parallels with the sampling of biological systems where a high sampling rate is required to confidently identify patterns in metabolic fluctuations. Both the jogger video and the biological sampling problems are governed by the Nyquist-Shannon sampling theorem which tells us that a function containing frequencies lower than B hertz can only be completely identified by collecting measurements at a series of points spaced $1/(2B)$ seconds apart or less.^{272,273}

The rapid acquisition rate of time-of-flight mass spectrometry (TOF-MS) measurements allows for sampling at a timescale that is relevant for a greater number of biological processes. However, MS alone lacks the necessary peak capacity for systems biology analyses, even when considering high-resolution methods that can provide a resolving power greater than $\sim 50,000$.^{274,275} This limited peak capacity may be alleviated through the coupling of mass spectrometry to one of several additional separations methods, notably ion mobility (IM).^{83,189} The ability of MS and IM-MS to perform proteomic and metabolomic analyses is unquestionable.^{10,13} The sensitivity, dynamic range, and ability to obtain accurate mass measurements, among other figures of merit, are the stronger suits of IM-MS.

Addition of the IM dimension to high-frequency biological mass spectrometry analyses allows for reduction of chemical noise (by partitioning inherent chemical noise to other areas of two dimensional conformation space) and also separates analytes on the order of milliseconds (causing no significant increase in acquisition time). The millisecond time-scale of these separations also allows for the addition of an LC- or gas chromatography (GC)-based separation before the mobility separation (yielding a three-dimensional data set). This added data dimensionality has several key benefits. For example, Clemmer and colleagues³⁷ have recently described LC-ESI IM-MS studies of the human plasma proteome whereby three-dimensional separations provided an enhanced dynamic range in concentration that was estimated to be 10^5 – 10^6 . Data from LC-IM-MS multiplexed arrangements illustrate the data density of such experiments from complex biological samples.

While exploration of the spatial dimension using IM and MS has already begun,²⁷⁶ there is significant room for improvement in the temporal dimension. Accompanying this improvement is a substantial need for improved techniques for coupling the system on which the analysis is being performed (*i.e.*, the organism) with the detection instrumentation (*i.e.*, the

ion mobility-mass spectrometer). Our efforts to improve this interfacing are reviewed in the following chapters.

Acknowledgements

Financial support for this work was provided by the National Institutes of Health-NIDA (#HHSN271200700012C), Vanderbilt University College of Arts and Sciences, Vanderbilt Institute of Chemical Biology, Vanderbilt Institute for Integrated Biosystems Research and Education, the American Society for Mass Spectrometry (Research award to J.A.M), the Spectroscopy Society of Pittsburgh, the National Institutes of Health (RC2DA028981), the US Defense Threat Reduction Agency (HDTRA-09-1-0013), the National Academies Keck Futures Initiative, Ionwerks Inc., and Waters Corp. We thank Todd Graham and Anthony Weil for their advice and assistance with the yeast studies, and Hod Lipson and Michael Schmidt for their guidance on machine learning. We also thank Whitney B. Ridenour and Richard M. Caprioli (Vanderbilt University) for assistance and use of the Synapt HDMS, which is supported by the Vanderbilt University Mass Spectrometry Research Core.

STATEMENT OF DISSERTATION

In regards to this project, my role has comprised the following contributions. I was the sole contributor of efforts to design and implement all online desalting techniques involving electrochemical and chromatographic means. The final desalter arrangement used in chapter 4, however, was a direct result of collaborative work between Dr. Christina Marasco and myself. I was the sole contributor of mass spectrometry data collection techniques for this platform. Data analysis was a collaborative effort between Dr. Christina Marasco and myself.

This work has far reaching implications for all of the biological sciences, but in particular, pharmacology, toxicology, and natural product synthesis. Online analyses of live cellular cultures afford the user an expedient detectable return on variable input parameters. It is this quick return that provides the opportunity to study dynamics the effect of highly variable input parameters such as various media conditions and challenges that may be used on a microbial culture to generate a specific natural product.

I believe this type of work has not been demonstrated previously because it is unusual to have access to and expertise in so many varying analytical and biomedical engineering fields (*i.e.*, microfluidics, chromatography and mass spectrometry), and the few that do have access to these fields are not studying systems biology through improved network dynamics detection. The online solid phase extraction device (outlined in chapter 3) is the predominant reason this type of work has been successful, and previous strategies of this caliber do not prioritize dynamics (as evidenced by the fact that most send the incoming sample stream to waste for a significant portion of the cycle).

CHAPTER II

SYSTEMS BIOLOGY MEASUREMENTS USING ION MOBILITY-MASS SPECTROMETRY

1. Introduction

As stated previously, most modern biological approaches choose to either rapidly sample a single aspect (*e.g.*, the electrochemical detection of glucose and the use of green fluorescent protein as a means of monitoring translation) or infrequently sample a more comprehensive set of data (*e.g.*, proteomics). Intermittent sampling results in a fractional snapshot of the system, upon which biological inferences must be placed. When considering the turnover rate of certain enzymatically catalyzed reactions (*e.g.*, millimolar per second rates for ATP, ADP, and cytosolic glucose) or the rate of ribosomal translation (*i.e.*, six to nine amino acids per second for a eukaryotic cell), for example, single minute sampling resolution is considered coarse.²⁶⁹⁻²⁷¹ If likened to a video of a jogger on a treadmill, the need for rapid sampling rates in systems biology studies can be explained as follows. If one wishes to use a video to analyze how the jogger moves and how the body's joints and structure work in unison to produce forward propulsion then a video with a very low sampling/frame rate would not be very useful. For example, if studying the jogger's motion through a 1 frame-per-second (fps) motion video the jogger may appear to be moving quite slowly and disjointedly, or perhaps may appear to not be moving at all. For this study a standard 30 fps (or faster) video would be of most use. This example draws many parallels with the sampling of biological systems where a high sampling rate is required to confidently identify patterns in metabolic fluctuations. Both the jogger video and the biological sampling problems are governed by the Nyquist-Shannon sampling theorem which tells us that a function containing frequencies lower than B hertz can only be completely

identified by collecting measurements at a series of points spaced $1/(2B)$ seconds apart or less. System dynamics is considered to be one of the key aspects of systems biology, thus necessitating the development of new rapid sampling techniques and platforms.¹

Once one has decided to drastically increase the sampling rate of their method the challenge still remains, how does one sample a biological system multiple times over the course of an experiment without destroying or even perturbing that system? If compared to a human clinical setting, when a doctor wishes to know the overall state of a patient, he/she may perform a comprehensive blood test. However, when forming the basis of an analytical platform, a more simplified system such as cell cultures are used, and cells don't possess a comparable "blood sample" to be taken. One solution is to run numerous duplicate systems in parallel, sacrificing one population for every sample collected; this drastically increases labor and speculatively assumes that all the populations are exact biological replicates of one another, which is highly unlikely.

The exometabolome or metabolic footprint represents an opportunity to bridge this gap. The exometabolome is everything that is secreted or excreted from the cell and is rich in cellular and population conditional information. This means the exometabolome has the potential to include proteins, lipids, glycans, metabolites, and in some bacterial and viral cases, nucleic acid material. It has been shown that this material can be used to infer intercellular processes and overall system states.^{277,278} The logical next step is identifying a technology that is able to sustain live cell populations, while also granting access to the cellular exometabolome. A viable technological candidate to meet these needs is microfluidics.

A. The multitrapping nanophysiometer

Microfluidics, or lab-on-a-chip (LOC) technology, spans multiple fields including engineering, physics, chemistry, and biology. This technology has implemented a shift in the traditional experimental techniques of cell and molecular biology towards small-scale on-chip research. This shift towards miniaturized chip devices comes with beneficial parameters. Low volumes of reagents may be used based on microfluidic device size and length of experiment. Also easier fluid handling on the microscale allows for better experimental control. Experiments conducted with microfluidic devices offer the potential of being inexpensive not only due to the decreased cost of reagents, but also because of low material cost as the devices are typically comprised of poly(dimethylsiloxane) (PDMS) and a glass slide or cover slip.^{279,280} The design and fabrication procedures allow for meticulous control of the device features, making the technology incredibly versatile. Because these devices consume picoliter to nanoliter volumes of reagents and/or cell culture medium, the extracellular contents including autocrine and paracrine signaling molecules are not diluted to the large extent experienced with cell culture and titer plate techniques.²⁸¹ In contrast to the macroscale, specific physical phenomena, such as diffusion, laminar flow, surface area-to-volume ratios, and other factors, when experienced on the microscale, have significant consequences in physiological processes and can greatly contribute to a more representative in vitro/in vivo correlation. By taking advantage of the numerous benefits of microfluidics researchers have been able to make measurements at the microscale that would otherwise not be possible.²⁸²

Cell trapping microfluidic devices sustain a cellular culture population by constantly perfusing fresh media through the device. The medium that passes through the device is typically directed to waste. This outlet stream, however, is rich in secreted and excreted material and can be used to monitor the exometabolome of the population. The Vanderbilt

Institute for Integrative Biosystems Research and Education (VIIBRE) Multitrap Nanophysiometer (MTNP), a microfluidic device used as miniature bioreactor, allows for studies on small populations of cells (1 to $\sim 10^5$). This is in stark contrast to traditional cell biology techniques which often require several orders of magnitude larger populations of cells. The MTNP lends itself to long-term optical measurements of the dynamic behavior of cells, including fluorescent labeling of cells to detect type, activation state, and signaling dynamics.^{281,283,284} The MTNPs can also be readily combined with microfabricated multielectrode arrays for electrochemical measurements of the metabolic activity of small numbers of cells and their rapid response to drugs and other perturbations.²⁸⁵⁻²⁹¹ Sensitivities approaching that required to monitor single cells have been achieved in preliminary work.²⁹²⁻²⁹⁷ Together these technologies are ideal for studying paracrine and autocrine signaling dynamics.

An additional benefit of these MTNP systems is the ease with which they can be used for stimulus-response experiments. Most MTNPs are designed with three input ports which are supplied with solvent/medium by three syringe pumps and a single output port. These input pumps can be run simultaneously or consecutively. The latter provides the opportunity to expose the cellular populations in the device to varying chemical stimulants (whether gradually or sudden) over the course of an experiment. These types of experiments can be of benefit to a wide range of applications, including pre-symptomatic response, biological applications of bifurcation theory, and glucose-stimulated insulin response, to name a few. Additionally, the output port, from which exometabolome rich medium elutes, can be connected online with a detector capable of analyzing the potentially complicated matrix of biomolecular material and also capable of detecting it at a rate germane to systems biology studies.

B. Ion mobility as a tool for measuring temporally dynamic living biological systems

The rapid acquisition rate of time-of-flight mass spectrometry (TOF-MS) measurements allows for sampling at a timescale that is relevant to a greater number of biological processes. However, MS alone lacks the necessary peak capacity for systems biology analyses, even when considering high-resolution methods that can provide a resolving power greater than ~50,000.^{274,275} This limited peak capacity may be alleviated through the coupling of mass spectrometry to one of several additional separations methods, notably ion mobility (IM), which is a post-ionization separation that resolves ions based on their relative size-to-charge ratio and occurs on the order of milliseconds.^{83,189} The ability of MS and IM-MS to perform proteomic and metabolomic analyses has been previously demonstrated.^{10,13} The sensitivity, dynamic range, and ability to obtain accurate mass measurements, among other figures of merit, are the stronger suits of IM-MS.

The simplicity of the design of IM makes the technology versatile and robust enough to be found in the commercial and military sectors, where it is used for the detection of explosive compounds. In the research laboratory, the millisecond timescale of the separations facilitates the multiplexed combination of ion mobility with higher repetition-rate sampling techniques such as MS. The addition of IM to MS can be likened to the coupling of liquid chromatography (LC) or gas chromatography (GC) to MS, where pre-ionization separations (GC and LC), which inherently have a longer separations timescale (minutes to hours), interface with the higher sampling rate MS (*e.g.*, microseconds for time-of-flight MS), allowing many spectra to be taken for a given LC or GC separation. The resulting data comprise an LC trace with an associated MS spectrum acquired at sub-second intervals, which is typically displayed in two dimensions (Figure 2.1(a)). The hydrophobic separation of LC is highly orthogonal to the m/z separation of MS and yields a spectrum where the molecular signals occupy a large and varied region of

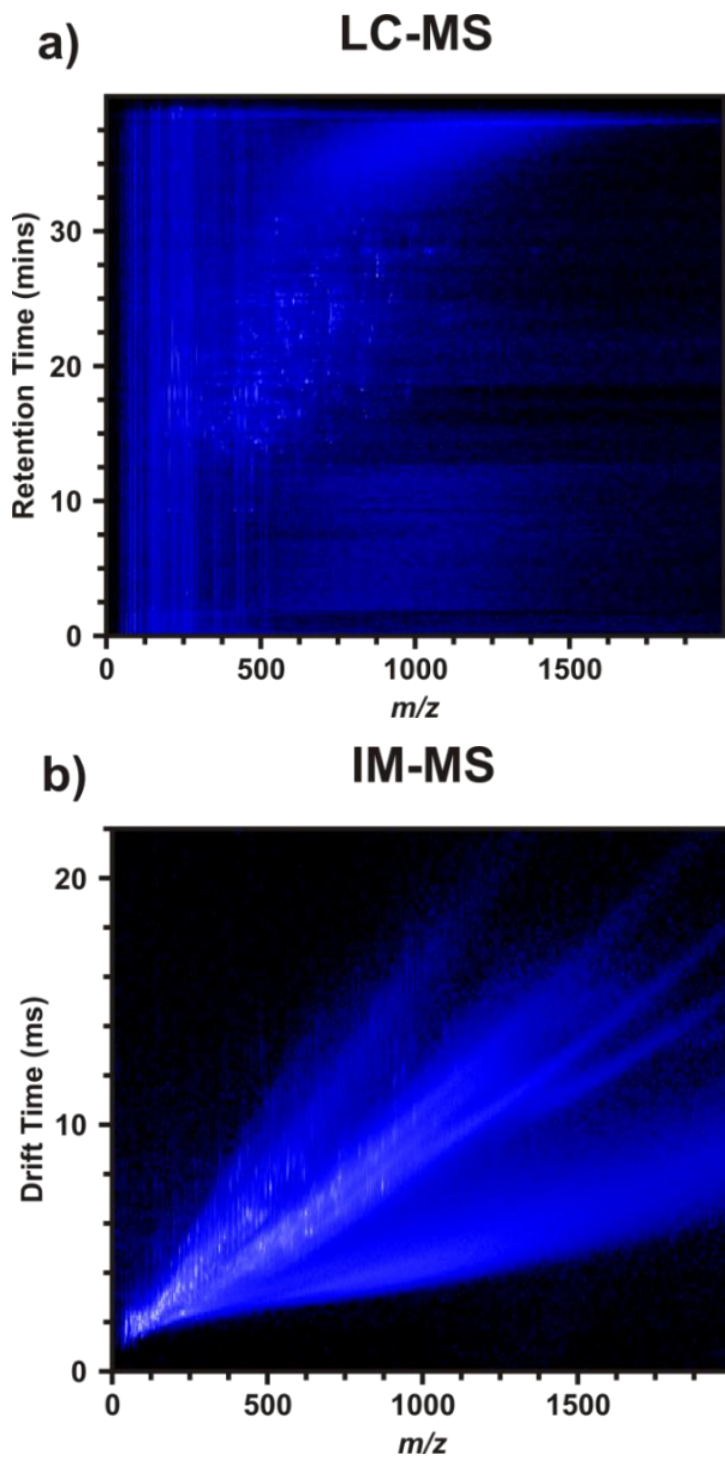


Figure 2.1. A comparison of the orthogonality of LC-MS and IM-MS. (a) The hydrophobic separation of LC is highly orthogonal to m/z separation of MS and yields a spectrum where the molecular signals occupy a large region of separations space. (b) The drift time of an ion, dictated by its gas-phase packing density, is not highly orthogonal to the mass differentiation of MS. This results in more concentrated occupation of separations space. This relationship produces lines of gas-phase packing density correlation (as seen in (b)) which are indicative of chemical class and provide an important means for analytical separations. Reprinted from reference 298.

separation space. This correlation is inversely related to the orthogonality of the two measurements.²⁹⁹ IM-MS is a similar marriage of two temporally disparate separations, with IM dispersing ions based upon their relative gas-phase packing density and charge state and occurring on the order of milliseconds, allowing for hundreds of MS spectra to be taken for a given IM separation. These data produce two-dimensional spectra, as shown in Figure 2.1(b), with the mass of the ion (m/z) displayed on the abscissa and drift time (the time it takes the ions to traverse the ion mobility drift cell in milliseconds) on the ordinate. The drift time of an ion, dictated by its gas-phase packing density, is not highly orthogonal to the mass differentiation of MS. This results in more concentrated occupation of separations space.

Advantages of the IM dimension include the ability to reduce chemical noise (by partitioning inherent chemical noise to other areas of two dimensional conformation space) and to perform separations on the order of milliseconds (causing no significant increase in total experiment time). The millisecond time-scale of these separations also allows for the addition of an LC- or GC-based separation before the mobility separation (yielding a three-dimensional data set). This added data dimensionality has several key benefits. For example, Clemmer and colleagues³⁷ have recently described LC-ESI IM-MS studies of the human plasma proteome whereby three-dimensional separations provided an enhanced dynamic range in concentration that was estimated to be 10^5 – 10^6 . Data from LC-IM-MS multiplexed arrangements illustrate the data density of such experiments from complex biological samples. An example spectrum of plasma from whole rat blood is shown in Figure 2.2 as a three dimensional scatterplot. Each ellipsoid in the spectrum represents a uniquely identified feature with the relative shapes of the ellipsoids in each dimension being governed by the associated resolution of each measurement axis. The relative size of each ellipsoid represents the relative intensity of the ion signal. Note that there are over 100,000 uniquely defined features contained within this dataset, compared

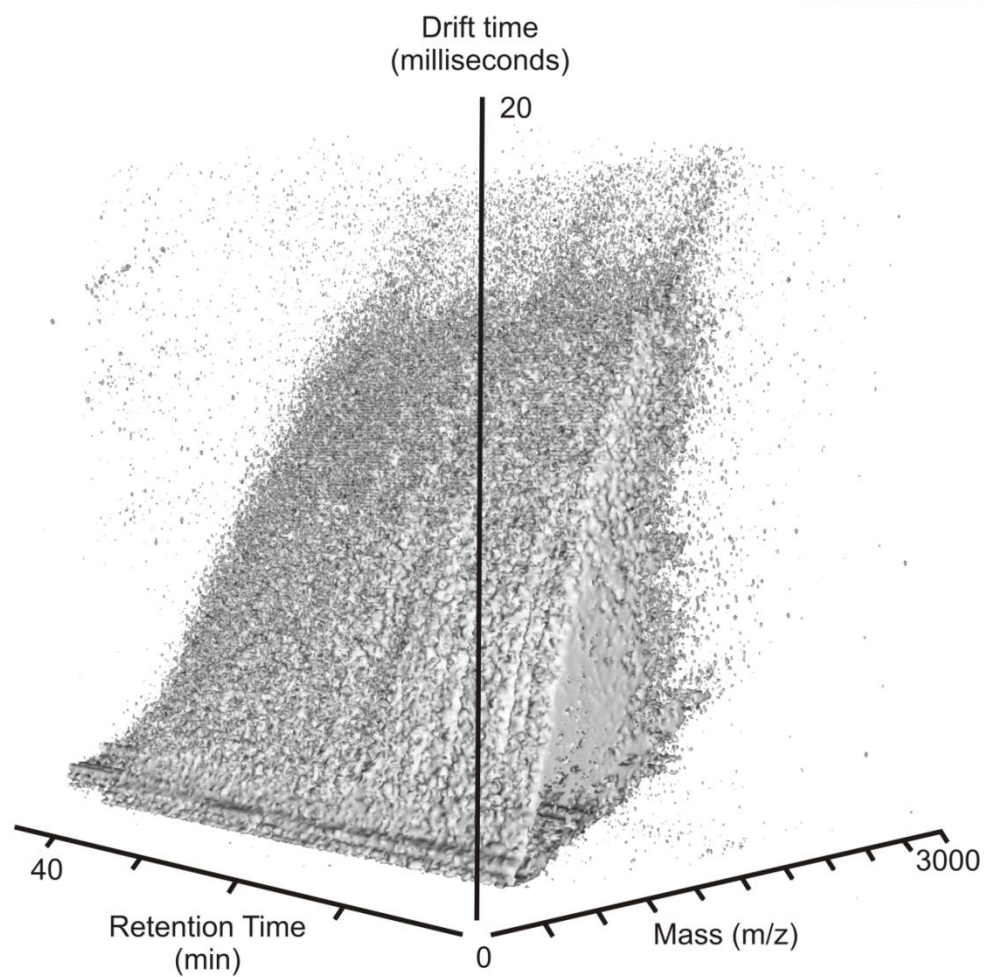


Figure 2.2. A three-dimensional scatter plot of an LC-ESI-IM-MS spectrum displaying plasma from whole rat blood. Each ellipsoid represents a unique molecular signal. The shape of each ellipsoid is governed by the relative resolution or resolving power of the three dimensions displayed (*i.e.*, drift time, retention time, and mass). The relative size of each ellipsoid represents the relative intensity of the ion signal. The points shown in this scatter plot occupy only one part in 105 of the possible distinct species that could be identified in this plot. Reprinted from reference 298.

with *ca.* 10,000 when performing IM-MS in the absence of LC. This represents only $\sim 10^{-5}$ of the possible molecules that could be uniquely specified in this scatterplot — another testimony of the peak capacity afforded by the three-dimensional separation.

C. Multidimensional data handling

Because of the large amounts of data generated in an (LC/GC) IM-MS analysis, translating the data to meaningful information can be challenging. Data acquired from IM-MS separations used in conjunction with any pre-ionization separation must first be discretized to finite retention time, drift time, and mass-to-charge values. Data must be aligned in all dimensions for cross-sample comparison. Open-source and commercial software is available that addresses several of these issues.³⁰⁰⁻³⁰² The use of internal calibrants and spectral feature alignment algorithms compensate for minor separation incongruencies. Additionally, isotopic envelopes must be collapsed into monoisotopic peaks and intensities normalized, commonly using total ion count. This ensures relevant and relatively quantitative sample-to-sample comparability. To date, software that defines peaks using mobility in conjunction with m/z and retention time is not widely available, as the processing and alignment of raw data in three dimensions are computationally expensive. However, developments in this area are forthcoming. The availability of open-source or commercially available software for peak identification will be necessary to fully utilize the potential of three or higher dimensions of separation.

Presently, these data are often discriminated using multivariate statistical analyses such as principal component analysis (PCA) and partial least squares-discriminate analysis (PLS-DA). In essence, these methods seek to distill data to two or three principal components that best describe the variability of the data. It is important that this approach allow the analytes that

contribute most significantly to differences in sample sets to be identified from tens of thousands of molecular signals — the PCA components each represent a particular spectrum of analytes that is representative of a specific difference between the two sets. In this manner, needles may be drawn from the haystacks of data present in very complex biological systems. This method has been employed extensively in metabolomic analyses and is considered a reliable method for untargeted analyses, allowing for the prioritization of peaks of interest for database searching using publicly available databases.^{11,12,303}

D. Combining IM-MS with microfluidics for cellular culture effluent analysis

Microfluidic chips have been successfully integrated with capillary electrophoretic (CE) separations of biomolecules.³⁰⁴⁻³⁰⁷ However, because CE is a condensed-phase separation, it still relies on liquid-phase physical properties for separation and typically requires 10's of minutes for separation. Several studies have focused on integrating the numerous benefits and flexibility of microfluidics with the sensitive analytical power of mass spectrometry.³⁰⁸ Some have used microfluidics to increase the ease and efficiency of proteomic analysis using on-chip immobilized enzymatic degradation for ESI and MALDI.^{309,310} Mellors et al. were able to demonstrate complete integration of the ionization source into the microfluidic chip³¹¹. In that study ESI was performed from the corner of the glass device without the need for external pumping or spray tips.

Integration of PDMS cell-trapping microfluidic devices, such as the MTNP,^{281,283,284} in an online manner with IM-MS involves sampling the continuously flowing output effluent of the MTNP. Fortunately, the flow rate (*ca.* 500 nL/min) and the general aqueous nature of this sample stream make it a good candidate for ESI analysis. This sample stream contains temporally related biomolecular signatures of the exometabolome of cellular populations

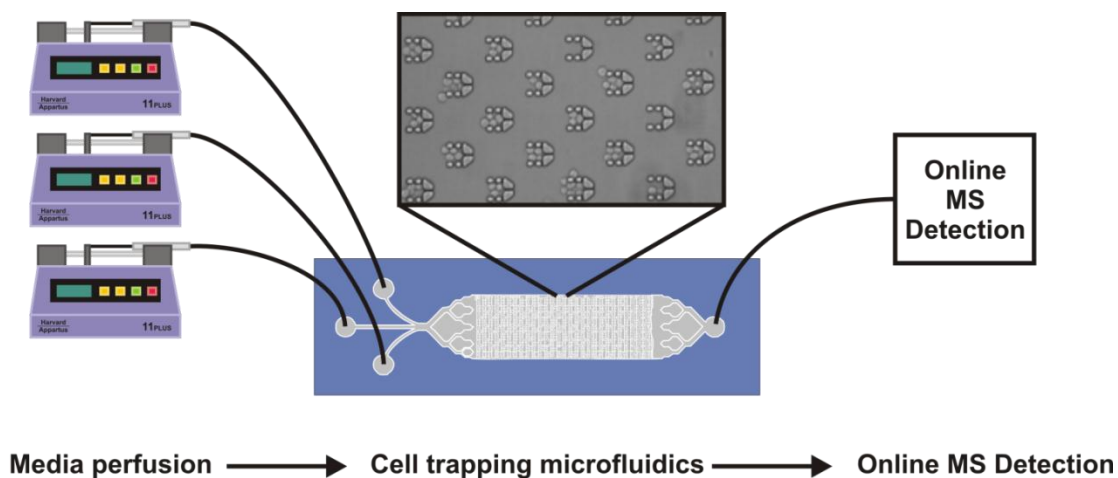


Figure 2.3. A schematic diagram for the online ESI-IM-MS analyses of the cellular exometabolome. Media is typically perfused using Harvard syringe pumps. Cell trapping microfluidic devices are fabricated from PDMS. These devices (not drawn to scale in this figure) are roughly 2 cm in total length and composed of 7000 cell traps which measure 18 μm wide and 18 μm deep. The interior space has a typical height of *ca.* 20 μm . Following perfusion of cell culture media across the cells, the sample effluent is subsequently analyzed by IM-MS. Reprinted from reference 312.

(Fig. 2.3)³¹². Media is typically perfused through the MTNP using syringe pumps. These devices (not drawn to scale in Figure 2.3) are roughly 2 cm in total length and are composed of 7000 cell traps that measure 18 μm wide and 18 μm deep. The interior space has a typical height of *ca.* 20 μm . Following perfusion of cell culture media across the cells, the sample effluent is analyzed *online* by ESI-IM-MS. This method serves as an option for the integrated and comprehensive online systems biology measurement of biological systems, potentially overcoming the difficulties related to sample fraction collection and system preservation.

In the sections to follow, the integration of PDMS microfluidic cell-trapping devices with ESI-IM-MS will be presented. The ability to explicitly control the conditions of the microenvironment of the device will be demonstrated. This is crucial for stimulus/response experiments where conditions may change quickly and frequently.

The future of systems biology research will lie not in the division of divergent and highly specified analyses of individual components of biological systems, but rather in the holistic and convergent simultaneous measurement of all parts of a biological system. It is the optimization of combining these aspects into a single experimental platform, while also overcoming the inherent difficulties, which will result in the greatest insight into these systems. An integrated IM-MS platform coupled to real-time experiments on small populations of live cells with the possibility of feedback^{291,313} will likely be useful for the present and future direction of systems biology– level experiments.

2. Methods

ESI-IM-TOFMS measurements for the preliminary desalting and diffusion studies were performed with a nanoflow-ESI ionization source held at +2.25 kV. After exiting the ESI tip the ions were directed through a 500 μm ID, 6 inch long steel capillary heated to 100°C and held at

ground potential. Upon exiting the steel capillary the ions were held in a keyhole ion funnel trapping region in order to be pulsed into the 14 cm long drift tube for temporally resolved measurement.²⁵⁸ Once the ionized species traversed the 4 Torr He-filled drift cell under the influence of a weak electric field held at -100 V potential at the front and -1900 V at the back plate, they were guided by ion optics into the low-pressure (*ca.* 10⁻⁸ Torr) TOFMS region. Two-dimensional spectra (arrival time versus *m/z*) of each sample were analyzed and compared using custom visualization software (Ionwerks, Houston, TX, USA) developed on the IDL platform (ITT Visual Information Solutions, Boulder, CO, USA). Desalting studies were performed using a 1 inch packed LC column. The 250 μm ID column was packed in-house with 30 μm C₁₈ beads. Cheminert (Valco Instruments Co. Inc., Houston, TX, USA) valves and an Eksigent nanoflow 2D LC pumping system (Eksigent Technologies, Dublin, CA, USA) was used to drive the desalting process discussed below. Mass calibration of the instrument was performed externally using a mixture of C₆₀ and C₇₀, which also serve as structural standards. A MALDI-TOFMS (Voyager DE-STR, Applied Biosystems, Foster City, CA, USA) operated in reflectron mode was used to confirm the identities of various signals.

Data for the yeast analyses were recorded on an Applied Biosystems Voyager DE-STR mass spectrometer. Data were processed using the Voyager Control Panel Version 5.10 (Applied Biosystems) and MALDI MS Imaging Tool, version 2.2.2 (developed by Markus Stoeckli, Novartis, Switzerland)³¹⁴. Both BY4741 and ATCC #9763 *Saccharomyces cerevisiae* strains were used. Cell stocks were initially stored at -80°C. A portion was plated on yeast peptone dextrose (YPD)-rich agar plates and allowed to grow for three days at 30°C. Inoculation was carried out overnight in synthetic minimal media (SD). Before experimentation, subculture cell density was confirmed using optical density (OD) measurements at 600 nm. The OD was confirmed to be in the optimal range of 0.5 to 1.0, indicating that the yeast cells were in the active phase of their logarithmic

growth. Throughout the course of the experiment deionized water was rinsed over the cells at a flow rate of 200 nL/min for 3 hours. The cells were captured in multitrap nanophysimeters for optical monitoring and to allow collection of the undiluted yeast secretome in the effluent.^{281,283}

Data for the Jurkat cell spectra were collected on a Synapt HDMS ion mobility-mass spectrometer platform (Waters Inc., Manchester, England). Data were processed using the Waters Driftscope 2.0 software package. Jurkat T cells (clone E6-1) were obtained from ATCC and cultured in RPMI 1640 medium supplemented with 10% FBS (ATCC) and 10 mg/ml Ciproflaxin (Cellgro). Cells were maintained in a sterile environment at 37°C with 5% CO₂. Supplied media was maintained at a flow rate of 200 nL/min. MTNP effluent was collected for off-line MALDI-IM-MS analysis.

3. Results and discussion

A. Preliminary studies

Our initial experiments have gauged the general compatibility of microfluidics liquid handling with IM-MS. Many variables were considered in order to validate suitable experimental conditions, including flow rates, measurement timing, pressure tolerances, and chemical compatibility (between necessary chemicals for biological microfluidics and IM-MS). Aimed at answering questions of compatibility, initial experiments sought simply to demonstrate that molecular events occurring inside the microfluidic device could be observed with confident identification and with appropriate temporal resolution. To this end, for our first experiments we used a microfluidic trap device with two inlets and one outlet and alternatively infused a blank methanol solution and a sample solution containing 20 µg/mL of a standard cardiac peptide (bradykinin, RPPGFSPFR). The infusion cycles were 10 minutes, meaning the blank

methanol solution was infused for 5 minutes followed by the sample solution for 5 minutes, etc. Figure 2.4 shows that not only could we detect small amounts of a biological sample through a trapping device but also that we could measure it with a temporal resolution of < 5 min and a very high signal-to-noise ratio between peptide and control blank infusion cycles. This also indicates that longitudinal diffusion between adjacent solution packets was minimal, providing confidence that secreted biomolecular material would not get displaced from its original temporal location in the flow stream. Although it appears that the noise level increases following the third injection cycle in all subsequent injection cycles the noise level remains at a steady state level. We speculate that this rising noise level plateaus when sufficient sample conditioning of the tubing between the MTNP and nESI source is achieved.

B. Saccharomyces cerevisiae

Given the demonstration of compatibility of microfluidics and IM-MS, it was important to test IM-MS as a detection method using a living biological system. *Saccharomyces cerevisiae* was chosen because it is a well-developed, well-understood system. It is also known for its resiliency as a biological system, enabling time-intensive experiments. *S. cerevisiae* cells were loaded into a trapping device and were supplied 100% deionized water. This water rinse activates a dormant state in the yeast cells with reduced metabolic activity.³¹⁵ The water rinse was begun at time zero and the progression of various ion species was monitored over time. Figure 2.5 shows images of budding yeast in an MTNP. Effluent from the experimental trapped yeast cells was spotted onto a MALDI plate every 5 minutes to retain time resolution, while not requiring extensive sample preparation. A sample spectrum (Fig. 2.5) displays the species that were monitored temporally in this experiment (Fig. 2.5). These three example sets of data show

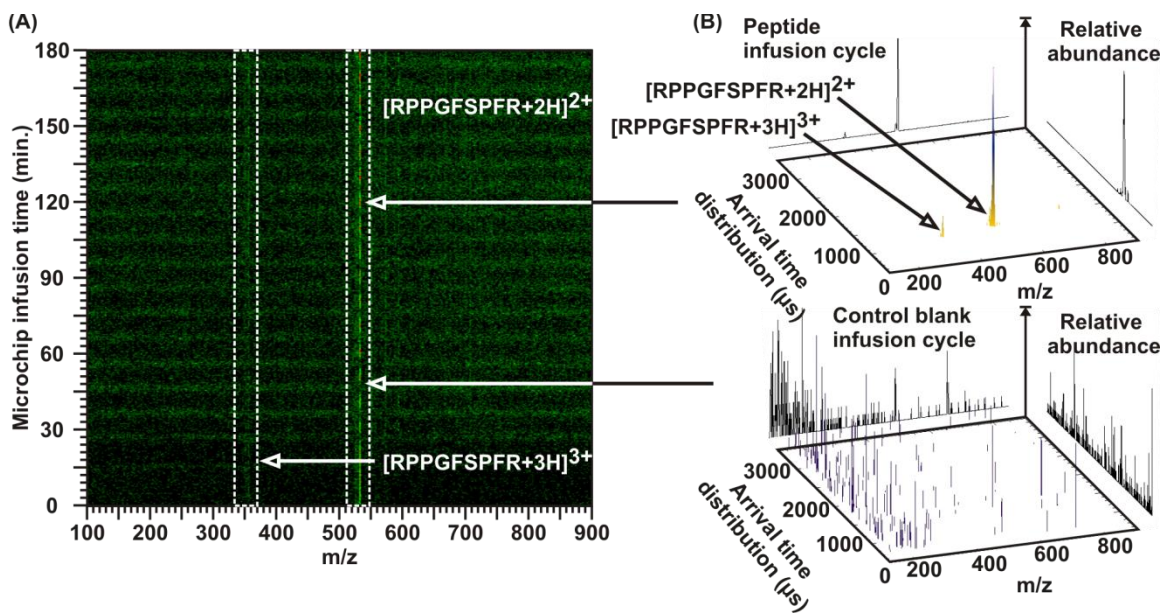


Figure 2.4. (A) Bradykinin standard (at a concentration of 20 $\mu\text{g}/\text{mL}$) and pure methanol were infused into a two-inlet, single-outlet microfluidic trap device. The two solutions were separately flowed through the trap in a consecutive fashion for 5 minutes each. The resulting m/z spectra demonstrated that not only was it possible to detect small amounts of biomolecular material through the trap but also that these materials could be measured with a temporal resolution <5 minutes. (B) 2D spectra during infusion of bradykinin (upper) and methanol alone (lower), plotted with different signal intensity scales. Due to the sharp detected distinction between the two flows, it can also be inferred that longitudinal diffusion between these two solution packets was minimal, providing confidence that secreted cellular material will not be displaced from its original temporal location in the flow stream. Reprinted from reference 312.

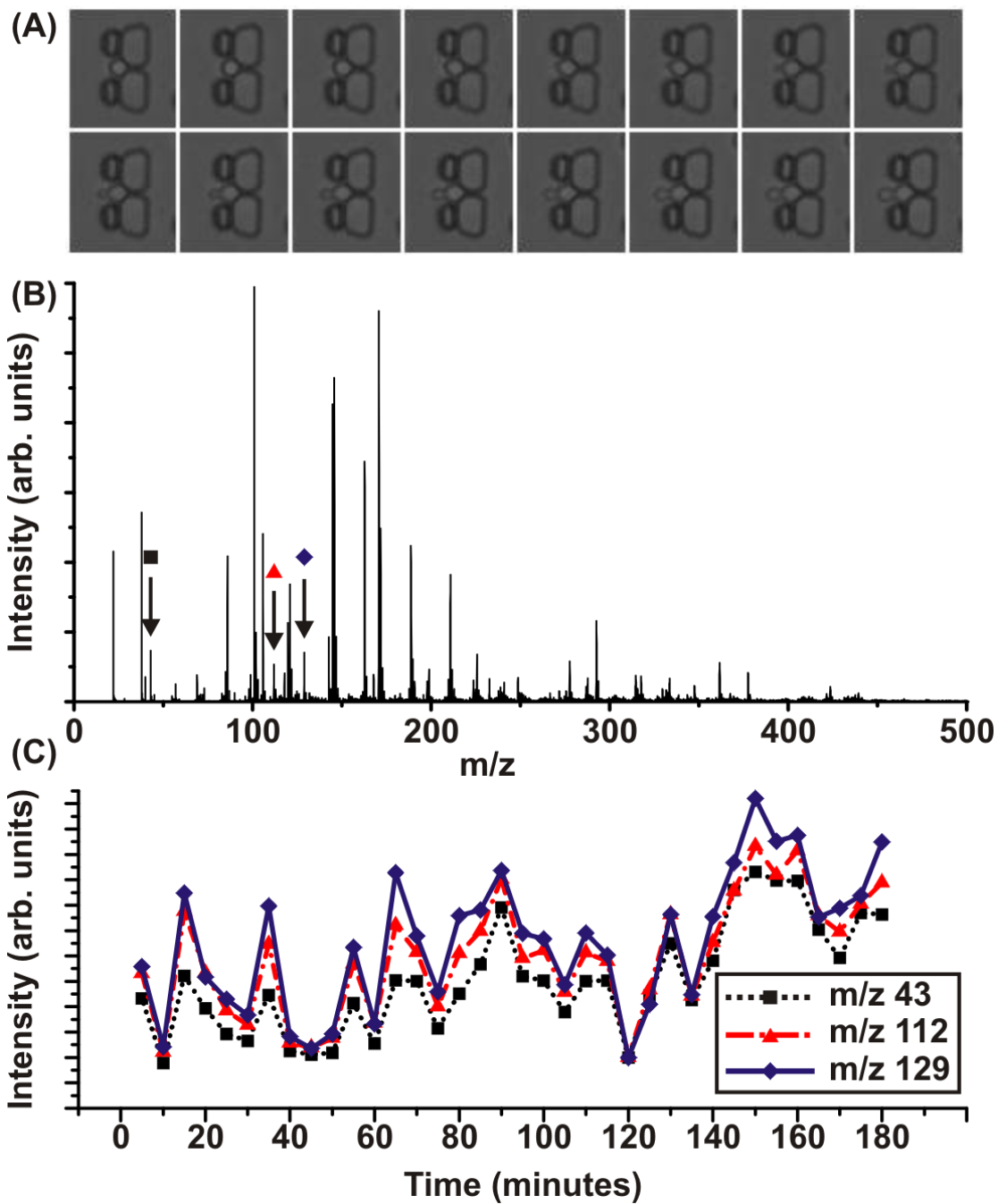


Figure 2.5. (A) Time-lapse images showing yeast that is budding while in an MTNP. (B) A MALDI-MS spectrum collected during the course of the water-induced dormancy state experiment. The samples were collected by spotting the effluent on a MALDI plate in a sequentially different position every 5 minutes. The three peaks marked were selected due to their observed increase in signal intensity over the 180 minute experiment. (C) The time-dependent signal intensities for the three species selected from a series of spectra as in (B), showing a marked increase in all three peaks after 180 minutes with a high degree of temporal correlation. Reprinted from reference 312.

an increase in relative abundance over time as the cells begin to enter their dormancy and also illustrate a highly correlated temporal response.

C. Jurkat cells

Jurkat cells at a density of *ca.* 1×10^6 /mL were loaded into the MTNP (Fig. 2.6) and supplied RPMI 1640 media. The effluent from the trap was flowed over a packed C₁₈ column for *ca.* 2 hours, theoretically saturating the column with cellular secretion material. This column was then rinsed of any contaminant material that was nonspecifically bound (using deionized water with 0.1% acetic acid) and then eluted (using methanol with 0.1% acetic acid) into an Eppendorf tube. The resulting IM-MS spectrum collected from this elution wash is presented in Fig. 2.6 and shows that this method is able to produce an abundance of signals, hundreds to thousands of different species, directly from biological cell trap effluent. When compared to the RPMI medium control (Fig. 2.6) a drastic increase in biomolecular material can easily be observed in the experimental spectrum. These data illustrate the use of reverse-phase chromatography for preconcentrating analytes and purging the effluent of media salts and non-pertinent material. This work demonstrates that in principle this technique should be effective, however, future chapters will demonstrate our efforts to make this system more automated and also to make it possible to perform the load/rinse/elute cycle on the order of a few minutes.

4. Conclusions

Systems biology focuses on a holistic approach to biological research. Intrinsic in this dogma is the need for accurate representations of network dynamics. Only through more rapid sampling can the kinetics and details of biological processes be fully observed and described. This necessitates the need for more improved detection strategies which excel at dynamic,

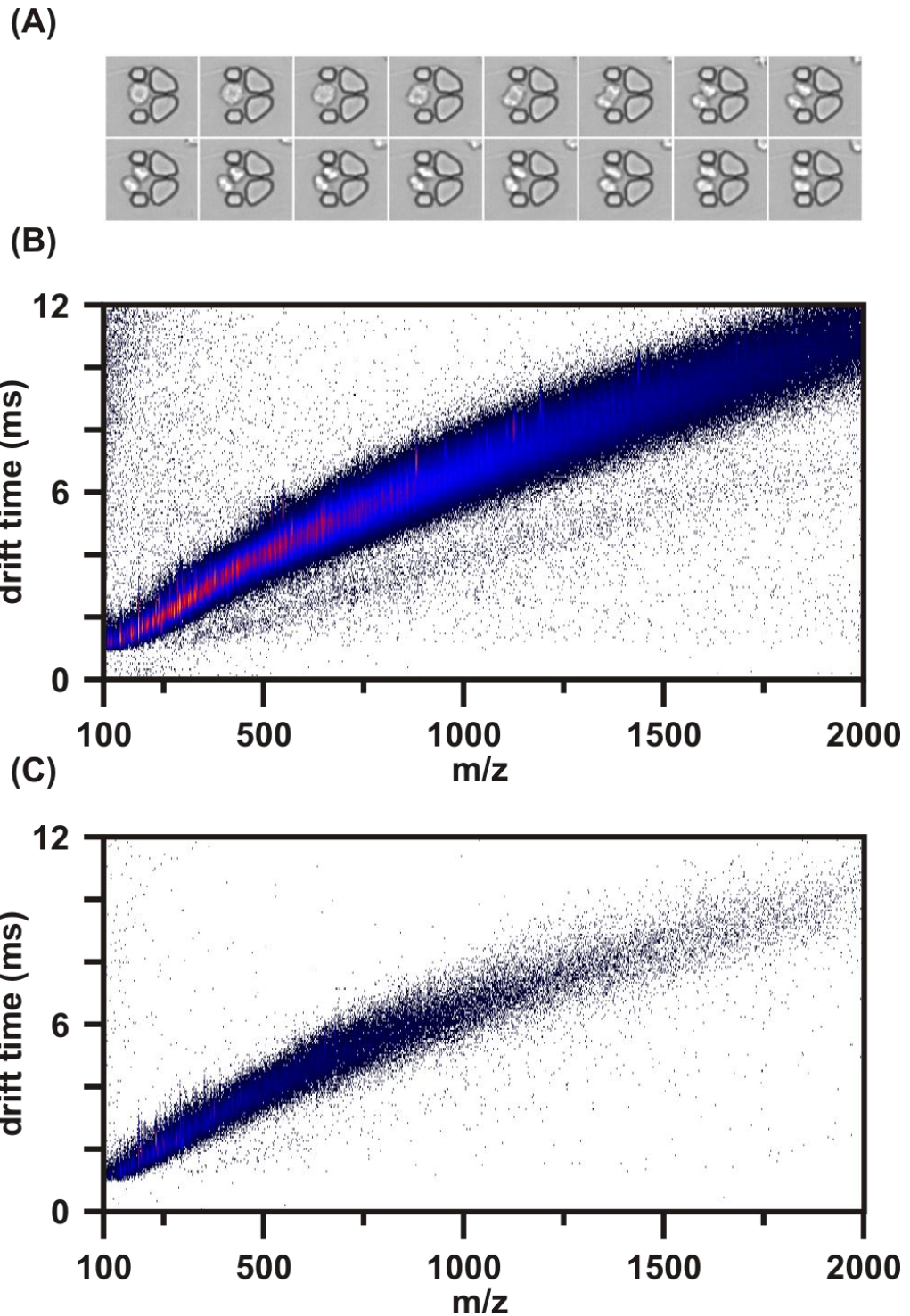


Figure 2.6. (A) Time-lapse images displaying multiplying Jurkat cells in an MTNP. (B) The resultant IM-MS spectrum collected from these cells with a desalting column load time of 2 hours to concentrate secreted material. The column was rinsed with 1 mL of water containing 0.1% acetic acid and then eluted with 50 μ L of methanol containing 0.1% acetic acid. A portion of this 50 μ L was spotted onto a MALDI plate and produced the IM-MS spectrum shown. (C) Control spectrum of medium used in spectrum (B) containing no cellular excretion. This medium was spotted on a MALDI plate under the same matrix conditions as the effluent from (B). Reprinted from reference 312.

broad and accurate measurements.

Advances in systems biology measurements which focus on improved dynamic detection strategies were presented in this chapter. Our preliminary work shows the potential for this system to provide temporally resolved systems biology data directly from complex cellular culture populations. Precise and expedient control of the microenvironment of the MTNP with regards to input concentrations (*i.e.*, stimuli) has been demonstrated (Fig. 2.4) and shows that biomolecular temporal events on the order of 5 minutes are observable with this platform. This accomplishment is critical for future stimulus/response experiments. The broad and temporally accurate detection capabilities of IM-MS have been demonstrated for complex biological samples originating from a sustained yeast cellular culture inside of a microfluidic device (Fig. 2.5). The potential of the combination of microfluidics and IM-MS has been shown by the sheer number of analytes detected from a simple Jurkat cell population (Fig. 2.6). This Jurkat cell data illustrates the abundance of secreted material which is observable with the use of ion mobility-mass spectrometry.

An important aspect of combining cell trapping microfluidics with IM-MS in a temporally accurate manner is the need for online sample preparation strategies. It is essential that these techniques remove suppression-causing contaminants (*e.g.*, salts) while also preserving the temporal dynamics of the continuous microfluidic flow stream. Much of the work presented in the remaining chapters is centered on perfecting this manner of online sample preparation.

Acknowledgements

Financial support for this work was provided by the Vanderbilt University College of Arts and Science, the Vanderbilt Institute for Integrative Biosystems Research and Education, the Vanderbilt Institute of Chemical Biology, the US Defense Threat Reduction Agency (HDTRA-09-1-

0013), the NIH and National Institute on Drug Abuse (1RO1GM092218- 01 and RC2DA028981), the National Academies Keck Futures Initiative, Ionwerks Inc., and Waters Corp. We thank Todd Graham and Anthony Weil for their advice and assistance with the yeast studies, and Hod Lipson and Michael Schmidt for their guidance on machine learning. We also thank Allison Price for her editorial assistance.

CHAPTER III

ONLINE SOLID PHASE EXTRACTION AS A MEANS OF OVERCOMING NON-VOLATILE INORGANIC ION MASS SPECTROMETRY SIGNAL SUPPRESSION

1. The history of charged droplet formation for purposes of analytical chemistry

The interactions of liquid and electricity is a topic that has garnered intense interest since man first harnessed electricity in the 1600s. Studies continued on this subject throughout the 17 and 1800's through the work of Alessandro Volta, Georg Ohm, Michael Faraday, and Friedrich Kohlrausch. In the late 1800's John William Strutt, also known as the third Baron Rayleigh or The Lord Rayleigh was interested, among many other things, in the theoretical basis of electrified water droplets and developed some basic principles that he detailed in some of his earlier works.³¹⁶⁻³¹⁸ One theory Lord Rayleigh established was that a fundamental limit exists to dictate the charge magnitude a droplet of liquid may assimilate before undergoing spontaneous droplet fission. This limit beyond which the surface tension of the liquid can no longer hold out against the force of the Coulombic charge repulsion is now known as the Rayleigh limit. Rayleigh proposed that beyond this limit the liquid would throw out "fine jets" of additional highly charged droplets to regain stability as highlighted in this passage from his 1882 publication:

*"When Q is great, the spherical form is unstable for all values of n below a certain limit, the maximum instability corresponding to a great, but still finite, value of n . Under these circumstances the liquid is thrown out in fine jets, whose fineness, however, has a limit."*³¹⁷

John Zeleny, as documented in two landmark publications in 1914 and 1917, was the first to observe these "jets" (later termed Rayleigh jets) and was able to photographically capture their bizarre behavior under various conditions of potential (Fig. 3.1(a) and (b)).^{319,320} Zeleny's technique of creating Rayleigh jets and ionized droplets from a tube became the basis of what is today known as electrospray ionization (ESI). After 1917, electrospray disappeared from the

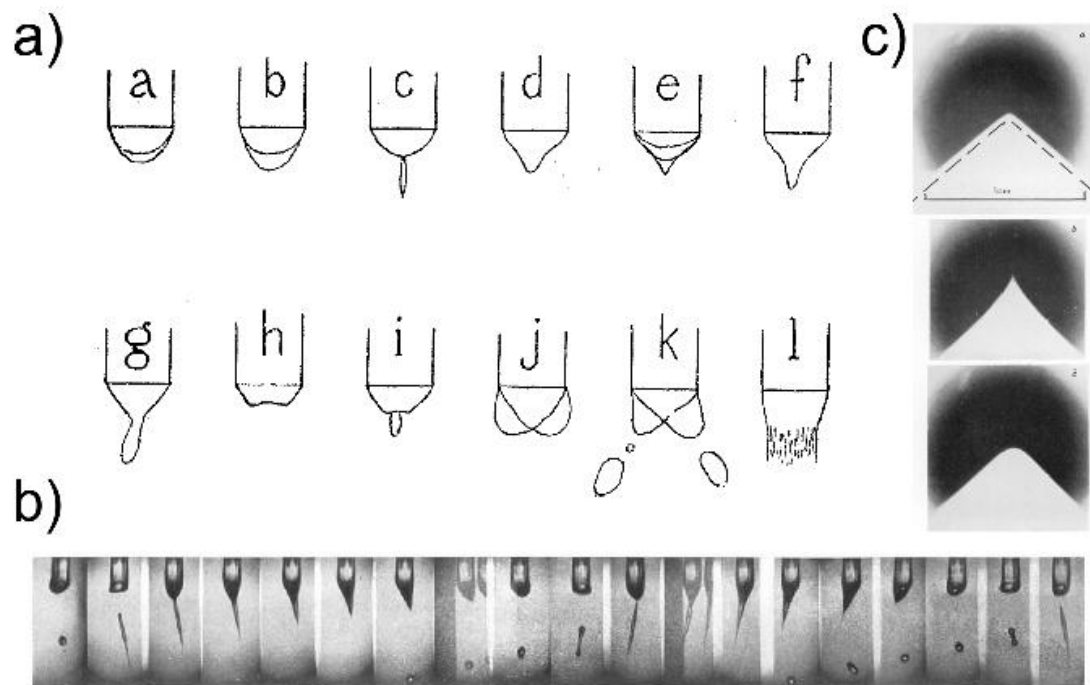


Figure 3.1. Images of the first observations of electrostatic sprays from a tubular sprayer. In 1914, John Zeleny was considered the first to document these sprays with his drawings shown in (a). Then in 1917, Zeleny became the first to photograph this spray as seen in (b). Taylor made a significant leap when he worked out the mathematical formation of this spray in 1964. A few of the images he gathered are shown in (c). From references 319-321.

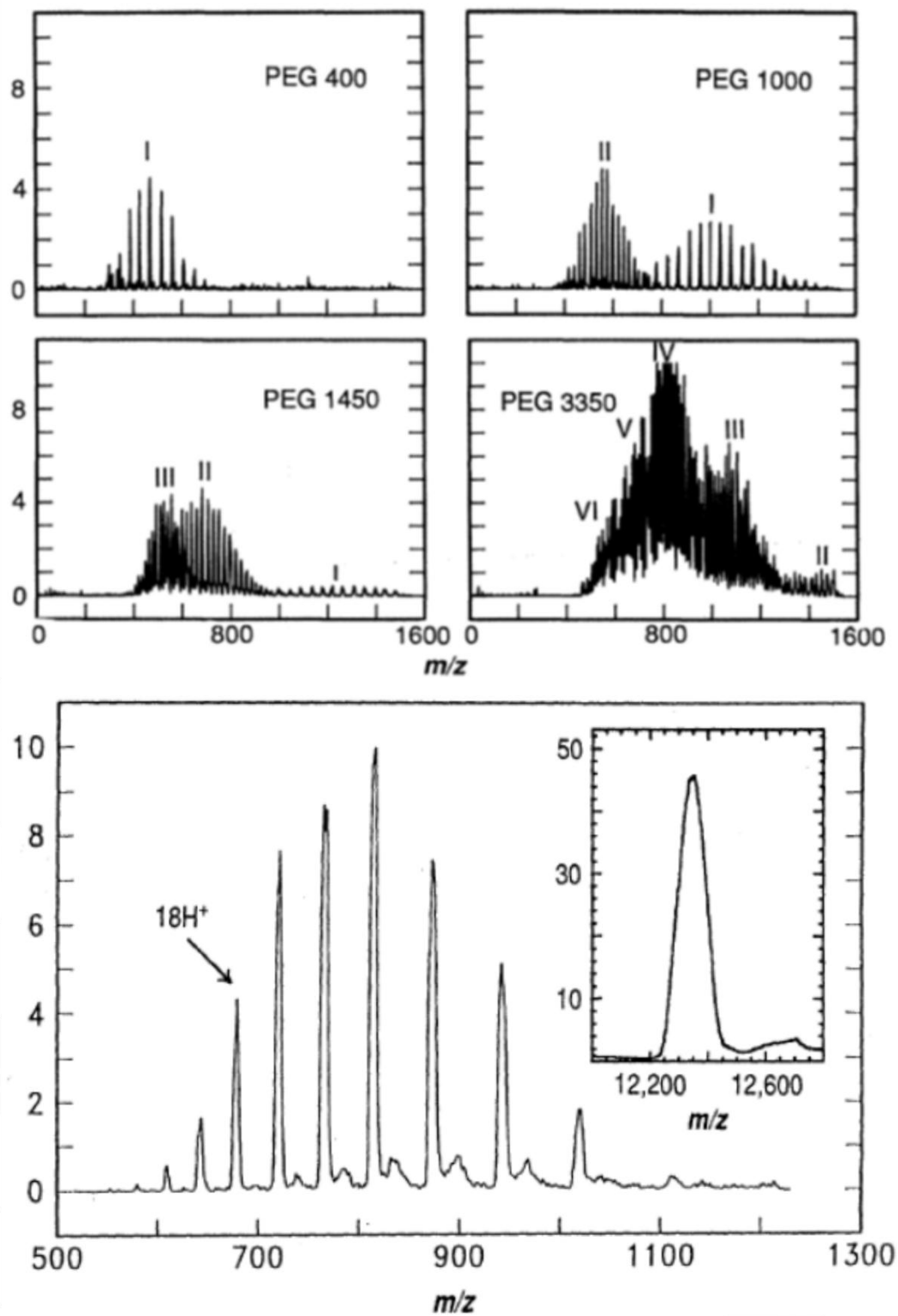


Figure 3.2. Spectra demonstrating the first use of ESI for analyzing high mass molecules. The spectra in the top half show PEG samples with average masses of 400, 1000, 1450, and 3350 Da. The spectrum below is Cytochrome C. The inset shows the result of an algorithm which transforms the multiply charged peaks into a singly charged combined peak. From reference 322.

literature for nearly 45 years until Victor E. Krohn Jr. explored its use as a means of aerospace propulsion in 1961.³²¹

In 1964, in the latter stages of his career, Sir Geoffrey Taylor rekindled his interest in electrical activity in thunderstorms, brushing up his knowledge by reading through Lord Rayleigh's works from over half a century earlier. Expounding upon the above quoted passage from Lord Rayleigh and also on the work of John Zeleny, Taylor developed an experiment to test the instability of these "fine jets" using glycerin and soap film (Fig. 3.1(c)).³²² As Taylor was the first to derive a mathematical model for this jet phenomenon in the context of a conducting spray tip, the geometrical anomaly took on his name: Taylor cone.

Later in the 60s, Malcolm Dole developed the charge residue model (CRM) which states that in charged droplets a sequence of Rayleigh instabilities or Coulomb explosions (with intermittent solvent molecule evaporation) causes smaller and smaller droplets to form until there is just one analyte molecule with a few adducted charge-containing solvent molecules. The last step explains that the "molecule becomes a free gas-phase ion by retaining some of its droplet's charge as the last of its solvent evaporates".³²³ Röllgen and coworkers³²⁴⁻³²⁶ furthered this theory beyond Dole's original experiments, which coincidentally involved special circumstances of ionization due to the polymeric system he was studying.³²⁷ In 1976, meteorologists Iribarne and Thomson proposed a slightly different theory on the formation of these gas-phase ions. Known as the ion evaporation model (IEM), this theory states that after a series of Rayleigh instability-related fissions, the field on the surface of the daughter droplets increases greatly. This highly charge-congested droplet surface is so densely packed that the analyte ion is able to overcome the surface tension of the solvent molecules and evaporate from the surface of the droplet.^{328,329} This opposing or rival view and the various researchers that

were won over on either side have inevitably helped spur the research and investigations further.

John Fenn, using his vast experience of free jet expansion, brought ESI into the modern age by providing “wings for molecular elephants”³³⁰ and solving a large number of mechanistic challenges that prevented the vaporization of large biomolecules on earlier electrospray devices. Fenn and coworkers’ initial success with ESI came when they altered Dole’s original design³²³ to avoid the drastic amounts of re-solvation that Dole was unknowingly causing.^{322,331} Once over this hurdle they showed that ESI could be used to ionize what was at that point-in-time considered the ‘unattainable’: proteins (Fig. 3.2).³²² Importantly, Fenn and coworkers took the stance that IEM was the most likely mechanism of ultimate ion formation in ESI, except when it came to large macromolecules (*i.e.*, large proteins and polymers) at which point they believed the CRM mechanism was most probable.³³² Fenn also expanded on the IEM mechanism by theorizing that a multiply-charged macro ion (which is charge-neutralized due to negative counter ions in solution) can experience Brownian motion within a droplet. In doing this the ion may, on occasion, cause one of its more terminal protonation sites to pick up a charge at the surface of the droplet. Once this happens, the charge may protrude beyond the boundaries of the droplet. This would cause repulsion between the macro ion terminal charge and the droplet surface, thus desorbing the rest of the molecule out of the droplet with it. This theory is still regarded by many as a very likely form of ion generation in ESI.

2. Fundamentals of electrospray formation

With the history and theoretical foundations in place, the utility of electrospray ionization is clear and can be successfully harnessed, though the phenomenon is still not entirely understood. The process begins by preparing a solution consisting of the analyte of interest and

a charge donor dissolved in a “sprayable” solvent. The analyte should be at a concentration appropriate for the detector and instrument being used and so will vary greatly accordingly. The charge donor identity and concentration is dependent on the analyte being investigated. For proteomic and small molecule investigations this charge donor is often a proton donor (*e.g.*, a strong acid) prepared at a 0.1% vol/vol concentration. Consequently, under the right conditions analyte ionization can occur without the aid of a charge donor through encouraged oxidation reactions at the electrospray tubing surface.³³³⁻³³⁵ The solvent in which these compounds are dissolved should be one of a moderate surface tension to allow the proper formation of a Taylor cone spray and a vapor pressure sufficient for reasonable evaporation before entering the instrument. Some common ESI solvents are listed in Table 3.1. Often for biomolecular/organic studies, a 50/50 mixture of water and methanol is used with a small percentage (*i.e.*, 0.1%) of a strong acid.

The prepared electrospray analyte solution is perfused through a metal (*e.g.*, stainless steel) tube of an inner diameter in the range of 100-300 μm at flow rates anywhere from 6 $\mu\text{L}/\text{min}$ to 2 mL/min for traditional ESI. This metal tube is held at a potential in the kV range and is aimed either directly (straight-on) or orthogonally towards the lower-potential instrument orifice. As the solution passes over and through the stainless steel tube, charge separation occurs where the applied charge forces like-charged ions away from the tube. Conversely, oppositely-charged species are drawn in or held more closely. In positive mode for example (where a positive potential is applied to the tube), all solution-phase positively-charged species are pushed through and away from the tip while natively negatively-charged species are drawn close to the charged tube, often inducing oxidation to complete the flow of electrons (as seen in Fig. 3.3(a)). This process of charge separation whereby a high localization of positively-charged species (in the case of positive mode ESI) is formed around the end of the tube facilitates

Table 3.1. Surface tension and vapor pressure values for some common ESI solvents. Values obtained from reference 336.

	All values in air at 20°C ³³⁶	
Solvent	Surface Tension (dyn/cm)	Vapor Pressure (bar)
Water	72.8	0.023
Propanol	23.7	0.024
Methanol	22.6	0.130
Ethanol	22.3	0.058
Isopropanol	21.7	0.044
Acetonitrile	19.1	0.093

protonation (through proton exchange reactions) of organic and biological species with basic functional groups.³³⁷ This charge separation process is also the driving force behind the formation of the Taylor cone. As the localized positively-charged pool of molecules attempts to escape the positive charge of the tube, the solution forms a swell at the center of the tube, somewhat owing to the fact that this singular point is the farthest from the tube these species can travel. As the amount of charge in the tip of this swell increases it comes to a point and a Taylor cone is formed. This cone formation is a combination of many forces, including the relief of charge repulsion between the accumulated ions, the “push” of the electrified tube on the ions of like charge, and the “pull” the solution experiences due to the opposing (or lower potential) charge of the orifice plate. This tip of the cone eventually reaches the Rayleigh limit and the Coulombic repulsion of all these positive charges overcomes the surface tension of the bulk solution which retains it. As the limit is reached, a volume of solution is able to separate from the bulk. Under higher strengths of electric field, this spray can take on many shapes including a varicose wave filament (seen in Fig. 3.3(b)³³⁸) which in fact, was also first theorized by Lord Rayleigh.³³⁹ Aside from a filament this spray can take on many other shapes as well depending on the specific spray parameters (tip voltage, flow rate, etc.), in order to obtain electrostatic stability.³⁴⁰ These pockets of solution that separate from the bulk solution, regardless of shape, initially contain a sufficient volume of solvent to stabilize the number of charges present. However, through the rapid evaporation of the high vapor pressure ESI solvent (table 3.1), the volume/charge ratio again reaches the Rayleigh limit and primary droplet fission occurs. The daughter droplets are expelled out of the original droplet from Rayleigh jets which spray orthogonal to the droplet vector (Fig. 3.3(c)).³⁴¹ This ejection has also been studied intently through experiments on levitated droplets (Fig. 3.3(d)).^{342,343} Studies on this fissioning process have shown that parent droplets have a much higher volume/charge ratio than the

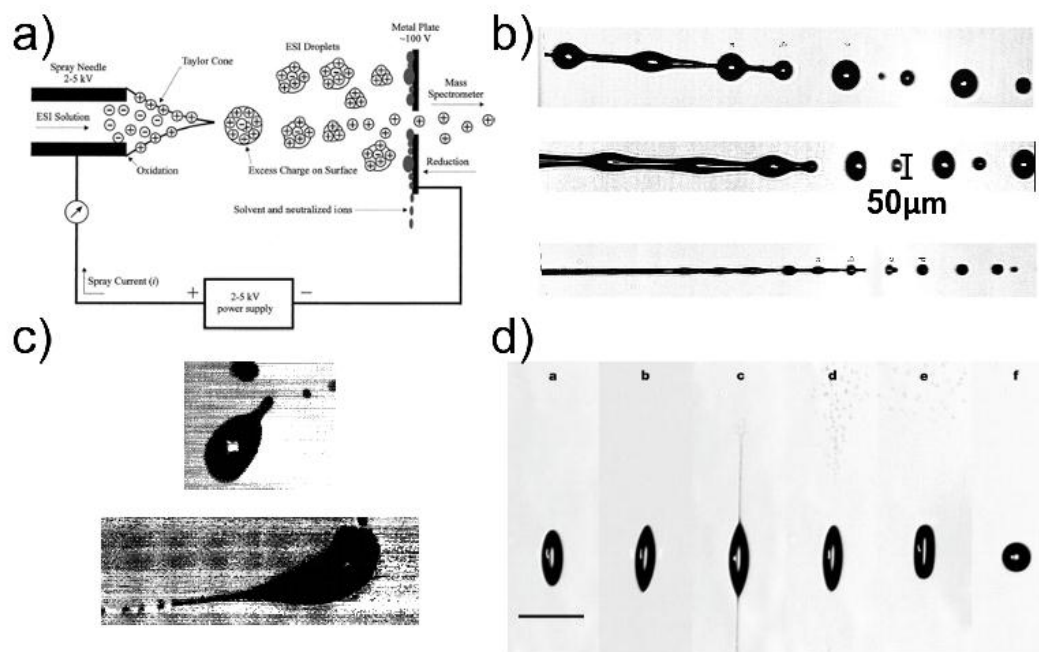


Figure 3.3. (a) Schematic of the electrospray process as depicted in reference 337. (b) A photograph of the varicose properties of the filament formed at the end of the electro spray cone, from reference 338. (c) Photographic observations of Rayleigh jet formation on electro sprayed droplets in mid-flight. Interestingly, droplet fission in this study was observed to always take place orthogonally to the electric field (from reference 341). (d) Photograph of Rayleigh jets formed on a levitating droplet and showing the return to the stable spherical shape in the final image on the right (from reference 342).

expelled daughter droplets^{344,345} (*i.e.*, daughter droplets take proportionally much more of the charge than they do the volume of the parent droplet).

This evidence gives credence to the theory that the predominance of charge resides on the parent droplets' surface and as daughter droplets are expelled they take with them not only most of the surface charge but also those analyte molecules which tend to reside near the surface of the droplet. Convincingly, it has been shown a number of times that the daughter droplets tend to be the major source of analyte ions observed.^{341,345,346} The large parent droplets that are left over after fission contain the remaining charge-paired ions.³⁴⁷ These findings imply that electrospray ion detection favors species which are more surface-active and, in fact, this implication has been demonstrated experimentally.^{348,349}

Beyond the point of initial parent droplet fission, there is a divide amongst researchers regarding the next series of steps. It is argued by Kebarle³⁵⁰ that present critical evidence³⁵¹⁻³⁵³ suggests Iribarne and Thomson's IEM mechanism as the most likely model for electrospray droplet evolution. Conversely, Kebarle also argues that multiply charged globular proteins most likely ionize and vaporize by way of Dole and Röllgen's CRM mechanism because the volume/charge ratio of the unsolvated proteins themselves are approaching the values required for Rayleigh instability.³⁵⁴ This phase in the electrospray process becomes increasingly more difficult to study as the droplets decrease in size and increase in velocity.

It has been mentioned that ionization predominantly occurs in the Taylor cone during charge separation at the end of the electrospray tip and can also occur at the electrospray tip surface through controlled oxidation reactions; however, apart from this some evidence suggests that ionization can also occur as far out as daughter droplet formation and fission. Studies on solution composition have produced environments where solution-phase protonation (such as in the Taylor cone during charge separation) is greatly hampered.³⁵⁵ This is

done by running positive mode ESI in extremely basic conditions such that any spare protons will immediately be consumed by the basic solution. In one such experiment the pH was adjusted to 10 using an ammonium hydroxide (NH_4OH) solution. In this solution one would expect the excess solution-phase cation (NH_4^+) to be the dominant charge-donating specie such that analyte ions would be observed as $[\text{M}+\text{NH}_4^+]^+$. The subsequent observation of a strong $[\text{M}+\text{H}]^+$ peak led to the prediction that NH_4^+ reacts with the analyte to produce ammonia gas (NH_3) and a protonated analyte. This reaction which normally would not occur in the solution-phase alone is bolstered by the complex chemical interactions between the reactants present in different states of matter and the contribution of the solution-phase proton affinity and gas-phase basicity strengths. However, in another experiment the same conditions were carried out by adjusting the pH with sodium hydroxide (NaOH). The persistent presence of the $[\text{M}+\text{H}]^+$ ion in this case has eluded explanation; however, the authors suggest that the onset of a corona discharge may have led to an atmospheric pressure chemical ionization (APCI) mechanism involving the production of H_3O^+ that acts as the main proton donor. Research in this regard is still ongoing and has not yielded definitive answers.

Performing electrospray ionization at nanoliter volume and size scales has yielded what initially appeared to be a very similar source type, dubbed nanoelectrospray ionization (nESI).³⁵⁶ Although nESI is operated under the same general conditions, a few caveats separate it from ESI in some very critical ways. Instead of using a stainless steel capillary with direct potential applied, a fused silica capillary (sometimes coated in gold) is used and charge is often applied by connecting it to a metal union fitting which is electrified. Nanoelectrospray typically operates at between 20-500 nL/min with a spray tip inner diameter of 1-100 μm . Because of these nano size regimes, nanospray produces droplets that are already in the nanometer diameter range. This causes the initial fission to occur much more quickly due to the increased charge/volume ratio.

This is different from standard electrospray in which case an additional fission step must occur in between primary droplet formation and the production of nanometer diameter sized droplets. In addition, it can be said that nanospray discourages droplet fission by spraying droplets that already have on average only one analyte molecule per droplet.³⁵⁷

3. Fundamentals of electrospray suppression

Contaminating sample matrices (*i.e.*, salts and other nonvolatile species) have long been known to have serious suppression effects on the electrospray process and in fact this suppression and its close relation to poor quantitation conditions is considered by many to be the major drawback to ESI. Familiarization with the mechanisms of charged droplet formation and fission is imperative to understanding the causes of this suppression. For this reason, most studies take a fundamental approach to assessing suppression effects. Many findings support the idea that the most likely suppression mechanism involves reduced evaporation efficiency.³⁵⁸⁻

³⁶² The main cause of this reduced evaporation is thought to be several-fold (Figure 3.4):

- (i) The nonvolatile contaminants raise the boiling point of the droplet through alteration of the colligative properties of the solution.
- (ii) Certain nonvolatile contaminants (*e.g.*, detergents) congregate at the surface of the droplet due to their increased surface activity and compete with analyte molecules for these sites. This increase in nonvolatile species at the surface of the droplet increases the surface tension and thereby decreases evaporation of solvent (by way of the CRM mechanism) and analyte (by way of the IEM mechanism) from the droplet.
- (iii) Some contaminants such as salts readily crystallize and, in turn, encourage co-crystallization with analyte molecules thereby locking them in the solid state and negating gas-phase mass spectrometric detection.

- (v) The sphere of hydration for strongly solvated ions (*e.g.*, Na⁺, K⁺, Li⁺) is very large and restricts mobility of not only the solvated ion but also surrounding analyte ions in the droplet bulk solution. This constrained mobility prevents ions that may initially exist in the bulk from migrating to the surface to be evaporated. In addition this large sphere of hydration charge protects the droplet by presenting uncharged solvent molecules on the droplet surface to the surrounding electric field.

Multiple studies on nanoelectrospray have noted its increased tolerance for nonvolatile contaminants.^{356,357} The authors of these studies claim this is a result of the differing mechanisms at play in the nanoelectrospray process compared to conventional electrospray. In electrospray it is argued, the primary droplets produced are electrostatically stable and present in the micrometer diameter range and therefore must undergo considerable solvent evaporation before the first Rayleigh instability is reached. This initial evaporation step is strongly discouraged as the high nonvolatile contaminant concentration causes the above mentioned effects to be heavily exacerbated. If the evaporation is facilitated by adding heat to the desolvation region the evaporation process produces highly concentrated small droplets which increases clustering of the salt molecules and dramatically increases the background noise (Fig. 3.5). Contrarily, in nanoelectrospray the primary droplets formed are already in the nanometer range and therefore undergo their first Rayleigh limited fission almost immediately.

4. A dual-column solid phase extraction strategy for online collection and preparation of continuously flowing effluent streams for mass spectrometry

With the rise of systems biology, biological research has experienced a shift of emphasis over the years from comprehensive measurements of the genome, transcriptome, and proteome to dynamic measurements of the metabolome. Methods such as DNA microarrays

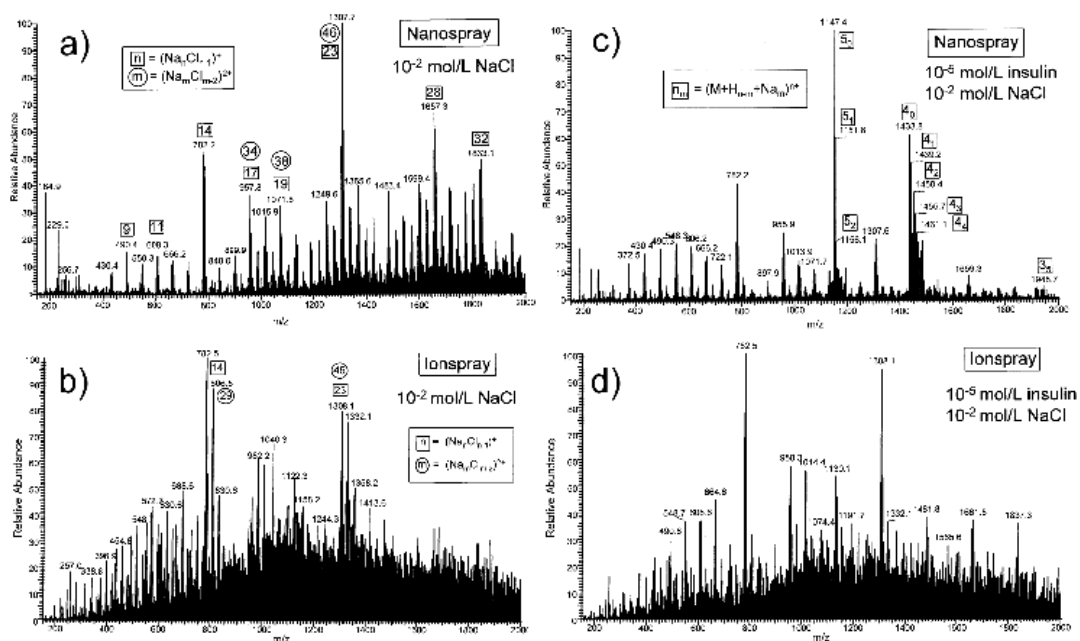


Figure 3.5. Examples of salt clustering and ion suppression (from reference 357). Panels (a) and (b) show nanospray and electrospray (ionspray) spectra of 10mM NaCl. Note the increased background noise in the lower spectrum which the authors attribute to “differently charged larger salt cluster ion species”. Spectra (c) and (d) demonstrate the increased sensitivity of insulin (at 10 μ M) in 10mM NaCl.

and two-hybrid screening, which have been critical for the advances in genomics and proteomics, are less useful for establishing the instantaneous metabolic state of an organism. Instead, techniques more capable of rapid analysis have come to the forefront of biological research due to the highly transient nature of the metabolome. Temporal integrity has become a vital component in these analyses, especially in fields such as cellular dynamics, where sufficiently frequent global metabolomics measurements can provide an understanding of internal metabolism kinetics.³⁶³ A faster sampling frequency and a greater number of detectable analytes allow for a more comprehensive interpretation of the system. Analyses on these timescales and breadth are well suited for the fast, broad detection capabilities of mass spectrometry (MS).

Mass spectrometry, when paired with electrospray ionization, is capable of complex and dynamic liquid sample analysis, making it a unique fit for the measurement of dynamic living systems. However, the application of MS in these areas has been encumbered in the past by the need to prepare all samples to remove the abundant low-volatility inorganic salts essential to life. Salts, or electrolytes, are used by cells as a general means of maintaining a precise osmotic balance and resting transmembrane potentials. In addition, they are required by certain cell types for other functions, such as muscle contraction (*e.g.*, heartbeat), nerve signaling, and blood homeostasis. Electrolytes are found in varying concentrations in extracellular and intracellular fluids, and levels rise and fall through ingestion and perspiration.³⁶⁴ To sustain cell viability in culture, cell culture medium contains these essential salts, typically at concentrations of 100-150 mM.^{365,366} These salts significantly interfere with the processes required to ionize and vaporize the sample prior to mass analysis. The suppression of ion signal in ESI involves charge competition mechanisms during ionization and decreased sensitivity due to a division of ion signal across multiple salt cluster species.^{360,361,367}

There are several techniques available to remove contaminant salts from biological samples in an offline, or quasi-offline fashion, including but not limited to solid phase extraction (SPE), liquid chromatography (LC), and capillary electrophoresis (CE). Collecting samples such as blood, lymph, serum, plasma, or cell culture medium effluent from a dynamic system (*e.g.*, living organism or live cell culture) and preparing the samples offline result in an accumulation of samples and a proportional increase in sample preparation time. Additionally, the collection of fractions in this manner results in averaging of dynamic responses with a temporal resolution proportional to the duration of each fraction collection. In order to properly sample dynamic fluctuations, the frequency with which these samples are collected must be no less than half the frequency of the highest fluctuation required by the Nyquist-Shannon sampling theorem.^{272,273} For example, if a biomolecular secretion is oscillating at a frequency on the order of 0.1 min^{-1} (as may be seen in glucose-stimulated insulin secretion³⁶⁸), each sample fraction collection must contain no more than 5 minutes of secreted material (assuming continuous collection and no sample loss) in order for the oscillation to be observable without aliasing.

Separation techniques such as LC and CE can perform sufficient online salt removal, but often at the cost of losing significant temporal resolution. Numerous online SPE methods exist in the patent and research literature;³⁶⁹⁻³⁸¹ however, these methods can suffer from extensive sample loss, inadequate handling of contaminant streams, and/or poor time resolution. Additionally, many of these online techniques are used exclusively to process fractionated samples, not continuous sample streams. Dynamic measurement requirements necessitate several modifications for such methods to be integrated into a rapid-sampling platform. These modifications require the apparatus to accept a constantly flowing sample stream, whereas most current online preparation methods utilize single or discrete injections for sample introduction (similar to an LC autosampler). Another modification includes a second column to

continue to accept sample eluent while the first column is being prepared for analysis. This minimizes sample waste and therefore loss of valuable information and temporal resolution. A waste cycle needs to be incorporated so that contaminants (salt, etc.) are not directed towards the mass spectrometer, as this could cause fouling and plugging of nano-junctions and orifices, which is of particular relevance to ESI. Lastly, the apparatus would ideally be miniaturized in order to accept and prepare the output flow of various cell culture microfluidics, which could be as low as 50 to 500 nL/min.

With these considerations in mind, we designed and implemented a three-valve, dual-column online SPE apparatus that is able to (i) handle a continuously flowing sample stream (without directing to waste), (ii) direct contaminants to a separate waste port during washing, (iii) analyze flow rates on the order of 500 nL/min or less and, (iv) provide variable preconcentration durations to optimize temporal resolution based on analyte concentrations. In these studies we implemented our online dual-column SPE apparatus in conjunction with a poly(dimethylsiloxane) (PDMS) microfluidic bioreactor as proof-of-concept of this approach. Specifically, we have used a cell trapping microfluidic device known as a Multitrap Nanophysiometer (MTNP).^{281,283,288,312} This device is designed to trap and sustain cultures of adherent and non-adherent cells. We sequentially perfused solutions of varying biomolecular identities through the microfluidic bioreactor to simulate the dynamic online output of a cellular culture for temporally coherent preparation of this continuous bioreactor effluent stream for ESI-MS.

5. Experimental

Desalting Instrumentation. SPE columns are made of 360 μm OD/100 μm ID fused silica tubing and are packed with 3 μm , 300 Å, C₁₈ phase Jupiter Bulk Packing

(Phenomenex, Torrance, CA) using a PIP-500 Pressure Injection System (New Objective, Woburn, MA). Packing was performed at *ca.* 1000 psi, with column length ranging from 10-15 cm. Similar to typical chromatography specifications, these columns are replaced following *ca.* 200 injections, and are noted to retain consistent load and elution characteristics throughout. The Phenomenex Jupiter phase has been found to have an 80% recovery rate with a small molecule, hematin (Fig 3.6). Three 10-port Nanovolume UPLC Valves with 360 μm fittings, C72MH-4690ED (VICI Valco Instruments Co. Inc., Houston, TX), were used to implement the online desalting apparatus. Valve actuation was automated using VCOM software v1.1.01 (VICI Valco Instruments Co. Inc., Houston, TX). The aqueous solvent and both organic solvent lines, running at 500 nL/min, were supplied with an Eksigent Nanoflow Metering System (AB SCIEX, Framingham, MA). Additionally, 360 μm OD/50 μm ID PEEK tubing was used between all junctions and throughout the entire assembly except for the SPE columns.

Sample/Solvent Preparation. RPMI-1640 media (ATCC, Manassas, VA) was mixed with Val⁵-Angiotensin I and Val⁵-Angiotensin II (Sigma-Aldrich, St. Louis, MO) to make 5 $\mu\text{g}/\text{mL}$ standard solutions of each. Aqueous solvent (solvent A) is composed of 95% distilled deionized water (DDW, 18.2 M Ω cm) and 5% Chromasolv methanol (Sigma-Aldrich, St. Louis, MO) with 0.1% formic acid (Fisher Scientific, Pittsburgh, PA). Organic solvent (solvent B) is composed of 95% Chromasolv methanol (Sigma-Aldrich, St. Louis, MO) and 5% DDW with 0.1% formic acid (Fisher Scientific, Pittsburgh, PA).

Microfluidic Bioreactor/Online SPE Apparatus. A MTNP microfluidic device designed to culture mammalian cells was used to simulate the biological microenvironment.^{281,283,288,312} This device was fabricated in-house out of PDMS and silanized with 2-

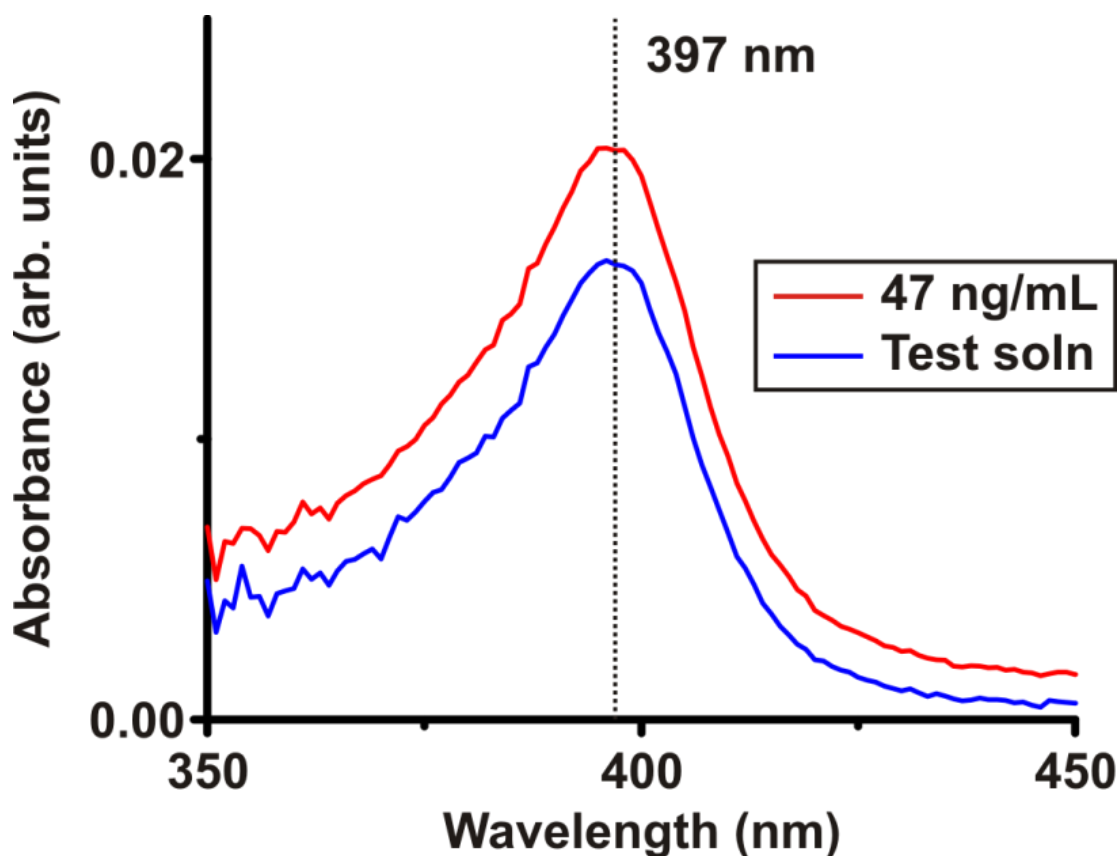


Figure 3.6. Absorbance spectra resulting from the samples measured. For the analysis of the recovery of the SPE columns used in this strategy we have performed UV-Vis absorbance measurements on solutions of hematin. We have dissolved hemin (Sigma Aldrich) in 0.1M NaOH to substitute the chloride moiety for a hydroxyl moiety and thereby produce the water soluble hematin. A Cary 100 Bio UV-Visible spectrophotometer was used to measure the absorbance of a blank, which constituted the elution solvent (i.e., 95% methanol, 5% water, with 0.1% formic acid). Also measured was a 47 ng/mL solution of hematin. This represented a 100% recovery event of a 100 ug/mL hematin solution from a sample loop with a total volume of 0.47 uL (roughly 24cm of 0.002" ID/360 um OD PEEK tubing). Next a sample solution was measured. This sample solution was generated by filling the sample loop (described previously) with a 100 ug/mL solution of hematin (in 0.1M NaOH) and loading this onto a column that was bomb loaded (as in the experimental section of the main article), to a length of 11.4 cm with 3 μ m, 300 Å, C18 phase Jupiter Bulk Packing (Phenomenex, Torrance, CA) using a PIP-500 Pressure Injection System (New Objective, Woburn, MA). Upon collection of the elution solution (which amounted to only about 2 uL), the sample was diluted to 1mL and measured on the UV-Vis. At the peak of the absorbance band (397 nm) the sample (blue) spectrum reached an absorbance level of 80% of the total 100% recovery solution spectrum (red). This corresponded to absorbance values of 0.016 above baseline for the sample (blue) and 0.020 for the 100% recovery solution (red). The red line indicates the spectra for the 100% recovery calibrant hematin solution. The blue is the result of the actual sample that was eluted from the column. The black spectrum was the blank.

[methoxy(polyethyleneoxy)propyl]-trimethoxysilane (Gelest, Morrisville, PA) to minimize analyte adhesion.³⁸² No cells were used in this proof-of-concept study. Online sample effluent from a dynamic biological system was simulated by using a PicoPlus syringe pump (Harvard Apparatus, Holliston, MA) to perfuse media solutions through the PDMS bioreactor.

Mass Spectrometry Analysis. All mass spectrometry analyses were conducted on a Synapt G2 (Waters Corp., Milford, MA) time-of-flight mass spectrometer (TOFMS) with a nano-electrospray ionization (nESI) source. Data were collected in continuous fashion to demonstrate the characteristics of the desalting apparatus.

6. Results and discussion

A detailed examination of prior strategies for continuous flow stream online desalting showed that these techniques did not meet our requirements for dynamic cellular studies. To address these needs we propose the present dual-column solid phase extraction strategy. The following describes (i) the metrics and design criteria for comparing allied desalting techniques, and (ii) the evaluation and validation of the dual-column solid phase extraction strategy.

A. Metrics and design criteria

There are several techniques available to desalt time-course or time-correlated samples for mass spectrometry in an offline or online fashion (Table 3.2). In these types of analyses the general workflow follows the basic scheme and order of (i) sample/fraction collection (*i.e.*, from the organism or bioreactor), (ii) sample preparation (*i.e.*, desalination), and (iii) sample analysis. An important distinction is made here to differentiate offline from online experimental protocols. In this work, offline techniques are defined as those where sample/fraction collection, sample preparation, and sample analysis are performed in separate locations or on

Table 3.2. Typical relative figures of merit for methods commonly used for the removal of salt from biological samples

Desalting techniques	Relative figure of merit				
	Acceptable flow rate	Sample loss ^a	Ability to pre-concentrate ^b	Commercially available	Representative references
<i>Continuous sample treatment (i.e., online)</i>					
Dual-column solid phase extraction	nL/min to mL/min	No	Yes	No	Present studies
Online microdialysis	nL/min to μ L/min	No	No	No	389-391
Single-column solid phase extraction	nL/min to mL/min	Yes	Yes	Yes	372,373,377,379-381
Capillary electrophoresis	nL/min to μ L/min	Yes	Yes	Yes	385-388
Liquid chromatography	μ L/min to mL/min	Yes	Yes	Yes	383,384
<i>Discrete sample treatment (i.e., offline)</i>					
Solid phase extraction	N/A	No	Yes	Yes	392
Microdialysis	N/A	No	No	Yes	393
Capillary electrophoresis	N/A	No	Yes	Yes	394,395

^a Distinguishes the prospect of this technique to direct the incoming flow stream to waste

^b Specifies the capacity of the technique for allowing sample material to accrue in some manner

separate non-connected pieces of equipment. This is often accomplished by storing samples in discrete containers (*e.g.*, well plates or microcuvettes). Online techniques are those where these steps are performed on the same piece of equipment; all parts and processes are fluidly connected in series without human intervention occurring between steps. The techniques listed as “Continuous sample treatment” in Table 3.2 are those which are able to accept a continuous incoming flow stream, purge it of contaminants such as salts, and subsequently direct it to a detector. Online capillary electrophoresis and liquid chromatography are not exclusively used to prepare continuous samples streams; however, in principle they are capable of doing so, and there are examples of this type of implementation in the literature.³⁸³⁻³⁸⁸

The most common offline techniques, such as SPE, dialysis, and CE, are generally straightforward methods to implement using well-established protocols. When used to desalt time-correlated samples offline, these types of techniques require that sequential fractions be collected in order to store and later prepare the samples elsewhere. The time-consuming sample preparation protocols which follow are often countered by collecting fewer fractions or pooling fractions. This, however, leads to lower sampling frequency and increased averaging of analyte levels, and precludes the observation of high-frequency perturbations. Additionally, offline sample preparation often involves multiple transfer steps that may contribute to sample losses.

Online methods of desalting, such as LC,^{383,384} online CE,^{385-388,396-398} and online single-column SPE,³⁶⁹⁻³⁸¹ do not suffer as much from long preparation times since sample collection and sample detection is integrated with the sample preparation. They do, however, encounter challenges related to sample loss and sampling frequency. LC, CE, and SPE utilize one column/capillary to do all sample accumulation, processing, and eluting. This dictates the use of discrete samples, or in the case of a continuous sample stream, that the incoming sample

stream be directed to waste while the single column is being prepared. This sample loss is detrimental to a complete temporal record (*i.e.*, between input and output streams) since the analyte and information inherent to this lost material are unrecoverable. In terms of continuous flow, packed phase column-based techniques (such as LC and SPE) and open capillary column techniques (such as CE) are generally able to accept a wide range of collection flow rates. In these online techniques, analytes must physically stop for a period of time (whether it be on the LC or SPE column or in the CE capillary) in order to carry out the physical separation of salts from analytes of interest. While this does increase averaging of molecular signal and preparation duration, it also provides an opportunity to preconcentrate low abundant signals.

Microdialysis methods as described in the recent literature are a viable option for continuous online sample analyses.^{391,393,399-401} They have the best potential for high temporal integrity because it involves diffusional forces across a concentration gradient in an often constantly flowing solution stream. Ignoring the potential for loss of low molecular weight material through the dialysis membrane itself, online microdialysis does not require the incoming sample stream to be diverted to waste and therefore retains all incoming analyte material. Microdialysis, when paired with MS, may require post-dialysis solvent conditioning for optimal ESI performance and consequently analyte dilution. It should be noted that flow rate and back pressure need to be optimized for fundamentally different processes in both microdialysis and for ESI and that these values may be dissimilar depending on the arrangement that is used. Cell trapping microfluidics, such as the MTNP used in this work, function at flow rates on the order of 500 nL/min with minimal back pressure (conditions required for cell viability).

Dual-column online SPE, such as that presented here, has the potential to provide a method of desalting which provides favorable figures of merit for those outlined. The use of two

columns negates sample loss by accepting the continuous sample stream on one column while the other column is being purged and eluted. The preparation time, while not as expedient as online microdialysis, is variable and can, in principle, achieve temporal resolution depending only on the number of columns utilized and the duration necessary to wash out salts given the particular column characteristics. The non-instantaneous nature of the preparation also provides the opportunity to preconcentrate the sample should it be necessary for the detection of low abundance analytes. Additionally, similar to most column-based methods, it is better suited for low collection/sample flow rates.

B. Method validation.

The valve arrangement presented here (Fig. 3.7(a), (b)) uses a six-step cycle (Fig. 3.7(c)) which provides a constant loading condition, ensuring that all analyte material in the online sample effluent will be collected if desired. In addition, contaminants are rinsed from the SPE columns during a purge step which is directed to waste. Valve cycle steps can be scaled in time uniformly to yield a cycle which is better for detecting high frequency oscillations (short step durations) or one which is better for detecting very low abundance analytes (long step durations). Figure 3.7(c) outlines the valve switching scheme for online sample preparation. In step 1, the valve orientation is as pictured in Figure 3.7(a), such that SPE column A is loaded with online sample effluent and SPE column B is desalting a sample plug and sending salts to waste. Valve 3 is switched such that SPE column A is receiving sample effluent and SPE column B is eluted and directed towards the MS for ion detection. Because this is the first cycle, column B has not actually been loaded with any analytical material at this time and so this elution is blank (as observed later). After this, valve 3 is switched so that SPE column B is equilibrated with aqueous solvent in preparation for its subsequent loading step. SPE column A continues to load

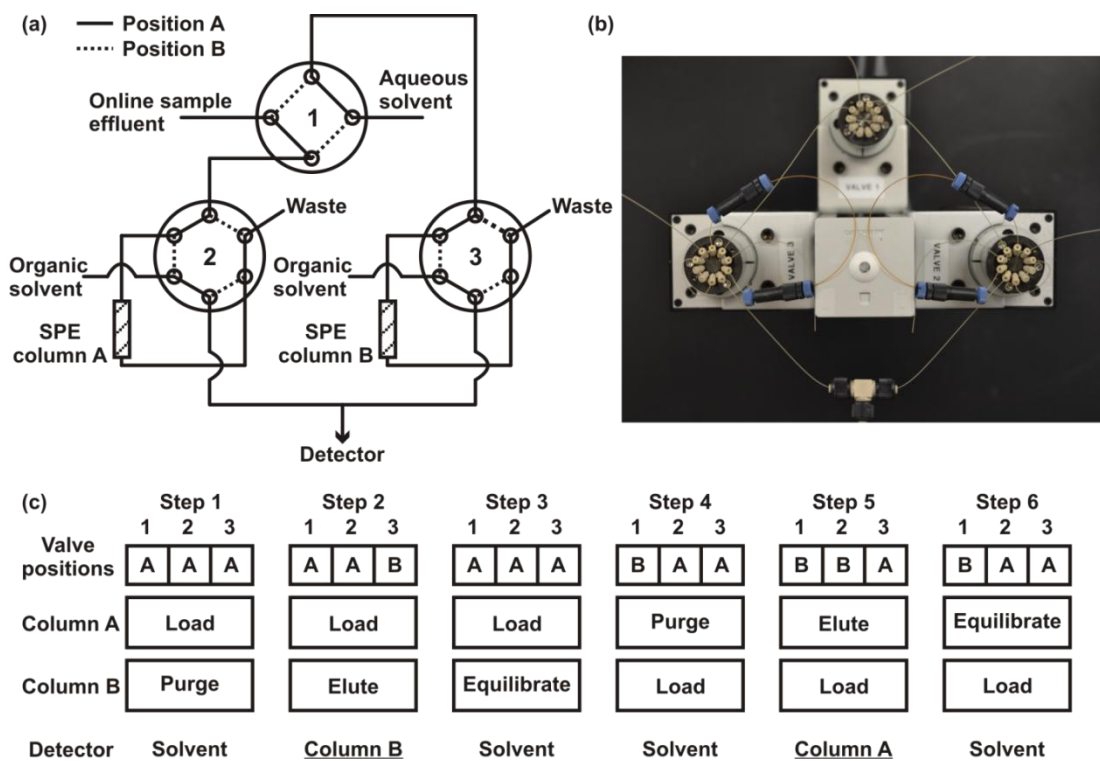


Figure 3.7. (a) The three-valve arrangement used in the online SPE experiments. All three valves were individually actuated by coordinated, automatic computer control. The legend indicates the valve orientation notation. (a) Simplified diagram showing 4- and 6-port valves. (b) Implementation of (a) using 10-port valves with unused ports being capped. (c) A chart showing the sequence of states for valves (listed in numerical order), SPE column A, SPE column B, and the detector (MS) through the six-step cycle.

sample throughout the equilibration of SPE column B. Next, valve 1 is switched such that the online sample effluent is directed to the newly equilibrated SPE column B. SPE column A is purged with water at this step, allowing for desalination of the sample collected on the column. Valve 2 is switched and SPE column A is eluted with organic solvent, while SPE column B is left in the loading position. Lastly, valve 2 is switched to equilibrate SPE column A and the SPE apparatus starts the entire cycle again. Note that the MS is analyzing a sample for only two of the six steps. Were Fig. 3.7 implemented in triplicate, it would be possible for six samples to be interleaved without sample loss or overlap, enabling analysis, for example, of three parallel bioreactors that could provide one control and two different experimental conditions near simultaneously.

Various standards were perfused through a MTNP microfluidic bioreactor and onto the dual-column online SPE apparatus to validate temporal response and reproducibility (Fig. 3.8(a)). Figures 3.8(b) and 3.8(c) depict the valve timing and resulting total ion chromatogram (TIC), respectively, for the online SPE apparatus. The valve cycle produces a pattern of two alternating sets of peaks (*i.e.*, every other peak originates from the same column). When the time-step durations are set equally, this yields a single time period of elution followed by two time periods of clean solvent, hence the rise and fall shape of the chromatogram. Importantly, the length of these time steps can be adjusted to shorter durations to emphasize temporal dynamics or longer durations to extend preconcentration steps and thereby aid in identifying lower abundance signals. In Figures 3.8 and 3.9 the time steps were set to one minute, yielding three minutes of load time, and one minute each for purging, eluting, and equilibrating. Using this timing scheme the limit of detection for a model metabolite (hematin) was observed to be 50 ng/mL or *ca.* 75 pg (118 fmol) of total material (see Table 3.3 for details).

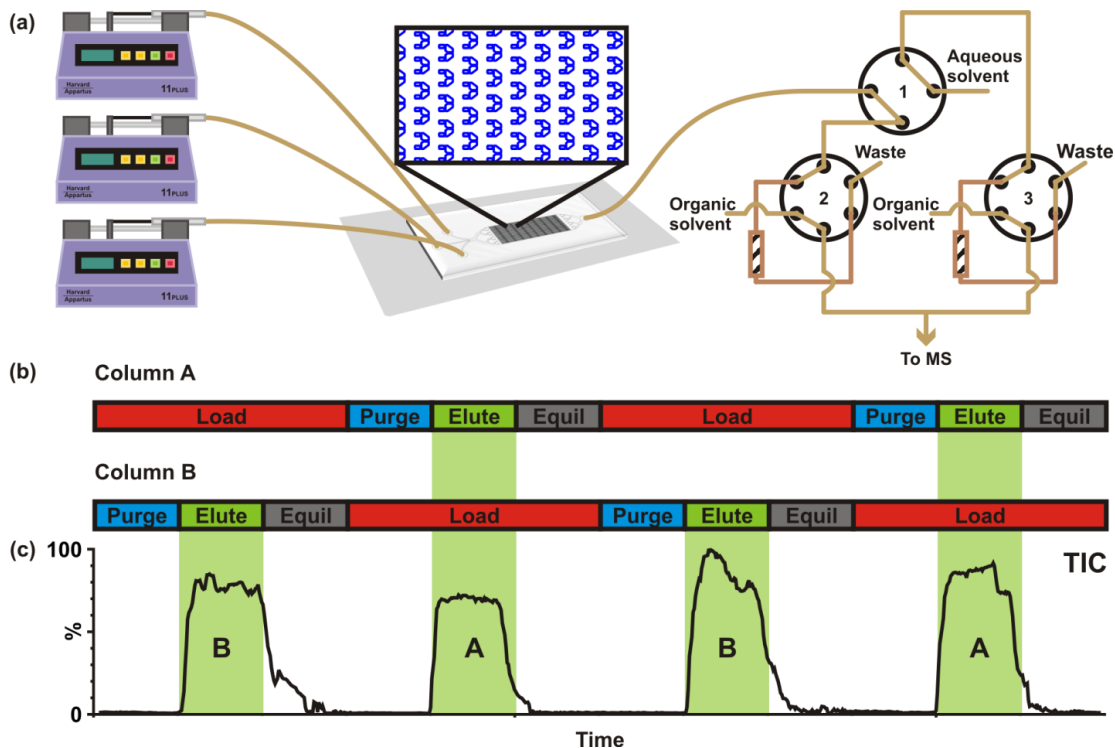


Figure 3.8. Experimental scheme with valve timing and sample elution for the online apparatus. (a) Scheme depicting how the various sample solutions were perfused through a MTNP microfluidic device and then into the desalting apparatus. This arrangement was chosen to simulate a dynamically varying continuous sample stream originating from a live cell bioreactor. (b) Chart illustrating the valve cycle. Importantly, the chart shows that the loading step is continuous and occurs on one column while the other column is purged of contaminants, eluted to remove analyte material, and then equilibrated to prepare for the next loading cycle. (c) An example total ion chromatogram (TIC) showing the typical peak and trough pattern produced from the cycle shown in (a). The peaks are labeled based on the column from which the analytes are eluted.

Table 3.3. Quantitative data demonstrating the limits of detection for the dual-column online solid phase extraction desalter. The previously mentioned procedure (Fig. 3.6/Experimental section) was used to produce hematin standards at concentrations of 1000, 500, 100, 50, and 10 ng/mL. These hematin standards were run through the desalter setup (presented in figure 2) to evaluate the system's limit of detection. The overall integrated peak areas for the resulting chromatograms are presented in Table S1. Interestingly, since these solutions were made in 0.1 M NaOH, these samples also contained an unusually high amount of salt (4 g/L). These samples were not preprocessed in any way prior to running through the online SPE desalter.

Hematin (in 0.1M NaOH)

Concentration (ng/mL)	Molarity (nM)	Total material (pg) [†]	Total moles (fmol)	Integrated area [*]
1000	1578.38	1500	2367.57	3.23E+04
500	789.19	750	1183.79	2.21E+03
100	157.84	150	236.76	914
50	78.92	75	118.38	273
10	15.78	15	23.68	0

[†] With a load time of 3 min at 500 nL/min

^{*} Using a MassLynx peak to peak amplitude of 200

In order to simulate dynamic cellular output, three syringe pumps were connected to the inlets of an MTNP microfluidic bioreactor device (Fig. 3.8(a)). The first pump delivered a solution containing 5 $\mu\text{g}/\text{mL}$ of Val⁵-Angiotensin I (Standard #1) in RPMI 1640 medium through the device and into the desalting apparatus for 15 minutes, followed by delivery by the second pump of RPMI 1640 medium (without any additives) for 15 minutes, and then the third pump delivered 5 $\mu\text{g}/\text{mL}$ of Val⁵-Angiotensin II (Standard #2) in RPMI 1640 medium for an additional 30 minutes. After this, RPMI 1640 medium was flowed for 30 minutes using the second pump, followed by clean deionized water for 80 minutes using the first pump, which originally delivered Angiotensin I (sequence shown in Fig. 3.9(a)).

In Figure 3.9(b), the data show a total ion count increase for 30 minutes, at which point the ion signal reaches a steady state, and then decreases after the deionized water has been flowing for *ca.* 30 minutes. The TIC peaks displayed in Fig. 4b were integrated to determine the repeatability of these elution cycles. Importantly, only the peaks occurring from minute 27 to minute 120 were used, as this was considered the time over which the signal was in equilibrium. The peak areas were found to have a percent relative standard deviation of *ca.* 15% throughout these experiments. Note that intracolumn (only for column A or B) reproducibility and intercolumn (for both column A and B) reproducibility are 14.6 % ($n = 16, m = 2$) and 15.0 % ($n = 32$), respectively. Figure 3.9(c) shows the extracted ion chromatogram for Val⁵-Angiotensin I, m/z 642.40. These data show that although Val⁵-Angiotensin I was perfused at minute 0, it was not detected until the second cycle (minute 6), owing to the inherent blank first cycle (discussed above). Additionally, the signal for Val⁵-Angiotensin I was not greatly reduced until minute 25 and residual traces of m/z 642.40 were observed throughout the experiment. This hysteresis is typical when using C₁₈ phase SPE columns and can be mitigated by using more rigorous column conditioning methodologies.⁴⁰² Figure 3.9(d) shows an extracted ion chromatogram (XIC) for

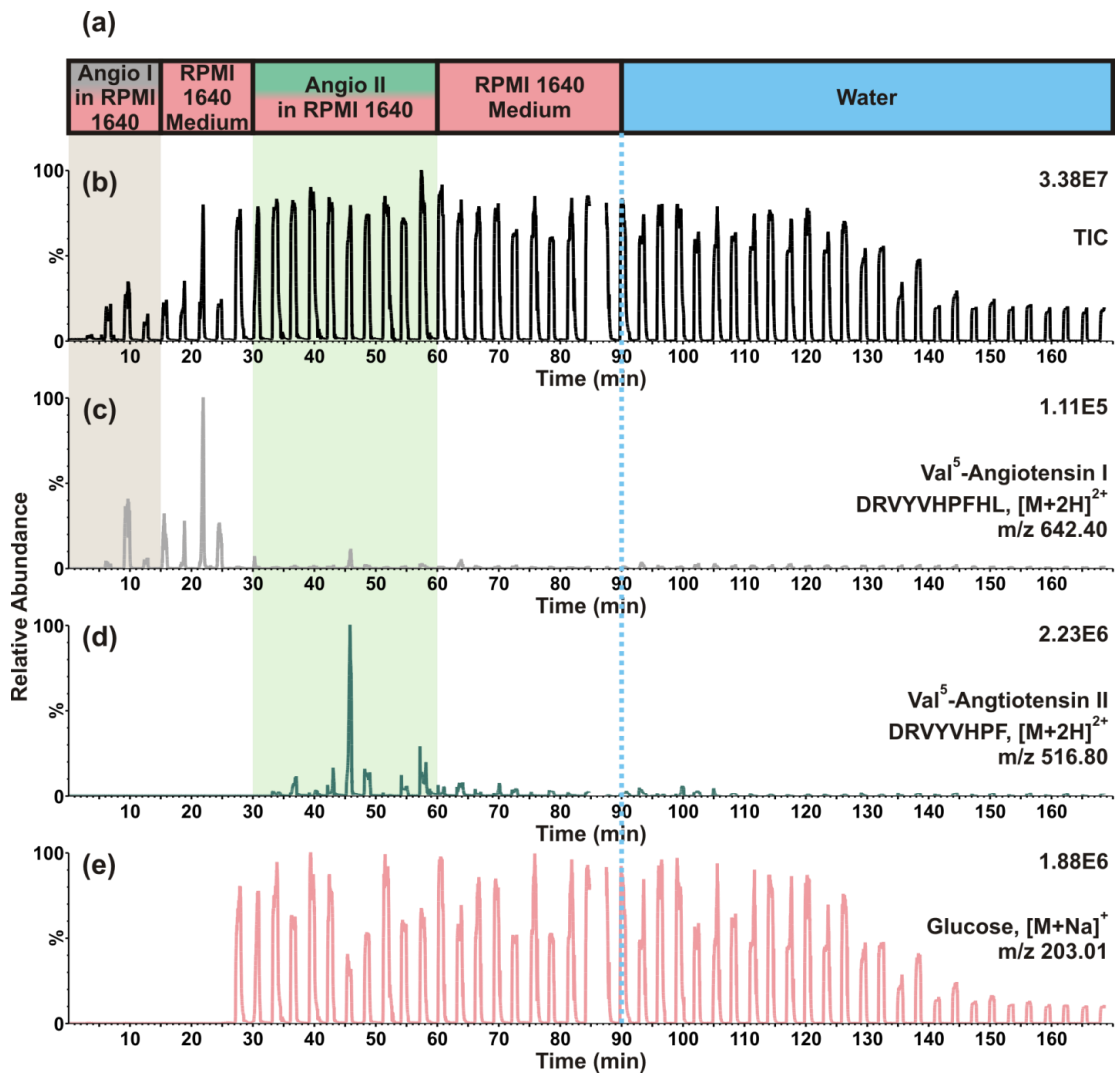


Figure 3.9. A variable analyte concentration experiment, showing perfusion of different analytes (in RPMI 1640 medium) and H₂O through the MTNP, to characterize the online SPE desalting apparatus. (a) A chart showing the progression of solutions through the apparatus over the course of a 170-minute experiment. (b) The TIC for the experiment. (c-e) Extracted ion chromatograms for (c) Standard #1, Val⁵-Angiotensin I, m/z 642.40, (d) Standard #2, Val⁵-Angiotensin II, m/z 516.80, and (e) the [M+Na]⁺ ion of glucose, m/z 203.01, in the RPMI common to the first four analytes. The asterisk (*) corresponds to a break in the data between minutes 86 and 88, which was the result of the data file reaching its maximum length and the initialization of a second file. The two files were combined based on their accurate time tags

Val5-Angiotensin II, m/z 516.80. Similar to Val5-Angiotensin I, the signal for Val5-Angiotensin II appears at the second cycle and some hysteresis is observed. In Figure 3.9(e), the XIC for glucose ($[M+Na]^+$, m/z 203.01) is shown. Glucose was a unique identifier of cellular media in these experiments (*i.e.*, only present in the RPMI 1640 media). RPMI 1640 medium was present from 0-90 minutes in this time course; however, the ion signal for glucose was not detected until minute 27. These results suggest changes in column affinity as other cellular material began to bind and interact with the column. Glucose was also susceptible to hysteresis, as evidenced by the lingering signal even 60 minutes after RPMI 1640 medium was discontinued. Alternatively, the hysteresis effect could be related to carbohydrate affinity for silica surfaces (*e.g.*, C_{18} phase bead surface). Increasing the time-step duration (and thereby decreasing the resolution) allows one to better observe lower abundance analytes and mitigates the observed hysteresis. Decreased hysteresis is accomplished due to a longer elution step, which ensures that more material is removed from the SPE column every cycle. To further assess the repeatability of these elutions, the peaks resulting from glucose specifically (from minutes 27-120), were integrated and found to have percent relative standard deviations of *ca.* 20% for both intracolumn and intercolumn precision. Regardless, this apparatus exhibits satisfactory desalting capabilities, as shown in Figure 3.10. In the absence of any form of desalting, a stable electrospray was not able to be generated and therefore no ions were observed. With the use of the dual-column SPE apparatus, an abundant analyte signal was observed for both model peptides.

This apparatus demonstrates the capability to successfully analyze and ionize small peptide analytes within a continuous salt-rich sample stream using dual-column online SPE desalting techniques (Fig. 3.9). This capability is required when performing analyses on lab-on-a-chip/microfluidic bioreactor devices or other bioreactors where analyses need to be performed

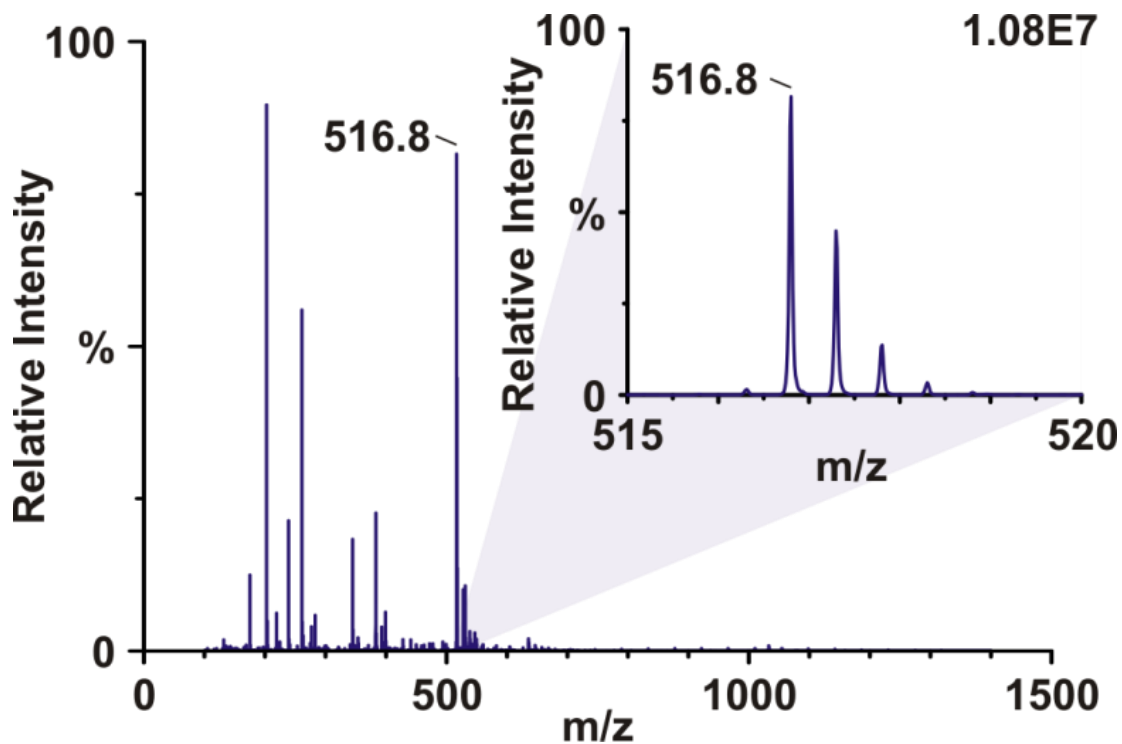


Figure 3.10. Demonstration of desalting capabilities of the dual-column SPE apparatus when used to assess an online dynamically fluctuating flow stream. (a) Combined mass spectrum from minute 45 to 48 showing the peptide DRVYVHPF from desalted cell culture medium. (b) Inset of the mass spectrum for the region immediately surrounding the peptide DRVYVHPF (standard #2, Val⁵-Angiotensin II), at m/z 516. In a companion experiment without desalting, a stable spray could not be produced for this sample without first desalting it, thus no ions were observed and no spectrum was generated

online in a temporal fashion and with small sample amounts. Measurements on this timescale were previously time-consuming due to the offline nature of most preparation work-flows. By keeping the sample online and preparing sample material using two SPE columns in parallel, sample loss is negated and sample preparation time is drastically reduced. Thus more frequent measurements and comprehensive data can be used to interpret biological systems.

For a representative experiment to demonstrate the applicability of this strategy to collect data from a biological system, we have presented here, spectra collected from a microfluidically-cultured population of insulinoma (Rin-m5f) cells. Upon exposure of the cells to glucose a number of signals were detected³. Among these was the clear presence of a protein of similar mass to ubiquitin (Fig. 3.11(c), (d)). This protein has been observed in similar traditionally-cultured offline studies of this nature.¹ Concurrent with these desalting/mass spectrometry analyses we also performed fluorescence analysis on these cells (Fig. 3.11(a), (b)). Fluo-4 fluorescent calcium indicator dye used was used in conjunction with a Nikon Eclipse Ti inverted fluorescence microscope for visualization. This data demonstrates the potential for this strategy to be used for analysis of biological systems and also in conjunction with other analytical techniques to aid in systems-level studies.

7. Conclusions

We have described a strategy with a demonstrated ability to perform temporally resolved online desalination of a continuous sample stream at a resolution of three minutes with minimal loss of analyte and a lower limit of detection in the fmol to pmol range for small molecules. Under these conditions recoveries of *ca.* 80% are obtained even at fmol loadings. These experiments show that highly dynamic analyte fluctuations can be observed and non-volatile contaminants can be removed prior to downstream ESI-MS. Continuous online

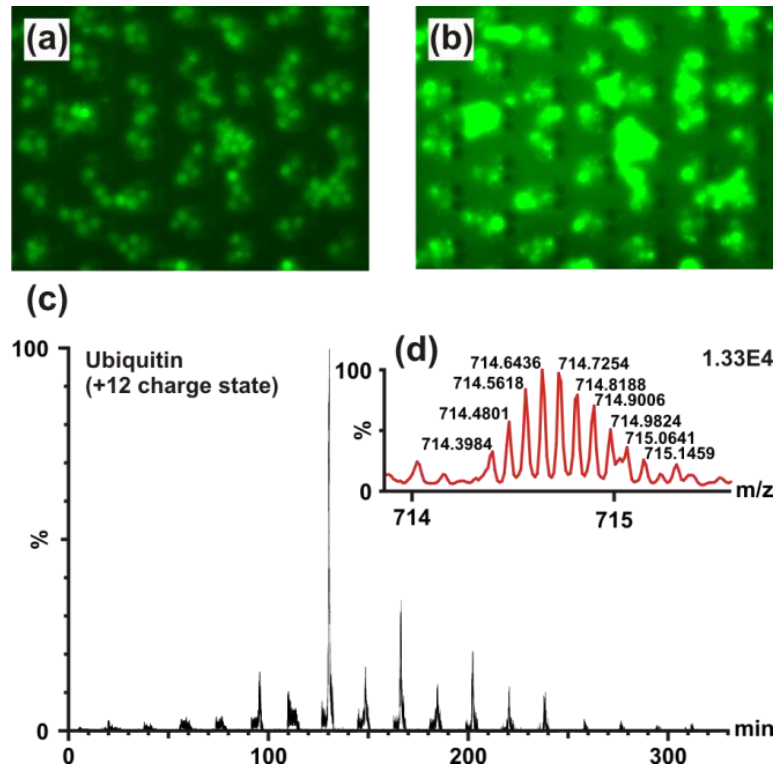


Figure 3.11. Data from a microfluidically-cultured population of insulinoma (Rin-m5f) cells. (a) Fluorescence microscopy showing baseline calcium secretion. (b) Calcium secretion upon exposure to glucose. (c) The extracted ion chromatogram (XIC) for the 12+ charge state of ubiquitin (the highest intensity isotopic peak, m/z 714.64, was chosen for visualization of the XIC). (d) The resulting mass spectrum of ubiquitin.

desalination provides a decrease in sample preparation time compared to fractionation (on the order of 10-30 minutes per sample). Importantly, we demonstrated the ability to observe analyte concentration changes in less than five minutes. This feature could prove useful for metabolic flux analyses and metabolic control analyses. This apparatus can also be used to prepare fractionated samples; however, the most beneficial application will be the study of the dynamic metabolic output of living systems or organisms.

Acknowledgements

Financial support for this work was provided by the NIH (R01GM092218 and RC2DA028981), the US Defense Threat Reduction Agency (HDTRA-09-1-0013), the Vanderbilt University College of Arts and Sciences, the Vanderbilt Institute of Chemical Biology, and the Vanderbilt Institute for Integrative Biosystems Research and Education. We thank Allison Price for her editorial assistance.

CHAPTER IV

REAL-TIME CELLULAR EXOMETABOLOME ANALYSIS WITH A MICROFLUIDIC-MASS SPECTROMETRY PLATFORM

1. Introduction

Cellular response is a complex phenomenon that manifests both physically and chemically. While physical responses can most often be analyzed visually, chemical responses are difficult to characterize even with modern detection methods. Adding to the difficulty is the influence of timing when dealing with cellular response. When responding to a biochemically altering stimulus, such as naïve T cell response to an antigen presented by a dendritic cell, a cell undergoes a series of biochemical pathway shifts that allow it to adapt to its new conditioned state. The cell's temporal response, therefore, provides insight into the interspersed pathway shifts that occur throughout the various stages of stimulus exposure. Temporal response is especially relevant to toxicology, where, despite experiencing a toxin and undergoing numerous metabolic shifts, an organism may not show observable external symptoms until much later, when effective treatments are no longer as useful.

Nonetheless, time remains a largely underappreciated or neglected variable in most comprehensive cellular response experiments, not as much for its perceived lack of value as for its difficulty of precise temporal resolution and control of measurements. Biological measurements typically take one of two forms; either they sample a small number of targets very frequently (*e.g.*, immunoassay or fluorescence measurements) or they sample a plethora of targets over a broad time span (*e.g.*, proteomic workup). The limitations of current methodological strategies and detection technologies stymie the combination of these two approaches. The most comprehensive analysis would track as many analytes as possible and sample these analytes as frequently as possible to capture the truly dynamic properties of

metabolic responses. As the frequency of sample collection is increased, previously unidentified patterns in signal response may begin to emerge, according to the Shannon-Nyquist theorem, which states that in order to properly characterize a pattern containing a frequency of Y , the sampling must occur at an interval greater than $1/(2Y)$.^{272,273} Also, increasing the sampling frequency may reduce the possibility of aliasing, wherein rapidly varying phenomena are undersampled in violation of the Shannon/Nyquist theorem to produce misleading results.

With the approach in place, a major logistical problem still remains: how does one sample a biological system multiple times over the course of an experiment without destroying, or even perturbing, that system? The exometabolome, or suite of biomolecules that are secreted or excreted from a cell into the surrounding matrix, represents a promising target. The exometabolome has been demonstrated as a viable indicator of internal cellular processes and can be easily assessed without any disturbance of the system from which it originates.^{278,404} Changes in exometabolomic species transport provide information on the current state of the cell population, which can lead to a more thorough understanding of the particular cell's biology and to the ability to control the cell's behavior.

The cell is constantly surveilling the surrounding environment. Perceived changes in this microenvironment lead to alterations of intracellular and intercellular signaling, which in turn lead to shifts in gene regulation and modifications in protein and metabolite production. Depending on the signal received, the intracellular processes enacted may lead to the secretion of another signaling factor to extend the complex web of communication. These signaling factors are produced by a given cell for communication with 1) nearby cells of the same type (autocrine signaling), 2) adjacent cells (juxtacrine signaling), 3) nearby cells of a different type (paracrine signaling), and 4) distant cells (endocrine signaling). The exometabolome not only

includes traditional signaling molecules, but also enzymatically produced metabolites of xenobiotics (*i.e.*, drugs, toxins) introduced to cells.

The Vanderbilt Institute for Integrative Biosystems Research and Education (VIIBRE) Multitrap Nanophysiometer (MTNP) is a poly(dimethylsiloxane) (PDMS) microfluidic device that functions as a miniature bioreactor. In contrast to traditional cell biology techniques that often require cellular populations on the order of $>10^8$, the MTNP allows for studies on small populations of cells or simple organisms ($<10^5$). The MTNP has been used for long-term optical measurements of the dynamic behavior of cells, including fluorescent labeling of cells to determine type and activation state and detect signaling dynamics.^{281,283,284} This device provides a framework on which to study numerous cells, *i.e.*, T cells, beta cells, and breast cancer cells, as it traps both non-adherent and adherent cells with structural barriers instead of with chemical surface modification that may cause cells to be exposed to higher shear stresses resulting from direct contact with fluid flow. The MTNP is well suited to detect secreted molecules in cellular effluent, and it is also unique in its ability to provide a system for investigating the dynamic response of a cell population to a stimulus. The constant perfusion design of the microfluidic bioreactor gives rise to a platform component capable of real-time alteration and control of the cellular microenvironment, in addition to providing an opportunity for monitoring the effluent output from the device.

The complexity of biological samples often overwhelms standard screening techniques seeking to discover biomarkers of disease or rapidly assess drug efficacy. This unique problem warrants an analytical technique capable of both rapid screening of samples and sufficient sensitivity to account for the many analytes in low abundance that typically comprise metabolomic and signaling experiments, which often either defy detection or appear collectively as chemical noise. The use of mass spectrometry (MS) as the leading detection method of

proteomic,⁴⁰⁵ lipidomic,⁴⁰⁶ and glycomic⁴⁰⁷ studies has led to many advances in elucidating the complexity of the cell.

The combination of constant microfluidic perfusion bioreactors with mass spectrometry has the potential to rapidly screen cell effluent for secreted species indicative of internal metabolic perturbations. Several studies have taken on the challenge of integrating these technologies to produce a powerful analytical platform. In an early experiment, Chan *et al.* verified that using PDMS bioreactor devices to transfer samples into the electrospray ionization mass spectrometer (ESI-MS) did not contaminate the samples.³⁰⁹ On-chip ultrafiltration and analyte pre-concentration for high-throughput small molecule screening with ESI-MS were performed with the resulting detection sensitivity shown to increase by one to two orders of magnitude over off-chip screening strategies.³¹¹ A significant impairment in coupling cellular bioreactor microfluidic devices with online-MS is in the suppression of signals of interest by salts present in biological samples. To combat this problem, some form of desalting is typically performed offline, using either a solid phase extraction (SPE) column and vacuum manifold or some form of liquid chromatography. These techniques desalt samples by providing a functionalized surface for which salts and analytes have differing affinities. For example, liquid chromatography (LC) typically uses C₁₈ columns, which provide good affinity binding sites for non-polar molecules but lack sufficient interaction prospects for salts, thereby allowing for an aqueous rinse to clear the column of salts and a subsequent organic elution of analytes without the suppressing contributions from salts. These methods, while providing an efficient means of desalination, come at the expense of temporal resolution, and they are not designed for online analysis. One recent development in the online desalting of effluent from a microfluidic bioreactor is the work of Chen *et al.*, which incorporates a packed micro-solid phase extraction column.³⁷⁸

We have previously demonstrated the ability to rapidly desalt a continuous sample stream using online SPE.³¹² This work directly translates to the processing of continuous sample streams originating from a MTNP. Using online SPE for such applications provides a surface for which analytes of interest have affinities but unwanted salts do not. This allows for variable duration periods of pre-concentration of the analytes.

As an initial proof of concept experiment for this integrated platform, we selected cellular memory of drug exposure, specifically Jurkat T cell memory of cocaine, for ease in identification of known drug metabolites and for its unique biological information. The choice of cell type was based upon cocaine's classification as an immunosuppressive agent, whether by mechanisms of direct and/or indirect actions on immune cells. Findings from experiments tying cocaine to immune function suppression have been contradictory at times,⁴⁰⁸⁻⁴¹² most likely because of the complex biological systems under investigation and wide variety of experimental procedures. A major hurdle in determining these mechanisms is the lack of an assay capable of tightly controlled environmental parameters, temporal robustness to avoid loss of intermittent changes, and multi-parameter sampling for unique evidence of experimental variable interconnection. The platform proposed herein allows for such an assay to be conducted. Through the comparison of naïve Jurkat T cells and those with prior cocaine exposure on this platform, differences in cocaine metabolism may be detected. Figure 4.1 demonstrates the experimental concept. Exposure of a naïve cell to cocaine may lead to a certain exometabolomic profile which defines the state of the cell. However, when a cell with prior cocaine experience receives a subsequent dose, the exometabolomic profile may either be identical to that of the naïve cell under exposure or distinguish the cell as unique. With a near real-time readout of cellular metabolic events on our integrated microfluidic-solid phase extraction-ion mobility-

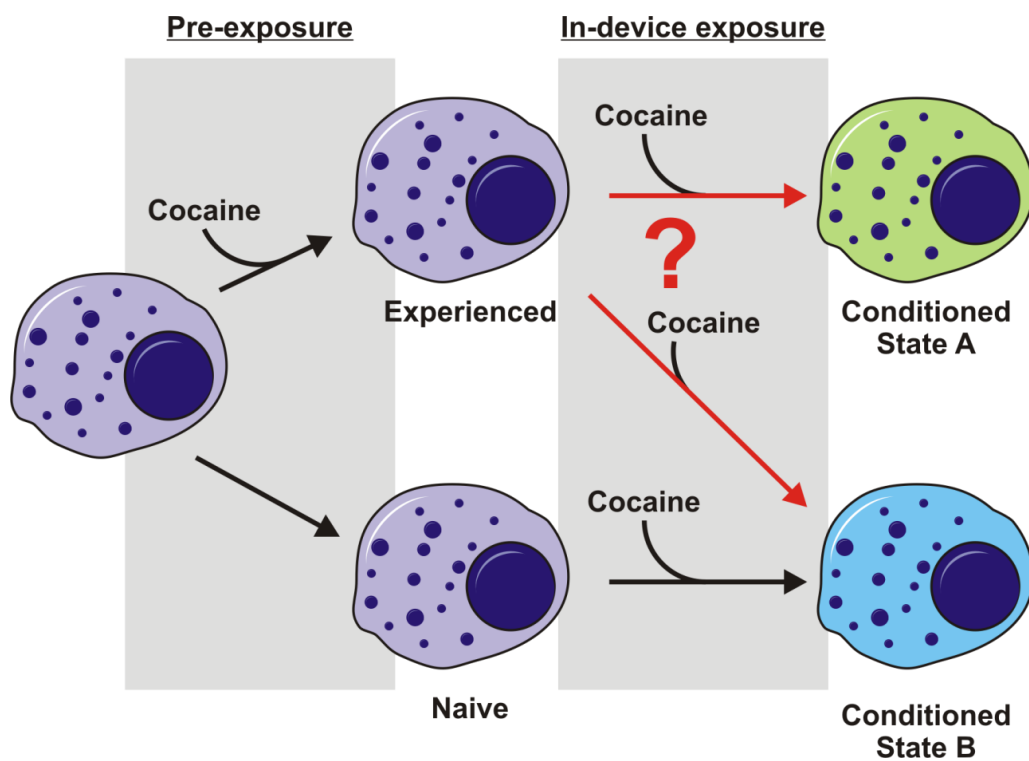


Figure 4.1. Experimental scheme showing the potential cell fates (in terms of exometabolomic profiles), demonstrated here as color change, for naïve and cocaine-experienced cells upon exposure to cocaine in a microfluidic bioreactor.

mass spectrometry platform, it may be possible to determine variations in exometabolomic profiles that will provide evidence of cellular memory of cocaine exposure.

2. Methods

A. Microfluidic bioreactor design and fabrication

The VIIBRE Multitrap Nanophysiometer (MTNP) was previously designed in AutoCAD and converted to a chrome mask on glass (Advance Reproductions, North Andover, MA). A silicon master was produced through photolithography methods which include spinning a negative photoresist, SU-8, onto silicon wafers, exposing them to UV light through the desired mask to crosslink the SU-8, then developing to remove non-cross-linked polymer.⁴¹³ Poly(dimethylsiloxane) (PDMS) (Sylgard 184 Elastomer Kit, Dow Corning, Midland, MI) was then cast onto the silicon and SU-8 master, cured, and removed from the master. Inlet and outlet ports were punched and PDMS replicas were bonded to glass coverslips by O₂ plasma treatment (Harrick Plasma Cleaner, Ithaca, NY).

PDMS Surface Modification

Liquid 2-[methoxy(polyethyleneoxy)₆₋₉propyl]trimethoxysilane (PEG-silane) was obtained from Gelest (Morrisville, PA). Immediately following plasma treatment, devices were intubated and a 2% solution of PEG-silane in 95% ethanol, 5% H₂O, and 11 mM acetic acid was injected until the device interior was filled. Devices were allowed to incubate at room temperature for 10 minutes followed by a rinse with ethanol, then water. A final incubation on a hot plate at 110°C for 10 minutes was then performed to evaporate any remaining solvent and

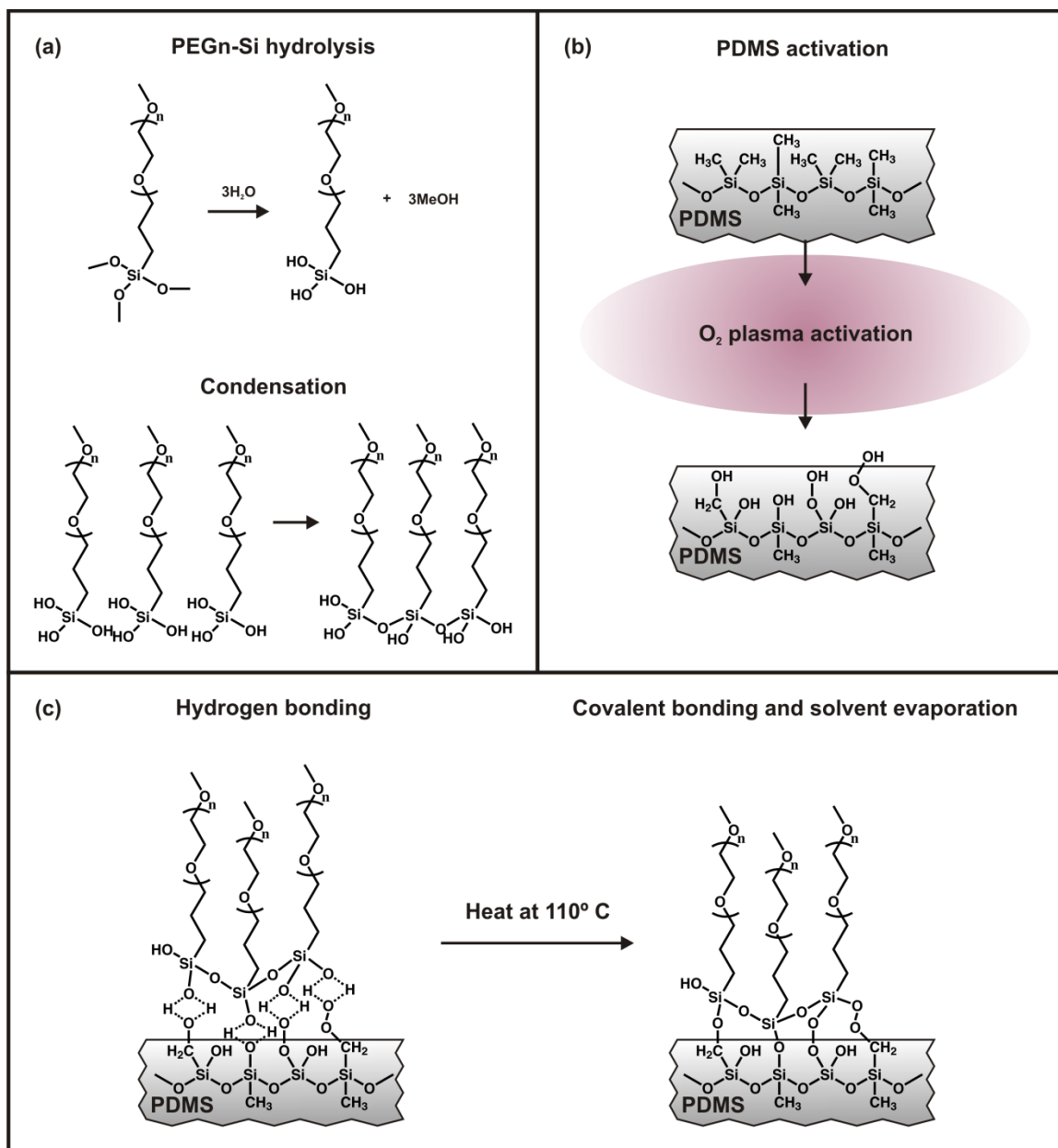


Figure 4.2. PDMS silanization scheme showing hydrolysis of methoxy group from PEGn trimethoxysilane to form silanol groups (A) and the steps of PDMS activation (B(i)), silane deposition (B(ii)), condensation of the silane into chains (B(iii)), hydrogen bond formation between silanol and oxidized PDMS surface (B(iv)), and covalent bond formation between silane and PDMS surface (B(v)).

complete the surface modification. Supplemental Figure 4.2 portrays the steps in the covalent surface modification of PDMS.

After at least 24 hours at room temperature, each device was perfused with fluorescently labeled insulin at a rate of 500 nL/min for 30 minutes and then rinsed with Ringer's buffer (118 mM NaCl, 5.4 mM KCl, 2.5 mM CaCl₂, 1.2 mM MgSO₄, 1.2 mM KH₂PO₄, 20 mM HEPES) for another 30 minutes. Images were collected every 15 seconds during the perfusion and rinsing stages with an inverted Nikon Eclipse Ti-e fitted with a 495 nm/521 nm excitation/emission filter set for fluorescent imaging of adsorbed insulin. Images were aligned and processed with Image J for comparison of total fluorescence intensity.

B. Cell culture and "in-culture" cocaine exposure

Jurkat T cells (clone E6-1, TIB-152) (ATCC, Manassas, VA) were cultured in 90% RPMI 1640, 10% fetal bovine serum (FBS, heat inactivated) (Lonza, Allendale, NJ) at 37°C, 5% CO₂ according to the manufacturer's instructions.

In-culture cocaine exposure experiments were performed as follows (Figure 4.3). Two populations of Jurkat T cells (passage 6, 2 million cells/ml, 500 µL, in biological triplicate) from the same culture flask were added to two separate microcentrifuge tubes. Both tubes were centrifuged at 200 × g for 2 minutes and supernatant was removed. Cells in tube one were resuspended in 500 µL of RPMI 1640 and incubated for 54 minutes at 37°C, 5% CO₂. The cells were then centrifuged as above and resuspended in RPMI with cocaine at 60 µg/ml, then incubated for another 54 minutes. This cell population received two more steps of media switching, RPMI then cocaine, for a total of four 54-minute exposure periods. Each time the cells were centrifuged, the supernatant was reserved for protein precipitation and metabolomic analysis. Since these cells lacked pre-exposed to cocaine, they were termed "naïve."

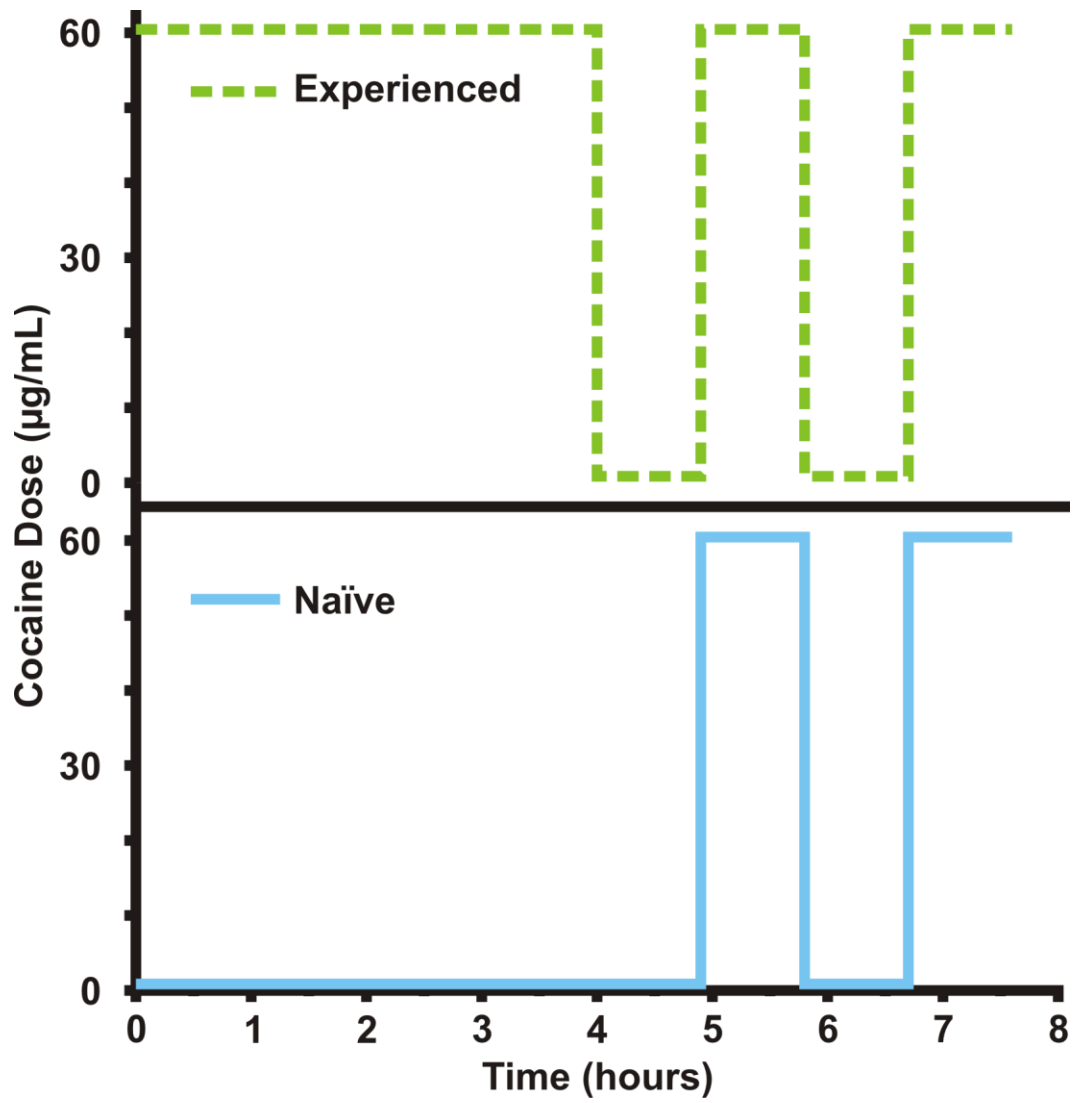


Figure 4.3. Cocaine exposure scheme for both in culture and online cell experiments showing the time course of cocaine administration to naïve (blue) and experienced (green) T cell populations.

Cells in the second tube were resuspended in 500 μL of cocaine in RPMI 1640 (60 $\mu\text{g}/\text{ml}$) and incubated for 216 minutes at 37°C, 5% CO_2 . After this period, cells were again centrifuged and then exposed in the same manner as tube one with alternating exposure to plain RPMI 1640 and cocaine. Supernatant from these samples was also kept for metabolomic analysis. Since these cells had an extended cocaine pre-exposure period, they were termed “experienced.”

In order to investigate the cocaine degradation over the time course of the experiment, samples of cocaine in RPMI were incubated in the same conditions as the cells and sampled at each 54-minute time point starting at time zero and ending at 10.5 hours.

C. Metabolomics sample preparation and UPLC-ESI-IM-MS analysis

As each 54-minute time point was taken, supernatant was placed on ice to halt any continued metabolite modifications and immediately processed for protein removal with cold methanol. To each 300 μL supernatant sample, 900 μL of cold methanol was added, vortexed, allowed to sit for 10 minutes at 4°C and then centrifuged at maximum speed for 10 minutes in a Heraeus Fresco 21 temperature-controlled centrifuge (Thermo Scientific). Supernatant was transferred to a new microcentrifuge tube and kept at 4°C until all samples were collected and processed. All samples were then dried down in a Savant DNA 110 Speedvac overnight with low heat and reconstituted in 300 μL 5% methanol/95% water (0.1% formic acid).

Samples were placed in the sample tray of the NanoAcquity UPLC with autosampler (Waters, Milford, MA), which remains cooled to 4°C to prevent sample degradation. Ultra performance liquid chromatography was performed on 1 μL samples loaded on a HSS C_{18} , 1.8 μm particle size column with mobile phase A (0.1% formic acid in H_2O) by ramping from 100% mobile phase A to 100% mobile phase B (0.1% formic acid in MeOH) over 11 minutes, then holding at 100% mobile phase B for 2 minutes. Ion mobility-mass spectrometry and MS^E were

then performed on the eluted analytes using the Synapt G2 ion mobility-mass spectrometer (Waters, Milford, MA). Quality control samples were dispersed every 10 samples in the Waters MassLynx v4.1 software sample list among technical triplicates of each biological sample.

D. Online cell loading and experimentation

Prior to experimentation, 500-1000 μL of cell suspension was removed from culture flasks. Cells at passage 6 were used for experiments. Cells were then gently pelleted and aspirated into polyether ether ketone (PEEK) tubing connected to pump-controlled syringes. The flow direction of the pump was reversed upon intubation of the MTNP and cells were collected into microfluidic traps for experimentation. Cell-loaded devices were then perfused with selected media components and bright-field images were collected by an inverted Nikon Eclipse Ti-e (Nikon Instruments, Melville, NY). Cells in the MTNP were maintained at 37°C and 5% CO_2 during experimentation.

For T cell cocaine metabolism studies, populations of naïve T cells and experienced T cells (exposed to cocaine at 60 $\mu\text{g}/\text{mL}$ in RPMI 1640 for 4 hours) were stimulated with either cocaine (60 $\mu\text{g}/\text{ml}$ in RPMI 1640) or RPMI 1640. Cells were initially exposed to plain RPMI media for 54 minutes, followed by exposure to cocaine at 60 $\mu\text{g}/\text{mL}$ in RPMI for 54 minutes. Both steps were repeated for a total of four steps. Experiments with naïve and experienced cells were performed on the same day, in series, to exclude any variation in cell population from day to day. The cocaine exposure scheme is the same as the in-culture exposure, shown in Figure 4.3.

E. Solid phase extraction desalter

Columns are made of 360 μm OD/100 μm ID fused silica tubing and are bomb-loaded in house with 3 μm , 300 Å, C_{18} phase Jupiter Bulk Packing (Phenomenex, Torrance, CA) using a PIP-

500 Pressure Injection System (New Objective, Woburn, MA). Three 10-port Nanovolume UPLC Valves with 360 μm fittings, C72MH-4690ED (VICI Valco Instruments Co. Inc., Houston, TX) were used for the valve arrangement (Figure 4.4). The aqueous solvent and both organic solvent lines, running at 500 nL/min, were supplied with an Eksigent Nanoflow Metering System (AB SCIEX, Framingham, MA), which has four independent flow channels. The output lines from the two downstream valves were connected with a micro-T junction and fed directly into the mass spectrometer via a nano-electrospray ionization (nESI) source. Cheminert 360 μm unions (with 100 μm bore) were used for all tubing-to-tubing connections (not shown). Only fittings for 360 μm OD tubing were used as the more popular 1/16" fittings requiring sleeves to connect to smaller bore tubing instigated leakage at high backpressures. Other than the columns, which were made of fused silica, 360 μm /50 μm PEEK tubing was used. Prior to experimental use a 2 $\mu\text{g}/\text{mL}$ solution of polyarginine was run through the system to bind all non-reversible interaction sites. Elution cycles were then run overnight to ensure all reversibly bound material was removed before experimentation. Sample loops were added to the system (as seen in Figure 4.4) to reduce backpressure buildup.

F. Online cell effluent desalting and mass spectrometry analysis

All online cell effluent experiments were conducted using PDMS MTNP devices. Cellular effluent from the device was processed online prior to mass spectrometry analysis using the online SPE desalter in Figure 4.4. Cell effluents, driven by syringe pumps upstream of the bioreactor, were filtered with an inline filter (1 μm stainless steel frit, followed by a 0.5 μm polymer mesh, IDEX Health & Science, Oak Harbor, WA) and loaded into each sample loop. Sample loops, which were made of 360 μm OD/250 μm ID tubing, were 12.2 cm long, providing a sample loop volume of 6 μL . The continuous sample stream was diverted into each sample

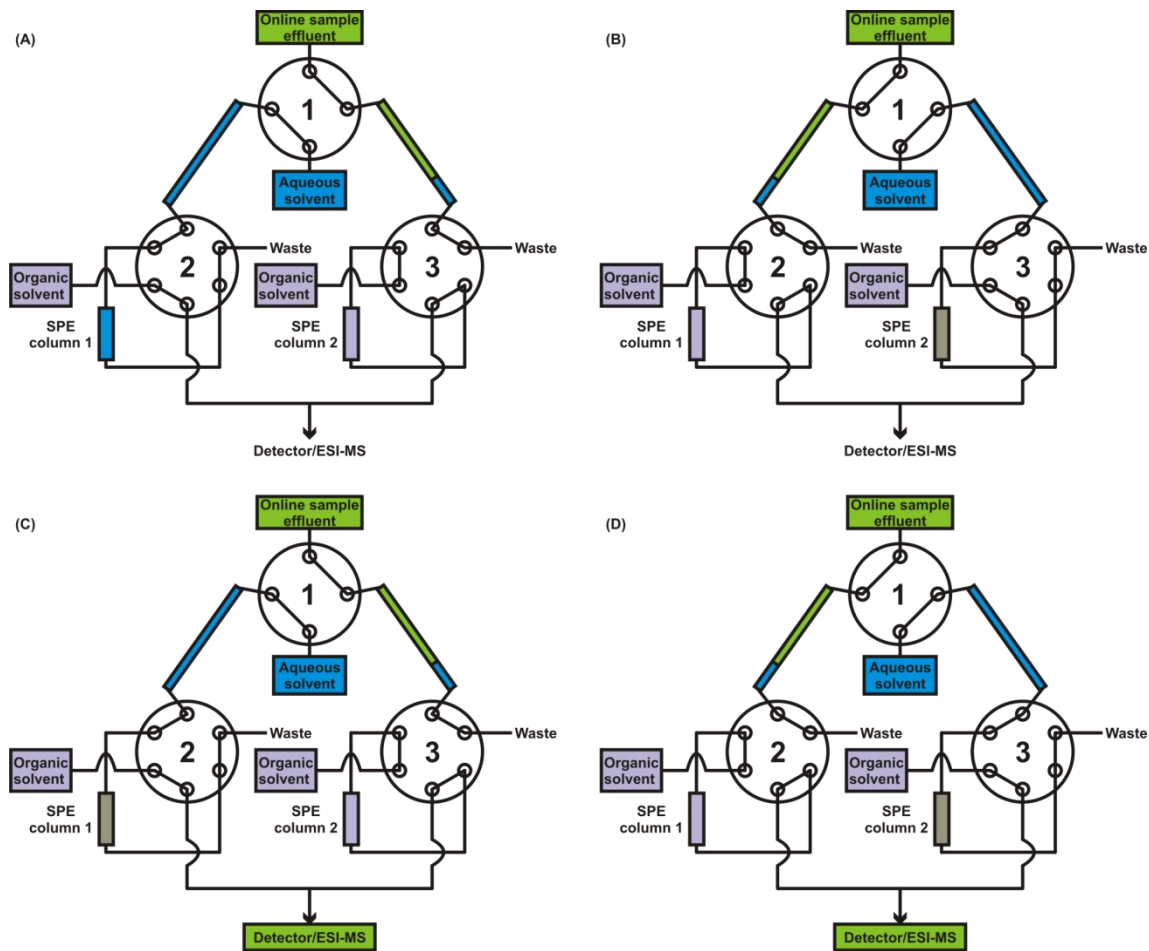


Figure 4.4. Solid phase extraction desalter setup starting from initial sample effluent flow incorporates 2 sample loops, 3 valves, and 2 C18 columns. During (A), sample effluent fills sample loop 2 for 9 minutes, while the aqueous solvent flows through sample loop 1, over column 1 and to waste. The organic solvent flows over column 2 and to the mass spectrometer. B) Upon switching of the valves, the sample effluent fills sample loop 1 for 9 minutes. Aqueous solvent forces the 1.5 μL head of aqueous solvent, the 4.5 μL of sample effluent, and an additional 2.1 μL of aqueous solvent over column 2 to equilibrate the column, load the sample, and rinse away the salts. Organic solvent runs through column 1 and to the detector. C) The next valve switch again exchanges the sample loop filled by effluent, while column 1 is equilibrated, loaded, and rinsed. The analytes captured on column 2 are eluted by the organic solvent and sent to the detector. D) When the valves switch again, the sample effluent fills the opposite loop, column 2 is equilibrated, loaded, and rinsed, and column 1 is eluted with organic solvents and those analytes are sent to the detector. The pattern repeats until the experiment is completed.

loop for exactly 9 minutes at 500 nL/min, thus filling the sample loop to 75% capacity. Because water was always flowing through these sample loops immediately prior to sample flow, a plug of 1.5 μL of water preceded each sample effluent plug. This plug served to quickly and roughly equilibrate the column with an aqueous solvent. Once the loop was filled to 75% with online sample effluent, the small water plug and sample effluent were passed over the column, using the aqueous solvent line to generate the necessary backpressure. Once the effluent had cleared the sample loop and had been entirely passed over the column, an additional 2.3 minutes or 2.1 μL of aqueous solvent (H_2O with 0.1% formic acid) was run over the column to serve as the rinsing/purging step to remove residual salts. Following the salt purge, the column was eluted with organic solvent (90% methanol, 10% H_2O , 0.1% formic acid). Each step of this process from the initial effluent flow through the SPE desalter is illustrated in Figure 4.4. Data were collected using MassLynx software (Waters Corp., MA) by Data Dependent Analysis (DDA) method cycle files, where each column elution was collected as an individual file. Collecting each column elution as individual data files aided sample analysis, as explained later.

G. Data processing and multivariate statistical analysis

Resulting data sets from both online and in-culture experiments were processed using Waters MarkerLynx software along with Umetrics Extended Statistics software for multivariate statistical analysis (Waters Corp., MA). All spectra were corrected to sodiated HEPES buffer ($[\text{M}+\text{Na}]^+$ exact mass 261.0888), centroided, and peaks were normalized to 10,000 counts per sample. Only spectra from samples analyzed through UPLC were deisotoped and underwent chromatographic peak detection. Data from online experiments were processed by a combined scan range. An intensity threshold was set for all data at 1000. Principal component analysis (PCA) with Pareto scaling was performed to verify initial sample grouping. Further statistical

analysis with orthogonal partial least squares-discriminate analysis (OPLS-DA) was performed to identify significant contributors for group separation.

3. Results

A. Platform integration and evaluation

Successful integration of the platform has been achieved, as shown in Figure 4.5. The microfluidic bioreactor (MTNP) is controlled upstream by Harvard Apparatus syringe pumps, viewed under the Nikon Eclipse Ti-e for optional fluorescent and bright field imaging acquisition, and outfitted with a stage incubator for control of temperature, gas, and humidity. The effluent exiting from the MTNP flows through two inline filters for catching cell debris (1 μm stainless steel frit, followed by a 0.5 μm polymer mesh, IDEX Health & Science, Oak Harbor, WA). Once through the filters, the effluent fills one of the two sample loops vented to open air to avoid high backpressures in series with the compliant microfluidic device. After the effluent undergoes salt removal by the solid phase extraction desalting system, it is directed into the nESI source and sprayed into the Waters Synapt G2 nESI-IM-MS.

Initial work, which paired a previous arrangement of the online SPE design with MTNPs, resulted in ruptured devices. When LC pumps were used to rinse and elute the SPE columns, pressure would build up behind the column. When the valve was switched so that the MTNP was directly in series with the column, this high backpressure (>200 psi), would cause massive flow reversal and induce the PDMS device to physically delaminate from the glass to which it was bonded. This problem was mitigated by altering the valve arrangement to incorporate sample loops. By cutting off the direct pathway between the columns and the microfluidics, the

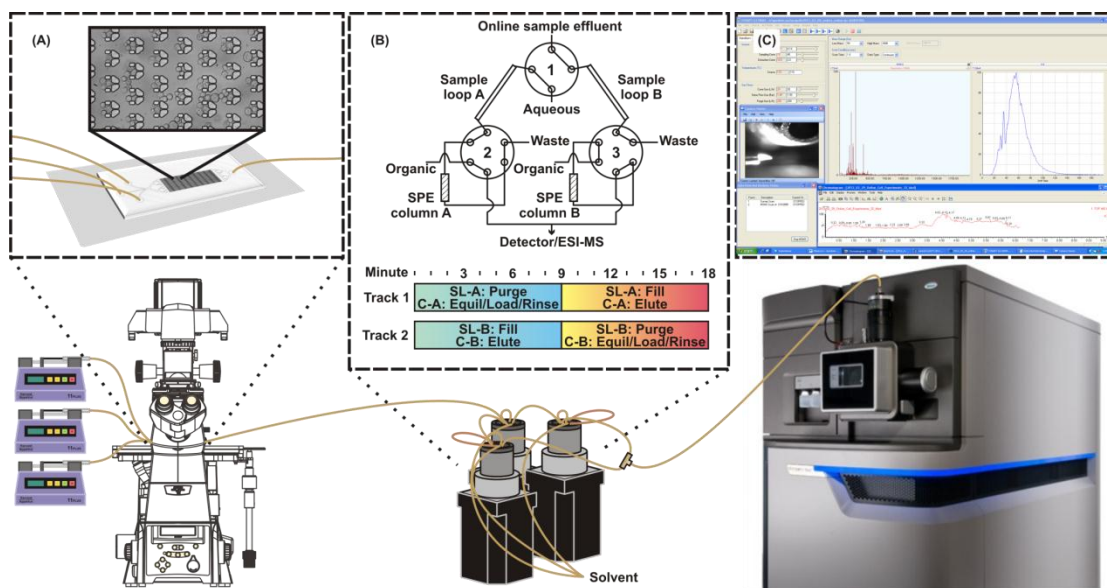


Figure 4.5. MTNP-SPE-nESI-IM-MS platform with Harvard Apparatus syringe pumps, Nikon Eclipse Ti-e inverted fluorescence microscope with stage incubator, solid phase extraction desalter with Eksigent and NanoAcquity pumps for solvent flow control, nanoelectrospray ionization source for continuous flow sample analysis in the Waters Synapt G2 ion mobility-mass spectrometer. Beyond the initial experimental setup, all components are fully automated and capable of running multi-hour experiments limited by the lifetime of cells in the MTNP.

buildup of pressure that occurred during rinsing/eluting was unable to take the least resistive path to the compliant microfluidic device and would instead be vented to the waste port, as shown in Figure 4.4. Although in extreme cases the inline filters downstream of the microfluidic device may become clogged with cells, thus interfering with effluent flows, this is a rare occurrence and can be prevented by using new filters for each experiment in addition to open-outlet cell loading (allowing cells to exit the device during loading before attaching to the downstream components).

The sample loop addition to the valve arrangement allowed for a two-step valve configuration, a simplification of the previous version. The new two-step arrangement generated a saw-toothed pattern as opposed to the rise-and-fall delta-function pattern observed with previous arrangements¹⁸. In this 180-minute experiment, an 18-minute-long cycle was used, producing an elution peak every 9 minutes. The sample loop volume was designed specifically to hold 9 minutes of sample effluent (4.5 μL at 500 nL/min flow rate). This cycle duration was determined to be optimal based on analyte concentrations. The file acquisition was set to account for the delay time from the device to the nESI source such that one column elution was captured per file while accounting for the roughly 12-second software delay between file acquisitions. Pump switching for control of the MTNP perfusion media was also timed with the SPE desalter valve switching.

Removal of salts in an online manner greatly increases signal-to-noise ratio. Yet with the low number of cells and high concentration of media components, detecting low concentrations of analytes is challenging. The signals are also affected by the dynamic range ($\sim 10^5$) of the mass spectrometer.²⁶⁴ Presumably, post-desalting, and given cellular utilization of nutrients in the media, HEPES at 10 mM is the analyte of greatest concentration. The high concentration of this species limits the lower range of detection of exometabolomic contents to roughly five orders of

magnitude lower. This HEPES concentration can be reduced if necessary, but as its purpose is to buffer the media to maintain a physiological pH, there could perhaps eventually be a tradeoff. While detection of low concentration species remains a challenge, the ongoing advances in mass spectrometry technology will increase the detection capabilities of this system.

B. PDMS surface passivation for increased signal-to-noise ratio

The use of a biological model for testing the instrumentation platform does have a major downside in the form of potential loss of metabolite signal due to adsorption to PDMS bioreactor surfaces. Rectification of these types of issues requires changing the microfluidic device material or modification of PDMS surface properties. Switching device materials, and thus the techniques for producing such devices, often requires substantial changes in infrastructure as well as loss of desirable PDMS properties such as optical clarity and low feature size. Surface modification is more plausible, as procedures can be added onto existing fabrication or experimental methods. A variety of types of surface modification of PDMS microfluidic devices have been investigated, such as chemical vapor deposition, sol-gel coating, silanization, surfactant coating and dynamic coating.^{414,415} Due to the nature of this combined technology platform with mass spectrometry downstream of the microfluidic device, care must be exercised in the selection of a surface modification method. The presence of species in the bioreactor effluent necessary for the alteration of the PDMS surface can lead to complications in the detection of desired cell secretions due to issues of dynamic range. Instability of species used in surface modification can additionally lead to adsorption of secreted cellular materials to PDMS. A stable, inert coating is crucial for downstream mass spectrometry. Surfactants and dynamic coating methods are not appropriate for this application as the presence of electrostatically bound polymer or added analytes to the solution are not compliant with

detecting low levels of cellular signals. One method leading to a covalently bound surface modifier is silanization. Though silanes are often deposited on surfaces through chemical vapor deposition and can result in the production of chlorine gas, ethoxy- and methoxy-silanes can be purchased in a liquid form, resulting in ease of application to PDMS surfaces for the prevention of non-specific adsorption.

While insulin is not necessarily a prime target of these experiments, it serves as an example of the potential complications from non-specific adsorption. Though high sensitivity is characteristic of mass spectrometry, this system seeks to identify secreted molecules from roughly 10^5 cells. Detecting these low-level signals becomes a greater challenge when a portion of the signal is lost due to interactions with seemingly inert materials. Although the PDMS passivation schemes returned positive results (data provided in Supplemental Material Figure 4.6), some metabolite, peptide or protein species, such as insulin, are particularly “sticky” to most polymer and glass. In testing the capabilities of the system, we have noticed drastic reduction in and even absence of signal from insulin standards over time, even at low temperatures. Additionally, insulin hysteresis in the combined platform has been discovered after as long as 4 days of continuous perfusion of the SPE desalter tubing and columns. While the columns may be a source of insulin retention, this particular hysteresis occurred with freshly made columns, pointing to an alternate source of contamination as the culprit. The remaining sources of contamination could be from insulin retention in the PEEK and/or fused silica tubing lines, the valve rotors, or even on the source block or cone of the mass spectrometer. Insulin adsorption does not merely lead to a contamination problem; it also leads to reduction in the overall insulin signal.

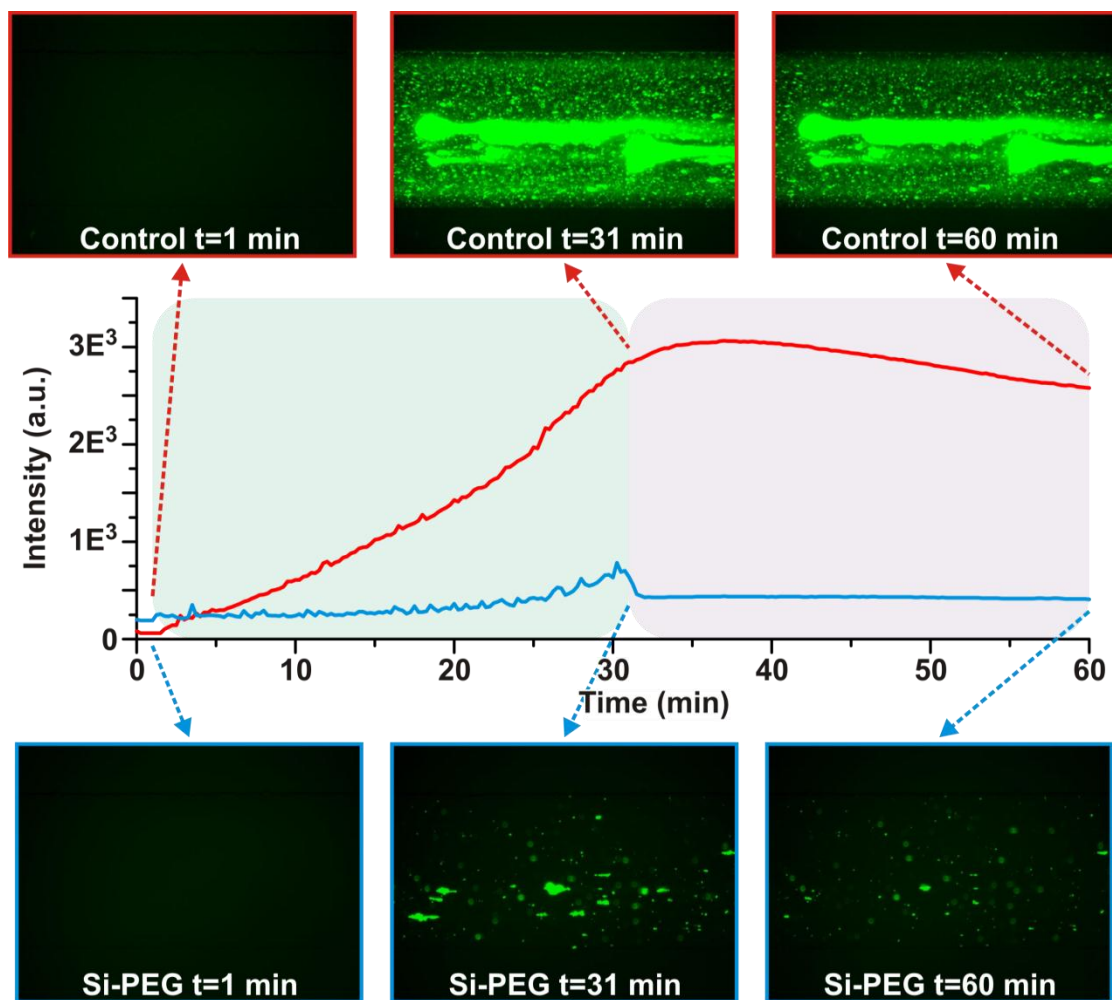


Figure 4.6. PDMS channels were perfused FITC-insulin for 30 minutes (green), followed by 30 minutes of rinsing with Ringer's solution (pink). The top three fluorescent images show the surface bound insulin at 1 min, 31 min, and 60 min, with the bottom three images corresponding to the surface modified channels. Silanized PDMS channels (blue line) retain (at maximum) only 25% of the total insulin retained by untreated PDMS (red line).

C. Comparison of UPLC-ESI-IM-MS to MTNP-SPE-nESI-IM-MS

A significant reduction in time is among the benefits of continuous sample flow from the microfluidic bioreactor to the solid phase extraction desalter and into the nESI-IM-MS. This integrated platform allows for the setup (~2-3 hours), execution (~4-8 hours), and data collection (no additional time) in the course of a day. Traditional in-culture experiments with UPLC-ESI-IM-MS analysis possibly require less initial setup (~1 hour), roughly the same execution time (~4-8 hours), significant additional sample processing time (~15-20 hours including overnight sample evaporation), and data collection (~50 hours for 120 samples with a 25-minute UPLC time per sample) for a total of *ca.* 4 days until data are ready for processing compared to 1 day for the platform developed in this work.

Another advantage of the integrated platform compared to in-culture experiments is in the ease of obtaining mass spectra at multiple time points. Our process is automated with constant media perfusion control timed with the switching of the SPE desalter valves as well as the data file collection timing. With the in-culture experiments, a lengthier process is required to collect a single time point. The cell suspension must be centrifuged for 2 minutes, the supernatant removed, and the cell pellet resuspended in new media. The length of time required for this media change is on the same order of the time points taken with the integrated platform. Repeated centrifuging and pellet aspiration can introduce unnecessary stress to the cells, which may produce an exometabolomic profile resulting from both the media exposure and additional cell stress.

One downside compared to liquid chromatography data is the absence of retention time information. While the solid phase extraction desalter uses a column similar to those found in an LC system, any slight timing discrepancy from one file collection to the next prevents the use of any retention time data. Confounding this issue is the fact that processing data within the

Waters MassLynx software without retention time data available prevents the option for the removal of isotopes from the data. While this is a hindrance in some respects (roughly 3 times more peaks, redundant data, etc.), it can prevent the accidental removal of isobaric peaks of interest from the study.

D. Cocaine metabolism in naïve and experienced T cells

Online Cellular Analysis: Two populations of Jurkat T cells were compared in this study: naïve T cells that had never been exposed to cocaine and experienced T cells that had been incubating in cocaine at 60 µg/ml in RPMI 1640 for 4 hours prior to online experimentation. As shown in Figure 4.7, a high degree of variance was observed based not only on what type of media was present in the bioreactor (*i.e.*, plain RPMI media or cocaine RPMI media), but also whether the cells experienced cocaine earlier in the day (*i.e.*, whether the cells were experienced or naïve to cocaine exposure). The major unique contributors to group separation between naïve and experienced exometabolomic profiles included m/z 283, m/z 187, m/z 399, m/z 157, and m/z 337 (all at elevated abundance in the experienced group compared to the naïve group). The metabolites contributing to group separation between types of media to which cells were exposed in the MTNP consisted of m/z 312, m/z 182, m/z 304, m/z 290, and m/z 150. Though the data analysis pipeline prevented removal of isotopes, any m/z present in the list of top contributors negated the inclusion of their respective isotopes from these lists.

Benzoyllecgonine (BE) (m/z 290 as $[M+H]^+$, m/z 312 as $[M+Na]^+$), a primary metabolite of cocaine, was identified as a contributing factor to the separation between the cocaine exposure steps and plain RPMI steps as well as to naïve cells and experienced cells. Analysis of this metabolite over the time course of the experiment revealed an expected increase during cocaine exposure steps, but also showed a significant increase from naïve to experienced cells (p

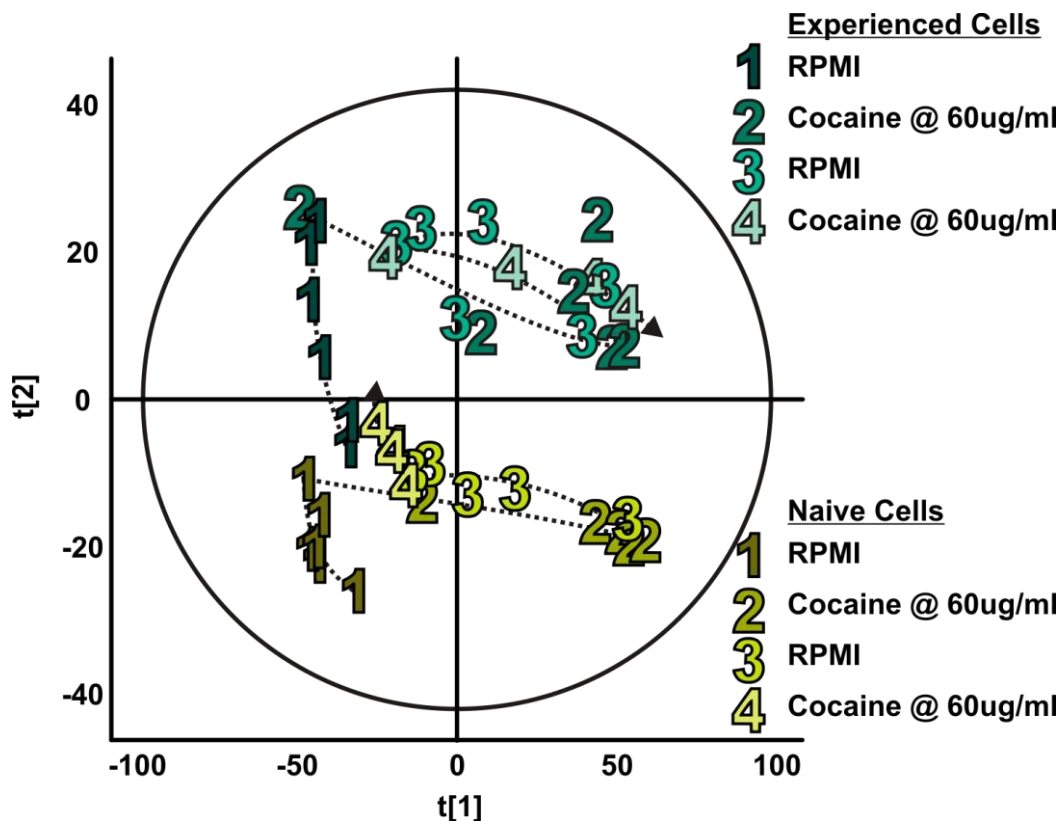


Figure 4.7. Walking principal component analysis of exometabolomic profiles of naïve (shades of yellow) and cocaine-experienced (shades of turquoise) Jurkat T cells obtained with on-line cellular analysis. Each numerically labeled data point represents a 9-minute column elution, with 6 data points collected per step (all marked with the step number and connected in order of collection with the dotted line). In steps 1 and 3, both cell populations received plain RPMI. In steps 2 and 4, both received cocaine in RPMI at 60 µg/ml. As profiles switch from RPMI to cocaine exposure, the data points move towards the right and vice versa, with the exception of naïve cell step 4, which stays closer to step 1. Further analysis of the data reveals this inconsistency may be explained by the death of the cells. Data were grouped not only based on the experimental step, but also by the experience level of the cells, as the cells receiving a 4-hour pre-incubation in cocaine group separately from those that did not receive this dose.

value = $5.7E^{-4}$) (Figure 4.8). Fragmentation spectra revealed fragment ions m/z 82, m/z 91, m/z 105, m/z 150, m/z 168, m/z 182 and m/z 272, as shown in Figure 4.8. Analysis of the remaining top three contributors to separation based on media revealed cocaine at m/z 304, anhydroecgonine methyl ester (AEME) at m/z 182 (produced from dehydration of ecgonine methyl ester (EME) rather than the pyrolysis of cocaine), and ecgonine aldehyde, the decomposition product of EME, at m/z 150. Cocaine metabolic pathways are described in Figure 4.9.

To verify that this increased BE abundance was not purely a result of non-enzymatic hydrolysis of cocaine to BE in aqueous solutions over the time course of the experiment, an experiment replicating the naïve and experienced cell experimental time course was performed with the omission of the Jurkat T cells. In order to compare the experiment with cells to that without cells, we normalized the BE intensity to the cocaine intensity. On average, the percent of the total normalized BE from non-enzymatic hydrolysis was 34.1% in step 2 of the naïve cell experiment while the corresponding percentage for step 2 of the experienced cell experiment was 34.5%.

The time course of additional metabolites is provided in Figure 4.10, including cocaine metabolites anhydroecgonine (AHE) (m/z 168) and hydroxybenzoylecgonine (HOBE) (m/z 306), as well as several unknown metabolites (m/z 330, m/z 475, m/z 678). Some of these additional metabolites have higher abundance in the cocaine-experienced population while others have no overall change in abundance. Overall, BE, AHE, and m/z 645 show significant increases from naïve to experienced cell population (p - values = $5.7E^{-4}$, $1.12E^{-3}$, and $1.60E^{-3}$ respectively). While AHE is a typical product of AEME (the pyrolysis product of cocaine), some reports have shown the metabolic pathway from cocaine into AEME and AHE could result from loss of water of EME or ecgonine (EG).⁴¹⁶ While there is much evidence that AEME and AHE can form as a result of

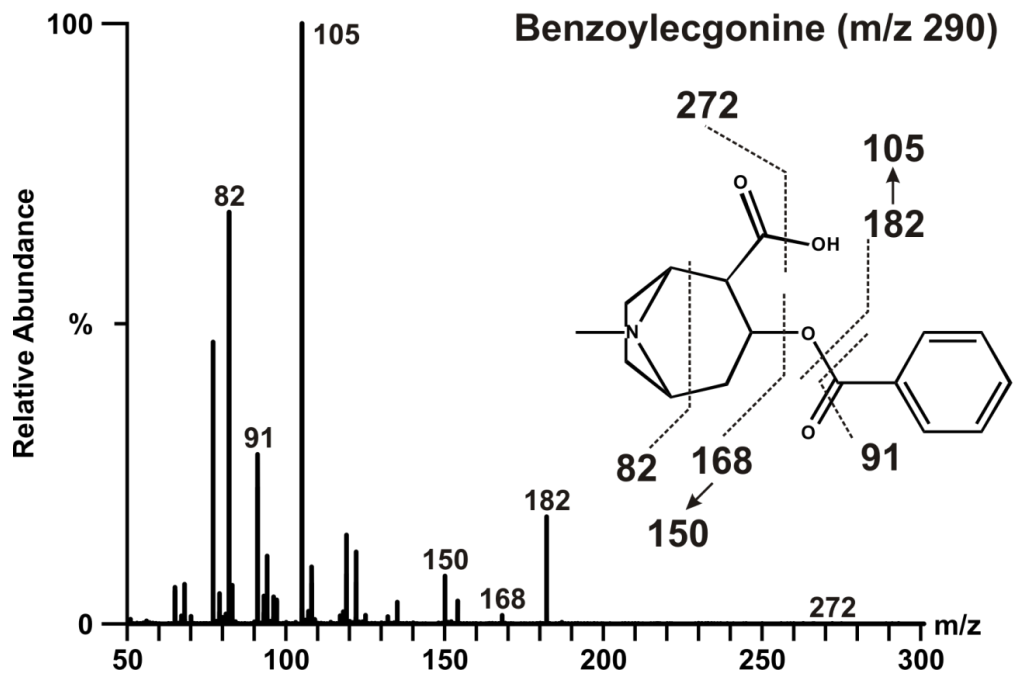
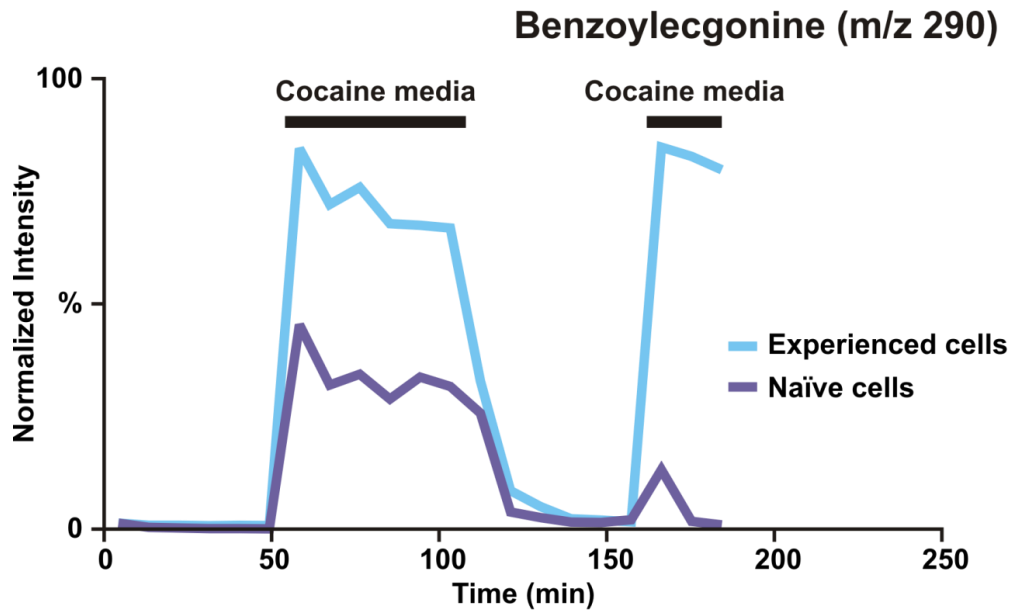


Figure 4.8. Top: Benzoylecgonine (BE) time course data for experienced (blue) and naïve (purple) cells. While data were gathered sequentially, plots are overlaid to highlight the increased abundance of BE in experienced cells. The absence of the expected increase in BE corresponding to step 4 (the last step of cocaine exposure) provides further evidence of cell death due to lack of cocaine metabolism. Bottom: The fragmentation spectra of BE are shown with parent ion of m/z 290.

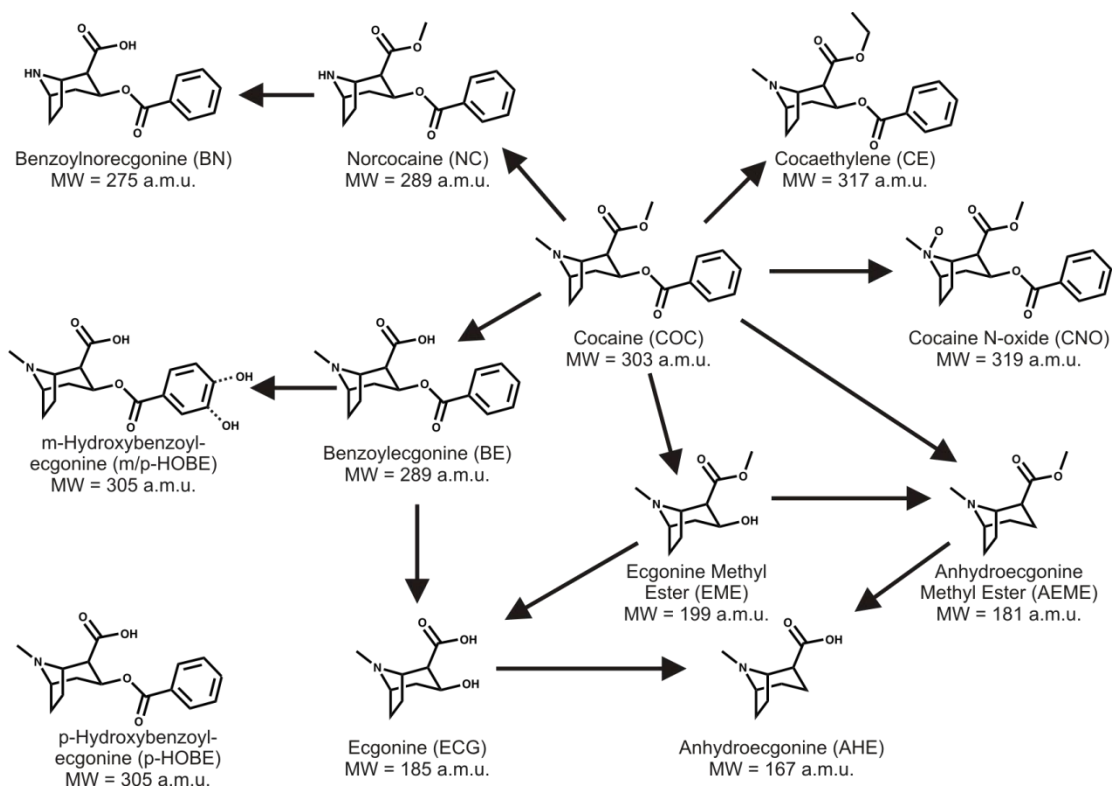


Figure 4.9. Metabolism of cocaine showing molecular weight for each metabolite.

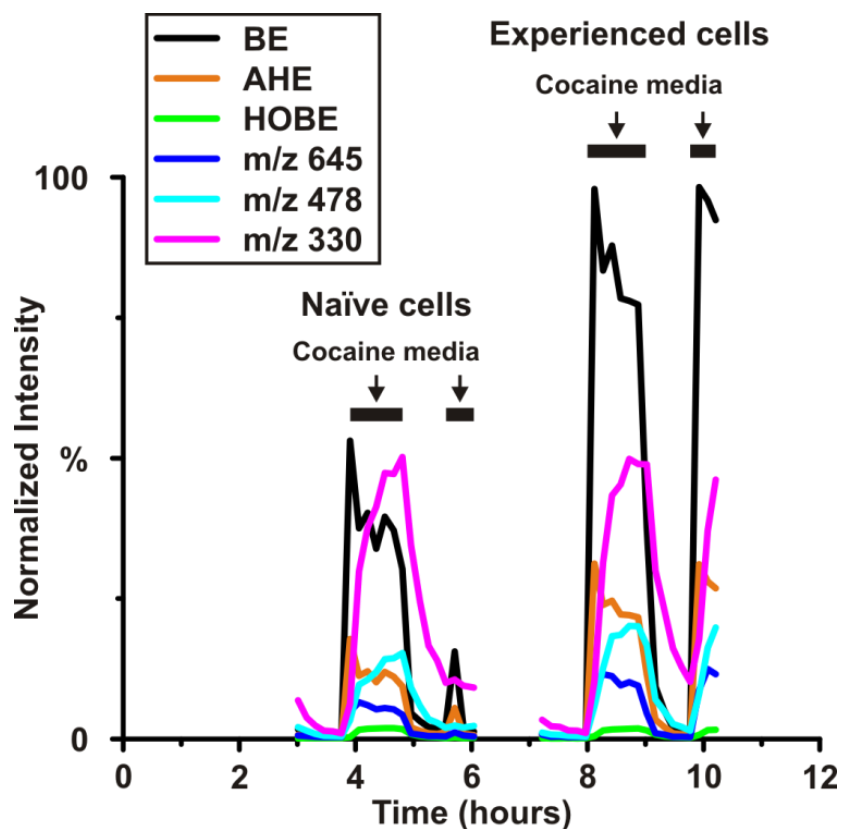


Figure 4.10. Additional metabolite time course data are shown compared to BE. Experimental conditions for each group of cells are shown above the graph with solid black lines indicating exposure to cocaine media. Anhydroecgonine (AHE) and hydroxybenzoylecgonine (HOBE), two additional metabolites of cocaine, provide examples of both variation between naïve and experienced cell groups in the case of AHE and consistency between these two groups in the case of HOBE. The increases in BE and AHE from naïve to experienced groups are statistically significant with respective p values of $5.7E^{-4}$ and $1.12E^{-3}$. Three unidentified m/z 645, m/z 478, and m/z 330 that contribute to the separation between media exposure groups are also shown. The features at m/z 330 and m/z 478 show no statistical significance between naïve and experienced cell groups while the increase in m/z 645 is statistically significant ($p = 1.6E^{-3}$).

the analysis technique, this is typical of gas chromatography separations that require vaporization of compounds, thus risking alteration of thermolabile compounds such as cocaine and its metabolites.⁴¹⁷ Electrospray ionization is utilized when this type of compound is under investigation.

E. In-culture cellular analysis

To compare this instrumentation platform, as well as the resulting biological data of naïve and cocaine-experienced T cells, with the current standard in mass spectrometry analysis of biological samples, the online experiment was replicated in culture and samples were analyzed with UPLC-ESI-IM-MS. Figure 4.11 shows the PCA plot demonstrating sufficient variance when comparing steps 1 and 3 (plain RPMI 1640 exposure) with steps 2 and 4 (cocaine exposure). Unlike the online experiment, separation between cocaine-experienced cells and naïve cells is not achieved, with exception of the initial RPMI exposure of the naïve cell populations. While one major difference is the number of time points per step of media exposure, as discussed previously, replicating the 9-minute time point sampling of the online system would confound the length of time needed for media switching, as well as inflict unnecessary stress on the cells.

4. Conclusions

A. Platform capabilities and shortcomings

We have described the analysis and proof of concept of a technology platform for near real-time detection of the cellular exometabolome based on the combination of a microfluidic bioreactor, an online SPE desalting arrangement, and mass spectrometry. A great

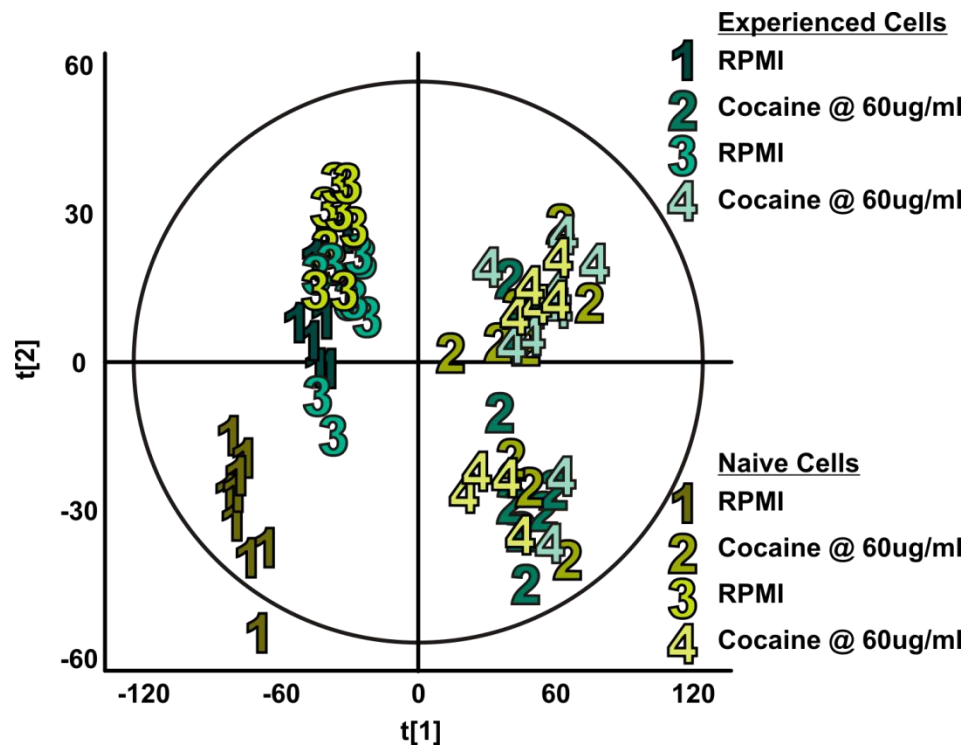


Figure 4.11. Walking principal component analysis of exometabolomic profiles of naïve (shades of yellow) and cocaine-experienced (shades of turquoise) Jurkat T cells using in-culture analysis. Each numerically labeled data point represents the end point of a 54-minute exposure to the indicated media. As with the online experiment, during steps 1 and 3 both cell populations received plain RPMI, while during steps 2 and 4 both received cocaine in RPMI at 60 μ g/ml. Variance between step 1 and 3 and steps 2 and 4 results in unsupervised grouping according to media exposure type. Separation between naïve and experienced cell groups, particularly when under cocaine exposure, does not occur to the same degree, as yellow and turquoise points corresponding to steps 2 and 4 are heavily intermixed.

strength of this platform is in its adaptability to different cell types and experimental conditions. Microfluidic cell trapping devices can be customized to the size of any adherent or non-adherent cell type. In this work, we demonstrate cell trapping and experimentation on naïve and cocaine-experienced Jurkat T cells. While this work shows only one model system based around cocaine exposure, the environmental stimuli are limited only by the number of pumps one has available for providing variable perfusion conditions and the temperature change and gas exchange rates an incubator is capable of generating. The online SPE desalting arrangement allowed for sufficient desalting to permit a temporal resolution of 9 minutes. While this temporal resolution is not by any means a significant advance for cellular chemical detection methods, because it is dictated by the analyte abundance and detection capabilities of the TOF mass analyzer, it is (depending on the mass analyzer) the best resolution possible for this biological system using mass spectrometry. Because it is trivial to scale the loading time in this arrangement based on detection power, we believe a technology platform of this general system will be of considerable utility to the biological community, particularly as mass analysis detectors improve in the coming years.

B. Cellular memory of cocaine experience

Cocaine metabolism in naïve and experienced Jurkat T cells was investigated with this near-real time platform developed for the study of the cellular exometabolome. It is well known that cocaine has an effect on immune cells, and that possibly there is some cell memory of prior cocaine exposure,⁴¹⁸ though there has been no prior demonstration of this suggestion. With the advent of this innovative platform, unique metabolic profiles are obtained that are absent from the “in-culture” data or perhaps lost due to the increased sample processing and UPLC analysis time. Upregulation of cocaine metabolism into benzoylecgonine in experienced cells

demonstrates one contributor to the unique exometabolomic profile resulting from previous cocaine experience. Anhydroecgonine, as well as unknown metabolites m/z 645 and m/z 478, are also upregulated in cell populations with prior cocaine exposure, leading to the possibility of indicators of immune cell memory of cocaine other than cocaine metabolites alone.

While there is a previously reported non-enzymatic degradation rate of cocaine into benzoylecgonine at physiological temperatures and pH,⁴¹⁹ we were able to confirm a rate specific to this platform. Through comparison of the BE to cocaine ratios from naïve and experienced cell experiments, as well as the platform absent of cells, it is evident that the portion of BE abundance from non-enzymatic degradation does not entirely explain the significant increase in BE during the cocaine exposure steps in the experienced cells, indicating the response is due to a unique exometabolomic profile of T cells with prior cocaine exposure. Further analysis of cellular memory of cocaine exposure is warranted based upon these findings.

Acknowledgements

Financial support for this work was provided by the NIH (R01GM092218 and RC2DA028981), the US Defense Threat Reduction Agency (HDTRA-09-1-0013), the Vanderbilt University College of Arts and Sciences, the Vanderbilt Institute of Chemical Biology, and the Vanderbilt Institute for Integrative Biosystems Research and Education. We thank Allison Price for her editorial assistance.

CHAPTER V

CONCLUSIONS AND FUTURE DIRECTIONS

As stated previously, systems biology seeks to describe the function of a biological system using a holistic, multiscale approach. This approach encompasses the analyses of molecular classes such as the genome, transcriptome, proteome, and metabolome (among others) of a biological system. Systems biology asserts that while understanding genes and proteins is important, the most important aspects going forward are more closely related to the system's network structure and network dynamics.¹ Researchers of systems biology have adopted a hybrid discovery-driven/hypothesis-driven approach to meet these challenges. The first step of this proposed approach is to define all of the components in the system. Then, by systematically perturbing this system, while monitoring all of these components, one is able to use computational biological methods to generate a network structure model of what is observed. This model will define all components of the system in terms of their mathematical relationship with all other components. With this model in hand the researcher/computational method generates a new perturbation that best tests that network structure model. From here, subsequently more refined models are produced until all perturbation reactions can be justified by the model.²

The system described in this text currently boasts the ability to measure dynamic biomolecular signals with a detector that is both highly sensitive and has a broad identity detection range. We have demonstrated the ability of the cell-trapping microfluidics to precisely control the microenvironment and the IM-MS's ability to precisely monitor this control.

We are currently automating this experiment for a “robot scientist” approach^{420,421} with closed-loop control and symbolic regression of the underlying metabolic dynamical equations.^{422,423} An automated microformulator will assemble on demand media whose various components and additional stimuli or toxins are stored separately and can be supplied independently or in combination with one another. Ultimately both the control of the microformulator and the quantitative analysis of the data will be provided through machine-learning algorithms developed by Lipson et al. at Cornell.⁴²²⁻⁴²⁴ Their self-modeling algorithm interprets the media components/stimuli as variable inputs and monitors the mass and other biological signals as outputs. Once the first data set is sent electronically from our platform to Cornell the algorithm will interpret the data and identify candidate models for the biological system’s metabolic network dynamics. The algorithm will then select a set of media conditions which it determines would best discriminate between the candidate models. This media condition command will then be relayed back to the microformulator and the new media mixture is supplied to the cell population for the next experiment, thus producing a self-investigating robot scientist that derives a model of the metabolic or signaling network under investigation (Fig. 5.1). With the present microfluidic-IM-MS platform running in tandem with feedback control and self-learning algorithms as shown in Figure 5.1, this experiment will begin to collect data and make true systems biology measurements.

Alterations to trap designs could easily make the system amenable to many different types of studies. One study that is of particular interest involves the use of differential, multiplexed IM-MS data interpretation. Figure 5.2 displays a microfluidic chip design which allows for the trapping of two different cell populations to investigate paracrine and autocrine signaling. Media is provided to the system through the left-most inlet. The first outlet allows for desalting and IM-MS characterization of any background contributions from the media

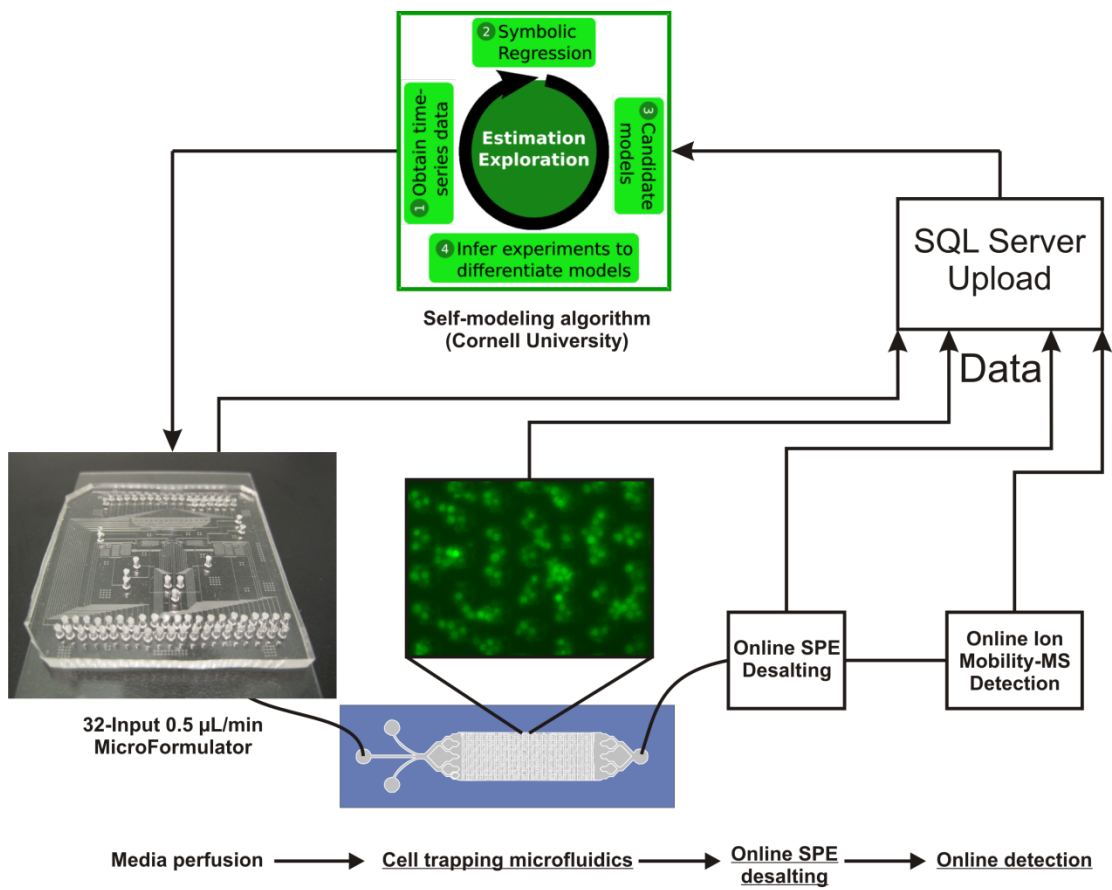


Figure 5.1. Robot scientist schematic. In this proposed experiment a microfluidic device, sustaining a live cell culture and under inspection by a microscope, is perfused with cell culture medium from a MicroFormulator. The MicroFormulator is able to mix and perfuse up to 32 different solutions to produce unique combinations of medium components and/or cellular stimuli (*e.g.*, toxins, therapeutics). The output media from the device is run through the automated online dual-column desalter and subsequently analyzed by online IM-MS. The data collected from all components of the system (*i.e.*, the MicroFormulator, the microscope over the microfluidic device, the online desalter, and the IM-MS) is sent to Cornell through an SQL-enabled server. Cornell then performs its estimation exploration algorithm on the data to generate system models. The algorithm then sends out the next set of media conditions to the MicroFormulator. These conditions are chosen to best discriminate between the generated system models.

components. Media, including any added chemical or biological stimuli, flows over the first cell population and induces a response. This effluent is split, with a portion going to the second outlet, where it is desalted and analyzed by IM-MS to determine the differential, cell-induced changes relative to the base media. The other fraction of the first-trap effluent perfuses the second population of cells, and the effluent from this second trap is directed to the third outlet and analyzed to elucidate the cell-to-cell mediated response. All three outlets will be analyzed in real-time by using a custom-built multiplexed 8-channel IM-MS instrument currently under construction. This would allow for continuous sampling of up to 8 flow streams, all of which are handled independently throughout the instrument. This arrangement allows for simultaneous measurement of seven experimental channels and one control. Special software packages can be used to explore differential signals to easily determine which species are being produced as a result of being directly downstream of a different cell population.

There are numerous applications when one considers the various different cell types that can be sustained by this platform. Some of the applications this platform has been proposed to explore include everything from testing immune cells for long-term drug memory effects to diagnosing chemical and biochemical warfare agent exposure using pre-symptomatic exometabolome signatures. Additionally applications involving personalized medicine have been proposed. In these regards one could extract a cellular sample from a patient and (after isolating the appropriate cell type) expose these cells to the therapeutic in question and determine the patient's specific reaction to the treatment. This could be especially useful for chemotherapeutic prescriptions where oftentimes cocktails of chemotherapeutics are prescribed in hopes that one will have a beneficial effect. Meanwhile all the therapeutics that had no beneficial effects are potentially causing many side effects and reducing the quality of life for that patient.

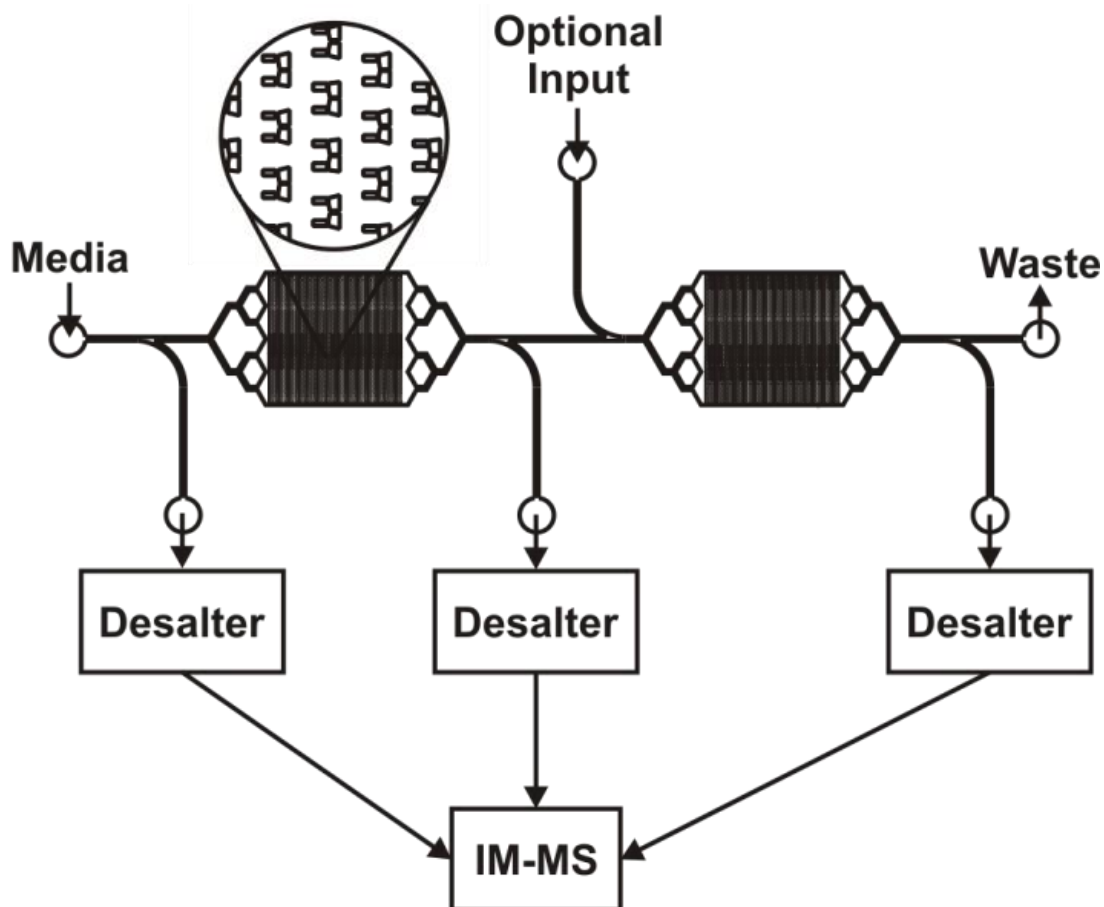


Figure 5.2. An example of a trap currently under development. This device will be used to perform differential studies whereby two cell populations can be probed simultaneously. Media will be supplied through the first inlet with a small portion running through the desalter and into the IM-MS to provide a control sample. Any paracrine or autocrine signaling material secreted by the first cell population would perfuse the second population, with a small fraction being collected by the second outlet. Finally the resultant secreted material from the second population would be analyzed through use of the third outlet port. These three signals could be analyzed in a differential manner to easily identify unique peaks in each effluent. Simultaneous IM-MS analysis could be achieved using a multiple nano-spray, multiple drift tube design as described in the text. Reprinted from reference 312.

With the platform designed, built and proven to be working for simple studies, the immediate tasks ahead will involve reducing the idiosyncratic logistical difficulties that tend to stymie progress and often lead to unproductive experiments. In order to most expediently overcome these challenges, the reader is directed to Appendix C.

Acknowledgements

Financial support for this work was provided by the Vanderbilt University College of Arts and Science, the Vanderbilt Institute for Integrative Biosystems Research and Education, the Vanderbilt Institute of Chemical Biology, the US Defense Threat Reduction Agency (HDTRA-09-1-0013), the NIH National Institute on Drug Abuse (RC2DA028981), the National Academies Keck Futures Initiative, Ionwerks Inc., and Waters Corp. We thank Todd Graham and Anthony Weil for their advice and assistance with the yeast studies, and Hod Lipson and Michael Schmidt for their guidance on machine learning.

APPENDIX A

ADAPTED REFERENCES

Portions of the work in the previous chapters are adapted from the following references.

CHAPTER I:

- McLean, J. A., Fenn, L. S. & Enders, J. R. Structurally Selective Imaging Mass Spectrometry by Imaging Ion Mobility-Mass Spectrometry. In *Mass Spectrometry Imaging: Principles and Protocols (Methods in Molecular Biology)* Vol. 656 (eds S. S. Rubakhin & J. V. Sweedler) 363-383 (Springer, 2010).
- Enders, J. R., Kliman, M., Sundarapandian, S. & McLean, J. A. Peptide and Protein Analysis Using Ion Mobility–Mass Spectrometry. In *Protein and Peptide Mass Spectrometry in Drug Discovery* (eds Michael L. Gross, Guodong Chen, & Birendra Pramanik) 139-174 (John Wiley & Sons, Inc., 2011).
- Enders, J. R. & McLean, J. A. Chiral and structural analysis of biomolecules using mass spectrometry and ion mobility-mass spectrometry. *Chirality* **21**, E253-E264 (2009).
- Enders, J. R., Marasco, C. C., Kole, A., Nguyen, B., Sevugarajan, S., Seale, K. T., Wikswow, J. P. & McLean, J. A. Towards monitoring real-time cellular response using an integrated microfluidics-matrix assisted laser desorption ionisation/nanoelectrospray ionisation-ion mobility-mass spectrometry platform. *IET Systems Biology* **4**, 416-427, (2010).

CHAPTER II

- Enders, J. R., Marasco, C. C., Kole, A., Nguyen, B., Sevugarajan, S., Seale, K. T., Wikswow, J. P. & McLean, J. A. Towards monitoring real-time cellular response using an integrated microfluidics-matrix assisted laser desorption ionisation/nanoelectrospray ionisation-ion mobility-mass spectrometry platform. *IET Systems Biology* **4**, 416-427, (2010).
- Enders, J. R., Goodwin, C. R., Marasco, C. C., Seale, K. T., Wikswow, J. P. & McLean, J. A. Advanced Structural Mass Spectrometry for Systems Biology: Pulling the Needles from Haystacks. *Current Trends in Mass Spectrometry* July, 18-23, (2011).

CHAPTER III

- Enders, J. R., Marasco, C. C., Wikswow, J. P. & McLean, J. A. A Dual-Column Solid Phase Extraction Strategy for Online Collection and Preparation of Continuously Flowing Effluent Streams for Mass Spectrometry. Submitted to *Analytical Chemistry*.

CHAPTER IV

- Marasco, C. C., Enders J. R., Seale, K. T., McLean, J. A., & Wikswo, J. P. Real-Time Cellular Exometabolome Analysis with a Microfluidic-Mass Spectrometry Platform. In preparation for submission to *PLoS One*.

CHAPTER V

- Enders, J. R., Marasco, C. C., Kole, A., Nguyen, B., Sevugarajan, S., Seale, K. T., Wikswo, J. P. & McLean, J. A. Towards monitoring real-time cellular response using an integrated microfluidics-matrix assisted laser desorption ionisation/nanoelectrospray ionisation-ion mobility-mass spectrometry platform. *IET Systems Biology* 4, 416-427, (2010).

APPENDIX B
IMAGING MS PROTOCOL

Materials

1. Sample prepared for MALDI analysis (thin tissue section washed, fixed to MALDI plate, and MALDI matrix applied).

2. Mass and drift tube IM standards/calibrants. Mass standards correspond to peptides and proteins bracketing the mass range of interest. Ion mobility structural standards for DTIM are typically C₆₀ and C₇₀ fullerenes, because they exist in one structural form. These can be used for evaluating DTIM resolution and for day-to-day evaluation of instrument performance. Additionally, fullerenes can be used as mass standards as they are structurally separated from biomolecules in conformation space and provide a wide range of gas-phase reaction products resulting in peaks spanning a large mass range in increments of 24 Da. To validate gas pressure in DTIM, typically the peptide bradykinin (RPPGFSPFR) is used to compare collision cross section measurement with the accepted value of $242 \pm 2 \text{ \AA}^2$.²⁵ Bradykinin can be mixed with matrix of choice or a 1 mg/ml standard solution in H₂O can be combined 1:1 v/v with 20 mg/mL α -cyano-4-hydroxycinnamic acid in 50% methanol. Both calibrants can be applied to MALDI plate using the dried droplet method.⁴²⁵

3. Traveling wave IM standards/calibrants. As discussed previously, estimated collision cross sections obtained by TWIM require internal standards with corresponding absolute collision cross section values obtained using DTIM. Published absolute collision cross sections can be

obtained from several published databases, including (i) peptide collision cross sections determined by ESI,^{128,187} (ii) intact protein collision cross sections determined by ESI,¹⁵⁵ (iii) peptide collision cross sections determined by MALDI,⁶⁶ and (iv) biologically relevant carbohydrate, lipid, and oligonucleotide collision cross sections determined by MALDI.²²⁴

Methods

Performing Collision Cross Section Measurements Using DTIM

1. In order to take measurements, the samples for imaging (tissue, etc.) should be prepared the same as for conventional imaging MALDI-MS. Note: typically ionization is performed at the pressure of the DTIM (*e.g.*, 1–10 Torr), which results in moderate pressure MALDI. Thus some collisional cooling typically takes place after ionization and can result in matrix-adducted and cluster species. These can be dissociated prior to DTIM by performing injected ion experiments. Furthermore, matrix optimization may be required. One effect of moderate pressure MALDI that we have observed is that higher ion currents can be achieved at slightly lower matrix-to-analyte ratios (*i.e.*, 1,000–100:1) than those used in high-vacuum MALDI (*i.e.*, 10,000–1,000:1).

2. Following insertion of the sample target into the instrument, mass and ion mobility standard/calibrants are measured. In particular, to MALDI-IM-MS methods the laser pulse serves as the start signal (t_0) for measuring the IM arrival time distribution (t_{atd}). These time distinctions are necessary for the calculations in Step 4.

3. Following separation in the IM drift cell filled with an inert gas (1–10 Torr), ions are directed through a skimming and differential pumping region where the pressure is reduced from 1–10 to $\sim 10^{-8}$ Torr for mass analysis in the orthogonal TOFMS. The stop time for t_{atd} corresponds to

the ion injection time for the TOFMS measurement. Note: as developed in more detail in the theory section, typically helium is used because of its low mass and low polarizability relative to other inert gases. However, other drift gases or drift gas additives can be used to promote long-range interactions between the ion and drift gas. This is analogous to tuning selectivity in HPLC by changing the mobile or stationary phase that is used.

4. To perform the calculations as described in Chapter 1 (*e.g.*, equation [4]) the arrival time distribution must be corrected for time spent in regions outside of the drift cell (*i.e.*, time spent traversing from the MALDI plate into the drift cell, in skimming and differential pumping regions, and ion optic regions prior to the source of the TOFMS). This will result in the drift time (t_d) of the ions within the IM drift cell used in the calculation of collision cross section:

$$t_d = t_{atd} - t_{dte}$$

5. To determine the value of t_{dte} (*i.e.*, the drift time correction factor), IM separations are performed by varying the voltage across the drift cell while maintaining all other experimental parameters constant. The arrival time distribution measured at each drift voltage is then plotted versus the inverse of drift voltage ($1/V$). Provided the range of voltages used maintains ion separations under low field conditions, this plot will result in a linear correlation. If non-linearity is observed, a calculation of the low-field limit should be performed, because curvature in this plot indicates that mobility is not constant over the voltage range used. For electrostatic fields higher than the low-field limit, the ion velocity distribution depends less strongly on the temperature of the separation and the mean ion energy increases as it traverses the drift region. Consequently, K is no longer constant and depends on the specific ratio of the

electrostatic field to the gas number density (E/N) (see reference 50 for a derivation of calculating the low-field limit for a particular analyte). A linear regression of this data results in a y-intercept corresponding to $t_{d,c}$. The y-intercept of this plot corresponds to $t_{d,c}$ because it represents the limit of $t_d \rightarrow 0$ at infinite drift cell voltage. Also note that the accuracy with which this correction should be made is more important for shorter drift times and its significance is less important at longer drift times. For example, in fast separations as described for imaging IM-MS experiments the values of $t_{d,c}$ can approach the relative magnitude of t_d . Preferably at least five voltages should be used to define this line although for high-precision measurements as many voltages as is practical should be used. For the most accurate results, the drift time correction should be evaluated for each component in the IM profile. The motivation for evaluating individual drift time corrections arises from additional ion–neutral collisions in the differential pumping regions at the entrance and/or exit of the IM drift cell. In these regions the gas dynamics typically transition from viscous to molecular flow, *e.g.*, at the exit aperture of the drift cell at 1–10 Torr to the high vacuum ($\sim 10^{-8}$ Torr) of the mass spectrometer, respectively.

6. After the t_d has been determined from the t_{atd} , it can now be used to calculate the collision cross section, Ω , of the ion of interest through the equation [4]. Note that the equation for calculating collision cross section is derived from classical electrodynamics, and as such, great care should be exercised in the dimensionality of the units used. Specifically, the units for E should be expressed in CGS Gaussian units, *i.e.*, statvolts cm^{-1} , where 1 statvolt equals 299.79 V. Note that statvolts cm^{-1} is equivalent to statcoulombs cm^{-2} and that elementary charge, e , is 4.80×10^{-10} statcoulombs. By comparing empirically determined cross sections with theoretical results, it has been shown that the hard-sphere approximation is best suited for analytes larger than *ca.* 1,000 Da, which is typically the size range in which many biological measurements are

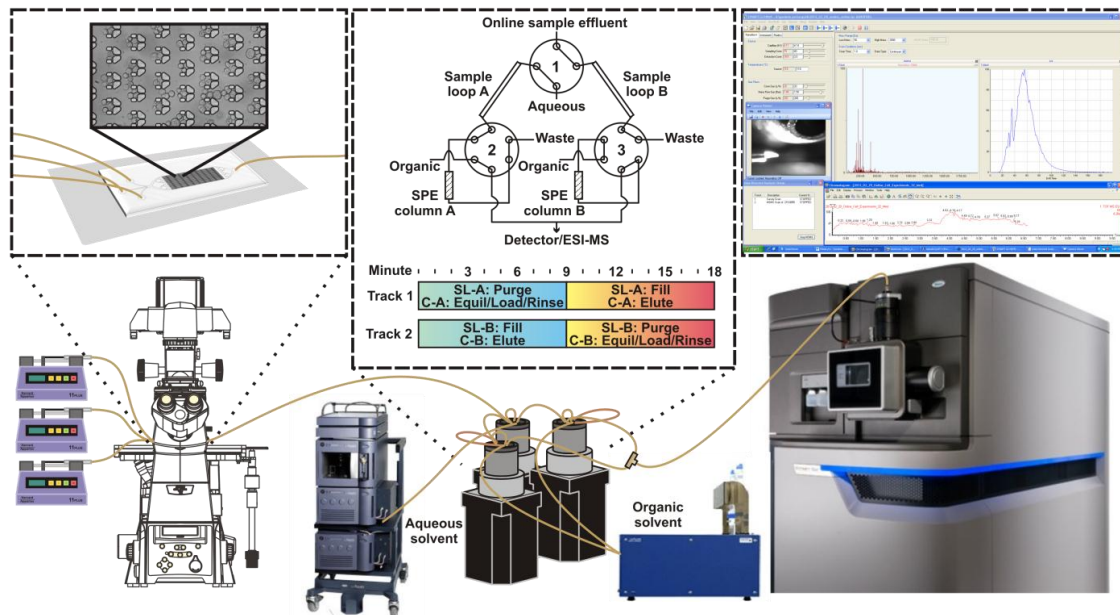
made. However, as the size of the analyte approaches the size scale of the drift gases used for separation, long-range interaction potential between the ion and neutral must be considered for accurate results.^{62,226,228}

7. After the collision cross section has been calculated, this can be further related to the structure using molecular dynamic simulations. More information about these computational methods can be found in more detail in other resources.⁶¹⁻⁶⁴

8. For calculating relative collision cross sections using traveling wave ion mobility-MS, there are two main procedures used which can be found in the literature.^{51,52}

APPENDIX C

PLATFORM TROUBLESHOOTING GUIDE



Liquid Management

Fittings and Connectors. Common thread types of fittings and connectors are shown in Fig. C.1. 10-32 thread type will most often be encountered when using 1/16" PEEK tubing for high-volume/high-flowrate applications. In order to use 10-32 1/16" PEEK connectors (as shown in top left) with 360 µm OD tubing, one must use IDEX Health and Science 'Green sleeves' (IDEX Health and Science F-242X). From IDEX: "Silica SealTight Sleeves are designed to connect 70 µm – 1mm OD capillary tubing to any standard 10-32 coned port normally intended for 1/16" OD tubing. The 1.6" long Silica SealTight sleeves withstand up to 50°C and can be finger tightened to hold up to 5,000 psi when using the NanoTight fittings". Luer lock connections will most often be used to connect 360 µm OD tubing to syringes for liquid perfusion. The use of 5/16-24 fittings involves a male part (*e.g.*, IDEX PN: P-888), which has threads on the outside, a female nut (IDEX PN: P-416), which has threads on the inside, and a ferrule piece (IDEX PN: F-152, for 360 µm OD tubing) which goes between those two parts. The ferrule receives force as the female nut is tightened and in doing so causes the ferrule to crimp the 360 µm OD PEEK or fused silica tubing. Fittings with 2-56 thread are common to VICI-Valco type fittings and will most commonly be used on VICI unions (VICI PN: C360UPK(G)4), and for valve fitting connectors (VICI PN: C360NFPKG, C360PPK, *See Valves*). Thread type 6-32 is found on coned nuts (*e.g.*, IDEX PN: F-124S) and is similar to ferrules (F-152) in the sense that it crimps 360 µm tubing directly.

CAUTION: When using connectors on tubing and using finger tightening it is generally not recommended to tighten very strongly when direct connector-to-tubing combinations are used. For example, when using an IDEX P-888 (5/16-24) union, where a PEEK ferrule directly crimps the 360 µm OD tubing, one should tighten just tight enough to not let the tubing pull out under moderate force. Tightening past this point leads to occlusion of the line (especially for PEEK tubing). When using fittings that require a 1/16" sleeve to connect to 360 µm OD tubing, more



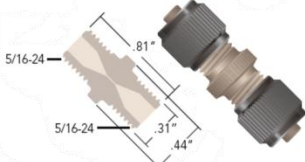

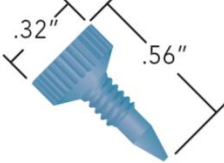
Image	Thread Type	Occurrence
	10-32 (Coned)	IDEX: F-120, P-659, P-770, P-727, P-742
	Luer Lock (Male)	IDEX: P-662, P-659
	5/16-24 (Female nut and male screw)	IDEX: P-662, P-888, P-772, front of Eksigent sytem
	2-56 (Male screws and female union)	VICI: C360UPKG4, C360NFPKG, C360PPK
	6-32	IDEX: F-124S, P-770, M-135, M-520, M-120x, M-130x, M-520

Figure C.1. A table detailing all the different types of threading used.

force can be used to tighten the fitting as the pressure applied must first penetrate the green sleeve before crimping the underlying 360 μm OD tubing.

Syringe Pumps. Media perfusion of microfluidic devices was carried out using a Harvard Apparatus Model '11' Plus Dual Syringe Pump with Serial Communication (MA1-70-2212). The syringe pumps drive the plunger of a syringe at a rate that is directly dependent on the user's inputted syringe inner diameter. Common syringe diameters can be found in the manual. When operating the syringe pumps, the 'pusher block brackets' (small black bars that screw into place to hold the disc shaped end of the syringe plunger) are often removed to provide a more level surface for the edge of the syringe plunger to rest against. Infusion can be performed manually using the pump's interface and LED screen, or automatically using the RS-232 data connection cables and either the pump control buttons or a macro written in *NIS Elements*. When operating manually the choice between infusion and withdraw can be selected based on the direction of the " \leftarrow FLOW \rightarrow " button. If operated using software and then disconnected and used manually, occasionally the " \leftarrow FLOW \rightarrow " button can become reversed. When operating the syringe pump it may become customary to press on the pusher block to expedite flow, however, after pressing on the block, the pump driving mechanism will 'kick' back, causing cessation of flow immediately thereafter. Use of syringe retainer is recommended, however, use of the syringe block bracket is not necessary. It is important to be sure the "Infuse limit switch adjuster" is placed at the maximum position (as shown on page 6 of the instruction manual) and tightened often (as use of the pump seems to loosen this adjuster).

Syringes. Commonly, 250 μL (Hamilton 81120 250 μL , Model 1725 TLL) or 500 μL (Hamilton 81220 500 μL , Model 1750 TLL) syringes are used to infuse media through

microfluidic devices. Syringe-to-360 μ m tubing connections are made using a PEEK female luer adapter assembly (IDEX Health and Science, P-662, 5/16-24 thread port connection, 0.006 in thru hole). This results in less leaking than that experienced when using 10-32 PEEK female luer lock adapter (IDEX Health and Science, P-659, 10-32 thread port connection, coned Female).

Tubing. Typically polyether ether ketone (PEEK) tubing is used wherever possible. An OD of 360 μ m with varying ID's (IDEX Health and Science, 1574, 1570, 1573, 1571) will be used for most applications (with 1/16" tubing being required very infrequently). Polymer tubing cutters (IDEX Health and Science, A-327, Standard Polymer Tubing Cutter for 1/16" and 1/8" tubing) are used to cut PEEK tubing to best ensure the severed end is not occluded. A main drawback to PEEK is the fact that noticeably large amounts of sample and biomolecular material have potential to adhere (reversibly and irreversibly) to its surfaces. This has been seen to cause, at times, massive tailing and memory effects. For this reason fused silica is used on sections of long uninterrupted tubing due to the glass's less adherent surface properties. Teflon tubing is available from IDEX as well (PNs: 1930, 1931, 1932, and 1933) in 360 μ m OD and 50-150 μ m IDs. Teflon is recommended as being compatible with all type of solvents, which could lead one to believe that chemical reactivity with this material is low relative to other types of tubing.

Microfluidic Device

Device Design. Microfluidic devices are designed in 2D through the use of AutoCAD or similar computer-aided design software. Designs are compiled by VIIBRE staff engineer (David Schaffer) and sent to Advanced Reproductions for creation of a chrome mask. It can take anywhere from two weeks to several months for a mask to be sent out and to arrive depending on how full the mask design is when drawings are submitted.

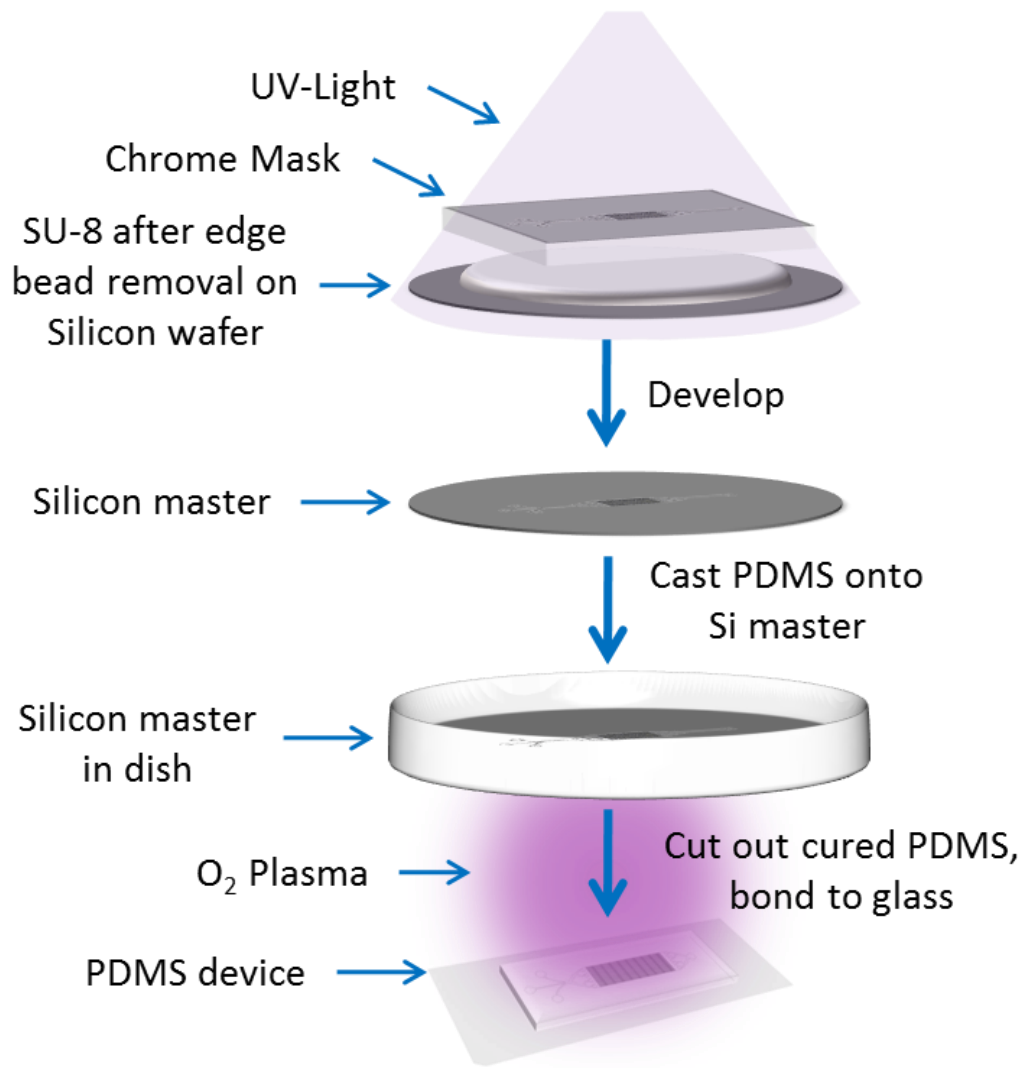


Figure C.2. Photolithography and replica molding diagram.

Photolithography. A master is created from the chrome mask through photolithography techniques. The protocol for a ~12um high T12 trap design such as those on Mask 38iii in the mask repository is as follows (Fig. C.2):

1. Silicon wafers are rinsed with acetone then isopropanol, dried under a stream of nitrogen, dehydration baked for 5 minutes at 180°C and allowed to cool to < 60°C
2. SU-8 2010 is spun on clean wafers for 10 seconds at 500rpm (acceleration of 2) followed by 35 seconds at 2500rpm (acceleration of 5)
3. The wafer is then covered with SU-8, soft baked under a ramped temperature from 50 to 95°C (2 min at 95°C), and allowed to cool to < 60°C
4. The edge bead is removed by spinning under a stream of edge bead remover
5. The mask is positioned over top of the SU-8 coated master with uncovered portions covered by ruby tape and exposed for 20-45 seconds at a 45 J/cm² dose
6. The master is covered, post-exposure baked with a temperature ramp of 180°C/hr, baked for 5 minutes at 95°C, and allowed to cool to < 60°C
7. The master is developed on the spinner for 3 minutes or until rinsing with isopropanol is completely clear
8. The master is hard baked with a temperature ramp of 120°C/hr, baked for 30 minutes at 180°C, and allowed to cool completely

Soft Lithography and Device Silanization. PDMS devices on glass coverslips are constructed through replica molding and silanized with a PEG-silane to prevent non-specific metabolite, peptide and protein adsorption. The protocol is as follows (Fig. C.3):

1. The cooled master is placed in a round petri dish, poured with mixed 10:1 Sylgard 84 elastomer: curing agent (until roughly 3-4mm deep), and degassed under vacuum until bubbles are gone
2. PDMS is allowed to cure for 4 hours at 60°C
3. Patterned areas are cut with a scalpel and removed from the master
4. Inlet and outlet ports are created by inserting a sharpened biopsy punch through the cut PDMS, patterned side up, with a sacrificial PDMS layer underneath to protect the punch, NOTE: Cores should be removed after each punch and can be aided by keeping a piece of wire inserted into the shaft of the punch stopping a few millimeters before the tip
5. Both sides of the PDMS are cleaned with tape and coverslips are cleaned with acetone and IPA
6. The device is placed patterned side up along with one of the coverslips on a 2"x3" glass slide and placed in the chamber of the Harrick Plasma cleaner *ca.* 3 inches from the back of the chamber
7. Device and coverslip are plasma activated under vacuum for 30-45 seconds, removed from the chamber and the device is placed patterned side down on the coverslip, NOTE: Tweezers can be used to lightly press on the top of the PDMS to assist with bonding if needed
8. Immediately after bonding, the PEG-Silane solution (2% in 95% EtOH, 5% H₂O, 10mM Acetic Acid) is flown through the device from the outlet until it just comes out the inlets
9. Devices are allowed to incubate at room temperature for at least 10 minutes and are then rinsed with EtOH and H₂O
10. Devices are incubated at 110°C for 10 minutes and allowed to cool

Priming. Prior to experiment, the microfluidic device is primed by first putting a drop of methanol on the outlet port, and allowing it to move by capillary action through the device. If it does not easily move, gently flick one end of the cover slip against the bench top. Devices that do not easily allow ethanol to flow in this way should not be used. The outlet can then be

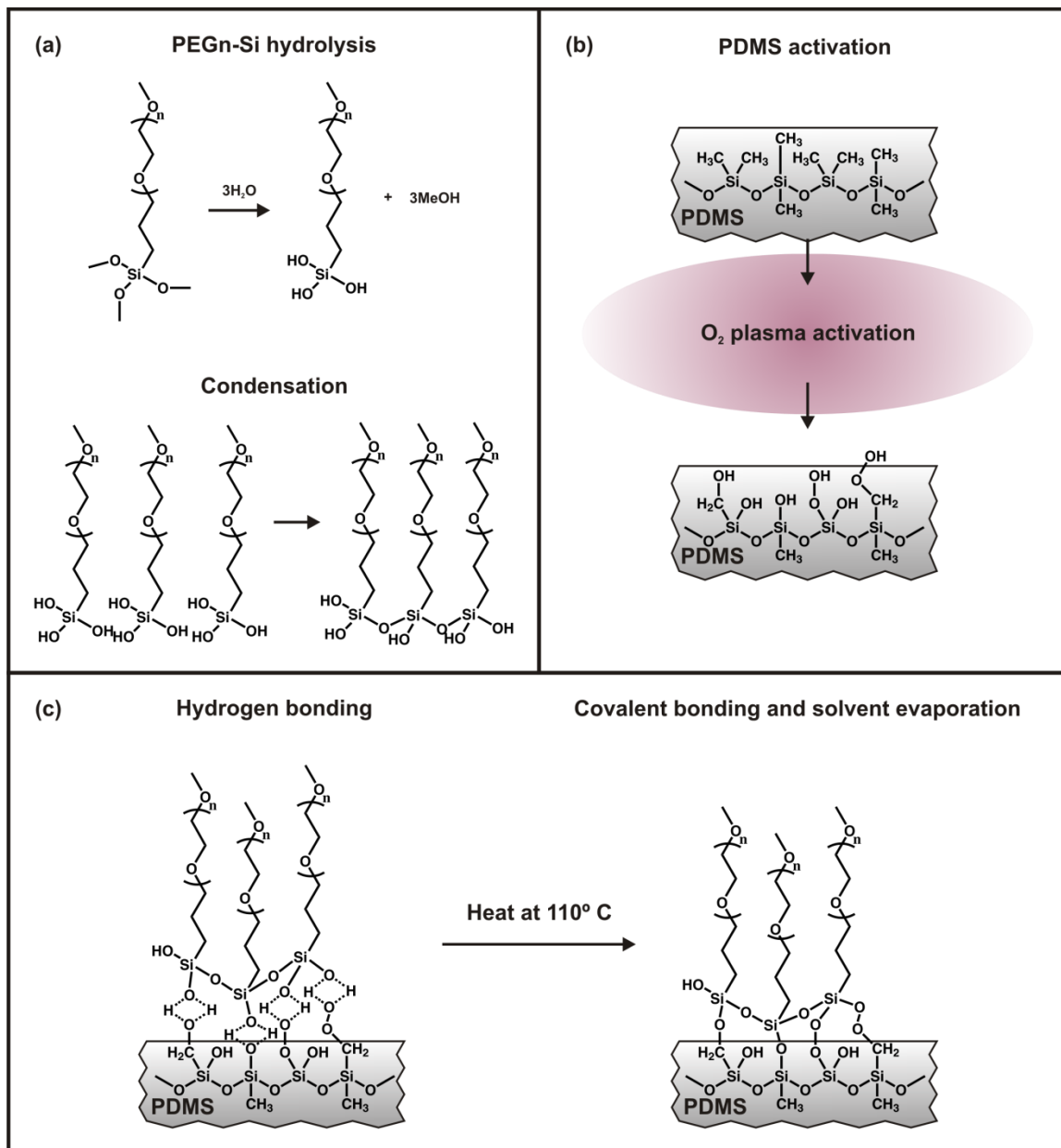


Figure C.3. PDMS silanization procedure.

intubated with PEEK tubing attached to a syringe containing the basic media for the experiment (*i.e.* RPMI or running buffer) and the plunger can be depressed until beads of media form on the inlets. The outlet and inlets should be covered with a drop of the same media before removing the PEEK tubing from the outlet.

Cells

Culture. Cells should be cultured according to manufacturer's instructions. Techniques will not be addressed herein as many cell culture resources exist.

Loading. An aliquot of cells is obtained just prior to experiment. For non-adherent cells, ~500uL of cell suspension is dispensed into a clear or light-colored microcentrifuge tube (dark colors are difficult to see through under the microscope). These cells can be used almost any day during the culturing procedure and volume dispensed adjusted to account for changing cell density. For adherent cells, sub-culturing procedures are followed to detach cells from surfaces of the culture flask. When cell suspensions are transferred to a centrifuge tube for trypsin removal, an aliquot is placed in an additional tube that is destined for the experiment. Cells are centrifuged according to culture instructions (typically low speed, ~100xg, is best). Media/trypsin is removed from the cell pellet and aliquot for the experiment is resuspended in desired media at the desired cell density (recommended at full density of split flask or greater). The cell suspension is transferred to a clear or light-colored microcentrifuge tube. For either adherent or non-adherent cell suspensions, aliquots are centrifuged at 1200 rpm for 2 minutes in McLean lab centrifuge (Eppendorf Minispin Plus) just prior to cell loading.

The tube of pelleted cells is placed in the orange foam tube holder and onto the stage insert, fitting over the four pegs on the insert. The microscope and software are both ready for

use (see below for instructions) and all syringes have been prepared and set to run forward on syringe pumps. The DIC optical configuration in NIS Elements is selected and the Ti-pad is checked for the halogen shutter to be open with the lamp in the on position and at 3V. The light will be physical visible if settings are correct. The stage is then positioned with the light immediately overtop of the open tube containing cells. Looking into the eye piece, the focus is adjusted to bring some portion of cells into focus. This can be tricky at first, but with experience it becomes easy to quickly bring cells into focus. The light path can be switched from the eye piece to the camera and play button hit to view the cells on the monitor. The end of the PEEK tubing into which the cells are to be loaded is then placed in the microcentrifuge tube (fluid should always be exiting the tubing when inserting into the cells to avoid any air bubbles) and pushed down towards the bottom to contact the cell pellet. It is useful to put a small kink in the tubing *ca.* 1.5 in from the end, but keep the bend <90 degrees. The plunger of the syringe attached to this tubing can be clamped to the pusher and the pump flow direction can then be reversed to withdraw cells into the PEEK tubing. There is a delay when the flow is reversed before suction occurs. For a flow rate of 500nL/min, it is around 1.5 minutes. The PEEK tubing should be constantly held in order to manipulate the location of the end relative to the cells. It is helpful during the loading process to adjust the exposure as needed and to move in and out of focus of the tubing end in order to view moving cells. Once cell movement into the tube is visually confirmed, loading continues for 3 minutes at 500nL/min with a 2 ft PEEK tubing length with an inner diameter of 50 μ m. If the tubing length, ID or the flow rate is altered, the amount of time for loading should be recalculated. Once the desired loading time has been achieved, the pump is reversed and plunger unclamped from the pusher. Again, there will be a delay before the flow is in the forward direction. During this time, the device should be intubated with tubing from the remaining forward flowing syringes. If the cells need to avoid the contents of the

syringe, the pump can be stopped right before the tubing is intubated, but a drop of liquid should be on the end while inserting the tubing to prevent air bubbles. The tubing containing the cells can then be intubated as well to begin the loading. The outlet tubing is also connected at this time. Note that if a given pump is stopped while cells are loaded into the device, some back flow of cells into those lines may occur. One way to prevent this is by putting crimped plugs of PEEK tubing into the remainder of the inlet ports during loading, then intubating with syringe tubing post-cell loading. Cells are allowed to load the device completely while the device is carefully moved into the stage incubator. Outlet tubing should not be connected until the rate of cells exiting the device has slowed significantly (Fig. C.4).

Microscopy

Nikon Eclipse Ti. The startup procedure must be followed or connection to the microscope/camera will not work correctly. Startup procedure is as follows:

1. If the computer has been shut down or logged off, it is started, logged into and allowed to load completely.
2. Power to all microscope components (except for the mercury arc lamp and the camera) is achieved by turning on the power strip on the back right of the cart.
3. If fluorescence images are to be taken, the mercury arc lamp power must be turned on separately from its power switch.
4. Once the initialization procedure has completed, the camera can be turned on from its power switch.
5. NIS Elements is then started.

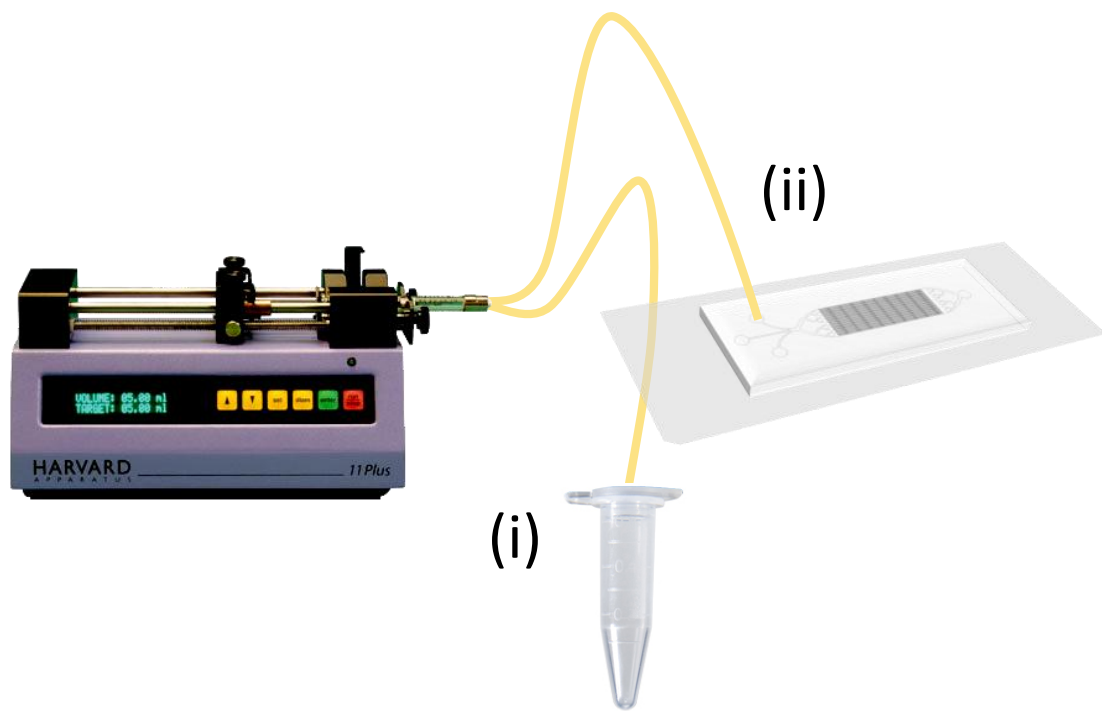


Figure C.4. Cell loading diagram

A common issue results from the software not loading the camera driver. In the event of this error message, close the software, wait and try to reopen again. This problem is just as likely a result of a faulty shut down procedure as it is from the startup procedure. Shut down procedure is as follows:

1. All desired image files are saved.
2. NIS Elements is closed.
3. The camera power is turned off from its specific power switch.
4. If the mercury arc lamp is on, its power switch can be set to off.
5. The power strip is then turned off.

NIS Elements. For detailed instructions on the use and capabilities of NIS Elements, consult the user guide located in the NIS Elements folder.

Incubator. Temperature, gas and humidity control can be achieved using the stage incubator. The gas line with luer lock fitting is attached to the incubator for CO₂ control, the tank turned on and the stop valve and needle valve on the back of the cart are adjusted appropriately. (The end of the tubing can be placed in a beaker filled with water to check the gas flow rate.) Once the device has been intubated and loading has begun, the device is carefully moved onto the stage incubator. It is important to have the stage incubator pressed into place on the stage before transferring the device. The clips are screwed into place to hold the cover slip, the side channels are filled with water to maintain humidity, and the lid of the incubator is placed carefully on top, allowing inlet and outlet tubing to rest between the top and bottom pieces. The incubator channel is then set to 37°C. Once the experiment is completed, the

channel is set to off and the gas turned off. The control box power is turned off with the microscope power strip.

Desalter Apparatus

Inline Filters. Inline filters have been used to prevent cellular debris escaping from the microfluidic device from entering the valves and column setup, where clogging is much more likely and problematic. Two types of inline filters are primarily used: black 0.5 μm PEEK frit inline filters (IDEX PN: M-120X) and natural colored 1 μm SST filter screen (IDEX PN: M-130X). Typically, these filters were replaced every experiment as it can be difficult to assess their level of occlusion.

Eksigent/desalting pumps. An Eksigent Nanoflow Metering System is used to supply the organic-based elution solvent. The Eksigent system is capable of flowing from 10-500 nL/minute from each of four independent channels, all of which are gas driven by 100psi of either air or nitrogen. Typically the organic solvent is perfused through the desalting apparatus at 500 nL/min. This flowrate was chosen to match the flow of the microfluidic bioreactors but also due to typical pressure constraints with regards to downstream columns and frits. To track this pressure, one must create a “Run Manager” flow profile. While this is running the pressure information is automatically collected and displayed on the chart on the main window of the Eksigent software. Maintenance and calibration must be performed routinely to ensure the pumps work efficiently and without the complications of air bubbles.

Waters NanoAcquity UPLC pump. The NanoAcquity pump is used to perfuse the desalting apparatus with aqueous solvent for the purpose of rinsing the columns of salt

contaminants. The NanoAcquity pump is controlled through the Binary Solvent Manager portion of the MassLynx program and set to a flow rate of 0.9 μ L/min in arrangement 2.

Valves. Three 10-port Nanovolume UPLC Valves with 360 μ m fittings, C72MH-4690ED (VICI Valco Instruments Co. Inc., Houston, TX), were used. These valves connect to the computer through a RS-232 daisy chain cable to the “2-position actuator control module”. The “manual controller”, the valve itself and the power supply cable also all connect to this control module (see Figure C.5). It is important to note that there are different models of controller modules and using the incorrect part will cause torque-related valve malfunction.

Columns. Columns are comprised of three components: the fused silica tubing, the chemically interactive silica packing phase, and the frit, which prevents the phase from escaping with the solvent flow. Columns are made from 360 μ m OD fused silica tubing. The ID of the tubing is chosen based on the size of the packing phase particles that are going to be used to pack the column. The packing phase used in these exometabolomic experiments was 3 μ m C18 silica phase (Jupiter 3 μ m C18 300 Å bulk packing phase, PN: 04A-4263, 404951-1, Phenomenex) and typically fused silica with 100 μ m ID and 360 μ m OD. Column frits are made by using the following protocol:

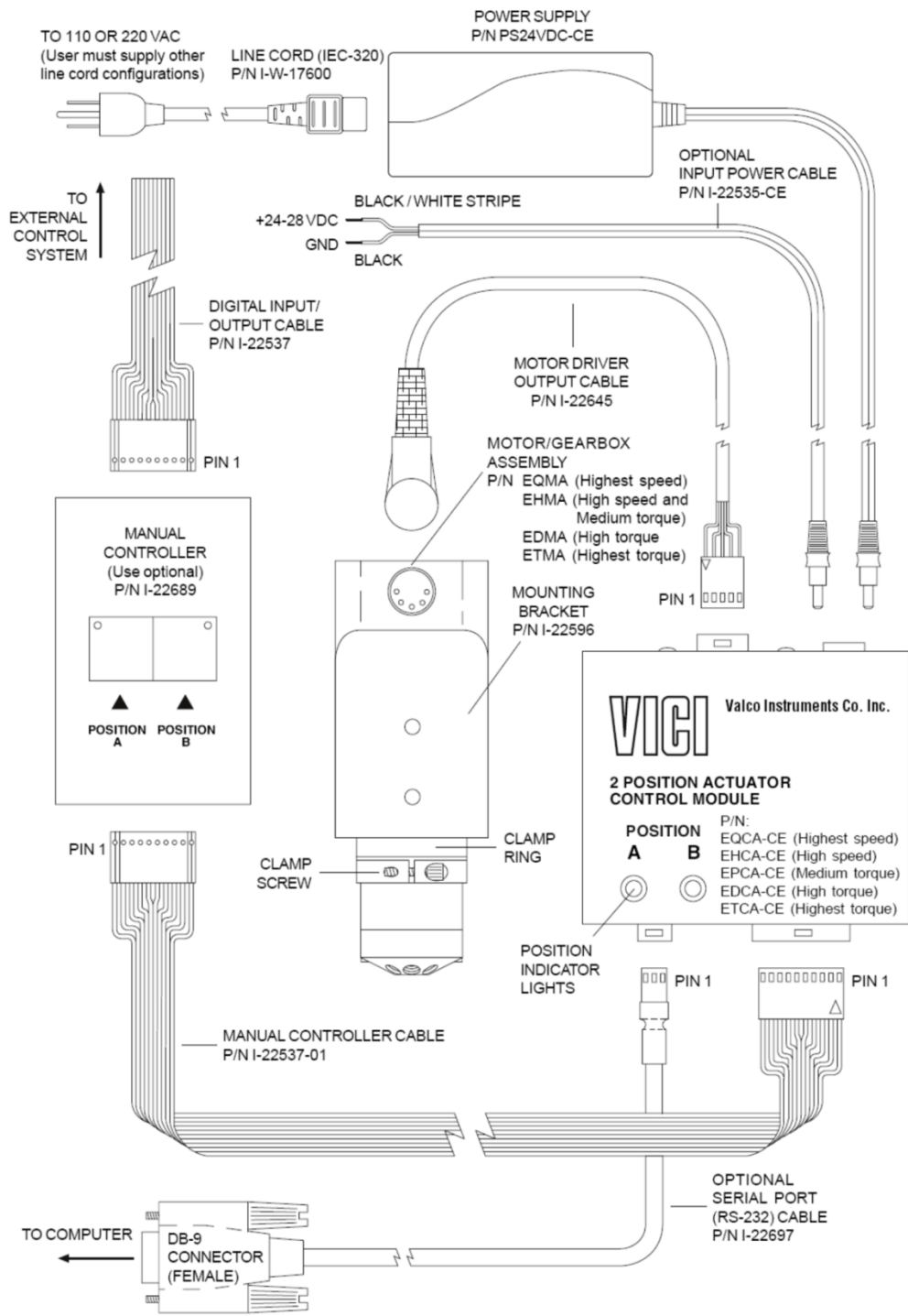


Figure C.5. Wiring and connection diagram for VICI/Valco/Cheminert actuated valves.

1. Mix 170 μL of KASIL (PQ [®]KASIL[®] 1 Potassium Silicate Solution) and 30 μL of formamide (F9037 SIGMA) in an Eppendorf tube. Vortex mixture.
2. Spin mixture down for <2min at a moderate RPM in a benchtop centrifuge. Yields a semi-solid lower layer of unusable polymerized material, and an upper layer of mixed unpolymerized material.
3. Dip pre-cut fused silica tubing into liquid upper layer for ~5-10 seconds. Liquid will rise into tubing due to capillary action.
4. Remove tubing from liquid and, keeping as still as possible, bake the fritted ends under a heating block for >3 hours/overnight at 100°C (Setting of 4.5 (high) on the VWR analog heatblock).
5. Cut frit to a few millimeters or shorter (depending on back pressure desired). Typical length for these experiments was a 1-2mm frit

Columns are bomb loaded using a New Objective Nanobomb apparatus (New Objective PIP-500 Pressure Injection System). The Nanobomb accepts an incoming air/nitrogen pressure of 1000 psi to generate the necessary pressure to drive the beads into the tubing. It is not necessary to use ultra-pure nitrogen as the gas is only used as a pressure source. Follow standard protocol for the Nanobomb and always wear eye protection.

Sample Loop. The sample loops in this experiment were made from fused silica tubing with the dimensions: 360 μm OD and 250 μm ID. This large ID allowed the sample loops to be much shorter.

Desalter Arrangements. There are two primary valve arrangements that have been used to desalt a continuous bioreactor sample stream. The first arrangement is a six-step arrangement, as depicted in Figure C.6, which was employed for multiple years and was used for

collecting most the preliminary data for the system. This cycle provides a constant loading condition, ensuring that all analyte material in the online sample effluent is collected. In addition, contaminants were rinsed from the SPE columns during a purge step which is directed to waste. Valve cycle steps can be scaled in time uniformly to yield a cycle which is better for detecting high frequency oscillations (short step durations) or one which is better for detecting very low abundance analytes (long step durations). Figure C.7(c) outlines the valve switching scheme for online sample preparation. In step 1, the valve orientation was as pictured in Figure C.6, such that SPE column A was loaded with online sample effluent and SPE column B was desalting a sample plug and sending salts to waste. Valve 3 was switched such that SPE column A was receiving sample effluent and SPE column B was eluted and directed towards the MS for ion detection. Because this is the first time through the cycle, column B has not actually been loaded with any analytical material at this time and so this elution is blank. After this, valve 3 was switched so that SPE column B was equilibrated with aqueous solvent in preparation for its subsequent loading step. SPE column A continued to load sample throughout the equilibration of SPE column B. Next, valve 1 was switched such that the online sample effluent was directed to the newly equilibrated SPE column B. SPE column A was purged with water at this step allowing for desalination of the sample collected on the column. Valve 2 switched and SPE column A was eluted with organic solvent, while SPE column B was left in the loading position. Lastly, valve 2 was switched to equilibrate SPE column A and the SPE apparatus started the entire cycle again. This cycle is depicted graphically in Figures C.7 and C.8.

If operated with dynamically varying solvent compositions (*i.e.*, not isocratic), solvent levels can be maintained such that the solvent composition reaching the detector does not experience predominantly aqueous or predominantly organic solvent. These changes in solvent composition have been observed to cause non-ideal ionization conditions at times. This solvent

maintenance as demonstrated in Figure C.8, can be achieved using the “Run Manager” in the Eksigent software. However, while trying to implement these strategies, numerous problems were experienced with regards to timing. Specifically, the file acquisitions system (Waters MassLynx) has an inherent delay between file acquisitions. Similarly, the Eksigent system has inherent delays between “Run Manager” profiles. These two separate delays made coordination of the two timing events very difficult to achieve. The two processes could be lined up to begin with but would eventually drift completely out of phase within a few cycles.

This arrangement suffered from problems associated with back pressure. As aqueous solvent was perfused over the columns, a high back pressure, usually on the order of 2000-3000 psi, was generated immediately preceding the columns. Because there was a direct “line of sight” between the SPE columns and the microfluidics, when the valves switched back to load from the microfluidics, this enormous back pressure plug would travel backwards and cause the PDMS device to delaminate from the glass cover slip.

The second arrangement was designed in response to the frequent problems experienced with back pressure when using the first arrangement. This second arrangement was designed to ensure that the microfluidics never had a direct “line of sight” with the SPE columns. In Figure C.9, it can be seen that the arrangement is almost identical to the previous design except for the incorporation of sample loops. This addition simplified the valve switching scheme required by shortening it to only two steps. To explain the arrangement: sample loops, which were made of 360 μm OD/250 μm ID tubing, were 12.2cm long, providing a sample loop volume of 6 μL . The continuous sample stream was diverted into each sample loop for exactly 9 min at 500 nL/min, thus filling the sample loop 75% of the way. Because water was always flowing through these sample loops immediately prior to sample flow, a plug of 1.5 μL of water preceded each sample effluent plug. This plug served to quickly and roughly equilibrate the

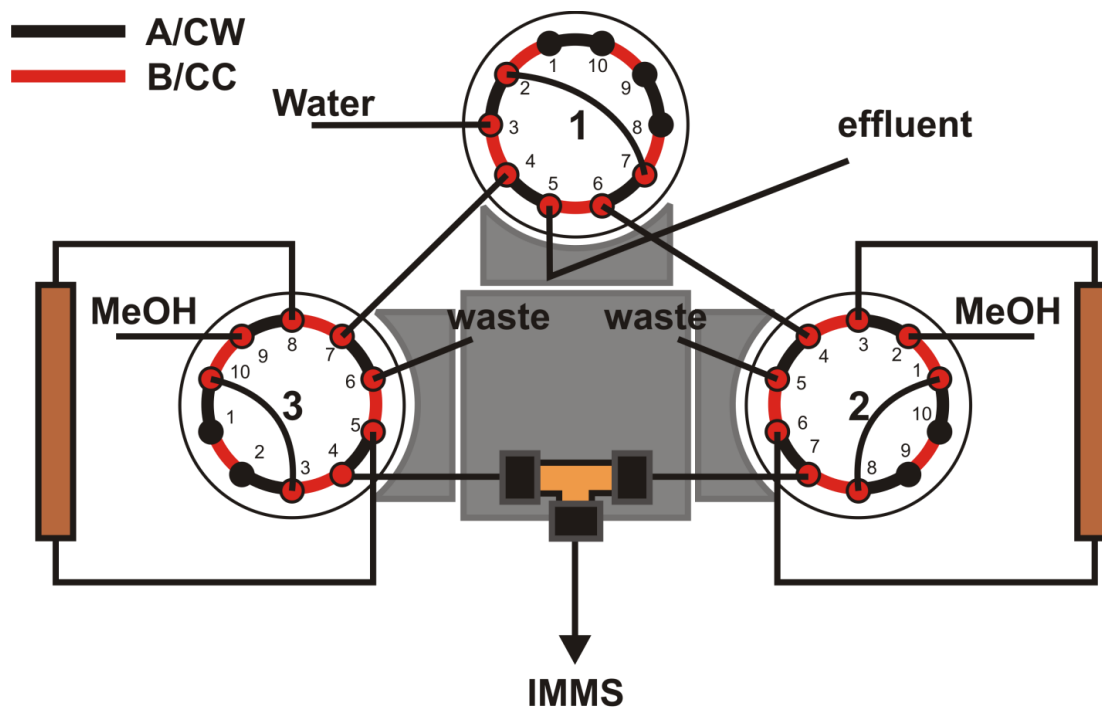
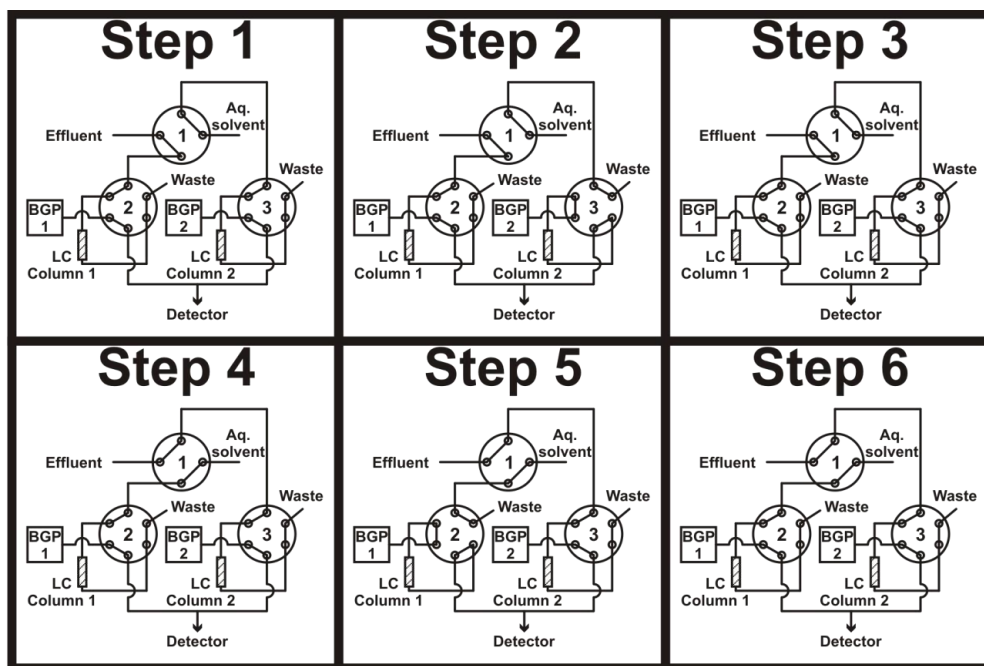


Figure C.6. Valve arrangement 1. This arrangement incorporated a 6-step valve cycle to achieve online SPE desalting. This arrangement was entirely capable of performing online desalting of a continuous sample stream, but suffered from back pressure problems when used for online desalting of PDMS bioreactor effluent.



Valve Positions

(CC - Counter clockwise, CW - Clockwise)

	① Step 1	③ Step 2	③ Step 3	① Step 4	② Step 5	② Step 6
Valve 1						
Valve 2						
Valve 3						

Figure C.7. Stepwise depiction of the 6-step desalting method using valve arrangement 1. The top portion shows the valve positions during each step. The chart in the bottom portion shows a graphical representation of these valve positions during each step, where the number in the circle between each step (at the top of the chart) is indicative of which valve is switching to achieve the next step.

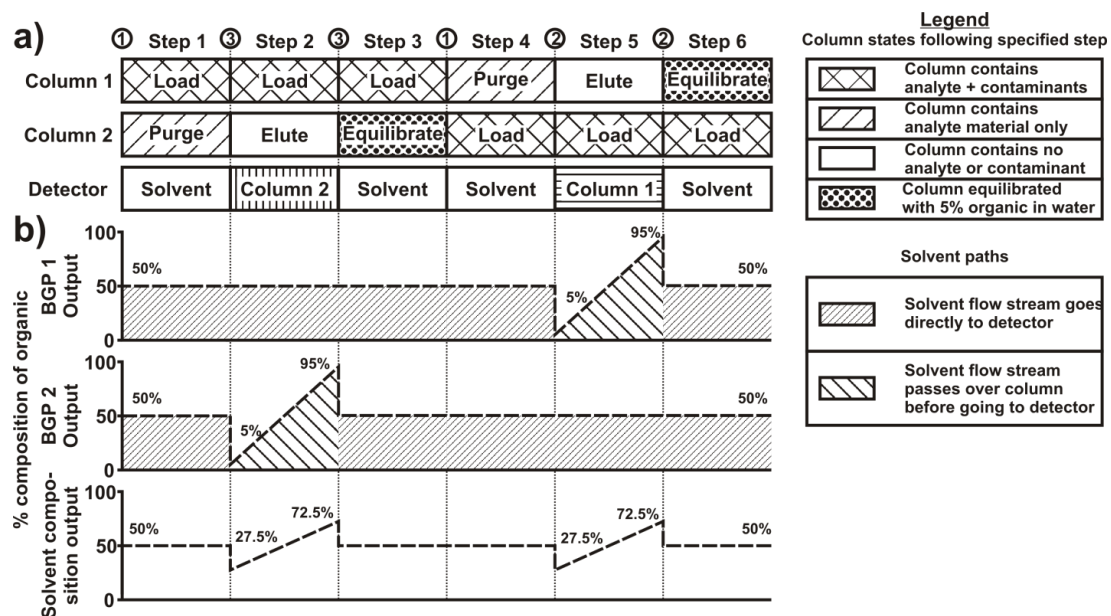


Figure C.8. Example of how valve arrangement 1 may be used in conjunction with automated varying flow, such as can be achieved with the Eksigent pump system.

column with an aqueous solvent. Once the loop was filled to 75% with online sample effluent, the small water plug and sample effluent were passed over the column, using the aqueous solvent line to generate the necessary backpressure. Once the effluent had cleared the sample loop and had been entirely passed over the column, an additional 2.3 min or 2.1 μL of aqueous solvent (H_2O with 0.1% formic acid) was run over the column to serve as the rinsing/purging step to remove residual salts. Following the salt purge, the column was eluted with organic solvent (90% Methanol, 10% H_2O , 0.1% formic acid). Whenever effluent was filling through a sample loop, the other end of the sample loop was open to a waste port. This allowed residual back pressure that may have been generated by the pumping of water over the columns to be alleviated out of the waste port instead of traveling upstream and delaminating the PDMS device. This cycle is depicted graphically in Figure C.10.

Additional arrangements were conceived but never built. The first design is based on valve arrangement 1 except for the inclusion of an analytical column (meant to perform true chromatography, as opposed to SPE) immediately preceding the mass spectrometer (Fig. C.11). This valve has a cycle similar to valve arrangement 1 (Fig. C.12). Importantly, the solvent composition passing over the analytical column would range between 52.5% and 95% organic as indicated in Figure C.13. This arrangement could prove useful for polar compounds which may require more harsh highly organic elution conditions.

Another arrangement that was designed but never built was one that was centered on efficient duty cycle. The basic cycle (from valve arrangement 1) contains 6 cycle steps. Only during two of these steps is there actually analyte material being eluted. This is due to the duration of the preparation process (*i.e.*, equilibrating, eluting, rinsing). By incorporating 6 columns one maximizes instrument analysis time (Fig C.14)

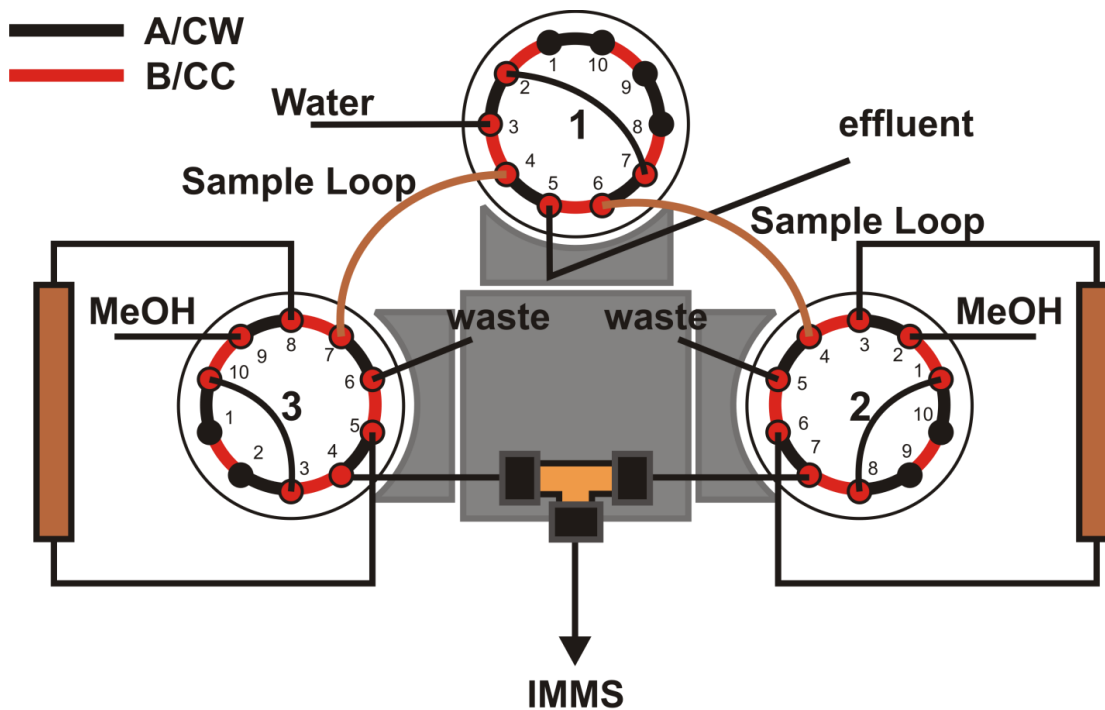
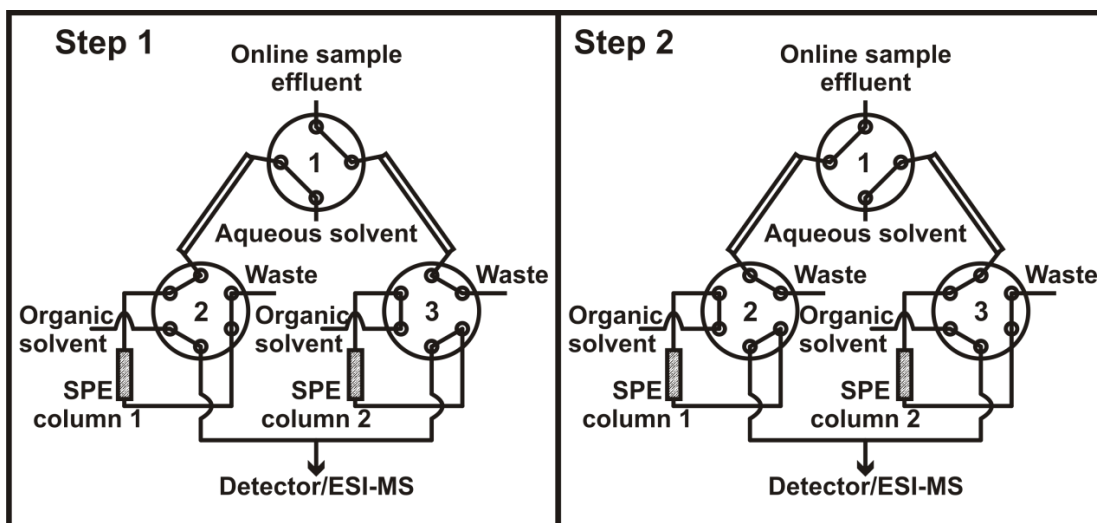


Figure C.9. Valve arrangement 2. This valve arrangement was a simplification of valve arrangement 1 and negated the effects of back pressure on the microfluidics by providing a waste port to vent excessive pressure. This arrangement incorporated a 2-step valve switching cycle to achieve online SPE desalting.



Valve Positions
(CC - Counter clockwise, CW - Clockwise)

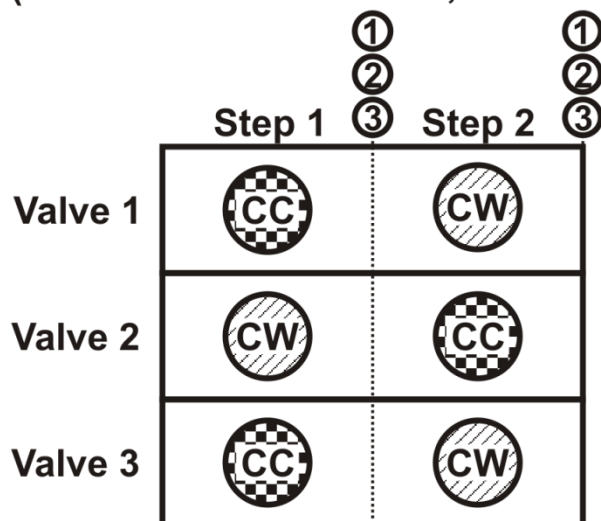
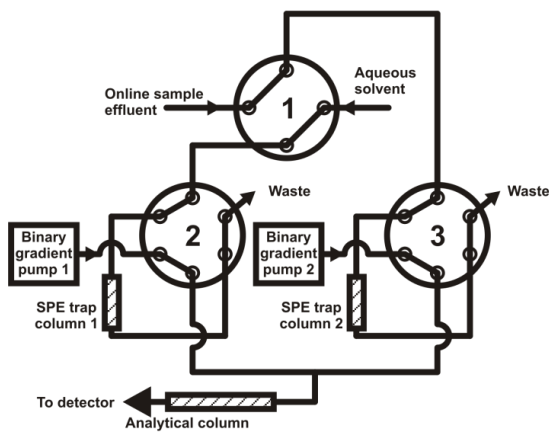


Figure C.10. Stepwise depiction of the 2-step desalting method using valve arrangement 2. The top portion shows the valve positions during each step. The chart in the bottom portion shows a graphical representation of these valve positions during each step, where the number in the circle between each step (at the top of the chart) is indicative of which valve is switching to achieve the next step.

All valves in counter-clockwise (CC) position



All valves in clockwise (CW) position

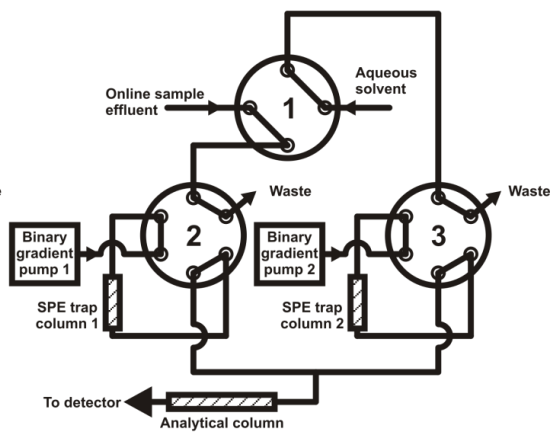
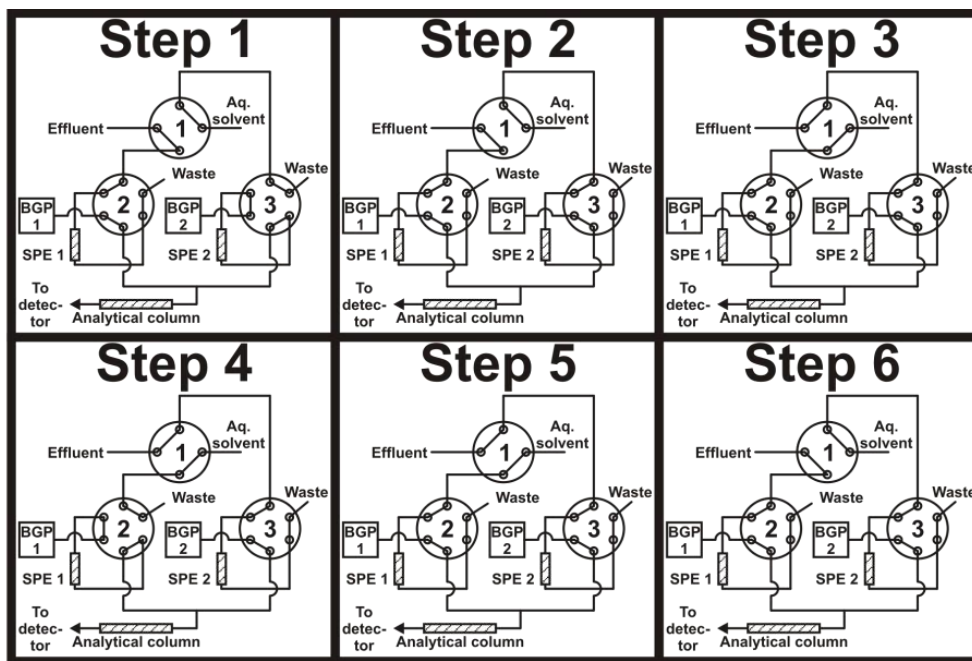


Figure C.11. Valve arrangement 3. Designed but never built due to the unreliable nature of the timing agreement between the Eksigent software and MassLynx program.



Valve Positions

(CC - Counter clockwise, CW - Clockwise)

	③ Step 1	③ Step 2	① Step 3	② Step 4	② Step 5	① Step 6
Valve 1	CW	CW	CC	CC	CC	CW
Valve 2	CC	CC	CC	CW	CC	CC
Valve 3	CW	CC	CC	CC	CC	CC

Figure C.12. Valve cycle steps for valve arrangement 3.

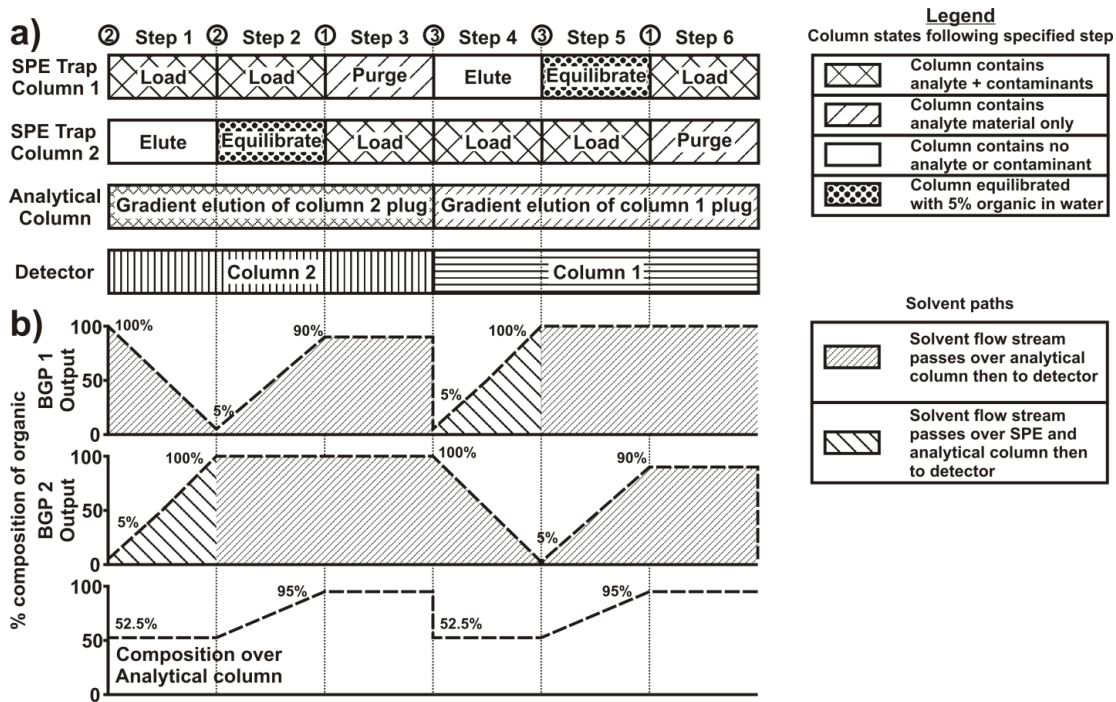


Figure C.13. Depiction of the solvent composition scheme for valve arrangement 3.

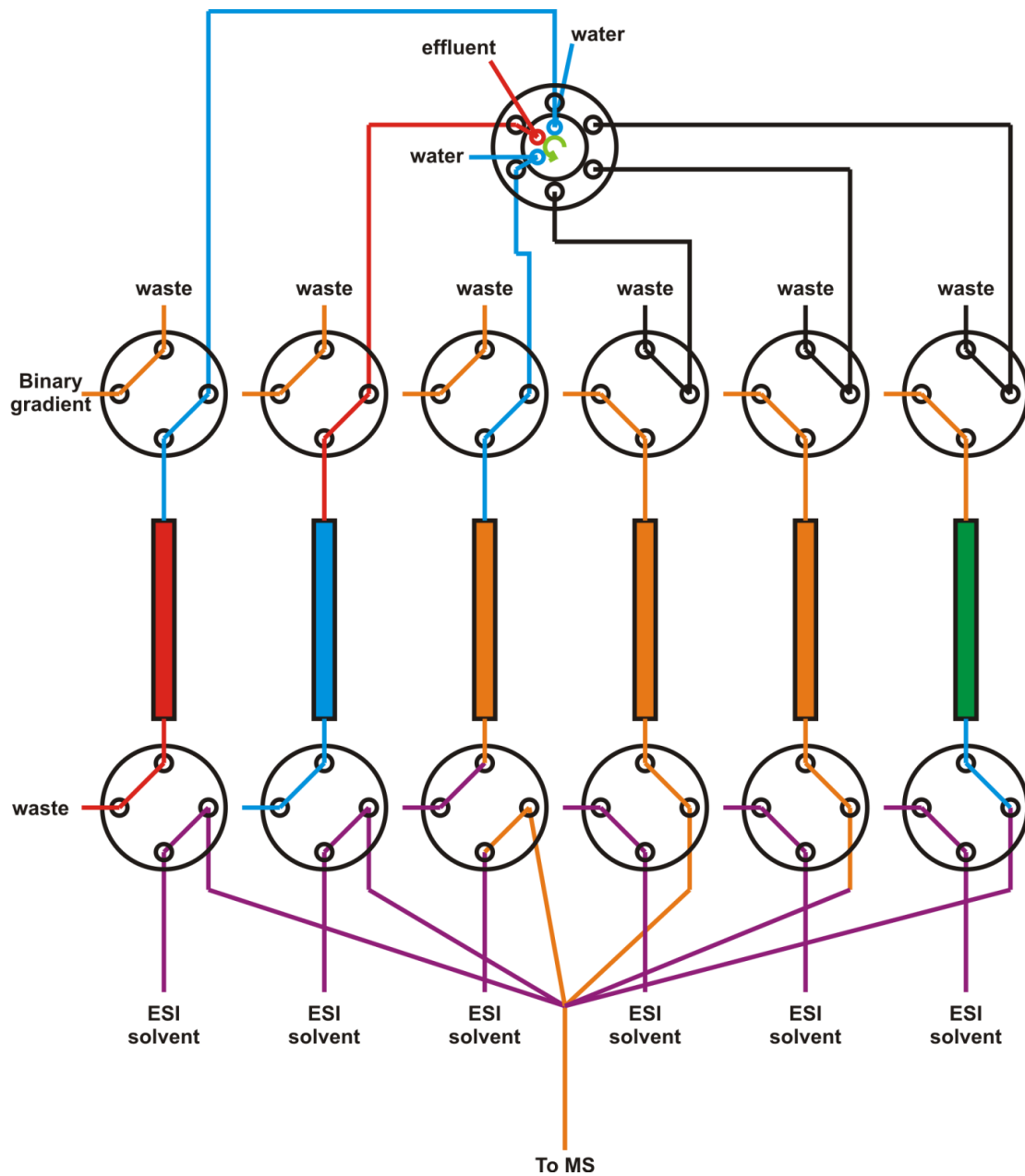


Figure C.14. A valve arrangement incorporating 6 columns. This arrangement was designed but never built.

Mass Spectrometry Data Acquisition

nESI Source. The nano-electrospray ionization (nESI) source is a probe “door” for the Waters Synapt G2 (Fig. C.15). The nESI source can produce a sufficient spray so long as the incoming flow is in the range of 200nL/min to 2 μ L/min. The output line of the online SPE desalter is connected directly to the nESI source. The incoming tube is connected with a PEEK fitting to a stainless steel union. The nanospray capillary connects to the other end of the union. This union and also the nanospray capillary are very susceptible to clogging when analyzing complex sample matrices such as bioreactor effluent.

Sample List. Continuous collection of discrete “files” of data for processing in MarkerLynx is accomplished by creating a sample list within MassLynx, analogous to UPLC type sample collection. Each sample is a set length of continuously running analytes eluted off of the columns. For the medium length sample loops (12.2 cm), an 8.8 minute data file is collected, allowing for delay time between each sample. Analogous data file length for the long sample loops (24.5 cm) is 17.8 minutes. Samples are named chronologically to prevent confusion. Once samples are ready to be acquired, the sample list can be saved and started.

Method File/Data Dependent Analysis. When performing online, real-time analyses, data collection can be quite onerous. In traditional discreet sample analysis, such as might be performed with LC or just by direct infusion, it may be customary to acquire a preliminary data file and search through this file to find the pertinent feature/peaks and then during a second acquisition, set up the instrument to fragment or better accentuate these features/peaks. When performing online, real-time analyses, it can be difficult to setup the instrument to collect the information most pertinent to your study because there is no indication of when this material

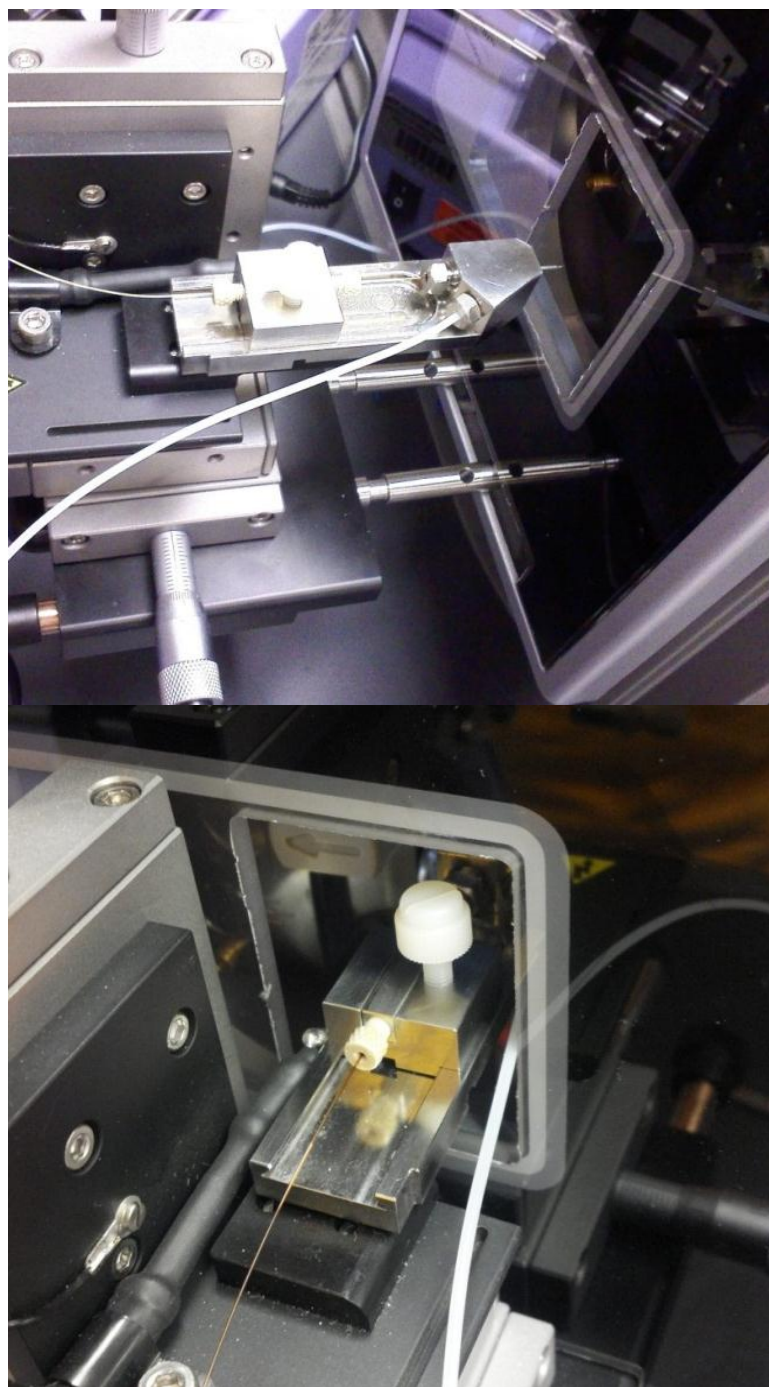


Figure C.15. The nESI source as it appears when the spray assembly is retracted (top) and during normal operating conditions (bottom).

will show up and it may only show up once and perhaps only for a very short period of time. For this reason it was quickly decided to acquire data using Data Dependent Analysis (DDA). MassLynx provides the option for this type of experiment in the MS method portion of the software. Within the DDA profile there are many options that can be used to tailor this type of acquisition to the experiment being performed. The DDA profile settings displayed in Table C.1 were used for most online cellular effluent acquisitions.

Mass Spectrometry Data Analysis

Once data files are collected, they can be transferred to a data analysis computer, aligned through MassLynx and processed with MarkerLynx and GEDI, if desired.

MassLynx Data Alignment. Data collected in the method described above does not correct, on-the-fly, or collect data to allow for a lock spray collection. To align the data, a peak of reasonable intensity and presence in all samples is chosen, commonly HEPES + Na⁺ (m/z = 261.0888 Da). Data is aligned by first opening any file in the data set in Chromatogram to set the file path, then in the MassLynx window selecting 'Tools', 'Automated Mass Measure'. In the AFAMM box, files desired to be aligned are double-clicked to change the red '✗' to a green '✓'. 'Automatic Peak Detection' parameters are set such that the lockspray mass is 261.0888, if aligning to HEPES, the mass window is +/-0.150 and background subtraction is not selected. Samples are then processed. Once complete an additional, centroided data file is created with the name as set in the 'Automatic Peak Detection' parameters. The sample list is then altered to include these new file names along with any standards that may be ideal to incorporate into the data processing. A method file for processing must be created within MassLynx by selecting 'Tools', 'Edit Method'. For this type of non-chromatographic data, 'Combined Scan Range' is

Table C.1. Parameters for MassLynx MS Tune DDA method file for the Synapt G2 used throughout chapter IV.

2012_03_06_ENDERS_880_ONLINE_MS_DDA_LOCK_FILE_trapCE_50.EXP			
[ACQUISITION]		[COLLISION ENERGY]	
Survey Start Time	0.00	Using MS Auto Trap Collision Energy (eV)	
Survey End Time	8.80	4.000000	
		Using MS Auto Transfer Collision Energy (eV)	
		0.000000	
[MS SURVEY]		[CONE VOLTAGE]	
Survey Start Mass	50.0000	Survey Use Tune Page CV	YES
Survey End Mass		MSMS CV Ramp Start Voltage	0.0
2000.0000		MSMS CV Ramp End Voltage	80.0
Discard uninteresting scans	NO		
Switch to MS/MS when rising	Intensity		
	above threshold		
Intensity Threshold	15.0		
Survey Scan Time	1.000		
Survey Interscan Time	0.024		
Survey Data Format			
Continuum			
ADC Sample Frequency (GHz)	3.0		
[MS/MS]		[INCLUDE]	
MSMS Start Mass	50.0	Precursor Selection	Included
MSMS End Mass	2000.0	Masses Take Priority	
Number of components	1	Use Include Masses List	YES
Switchback threshold (intensity / second)	10.0	Include Mass Range	600-1200
Use MSMS to MS Switch After Time	NO	Use Include File Masses	NO
Use MSMS to MS Switch After 1 Scan	NO	Include Window +/- (mDa)	100.0
Use MSMS to MS Switch After N Scans	YES	Include Retention Time Window	10.0
MSMS Switch After Scans	1.0		
MSMS Scan Time (sec)	1.000		
MSMS Interscan Time (sec)	0.024		
MSMS Data Format			
Continuum			
Use MS/MS ipr File	NO		
		[EXCLUDE]	
		Detected Precursor Inclusion	Using
		Real Time Exclusion	
		Detected Precursor Inclusion	Include
		After Time	
		Include After Time (s)	120.0
		Use Exclude Masses List	NO
		Use Exclude File Masses	NO
		Exclude Window +/- (mDa)	100.0
		FragmentationMode	CID
		[MOBILITY]	
		Use Precursor Drift Times	NO
		Maintain Mobility Separation	YES
		Calibration	Dynamic
		1	
[PEAK DETECTION]			
Use Intensity based Peak Detection	YES		
Peak Detection Window	3.0		
Deisotope Peak Selection	YES		
Charge State Tolerance Window	3.0		
Charge State Extraction Window	2.0		
Deisotope Tolerance Window	3.0		
Deisotope Extraction Window	2.0		

selected, with a threshold of 1000 and mass tolerance of 0.05. Deisotoping of the data is not possible in the 'Combined Scan Range' feature. The method file is then saved.

MarkerLynx. Once data is aligned and centroided, it can be processed with MarkerLynx for detection of peaks across the samples within the sample list. Data is processed by selecting 'MarkerLynx' from within the MassLynx window. In the box that appears, the appropriate project file which contains the data set to be processed, the altered sample list, and the method file are selected. The output file is named, all boxes checked, and data processed (a time-consuming process). Once the MarkerLynx file is created, samples are labeled both in terms of the experimental condition(s) and order of experiment for a "walking Principal Component Analysis (PCA)". For statistical analysis of the data, the 'XS' button is selected. This creates an Extended Statistics report (if not already produced during the data processing). Within Extended Statistics, the template is changed to PCA with pareto scaling and applied. Any plot can be double-clicked to enter the plots and something window. Data labels are changed to reflect given labels and desired plots and data lists are saved for further analysis. Groups are selected to produce OPLS-DA plots if needed for the particular data set.

Gene Expression Dynamics Identification (GEDI). If desired, data sets can be exported from Extended Statistics and processed with GEDI for the production of heat map style plots for enhanced data visualization. GEDI, along with documentation and instructions, is free for download. For large data sets (>16,000 columns), data cannot be copied or opened within Excel prior to transposition. To transpose data, it is first saved in Extended Statistics as a .dif file, and then opened as a new project. Within this new project area, the data can be transposed, selected, copied and then pasted in Excel. Once in Excel, the header is adjusted to comply with

GEDI input format and the file is saved as a tab delimited text file. If standards are to be subtracted, the data must be run as 'Static' even though it is dynamic data. From within GEDI, this file can be selected, and settings altered to those desired, typically 50 x 51 tiles, random seed with Pearson correlation. GEDI is then set to analyze. Once finished, averages of standards are calculated and subtracted from samples.

References

- 1 Kitano, H. Systems biology: A brief overview. *Science* **295**, 1662-1664, (2002).
- 2 Ideker, T., Galitski, T. & Hood, L. A new approach to decoding life: Systems biology. *Annual Review of Genomics and Human Genetics* **2**, 343-372, (2001).
- 3 *Examples of such databases are: Signal Transduction Knowledge Environment (STKE <http://www.stke.org/>); KEGG (<http://www.genome.ad.jp/>); EcoCyc (<http://ecocyc.org/>).*
- 4 Fodor, S. P. A., Read, J. L., Pirrung, M. C., Stryer, L., Lu, A. T. & Solas, D. Light-Directed, Spatially Addressable Parallel Chemical Synthesis. *Science* **251**, 767-773, (1991).
- 5 Schena, M., Shalon, D., Davis, R. W. & Brown, P. O. Quantitative Monitoring of Gene-Expression Patterns with a Complementary-DNA Microarray. *Science* **270**, 467-470, (1995).
- 6 Hughes, T. R., Mao, M., Jones, A. R., Burchard, J., Marton, M. J., Shannon, K. W., Lefkowitz, S. M., Ziman, M., Schelter, J. M., Meyer, M. R., Kobayashi, S., Davis, C., Dai, H. Y., He, Y. D. D., Stephanians, S. B., Cavet, G., Walker, W. L., West, A., Coffey, E., Shoemaker, D. D., Stoughton, R., Blanchard, A. P., Friend, S. H. & Linsley, P. S. Expression profiling using microarrays fabricated by an ink-jet oligonucleotide synthesizer. *Nature Biotechnology* **19**, 342-347, (2001).
- 7 Eng, J. K., McCormack, A. L. & Yates, J. R. An Approach to Correlate Tandem Mass-Spectral Data of Peptides with Amino-Acid-Sequences in a Protein Database. *Journal of the American Society for Mass Spectrometry* **5**, 976-989, (1994).
- 8 Anderson, N. L. & Anderson, N. G. Proteome and proteomics: New technologies, new concepts, and new words. *Electrophoresis* **19**, 1853-1861, (1998).
- 9 Gygi, S. P., Rist, B., Gerber, S. A., Turecek, F., Gelb, M. H. & Aebersold, R. Quantitative analysis of complex protein mixtures using isotope-coded affinity tags. *Nature Biotechnology* **17**, 994-999, (1999).
- 10 Aebersold, R. & Mann, M. Mass spectrometry-based proteomics. *Nature* **422**, 198-207, (2003).
- 11 Smith, C. A., O'Maille, G., Want, E. J., Qin, C., Trauger, S. A., Brandon, T. R., Custodio, D. E., Abagyan, R. & Siuzdak, G. METLIN - A metabolite mass spectral database. *Therapeutic Drug Monitoring* **27**, 747-751, (2005).
- 12 Wishart, D. S., Tzur, D., Knox, C., Eisner, R., Guo, A. C., Young, N., Cheng, D., Jewell, K., Arndt, D., Sawhney, S., Fung, C., Nikolai, L., Lewis, M., Coutouly, M. A., Forsythe, I., Tang, P., Shrivastava, S., Jeroncic, K., Stothard, P., Amegbey, G., Block, D., Hau, D. D., Wagner, J., Miniaci, J., Clements, M., Gebremedhin, M., Guo, N., Zhang, Y., Duggan, G. E., Maclnnis, G. D., Weljie, A. M., Dowlatabadi, R., Bamforth, F., Clive, D., Greiner, R., Li, L.,

- Marrie, T., Sykes, B. D., Vogel, H. J. & Querengesser, L. HMDB: the human metabolome database. *Nucleic Acids Research* **35**, D521-D526, (2007).
- 13 Dettmer, K., Aronov, P. A. & Hammock, B. D. Mass spectrometry-based metabolomics. *Mass Spectrometry Reviews* **26**, 51-78, (2007).
- 14 Want, E. J., Nordstrom, A., Morita, H. & Siuzdak, G. From exogenous to endogenous: The inevitable imprint of mass spectrometry in metabolomics. *Journal of Proteome Research* **6**, 459-468, (2007).
- 15 Fields, S. & Song, O. K. A Novel Genetic System to Detect Protein Protein Interactions. *Nature* **340**, 245-246, (1989).
- 16 Walhout, A. J. M. & Vidal, M. Protein interaction maps for model organisms. *Nature Reviews Molecular Cell Biology* **2**, 55-62, (2001).
- 17 Gavin, A. C., Bosche, M., Krause, R., Grandi, P., Marzioch, M., Bauer, A., Schultz, J., Rick, J. M., Michon, A. M., Cruciat, C. M., Remor, M., Hofert, C., Schelder, M., Brajenovic, M., Ruffner, H., Merino, A., Klein, K., Hudak, M., Dickson, D., Rudi, T., Gnau, V., Bauch, A., Bastuck, S., Huhse, B., Leutwein, C., Heurtier, M. A., Copley, R. R., Edlmann, A., Querfurth, E., Rybin, V., Drewes, G., Raida, M., Bouwmeester, T., Bork, P., Seraphin, B., Kuster, B., Neubauer, G. & Superti-Furga, G. Functional organization of the yeast proteome by systematic analysis of protein complexes. *Nature* **415**, 141-147, (2002).
- 18 Ho, Y., Gruhler, A., Heilbut, A., Bader, G. D., Moore, L., Adams, S. L., Millar, A., Taylor, P., Bennett, K., Boutilier, K., Yang, L. Y., Wolting, C., Donaldson, I., Schandorff, S., Shewnarane, J., Vo, M., Taggart, J., Goudreault, M., Muskat, B., Alfarano, C., Dewar, D., Lin, Z., Michalickova, K., Willems, A. R., Sassi, H., Nielsen, P. A., Rasmussen, K. J., Andersen, J. R., Johansen, L. E., Hansen, L. H., Jespersen, H., Podtelejnikov, A., Nielsen, E., Crawford, J., Poulsen, V., Sorensen, B. D., Matthiesen, J., Hendrickson, R. C., Gleeson, F., Pawson, T., Moran, M. F., Durocher, D., Mann, M., Hogue, C. W. V., Figeys, D. & Tyers, M. Systematic identification of protein complexes in *Saccharomyces cerevisiae* by mass spectrometry. *Nature* **415**, 180-183, (2002).
- 19 Eiceman, G. A. & Z., K. Introduction to Ion Mobility Spectrometry. in *Ion Mobility Spectrometry, Second Edition* (CRC Press, 2005).
- 20 Barnes, W. S., Martin, D. W. & McDaniel, E. W. Mass Spectrographic Identification of the Ion Observed in Hydrogen Mobility Experiments. *Physical Review Letters* **6**, 110-111, (1961).
- 21 McAfee, K. B. J. & Edelson, D. Identification and Mobility of Ions in a Townsend Discharge by Time-Resolved Mass Spectrometry. *Proceedings of the Physical Society of London* **81**, 382-384, (1963).
- 22 Gieniec, J., Mack, L. L., Nakamae, K., Gupta, C., Kumar, V. & Dole, M. Electrospray Mass-Spectroscopy of Macromolecules - Application of an Ion-Drift Spectrometer. *Biomedical Mass Spectrometry* **11**, 259-268, (1984).

- 23 von Helden, G., Wyttenbach, T. & Bowers, M. T. Inclusion of a Maldi Ion-Source in the Ion Chromatography Technique - Conformational Information on Polymer and Biomolecular Ions. *International Journal of Mass Spectrometry and Ion Processes* **146**, 349-364, (1995).
- 24 von Helden, G., Wyttenbach, T. & Bowers, M. T. Conformation of Macromolecules in the Gas-Phase - Use of Matrix-Assisted Laser-Desorption Methods in Ion Chromatography. *Science* **267**, 1483-1485, (1995).
- 25 Wyttenbach, T., vonHelden, G. & Bowers, M. T. Gas-phase conformation of biological molecules: Bradykinin. *Journal of the American Chemical Society* **118**, 8355-8364, (1996).
- 26 Shelimov, K. B., Clemmer, D. E., Hudgins, R. R. & Jarrold, M. F. Protein structure in vacuo: Gas-phase confirmations of BPTI and cytochrome c. *Journal of the American Chemical Society* **119**, 2240-2248, (1997).
- 27 Dwivedi, P., Wu, P., Klopsch, S. J., Puzon, G. J., Xun, L. & Hill, H. H. Metabolic profiling by ion mobility mass spectrometry (IMMS). *Metabolomics* **4**, 63-80, (2008).
- 28 Metz, T. O., Page, J. S., Baker, E. S., Tang, K. Q., Ding, J., Shen, Y. F. & Smith, R. D. High-resolution separations and improved ion production and transmission in metabolomics. *Trac-Trends in Analytical Chemistry* **27**, 205-214, (2008).
- 29 Dwivedi, P., Puzon, G., Tam, M., Langlais, D., Jackson, S., Kaplan, K., Siems, W. F., Schultz, A. J., Xun, L. Y., Woodsd, A. & Hill, H. H. Metabolic profiling of Escherichia coli by ion mobility-mass spectrometry with MALDI ion source. *Journal of Mass Spectrometry* **45**, 1383-1393, (2010).
- 30 Dwivedi, P., Schultz, A. J. & Hill, H. H. Metabolic profiling of human blood by high-resolution ion mobility mass spectrometry (IM-MS). *International Journal of Mass Spectrometry* **298**, 78-90, (2010).
- 31 Campuzano, I., Bush, M. F., Robinson, C. V., Beaumont, C., Richardson, K., Kim, H. & Kim, H. I. Structural Characterization of Drug-like Compounds by Ion Mobility Mass Spectrometry: Comparison of Theoretical and Experimentally Derived Nitrogen Collision Cross Sections. *Analytical Chemistry* **84**, 1026-1033, (2012).
- 32 Goodwin, C. R., Fenn, L. S., Derewacz, D. K., Bachmann, B. O. & McLean, J. A. Structural Mass Spectrometry: Rapid Methods for Separation and Analysis of Peptide Natural Products. *Journal of Natural Products* **75**, 48-53, (2012).
- 33 Myung, S., Taraszka, J. A., Lee, Y. J., Moon, M. H., Valentine, S. J., Koeniger, S. L. & Clemmer, D. E. Development of high-sensitivity ion trap-IMS-TOF techniques: A high-throughput nano-LC/IMS/TOF-separation of the Drosophila melanogaster proteome. *Abstracts of Papers of the American Chemical Society* **226**, U112-U112, (2003).

- 34 Liu, X., Plasencia, M., Ragg, S., Valentine, S. J. & Clemmer, D. E. Development of high throughput dispersive LC-ion mobility-TOFMS techniques for analysing the human plasma proteome. *Briefings of Funct. Genomics & Proteomics* **3**, 177-186, (2004).
- 35 Taraszka, J. A., Kurulugama, R., Sowell, R. A., Valentine, S. J., Koeniger, S. L., Arnold, R. J., Miller, D. F., Kaufman, T. C. & Clemmer, D. E. Mapping the proteome of *Drosophila melanogaster*: Analysis of embryos and adult heads by LC-IMS-MS methods. *Journal of Proteome Research* **4**, 1223-1237, (2005).
- 36 Valentine, S. J., Plasencia, M. D., Liu, X. Y., Krishnan, M., Naylor, S., Udseth, H. R., Smith, R. D. & Clemmer, D. E. Toward plasma proteome profiling with ion mobility-mass spectrometry. *Journal of Proteome Research* **5**, 2977-2984, (2006).
- 37 Liu, X. Y., Valentine, S. J., Plasencia, M. D., Trimpin, S., Naylor, S. & Clemmer, D. E. Mapping the human plasma proteome by SCX-LC-IMS-MS. *Journal of the American Society for Mass Spectrometry* **18**, 1249-1264, (2007).
- 38 Liu, X. Y., Miller, B. R., Rebec, G. V. & Clemmer, D. E. Protein expression in the striatum and cortex regions of the brain for a mouse model of Huntington's disease. *Journal of Proteome Research* **6**, 3134-3142, (2007).
- 39 Isailovic, D., Kurulugama, R. T., Plasencia, M. D., Stokes, S. T., Kyselova, Z., Goldman, R., Mechref, Y., Novotny, M. V. & Clemmer, D. E. Profiling of human serum glycans associated with liver cancer and cirrhosis by IMS-MS. *Journal of Proteome Research* **7**, 1109-1117, (2008).
- 40 Thomas, J. J., Bothner, B., Traina, J., Benner, W. H. & Siuzdak, G. Electrospray ion mobility spectrometry of intact viruses. *Spectroscopy-an International Journal* **18**, 31-36, (2004).
- 41 Knapman, T. W., Morton, V. L., Stonehouse, N. J., Stockley, P. G. & Ashcroft, A. E. Determining the topology of virus assembly intermediates using ion mobility spectrometry-mass spectrometry. *Rapid Communications in Mass Spectrometry* **24**, 3033-3042, (2010).
- 42 Uetrecht, C., Barbu, I. M., Shoemaker, G. K., van Duijn, E. & Heck, A. J. R. Interrogating viral capsid assembly with ion mobility-mass spectrometry. *Nature Chemistry* **3**, 126-132, (2011).
- 43 Ruotolo, B. T., Giles, K., Campuzano, I., Sandercock, A. M., Bateman, R. H. & Robinson, C. V. Evidence for macromolecular protein rings in the absence of bulk water. *Science* **310**, 1658-1661, (2005).
- 44 Benesch, J. L. P., Ruotolo, B. T., Simmons, D. A. & Robinson, C. V. Protein complexes in the gas phase: Technology for structural genomics and proteomics. *Chemical Reviews* **107**, 3544-3567, (2007).

- 45 Ruotolo, B. T., Hyung, S. J., Robinson, P. M., Giles, K., Bateman, R. H. & Robinson, C. V. Ion mobility-mass spectrometry reveals long-lived, unfolded intermediates in the dissociation of protein complexes. *Angewandte Chemie-International Edition* **46**, 8001-8004, (2007).
- 46 Jackson, S. N., Ugarov, M., Egan, T., Post, J. D., Langlais, D., Schultz, J. A. & Woods, A. S. MALDI-ion mobility-TOFMS imaging of lipids in rat brain tissue. *Journal of Mass Spectrometry* **42**, 1093-1098, (2007).
- 47 McLean, J. A., Ridenour, W. B. & Caprioli, R. M. Profiling and imaging of tissues by imaging ion mobility-mass spectrometry. *Journal of Mass Spectrometry* **42**, 1099-1105, (2007).
- 48 Revercomb, H. E. & Mason, E. A. Theory of Plasma Chromatography Gaseous Electrophoresis - Review. *Analytical Chemistry* **47**, 970-983, (1975).
- 49 Mason, E. A. *Ion Mobility: Its Role in Plasma Chromatography, in Plasma Chromatography*. (Plenum Press 1984).
- 50 Mason, E. A. & McDaniel, E. W. *Transport Properties of Ions in Gases*. (John Wiley & Sons, Inc., 1988).
- 51 Ruotolo, B. T., Benesch, J. L. P., Sandercock, A. M., Hyung, S. J. & Robinson, C. V. Ion mobility-mass spectrometry analysis of large protein complexes. *Nature Protocols* **3**, 1139-1152, (2008).
- 52 Williams, J. P. & Scrivens, J. H. Coupling desorption electrospray ionisation and neutral desorption/extractive electrospray ionisation with a travelling-wave based ion mobility mass spectrometer for the analysis of drugs. *Rapid Communications in Mass Spectrometry* **22**, 187-196, (2008).
- 53 Shvartsburg, A. A. & Smith, R. D. Fundamentals of Traveling Wave Ion Mobility Spectrometry. *Analytical Chemistry* **80**, 9689-9699, (2008).
- 54 Williams, J. P., Lough, J. A., Campuzano, I., Richardson, K. & Sadler, P. J. Use of ion mobility mass spectrometry and a collision cross-section algorithm to study an organometallic ruthenium anticancer complex and its adducts with a DNA oligonucleotide. *Rapid Communications in Mass Spectrometry* **23**, 3563-3569, (2009).
- 55 Bush, M. F., Hall, Z., Giles, K., Hoyes, J., Robinson, C. V. & Ruotolo, B. T. Collision Cross Sections of Proteins and Their Complexes: A Calibration Framework and Database for Gas-Phase Structural Biology. *Analytical Chemistry* **82**, 9557-9565, (2010).
- 56 Giles, K., Wildgoose, J. L., Langridge, D. J. & Campuzano, I. A method for direct measurement of ion mobilities using a travelling wave ion guide. *International Journal of Mass Spectrometry* **298**, 10-16, (2010).

- 57 Giles, K., Williams, J. P. & Campuzano, I. Enhancements in travelling wave ion mobility resolution. *Rapid Communications in Mass Spectrometry* **25**, 1559-1566, (2011).
- 58 Merenbloom, S. I., Flick, T. G. & Williams, E. R. How Hot are Your Ions in TWAVE Ion Mobility Spectrometry? *Journal of the American Society for Mass Spectrometry* **23**, 553-562, (2012).
- 59 Salbo, R., Bush, M. F., Naver, H., Campuzano, I., Robinson, C. V., Pettersson, I., Jorgensen, T. J. D. & Haselmann, K. F. Traveling-wave ion mobility mass spectrometry of protein complexes: accurate calibrated collision cross-sections of human insulin oligomers. *Rapid Communications in Mass Spectrometry* **26**, 1181-1193, (2012).
- 60 McLean, J. A., Fenn, L. S. & Enders, J. R. Structurally Selective Imaging Mass Spectrometry by Imaging Ion Mobility-Mass Spectrometry. in *Mass Spectrometry Imaging: Principles and Protocols (Methods in Molecular Biology)* Vol. 656 (eds S. S. Rubakhin & J. V. Sweedler) 363-383 (Springer, 2010).
- 61 Shvartsburg, A. A. & Jarrold, M. F. An exact hard-spheres scattering model for the mobilities of polyatomic ions. *Chemical Physics Letters* **261**, 86-91, (1996).
- 62 Wyttenbach, T., Witt, M. & Bowers, M. T. On the stability of amino acid zwitterions in the gas phase: The influence of derivatization, proton affinity, and alkali ion addition. *Journal of the American Chemical Society* **122**, 3458-3464, (2000).
- 63 Gidden, J. & Bowers, M. T. Gas-phase conformations of deprotonated and protonated mononucleotides determined by ion mobility and theoretical modeling. *Journal of Physical Chemistry B* **107**, 12829-12837, (2003).
- 64 Gidden, J. & Bowers, M. T. Gas-phase conformations of deprotonated trinucleotides (dGTT(-), dTGT(-), and dTTG(-)): The question of zwitterion formation. *Journal of the American Society for Mass Spectrometry* **14**, 161-170, (2003).
- 65 Fenn, L. S. & McLean, J. A. Biomolecular structural separations by ion mobility-mass spectrometry. *Analytical and Bioanalytical Chemistry* **391**, 905-909, (2008).
- 66 Tao, L., McLean, J. R., McLean, J. A. & Russell, D. H. A collision cross-section database of singly-charged peptide ions. *Journal of the American Society for Mass Spectrometry* **18**, 1232-1238, (2007).
- 67 Clemmer, D. E. & Jarrold, M. F. Ion mobility measurements and their applications to clusters and biomolecules. *Journal of Mass Spectrometry* **32**, 577-592, (1997).
- 68 Jarrold, M. F. Peptides and proteins in the vapor phase. *Annual Review of Physical Chemistry* **51**, 179-207, (2000).
- 69 Wyttenbach, T. & Bowers, M. T. Gas-phase conformations: The ion mobility/ion chromatography method. *Modern Mass Spectrometry* **225**, 207-232, (2003).

- 70 McLean, J. A., Ruotolo, B. T., Gillig, K. J. & Russell, D. H. Ion mobility-mass spectrometry: a new paradigm for proteomics. *International Journal of Mass Spectrometry* **240**, 301-315, (2005).
- 71 Wuthrich, K. NMR of Proteins and Nucleic Acids. 320 (Wiley, 1986).
- 72 Bax, A. Two-Dimensional Nmr and Protein-Structure. *Annual Review of Biochemistry* **58**, 223-256, (1989).
- 73 Wuthrich, K. The Development of Nuclear Magnetic-Resonance Spectroscopy as a Technique for Protein-Structure Determination. *Accounts of Chemical Research* **22**, 36-44, (1989).
- 74 Lipscomb, W. N. Experimental Crystallography. *Annual Review of Biochemistry* **58**, 223-256, (1953).
- 75 Kendrew, J. C., Dickerson, R. E., Strandberg, B. E., Hart, R. G. & Davies, D. R. Structure of myoglobin: a three-dimensional Fourier synthesis at 2Å resolution. *Nature* **185**, 422-427, (1960).
- 76 Perutz, M. F., Rossmann, M. G., Cullis, A. F., Muirhead, H., Will, G. & North, A. C. T. Structure of haemoglobin: a three-dimensional Fourier synthesis at 5.5Å resolution, obtained by X-ray analysis. *Nature* **185**, 416-422, (1960).
- 77 Blundell, T. L. & Johnson, L. N. *Protein Crystallography*. (Academic, 1976).
- 78 Covey, T. & Douglas, D. J. Collision Cross-Sections for Protein Ions. *Journal of the American Society for Mass Spectrometry* **4**, 616-623, (1993).
- 79 Loo, R. R. O. & Smith, R. D. Investigation of the Gas-Phase Structure of Electrosprayed Proteins Using Ion-Molecule Reactions. *Journal of the American Society for Mass Spectrometry* **5**, 207-220, (1994).
- 80 Hudgins, R. R., Woenckhaus, J. & Jarrold, M. F. High resolution ion mobility measurements for gas phase proteins: correlation between solution phase and gas phase conformations. *Int. J. Mass Spectrom. Ion Processes* **165/166**, 497-507, (1997).
- 81 Valentine, S. J., Counterman, A. E., Hoaglund, C. S., Reilly, J. P. & Clemmer, D. E. Gas-phase separations of protease digests. *Journal of the American Society for Mass Spectrometry* **9**, 1213-1216, (1998).
- 82 Taraszka, J. A., Counterman, A. E. & Clemmer, D. E. Gas-phase separations of complex tryptic peptide mixtures. *Fresenius Journal of Analytical Chemistry* **369**, 234-245, (2001).
- 83 Valentine, S. J., Kulchania, M., Barnes, C. A. S. & Clemmer, D. E. Multidimensional separations of complex peptide mixtures: a combined high-performance liquid chromatography/ion mobility/time-of-flight mass spectrometry approach. *International Journal of Mass Spectrometry* **212**, 97-109, (2001).

- 84 Moon, M. H., Myung, S., Plasencia, M., Hilderbrand, A. E. & Clemmer, D. E. Nanoflow LC/Ion Mobility/CID/TOF for Proteomics: Analysis of a Human Urinary Proteome. *Journal of Proteome Research* **2**, 589-597, (2003).
- 85 Myung, S., Lee, Y. J., Moon, M. H., Taraszka, J., Sowell, R., Koeniger, S., Hilderbrand, A. E., Valentine, S. J., Cherbas, L., Cherbas, P., Kaufmann, T. C., Miller, D. F., Mechref, Y., Novotny, M. V., Ewing, M. A., Sporleder, C. R. & Clemmer, D. E. Development of high-sensitivity ion trap ion mobility spectrometry time-of-flight techniques: A high-throughput nano-LC-IMS-TOF separation of peptides arising from a Drosophila protein extract. *Analytical Chemistry* **75**, 5137-5145, (2003).
- 86 Taraszka, J. A., Gao, X. F., Valentine, S. J., Sowell, R. A., Koeniger, S. L., Miller, D. F., Kaufman, T. C. & Clemmer, D. E. Proteome profiling for assessing diversity: Analysis of individual heads of Drosophila melanogaster using LC-ion mobility-MS. *Journal of Proteome Research* **4**, 1238-1247, (2005).
- 87 Valentine, S. J., Liu, X. Y., Plasencia, M. D., Hilderbrand, A. E., Kurulugama, R. T., Koeniger, S. L. & Clemmer, D. E. Developing liquid chromatography ion mobility mass spectrometry techniques. *Expert Review of Proteomics* **2**, 553-565, (2005).
- 88 Wyttenbach, T., Witt, M. & Bowers, M. T. On the question of salt bridges of cationized amino acids in the gas phase: glycine and arginine. *International Journal of Mass Spectrometry* **183**, 243-252, (1999).
- 89 Wyttenbach, T., Liu, D. F. & Bowers, M. T. Hydration of small peptides. *International Journal of Mass Spectrometry* **240**, 221-232, (2005).
- 90 Kohtani, M., Breaux, G. A. & Jarrold, M. F. Water molecule adsorption on protonated dipeptides. *Journal of the American Chemical Society* **126**, 1206-1213, (2004).
- 91 Liu, D. F., Wyttenbach, T., Carpenter, C. J. & Bowers, M. T. Investigation of noncovalent interactions in deprotonated peptides: Structural and energetic competition between aggregation and hydration. *Journal of the American Chemical Society* **126**, 3261-3270, (2004).
- 92 Hudgins, R. R., Mao, Y., Ratner, M. A. & Jarrold, M. F. Conformations of Gly(n)H(+) and Ala(n)H(+) peptides in the gas phase. *Biophysical Journal* **76**, 1591-1597, (1999).
- 93 Enders, J. R., Kliman, M., Sundarapandian, S. & McLean, J. A. Peptide and Protein Analysis Using Ion Mobility–Mass Spectrometry. in *Protein and Peptide Mass Spectrometry in Drug Discovery* (eds Michael L. Gross, Guodong Chen, & Birendra Pramanik) 139-174 (John Wiley & Sons, Inc., 2011).
- 94 Wyttenbach, T. & Bowers, M. T. Intermolecular interactions in biomolecular systems examined by mass spectrometry. *Annual Review of Physical Chemistry* **58**, 511-533, (2007).

- 95 Counterman, A. E., Hilderbrand, A. E., Barnes, C. A. S. & Clemmer, D. E. Formation of peptide aggregates during ESI: Size, charge, composition, and contributions to noise. *Journal of the American Society for Mass Spectrometry* **12**, 1020-1035, (2001).
- 96 Liu, D. F., Wyttenbach, T., Barran, P. E. & Bowers, M. T. Sequential hydration of small protonated peptides. *Journal of the American Chemical Society* **125**, 8458-8464, (2003).
- 97 Hudgins, R. R., Ratner, M. A. & Jarrold, M. F. Design of helices that are stable in vacuo. *Journal of the American Chemical Society* **120**, 12974-12975, (1998).
- 98 Counterman, A. E., Valentine, S. J., Srebalus, C. A., Henderson, S. C., Hoaglund, C. S. & Clemmer, D. E. High-order structure and dissociation of gaseous peptide aggregates that are hidden in mass spectra. *Journal of the American Society for Mass Spectrometry* **9**, 743-759, (1998).
- 99 Hudgins, R. R. & Jarrold, M. F. Helix formation in unsolvated alanine-based peptides: Helical monomers and helical dimers. *Journal of the American Chemical Society* **121**, 3494-3501, (1999).
- 100 Kinnear, B. S. & Jarrold, M. F. Helix formation in unsolvated peptides: Side chain entropy is not the determining factor. *Journal of the American Chemical Society* **123**, 7907-7908, (2001).
- 101 Counterman, A. E. & Clemmer, D. E. Large anhydrous polyalanine ions: Evidence for extended helices and onset of a more compact state. *Journal of the American Chemical Society* **123**, 1490-1498, (2001).
- 102 Taraszka, J. A., Counterman, A. E. & Clemmer, D. E. Large anhydrous polyalanine ions: substitution of Na⁺ for H⁺ destabilizes folded states. *International Journal of Mass Spectrometry* **204**, 87-100, (2001).
- 103 Kohtani, M. & Jarrold, M. F. The initial steps in the hydration of unsolvated peptides: Water molecule adsorption on alanine-based helices and globules. *Journal of the American Chemical Society* **124**, 11148-11158, (2002).
- 104 Counterman, A. E. & Clemmer, D. E. Gas phase polyalanine: Assessment of $i \rightarrow i+3$ and $i \rightarrow i+4$ helical turns in [Ala(n)+4H]⁴⁺ (n=29-49) ion. *Journal of Physical Chemistry B* **106**, 12045-12051, (2002).
- 105 Breaux, G. A. & Jarrold, M. F. Probing helix formation in unsolvated peptides. *Journal of the American Chemical Society* **125**, 10740-10747, (2003).
- 106 Hartings, M. R., Kinnear, B. S. & Jarrold, M. F. The energy landscape of unsolvated peptides: The role of context in the stability of alanine/glycine helices. *Journal of the American Chemical Society* **125**, 3941-3947, (2003).
- 107 Wyttenbach, T., Paizs, B., Barran, P., Brechi, L., Liu, D. F., Suhai, S., Wysocki, V. H. & Bowers, M. T. The effect of the initial water of hydration on the energetics, structures,

- and H/D exchange mechanism of a family of pentapeptides: An experimental and theoretical study. *Journal of the American Chemical Society* **125**, 13768-13775, (2003).
- 108 Counterman, A. E. & Clemmer, D. E. Compact -> extended helix transitions of polyalanine in vacuo. *Journal of Physical Chemistry B* **107**, 2111-2117, (2003).
- 109 Kohtani, M., Jones, T. C., Schneider, J. E. & Jarrold, M. F. Extreme stability of an unsolvated alpha-helix. *Journal of the American Chemical Society* **126**, 7420-7421, (2004).
- 110 Sudha, R., Kohtani, M., Breaux, G. A. & Jarrold, M. F. pi-helix preference in unsolvated peptides. *Journal of the American Chemical Society* **126**, 2777-2784, (2004).
- 111 Jarrold, M. F. Helices and sheets in vacuo. *Physical Chemistry Chemical Physics* **9**, 1659-1671, (2007).
- 112 Zilch, L. W., Kaleta, D. T., Kohtani, M., Krishnan, R. & Jarrold, M. F. Folding and unfolding of helix-turn-helix motifs in the gas phase. *Journal of the American Society for Mass Spectrometry* **18**, 1239-1248, (2007).
- 113 Wyttenbach, T., Bushnell, J. E. & Bowers, M. T. Salt bridge structures in the absence of solvent? The case for the oligoglycines. *Journal of the American Chemical Society* **120**, 5098-5103, (1998).
- 114 Hudgins, R. R. & Jarrold, M. F. Conformations of unsolvated glycine-based peptides. *Journal of Physical Chemistry B* **104**, 2154-2158, (2000).
- 115 Counterman, A. E. & Clemmer, D. E. Anhydrous polyproline helices and globules. *Journal of Physical Chemistry B* **108**, 4885-4898, (2004).
- 116 Antoine, R., Compagnon, I., Rayane, D., Broyer, M., Dugourd, P., Breaux, G., Hagemester, F. C., Pippen, D., Hudgins, R. R. & Jarrold, M. F. Electric dipole moments and conformations of isolated peptides. *European Physical Journal D* **20**, 583-587, (2002).
- 117 Counterman, A. E. & Clemmer, D. E. Magic number clusters of serine in the gas phase. *Journal of Physical Chemistry B* **105**, 8092-8096, (2001).
- 118 Myung, S., Julian, R. R., Nanita, S. C., Cooks, R. G. & Clemmer, D. E. Formation of nanometer-scale serine clusters by sonic spray. *Journal of Physical Chemistry B* **108**, 6105-6111, (2004).
- 119 Julian, R. R., Myung, S. & Clemmer, D. E. Spontaneous anti-resolution in heterochiral clusters of serine. *Journal of the American Chemical Society* **126**, 4110-4111, (2004).
- 120 Myung, S., Lorton, K. P., Merenbloom, S. I., Fioroni, M., Koeniger, S. L., Julian, R. R., Baik, M. H. & Clemmer, D. E. Evidence for spontaneous resolution of icosahedral proline. *Journal of the American Chemical Society* **128**, 15988-15989, (2006).

- 121 Myung, S., Fioroni, M., Julian, R. R., Koeniger, S. L., Baik, M. H. & Clemmer, D. E. Chirally directed formation of nanometer-scale proline clusters. *Journal of the American Chemical Society* **128**, 10833-10839, (2006).
- 122 Wu, C., Klasmeier, J. & Hill, H. H. Atmospheric pressure ion mobility spectrometry of protonated and sodiated peptides. *Rapid Communications in Mass Spectrometry* **13**, 1138-1142, (1999).
- 123 Shelimov, K. B. & Jarrold, M. F. Conformations, unfolding, and refolding of apomyoglobin in vacuum: An activation barrier for gas-phase protein folding. *Journal of the American Chemical Society* **119**, 2987-2994, (1997).
- 124 Fye, J. L., Woenckhaus, J. & Jarrold, M. F. Hydration of folded and unfolded gas-phase proteins: Saturation of cytochrome c and apomyoglobin. *Journal of the American Chemical Society* **120**, 1327-1328, (1998).
- 125 Woenckhaus, J., Hudgins, R. R. & Jarrold, M. F. Hydration of gas-phase proteins: A special hydration site on gas-phase BPTI. *Journal of the American Chemical Society* **119**, 9586-9587, (1997).
- 126 Jarrold, M. F. Unfolding, refolding, and hydration of proteins in the gas phase. *Accounts of Chemical Research* **32**, 360-367, (1999).
- 127 Mao, Y., Ratner, M. A. & Jarrold, M. F. One water molecule stiffens a protein. *Journal of the American Chemical Society* **122**, 2950-2951, (2000).
- 128 Hoaglund, C. S., Valentine, S. J., Sporleder, C. R., Reilly, J. P. & Clemmer, D. E. Three-dimensional ion mobility TOFMS analysis of electrosprayed biomolecules. *Analytical Chemistry* **70**, 2236-2242, (1998).
- 129 Wyttenbach, T. & Bowers, M. T. Gas phase conformations of biological molecules: The hydrogen/deuterium exchange mechanism. *Journal of the American Society for Mass Spectrometry* **10**, 9-14, (1999).
- 130 Sawyer, H. A., Marini, J. T., Stone, E. G., Ruotolo, B. T., Gillig, K. J. & Russell, D. H. The structure of gas-phase bradykinin fragment 1-5 (RPPGF) ions: An ion mobility spectrometry and H/D exchange ion-molecule reaction chemistry study. *Journal of the American Society for Mass Spectrometry* **16**, 893-905, (2005).
- 131 Clemmer, D. E., Hudgins, R. R. & Jarrold, M. F. Naked Protein Conformations - Cytochrome-C in the Gas-Phase. *Journal of the American Chemical Society* **117**, 10141-10142, (1995).
- 132 Shelimov, K. B. & Jarrold, M. F. "Denaturation" and refolding of cytochrome c in vacuo. *Journal of the American Chemical Society* **118**, 10313-10314, (1996).

- 133 Woenckhaus, J., Mao, Y. & Jarrold, M. F. Hydration of gas phase proteins: Folded +5 and unfolded +7 charge states of cytochrome c. *Journal of Physical Chemistry B* **101**, 847-851, (1997).
- 134 Mao, Y., Ratner, M. A. & Jarrold, M. F. Molecular dynamics simulations of the charge-induced unfolding and refolding of unsolvated cytochrome c. *Journal of Physical Chemistry B* **103**, 10017-10021, (1999).
- 135 Mao, Y., Woenckhaus, J., Kolafa, J., Ratner, M. A. & Jarrold, M. F. Thermal unfolding of unsolvated cytochrome c: Experiment and molecular dynamics simulations. *Journal of the American Chemical Society* **121**, 2712-2721, (1999).
- 136 Thalassinou, K., Slade, S. E., Jennings, K. R., Scrivens, J. H., Giles, K., Wildgoose, J., Hoyes, J., Bateman, R. H. & Bowers, M. T. Ion mobility mass spectrometry of proteins in a modified commercial mass spectrometer. *International Journal of Mass Spectrometry* **236**, 55-63, (2004).
- 137 McCullough, B. J., Eastwood, H., Clark, D. J., Polfer, N. C., Campopiano, D. J., Dorin, J. A., Maxwell, A., Langley, R. J., Govan, J. R. W., Bernstein, S. L., Bowers, M. T. & Barran, P. E. Characterisation of DEFB107 by mass spectrometry: Lessons from an anti-antimicrobial defensin. *International Journal of Mass Spectrometry* **252**, 180-188, (2006).
- 138 Woods, A. S., Koomen, J. M., Ruotolo, B. T., Gillig, K. J., Russel, D. H., Fuhrer, K., Gonin, M., Egan, T. F. & Schultz, J. A. A study of peptide-peptide using MALDI ion mobility o-TOF and ESI mass spectrometry. *Journal of the American Society for Mass Spectrometry* **13**, 166-169, (2002).
- 139 Ruotolo, B. T., Tate, C. C. & Russell, D. H. Ion mobility-mass spectrometry applied to cyclic peptide analysis: Conformational preferences of gramicidin S and linear analogs in the gas phase. *Journal of the American Society for Mass Spectrometry* **15**, 870-878, (2004).
- 140 Valentine, S. J., Sevugarajan, S., Kurulugama, R. T., Koeniger, S. L., Merenbloom, S. I., Bohrer, B. C. & Clemmer, D. E. Split-field drift tube/mass spectrometry and isotopic labeling techniques for determination of single amino acid polymorphisms. *Journal of Proteome Research* **5**, 1879-1887, (2006).
- 141 Taraszka, J. A., Li, J. W. & Clemmer, D. E. Metal-mediated peptide ion conformations in the gas phase. *Journal of Physical Chemistry B* **104**, 4545-4551, (2000).
- 142 Smith, D. P., Giles, K., Bateman, R. H., Radford, S. E. & Ashcroft, A. E. Monitoring copopulated conformational states during protein folding events using Electrospray ionization-ion mobility spectrometry-mass spectrometry. *Journal of the American Society for Mass Spectrometry* **18**, 2180-2190, (2007).
- 143 Badman, E. R., Hoaglund-Hyzer, C. S. & Clemmer, D. E. Monitoring structural changes of proteins in an ion trap over similar to 10-200 ms: Unfolding transitions in cytochrome c ions. *Analytical Chemistry* **73**, 6000-6007, (2001).

- 144 Wyttenbach, T., Liu, D. F. & Bowers, M. T. Interactions of the hormone oxytocin with divalent metal ions. *Journal of the American Chemical Society* **130**, 5993-6000, (2008).
- 145 Bernstein, S. L., Liu, D. F., Wyttenbach, T., Bowers, M. T., Lee, J. C., Gray, H. B. & Winkler, J. R. α -Synuclein: Stable compact and extended monomeric structures and pH dependence of dimer formation. *Journal of the American Society for Mass Spectrometry* **15**, 1435-1443, (2004).
- 146 Grabenauer, M., Bernstein, S. L., Lee, J. C., Wyttenbach, T., Dupuis, N. F., Gray, H. B., Winkler, J. R. & Bowers, M. T. Spermine binding to Parkinson's protein alpha-synuclein and its disease-related A30P and A53T mutants. *Journal of Physical Chemistry B* **112**, 11147-11154, (2008).
- 147 Valentine, S. J., Counterman, A. E. & Clemmer, D. E. Conformer-dependent proton-transfer reactions of ubiquitin ions. *Journal of the American Society for Mass Spectrometry* **8**, 954-961, (1997).
- 148 Li, J. W., Taraszka, J. A., Counterman, A. E. & Clemmer, D. E. Influence of solvent composition and capillary temperature on the conformations of electrosprayed ions: unfolding of compact ubiquitin conformers from pseudonative and denatured solutions. *International Journal of Mass Spectrometry* **187**, 37-47, (1999).
- 149 Badman, E. R., Hoaglund-Hyzer, C. S. & Clemmer, D. E. Dissociation of different conformations of ubiquitin ions. *Journal of the American Society for Mass Spectrometry* **13**, 719-723, (2002).
- 150 Myung, S., Badman, E. R., Lee, Y. J. & Clemmer, D. E. Structural transitions of electrosprayed ubiquitin ions stored in an ion trap over similar to 10 ms to 30 s. *Journal of Physical Chemistry A* **106**, 9976-9982, (2002).
- 151 Koeniger, S. L., Merenbloom, S. I. & Clemmer, D. E. Evidence for many resolvable structures within conformation types of electrosprayed ubiquitin ions. *Journal of Physical Chemistry B* **110**, 7017-7021, (2006).
- 152 Koeniger, S. L., Merenbloom, S. I., Sevugarajan, S. & Clemmer, D. E. Transfer of structural elements from compact to extended states in unsolvated ubiquitin. *Journal of the American Chemical Society* **128**, 11713-11719, (2006).
- 153 Koeniger, S. L. & Clemmer, D. E. Resolution and structural transitions of elongated states of ubiquitin. *Journal of the American Society for Mass Spectrometry* **18**, 322-331, (2007).
- 154 Segev, E., Wyttenbach, T., Bowers, M. T. & Gerber, R. B. Conformational evolution of ubiquitin ions in electrospray mass spectrometry: molecular dynamics simulations at gradually increasing temperatures. *Physical Chemistry Chemical Physics* **10**, 3077-3082, (2008).

- 155 Valentine, S. J., Counterman, A. E. & Clemmer, D. E. A database of 660 peptide ion cross sections: Use of intrinsic size parameters for bona fide predictions of cross sections. *Journal of the American Society for Mass Spectrometry* **10**, 1188-1211, (1999).
- 156 Srebalus, C. A., Li, J. W., Marshall, W. S. & Clemmer, D. E. Gas phase separations of electrosprayed peptide libraries. *Analytical Chemistry* **71**, 3918-3927, (1999).
- 157 Barnes, C. A. S., Hilderbrand, A. E., Valentine, S. J. & Clemmer, D. E. Resolving isomeric peptide mixtures: A combined HPLC/ion mobility-TOFMS analysis of a 4000-component combinatorial library. *Analytical Chemistry* **74**, 26-36, (2002).
- 158 Koeniger, S. L., Merenbloom, S. I., Valentine, S. J., Jarrold, M. F., Udseth, H. R., Smith, R. D. & Clemmer, D. E. An IMS-IMS analogue of MS-MS. *Analytical Chemistry* **78**, 4161-4174, (2006).
- 159 Merenbloom, S. I., Koeniger, S. L., Valentine, S. J., Plasencia, M. D. & Clemmer, D. E. IMS-IMS and IMS-IMS-IMS/MS for separating peptide and protein fragment ions. *Analytical Chemistry* **78**, 2802-2809, (2006).
- 160 Merenbloom, S. I., Koeniger, S. L., Bohrer, B. C., Valentine, S. J. & Clemmer, D. E. Improving the efficiency of IMS-IMS by a combing technique. *Analytical Chemistry* **80**, 1918-1927, (2008).
- 161 Fernandez-Lima, F. A., Becker, C., Gillig, K. J., Russell, W. K., Tichy, S. E. & Russell, D. H. Ion Mobility-Mass Spectrometer Interface for Collisional Activation of Mobility Separated Ions. *Analytical Chemistry* **81**, 618-624, (2009).
- 162 Barnes, C. A. S. & Clemmer, D. E. Assessment of purity and screening of peptide libraries by nested ion mobility TOFMS: Identification of RNase S-protein binders. *Analytical Chemistry* **73**, 424-433, (2001).
- 163 Ruotolo, B. T., Verbeck, G. F., Thomson, L. M., Gillig, K. J. & Russell, D. H. Observation of conserved solution-phase secondary structure in gas-phase tryptic peptides. *Journal of the American Chemical Society* **124**, 4214-4215, (2002).
- 164 Barran, P. E., Polfer, N. C., Campopiano, D. J., Clarke, D. J., Langridge-Smith, P. R. R., Langley, R. J., Govan, J. R. W., Maxwell, A., Dorin, J. R., Millar, R. P. & Bowers, M. T. Is it biologically relevant to measure the structures of small peptides in the gas-phase? *International Journal of Mass Spectrometry* **240**, 273-284, (2005).
- 165 Myung, S., Wiseman, J. M., Valentine, S. J., Takats, Z., Cooks, R. G. & Clemmer, D. E. Coupling desorption electrospray ionization with ion mobility/mass spectrometry for analysis of protein structure: Evidence for desorption of folded and denatured states. *Journal of Physical Chemistry B* **110**, 5045-5051, (2006).
- 166 Valentine, S. J. & Clemmer, D. E. H/D exchange levels of shape-resolved cytochrome c conformers in the gas phase. *Journal of the American Chemical Society* **119**, 3558-3566, (1997).

- 167 Kindy, J. M., Taraszka, J. A., Regnier, F. E. & Clemmer, D. E. Quantifying peptides in isotopically labeled protease digests by ion mobility/time-of-flight mass spectrometry. *Analytical Chemistry* **74**, 950-958, (2002).
- 168 Valentine, S. J. & Clemmer, D. E. Temperature-dependent H/D exchange of compact and elongated cytochrome c ions in the gas phase. *Journal of the American Society for Mass Spectrometry* **13**, 506-517, (2002).
- 169 Ruotolo, B. T. & Russell, D. H. Gas-phase conformations of proteolytically derived protein fragments: Influence of solvent on peptide conformation. *Journal of Physical Chemistry B* **108**, 15321-15331, (2004).
- 170 Lee, Y. J., Hoaglund-Hyzer, C. S., Taraszka, J. A., Zientara, G. A., Counterman, A. E. & Clemmer, D. E. Collision-induced dissociation of mobility-separated ions using an orifice-skimmer cone at the back of a drift tube. *Analytical Chemistry* **73**, 3549-3555, (2001).
- 171 Hoaglund-Hyzer, C. S. & Clemmer, D. E. Ion trap/ion mobility/quadrupole/time of flight mass spectrometry for peptide mixture analysis. *Analytical Chemistry* **73**, 177-184, (2001).
- 172 Stone, E., Gillig, K. J., Ruotolo, B., Fuhrer, K., Gonin, M., Schultz, A. & Russell, D. H. Surface-induced dissociation on a MALDI-ion mobility-orthogonal time-of-flight mass spectrometer: Sequencing peptides from an "in-solution" protein digest. *Analytical Chemistry* **73**, 2233-2238, (2001).
- 173 Badman, E. R., Myung, S. & Clemmer, D. E. Gas-phase separations of protein and peptide ion fragments generated by collision-induced dissociation in an ion trap. *Analytical Chemistry* **74**, 4889-4894, (2002).
- 174 Hoaglund-Hyzer, C. S., Lee, Y. J., Counterman, A. E. & Clemmer, D. E. Coupling ion mobility separations, collisional activation techniques, and multiple stages of MS for analysis of complex peptide mixtures. *Analytical Chemistry* **74**, 992-1006, (2002).
- 175 Sowell, R. A., Hersberger, K. E., Kaufman, T. C. & Clemmer, D. E. Examining the proteome of *Drosophila* across organism lifespan. *Journal of Proteome Research* **6**, 3637-3647, (2007).
- 176 Xun, Z., Sowell, R. A., Kaufman, T. C. & Clemmer, D. E. Lifetime proteomic profiling of an A30P alpha-synuclein *Drosophila* model of Parkinson's disease. *Journal of Proteome Research* **6**, 3729-3738, (2007).
- 177 Xun, Z. Y., Sowell, R. A., Kaufman, T. C. & Clemmer, D. E. Protein expression in a *Drosophila* model of Parkinson's disease. *Journal of Proteome Research* **6**, 348-357, (2007).

- 178 Xun, Z. Y., Sowell, R. A., Kaufman, T. C. & Clemmer, D. E. Quantitative proteomics of a presymptomatic A53T alpha-synuclein drosophila model of Parkinson disease. *Molecular & Cellular Proteomics* **7**, 1191-1203, (2008).
- 179 Xun, Z. Y., Kaufman, T. C. & Clemmer, D. E. Proteome response to the panneural expression of human wild-type alpha-synuclein: A Drosophila model of Parkinson's disease. *Journal of Proteome Research* **7**, 3911-3921, (2008).
- 180 Polfer, N. C., Bohrer, B. C., Plasencia, M. D., Paizs, B. & Clemmer, D. E. On the dynamics of fragment isomerization in collision-induced dissociation of peptides. *Journal of Physical Chemistry A* **112**, 1286-1293, (2008).
- 181 Counterman, A. E. & Clemmer, D. E. Cis-trans signatures of proline-containing tryptic peptides in the gas phase. *Analytical Chemistry* **74**, 1946-1951, (2002).
- 182 Alves, P., Arnold, R. J., Clemmer, D. E., Li, Y. X., Reilly, J. P., Sheng, Q. H., Tang, H. X., Xun, Z. Y., Zeng, R. & Radivojac, P. Fast and accurate identification of semi-tryptic peptides in shotgun proteomics. *Bioinformatics* **24**, 102-109, (2008).
- 183 Kurulugama, R. T., Valentine, S. J., Sowell, R. A. & Clemmer, D. E. Development of a high-throughput IMS-IMS-MS approach for analyzing mixtures of biomolecules. *Journal of Proteomics* **71**, 318-331, (2008).
- 184 Riba-Garcia, I., Giles, K., Bateman, R. H. & Gaskell, S. J. Evidence for structural variants of a- and b-type peptide fragment ions using combined ion Mobility/Mass spectrometry. *Journal of the American Society for Mass Spectrometry* **19**, 609-613, (2008).
- 185 Merenbloom, S. I., Bohrer, B. C., Koeniger, S. L. & Clemmer, D. E. Assessing the peak capacity of IMS-IMS separations of tryptic peptide ions in He at 300 K. *Analytical Chemistry* **79**, 515-522, (2007).
- 186 Thalassinos, K., Grabenauer, M., Slade, S. E., Hilton, G. R., Bowers, M. T. & Scrivens, J. H. Characterization of Phosphorylated Peptides Using Traveling Wave-Based and Drift Cell Ion Mobility Mass Spectrometry. *Analytical Chemistry* **81**, 248-254, (2009).
- 187 Henderson, S. C., Valentine, S. J., Counterman, A. E. & Clemmer, D. E. ESI/ion trap/ion mobility/time-of-flight mass spectrometry for rapid and sensitive analysis of biomolecular mixtures. *Analytical Chemistry* **71**, 291-301, (1999).
- 188 Hilderbrand, A. E., Myung, S. & Clemmer, D. E. Exploring crown ethers as shift reagents for ion mobility spectrometry. *Analytical Chemistry* **78**, 6792-6800, (2006).
- 189 Ruotolo, B. T., Gillig, K. J., Stone, E. G. & Russell, D. H. Peak capacity of ion mobility mass spectrometry: Separation of peptides in helium buffer gas. *Journal of Chromatography B-Analytical Technologies in the Biomedical and Life Sciences* **782**, 385-392, (2002).
- 190 Ruotolo, B. T., Gillig, K. J., Stone, E. G., Russell, D. H., Fuhrer, K., Gonin, M. & Schultz, J. A. Analysis of protein mixtures by matrix-assisted laser desorption ionization-ion mobility-

- orthogonal-time-of-flight mass spectrometry. *International Journal of Mass Spectrometry* **219**, 253-267, (2002).
- 191 Ruotolo, B. T., Verbeck, G. F., Thomson, L. M., Woods, A. S., Gillig, K. J. & Russell, D. H. Distinguishing between phosphorylated and nonphosphorylated peptides with ion mobility-mass spectrometry. *Journal of Proteome Research* **1**, 303-306, (2002).
- 192 McLean, J. A. & Russell, D. H. Sub-femtomole peptide detection in ion mobility-time-of-flight mass spectrometry measurements. *Journal of Proteome Research* **2**, 427-430, (2003).
- 193 Ruotolo, B. T., Gillig, K. J., Woods, A. S., Egan, T. F., Ugarov, M. V., Schultz, J. A. & Russell, D. H. Analysis of phosphorylated peptides by ion mobility-mass spectrometry. *Analytical Chemistry* **76**, 6727-6733, (2004).
- 194 Ruotolo, B. T., McLean, J. A., Gillig, K. J. & Russell, D. H. Peak capacity of ion mobility mass spectrometry: the utility of varying drift gas polarizability for the separation of tryptic peptides. *Journal of Mass Spectrometry* **39**, 361-367, (2004).
- 195 Ruotolo, B. T., McLean, J. A., Gillig, K. J. & Russell, D. H. The influence and utility of varying field strength for the separation of tryptic peptides by ion mobility-mass spectrometry. *Journal of the American Society for Mass Spectrometry* **16**, 158-165, (2005).
- 196 Woods, A. S., Ugarov, M., Egan, T., Koomen, J., Gillig, K. J., Fuhrer, K., Gonin, M. & Schultz, J. A. Lipid/peptide/nucleotide separation with MALDI-ion mobility-TOF MS. *Analytical Chemistry* **76**, 2187-2195, (2004).
- 197 Williams, J. P., Giles, K., Green, B. N., Scrivens, J. H. & Bateman, R. H. Ion mobility augments the utility of mass spectrometry in the identification of human hemoglobin variants. *Rapid Communications in Mass Spectrometry* **22**, 3179-3186, (2008).
- 198 Bernstein, S. L., Wytttenbach, T., Baumketner, A., Shea, J. E., Bitan, G., Teplow, D. B. & Bowers, M. T. Amyloid β -protein: Monomer structure and early aggregation states of A beta 42 and its Pro(19) alloform. *Journal of the American Chemical Society* **127**, 2075-2084, (2005).
- 199 Monien, B. H., Fradinger, E. A., Spring, S. M., Bernstein, S. L., Bowers, M. T. & Bitan, G. A novel approach to Alzheimer's disease therapy: Inhibition of A beta 42 oligomerization by C-terminal A beta 42 fragments. *Journal of Peptide Science* **12**, 147-147, (2006).
- 200 Spring, S. M., Bernstein, S. L., Lazo, N. D., Urbanc, B., Stanley, H. E., Bowers, M. T., Teplow, D. B. & Bitan, G. Towards inhibition of amyloid beta-protein oligomerization. *Understanding Biology Using Peptides* **19**, 515-516, (2006).
- 201 Henderson, S. C., Li, J. W., Counterman, A. E. & Clemmer, D. E. Intrinsic size parameters for Val, Ile, Leu, Gln, Thr, Phe, and Trp residues from ion mobility measurements of polyamino acid ions. *Journal of Physical Chemistry B* **103**, 8780-8785, (1999).

- 202 Valentine, S. J., Counterman, A. E., Hoaglund-Hyzer, C. S. & Clemmer, D. E. Intrinsic amino acid size parameters from a series of 113 lysine-terminated tryptic digest peptide ions. *Journal of Physical Chemistry B* **103**, 1203-1207, (1999).
- 203 Counterman, A. E. & Clemmer, D. E. Volumes of individual amino acid residues in gas-phase peptide ions. *Journal of the American Chemical Society* **121**, 4031-4039, (1999).
- 204 Shvartsburg, A. A., Siu, K. W. M. & Clemmer, D. E. Prediction of peptide ion mobilities via a priori calculations from intrinsic size parameters of amino acid residues. *Journal of the American Society for Mass Spectrometry* **12**, 885-888, (2001).
- 205 Mosier, P. D., Counterman, A. E., Jurs, P. C. & Clemmer, D. E. Prediction of peptide ion collision cross sections from topological molecular structure and amino acid parameters. *Analytical Chemistry* **74**, 1360-1370, (2002).
- 206 Barnes, C. A. S. & Clemmer, D. E. Assessing intrinsic side chain interactions between i and i+4 residues in solvent-free peptides: A combinatorial gas-phase approach. *Journal of Physical Chemistry A* **107**, 10566-10579, (2003).
- 207 Hilderbrand, A. E. & Clemmer, D. E. Determination of sequence-specific intrinsic size parameters from cross sections for 162 tripeptides. *Journal of Physical Chemistry B* **109**, 11802-11809, (2005).
- 208 Baumketner, A., Bernstein, S. L., Wyttenbach, T., Bitan, G., Teplow, D. B., Bowers, M. T. & Shea, J. E. Amyloid beta-protein monomer structure: A computational and experimental study. *Protein Science* **15**, 420-428, (2006).
- 209 Baumketner, A., Bernstein, S. L., Wyttenbach, T., Lazo, N. D., Teplow, D. B., Bowers, M. T. & Shea, J. E. Structure of the 21-30 fragment of amyloid beta-protein. *Protein Science* **15**, 1239-1247, (2006).
- 210 Teplow, D. B., Lazo, N. D., Bitan, G., Bernstein, S., Wyttenbach, T., Bowers, M. T., Baumketner, A., Shea, J. E., Urbanc, B., Cruz, L., Borreguero, J. & Stanley, H. E. Elucidating amyloid beta-protein folding and assembly: A multidisciplinary approach. *Accounts of Chemical Research* **39**, 635-645, (2006).
- 211 Krone, M. G., Baumketner, A., Bernstein, S. L., Wyttenbach, T., Lazo, N. D., Teplow, D. B., Bowers, M. T. & Shea, J. E. Effects of familial Alzheimer's disease mutations on the folding nucleation of the amyloid beta-protein. *Journal of Molecular Biology* **381**, 221-228, (2008).
- 212 Barran, P. E., Roeseke, R. W., Pawson, A. J., Sellar, R., Bowers, M. T., Morgan, K., Lu, Z. L., Tsuda, M., Kusakabe, T. & Millar, R. P. Evolution of constrained gonadotropin-releasing hormone ligand conformation and receptor selectivity. *Journal of Biological Chemistry* **280**, 38569-38575, (2005).

- 213 Liu, D. F., Seuthe, A. B., Ehrler, O. T., Zhang, X. H., Wyttenbach, T., Hsu, J. F. & Bowers, M. T. Oxytocin-receptor binding: Why divalent metals are essential. *Journal of the American Chemical Society* **127**, 2024-2025, (2005).
- 214 Loo, J. A. Studying noncovalent protein complexes by electrospray ionization mass spectrometry. *Mass Spectrometry Reviews* **16**, 1-23, (1997).
- 215 Leary, J. A., Schenauer, M. R., Stefanescu, R., Andaya, A., Ruotolo, B. T., Robinson, C. V., Thalassinos, K., Scrivens, J. H., Sokabe, M. & Hershey, J. W. B. Methodology for Measuring Conformation of Solvent-Disrupted Protein Subunits using T-WAVE Ion Mobility MS: An Investigation into Eukaryotic Initiation Factors. *Journal of the American Society for Mass Spectrometry* **20**, 1699-1706, (2009).
- 216 Loo, J. A., Berhane, B., Kaddis, C. S., Wooding, K. M., Xie, Y. M., Kaufman, S. L. & Chernushevich, I. V. Electrospray ionization mass spectrometry and ion mobility analysis of the 20S proteasome complex. *Journal of the American Society for Mass Spectrometry* **16**, 998-1008, (2005).
- 217 Heck, A. J. R. & van den Heuvel, R. H. H. Investigation of intact protein complexes by mass spectrometry. *Mass Spectrometry Reviews* **23**, 368-389, (2004).
- 218 Kaddis, C. S., Lomeli, S. H., Yin, S., Berhane, B., Apostol, M. I., Kickhoefer, V. A., Rome, L. H. & Loo, J. A. Sizing large proteins and protein complexes by electrospray ionization mass spectrometry and ion mobility. *Journal of the American Society for Mass Spectrometry* **18**, 1206-1216, (2007).
- 219 Alverdi, V., Mazon, H., Versluis, C., Hemrika, W., Esposito, G., van den Heuvel, R., Scholten, A. & Heck, A. J. R. cGMP-binding prepares PKG for substrate binding by disclosing the C-terminal domain. *Journal of Molecular Biology* **375**, 1380-1393, (2008).
- 220 Scholten, A., Aye, T. T. & Heck, A. J. R. A multi-angular mass spectrometric view at cyclic nucleotide dependent protein kinases: In vivo characterization and structure/function relationships. *Mass Spectrometry Reviews* **27**, 331-353, (2008).
- 221 Uetrecht, C., Versluis, C., Watts, N. R., Wingfield, P. T., Steven, A. C. & Heck, A. J. R. Stability and shape of hepatitis B virus capsids in vacuo. *Angewandte Chemie-International Edition* **47**, 6247-6251, (2008).
- 222 Lorenzen, K., Olia, A. S., Uetrecht, C., Cingolani, G. & Heck, A. J. R. Determination of stoichiometry and conformational changes in the first step of the P22 tail assembly. *Journal of Molecular Biology* **379**, 385-396, (2008).
- 223 Benesch, J. L. P. Collisional Activation of Protein Complexes: Picking Up the Pieces. *Journal of the American Society for Mass Spectrometry* **20**, 341-348, (2009).
- 224 Fenn, L. S., Kliman, M., Mahsut, A., Zhao, S. R. & McLean, J. A. Characterizing ion mobility-mass spectrometry conformation space for the analysis of complex biological samples. *Analytical and Bioanalytical Chemistry* **394**, 235-244, (2009).

- 225 Case, D. A., Cheatham, T. E., Darden, T., Gohlke, H., Luo, R., Merz, K. M., Onufriev, A., Simmerling, C., Wang, B. & Woods, R. J. The Amber biomolecular simulation programs. *Journal of Computational Chemistry* **26**, 1668-1688, (2005).
- 226 Mesleh, M. F., Hunter, J. M., Shvartsburg, A. A., Schatz, G. C. & Jarrold, M. F. Structural information from ion mobility measurements: Effects of the long-range potential. *Journal of Physical Chemistry* **100**, 16082-16086, (1996).
- 227 von Helden, G., Hsu, M. T., Gotts, N. & Bowers, M. T. Carbon Cluster Cations with up to 84 Atoms - Structures, Formation Mechanism, and Reactivity. *Journal of Physical Chemistry* **97**, 8182-8192, (1993).
- 228 Wyttenbach, T., vonHelden, G., Batka, J. J., Carlat, D. & Bowers, M. T. Effect of the long-range potential on ion mobility measurements. *Journal of the American Society for Mass Spectrometry* **8**, 275-282, (1997).
- 229 Gown, A. M. Genogenic immunohistochemistry: a new era in diagnostic immunohistochemistry. *Current Diagnostic Pathology* **8**, 193-200, (2002).
- 230 Ramos-Vara, J. A. Technical aspects of immunohistochemistry. *Veterinary Pathology* **42**, 405-426, (2005).
- 231 Steinkamp, J. A. Flow-Cytometry. *Review of Scientific Instruments* **55**, 1375-1400, (1984).
- 232 Seda, O., Tremblay, J., Sedova, L. & Hamet, P. Integrating genomics and transcriptomics with geo-ethnicity and the environment for the resolution of complex cardiovascular diseases. *Current Opinion in Molecular Therapeutics* **7**, 583-587, (2005).
- 233 Gabryelski, W. & Froese, K. L. Rapid and sensitive differentiation of anomers, linkage, and position isomers of disaccharides using High-Field Asymmetric Waveform Ion Mobility Spectrometry (FAIMS). *Journal of the American Society for Mass Spectrometry* **14**, 265-277, (2003).
- 234 Wei, X. & Li, L. Mass Spectrometry-Based Proteomics and Peptidomics for Biomarker Discovery in Neurodegenerative Diseases. *International Journal of Clinical and Experimental Pathology* **2**, 132-148, (2009).
- 235 Hoaglund, C. S., Valentine, S. J. & Clemmer, D. E. An ion trap interface for ESI-ion mobility experiments. *Analytical Chemistry* **69**, 4156-4161, (1997).
- 236 Jin, L., Barran, P. E., Deakin, J. A., Lyon, M. & Uhrin, D. Conformation of glycosaminoglycans by ion mobility mass spectrometry and molecular modelling. *Physical Chemistry Chemical Physics* **7**, 3464-3471, (2005).
- 237 Watson, A. D. Lipidomics: a global approach to lipid analysis in biological systems. *Journal of Lipid Research* **47**, 2101-2111, (2006).

- 238 Kemper, P. R. & Bowers, M. T. Electronic-State Chromatography - Application to 1st-Row Transition-Metal Ions. *Journal of Physical Chemistry* **95**, 5134-5146, (1991).
- 239 Verbeck, G. F. *Development of a variable-temperature ion mobility/time-of-flight mass spectrometer for separation of electronic isomers* Ph. D. thesis, Texas A&M University, (2005).
- 240 Bohrer, B. C., Mererbloom, S. I., Koeniger, S. L., Hilderbrand, A. E. & Clemmer, D. E. Biomolecule Analysis by Ion Mobility Spectrometry. *Annual Review of Analytical Chemistry* **1**, 293-327, (2008).
- 241 Merenbloom, S. I., Glaskin, R. S., Henson, Z. B. & Clemmer, D. E. High-Resolution Ion Cyclotron Mobility Spectrometry. *Analytical Chemistry* **81**, 1482-1487, (2009).
- 242 Furche, F., Ahlrichs, R., Weis, P., Jacob, C., Gilb, S., Bierweiler, T. & Kappes, M. M. The structures of small gold cluster anions as determined by a combination of ion mobility measurements and density functional calculations. *Journal of Chemical Physics* **117**, 6982-6990, (2002).
- 243 Mason, E. A. & McDaniel, E. W. Measurement of Drift Velocities and Longitudinal Diffusion Coefficients. in *Transport Properties of Ions in Gases* Ch. 2, 31-102 (John Wiley & Sons, 1988).
- 244 McDaniel, E. W. *Collision Phenomena in Ionized Gases*. (John Wiley & Sons, 1964).
- 245 Kanu, A. B., Dwivedi, P., Tam, M., Matz, L. & Hill, H. H. Ion mobility-mass spectrometry. *Journal of Mass Spectrometry* **43**, 1-22, (2008).
- 246 Steiner, W. E., Clowers, B. H., English, W. A. & Hill, H. H. Atmospheric pressure matrix-assisted laser desorption/ionization with analysis by ion mobility time-of-flight mass spectrometry. *Rapid Communications in Mass Spectrometry* **18**, 882-888, (2004).
- 247 Wyttenbach, T., Kemper, P. R. & Bowers, M. T. Design of a new electrospray ion mobility mass spectrometer. *International Journal of Mass Spectrometry* **212**, 13-23, (2001).
- 248 Dugourd, P., Hudgins, R. R., Clemmer, D. E. & Jarrold, M. F. High-resolution ion mobility measurements. *Review of Scientific Instruments* **68**, 1122-1129, (1997).
- 249 Giles, K., Pringle, S. D., Worthington, K. R., Little, D., Wildgoose, J. L. & Bateman, R. H. Applications of a travelling wave-based radio-frequency only stacked ring ion guide. *Rapid Communications in Mass Spectrometry* **18**, 2401-2414, (2004).
- 250 Pringle, S. D., Giles, K., Wildgoose, J. L., Williams, J. P., Slade, S. E., Thalassinou, K., Bateman, R. H., Bowers, M. T. & Scrivens, J. H. An investigation of the mobility separation of some peptide and protein ions using a new hybrid quadrupole/travelling wave IMS/oa-ToF instrument. *International Journal of Mass Spectrometry* **261**, 1-12, (2007).

- 251 Vakhrushev, S. Y., Langridge, J., Campuzano, I., Hughes, C. & Peter-Katlinic, J. Ion mobility mass spectrometry analysis of human glycourinome. *Analytical Chemistry* **80**, 2506-2513, (2008).
- 252 Buryakov, I. A., Krylov, E. V., Makas, A. L., Nazarov, E. G., Pervukhin, V. V. & Rasulev, U. K. Ion Division by Their Mobility in High Tension Alternating Electric Field. *Pisma V Zhurnal Tekhnicheskoi Fiziki* **17**, 60-65, (1991).
- 253 Buryakov, I. A., Krylov, E. V., Nazarov, E. G. & Rasulev, U. K. A New Method of Separation of Mult-Atomic Ions by Mobility at Atmospheric-Pressure Using a High-Frequency Amplitude-Asymmetric Strong Electric-Field *International Journal of Mass Spectrometry and Ion Processes* **128**, 143-148, (1993).
- 254 Krylov, E. V., Coy, S. L. & Nazarov, E. G. Temperature effects in differential mobility spectrometry. *International Journal of Mass Spectrometry* **279**, 119-125, (2009).
- 255 Krylov, E. V., Nazarov, E. G. & Miller, R. A. Differential mobility spectrometer: Model of operation. *International Journal of Mass Spectrometry* **266**, 76-85, (2007).
- 256 Shvartsburg, A. A., Tang, K. & Smith, R. D. Optimization of the design and operation of FAIMS analyzers. *Journal of the American Society for Mass Spectrometry* **16**, 2-12, (2005).
- 257 Shvartsburg, A. A., Bryskiewicz, T., Purves, R. W., Tang, K. Q., Guevremont, R. & Smith, R. D. Field asymmetric waveform ion mobility spectrometry studies of proteins: Dipole alignment in ion mobility spectrometry? *Journal of Physical Chemistry B* **110**, 21966-21980, (2006).
- 258 Sundarapandian, S., May, J. C. & McLean, J. A. Dual Source Ion Mobility-Mass Spectrometer for Direct Comparison of Electrospray Ionization and MALDI Collision Cross Section Measurements. *Analytical Chemistry* **82**, 3247-3254, (2010).
- 259 Reyzer, M. L., Hsieh, Y. S., Ng, K., Korfmacher, W. A. & Caprioli, R. M. Direct analysis of drug candidates in tissue by matrix-assisted laser desorption/ionization mass spectrometry. *Journal of Mass Spectrometry* **38**, 1081-1092, (2003).
- 260 Stone, E. G., Gillig, K. J., Ruotolo, B. T. & Russell, D. H. Optimization of a matrix-assisted laser desorption ionization-ion mobility-surface-induced dissociation-orthogonal-time-of-flight mass spectrometer: simultaneous acquisition of multiple correlated MS1 and MS2 spectra. *International Journal of Mass Spectrometry* **212**, 519-533, (2001).
- 261 Sun, W. J., May, J. C. & Russell, D. H. A novel surface-induced dissociation instrument for ion mobility-time-of-flight mass spectrometry. *International Journal of Mass Spectrometry* **259**, 79-86, (2007).
- 262 Domon, B. & Costello, C. E. A Systematic Nomenclature for Carbohydrate Fragmentations in Fab-MS MS Spectra of Glycoconjugates. *Glycoconjugate Journal* **5**, 397-409, (1988).

- 263 Chen, H. S., Rejtar, T., Andreev, V., Moskovets, E. & Karger, B. L. High-speed, high-resolution monolithic capillary LC-MALDI MS using an off-line continuous deposition interface for proteomic analysis. *Analytical Chemistry* **77**, 2323-2331, (2005).
- 264 Anderson, N. L. & Anderson, N. G. The human plasma proteome - History, character, and diagnostic prospects. *Molecular & Cellular Proteomics* **1**, 845-867, (2002).
- 265 Caprioli, R. M., Farmer, T. B. & Gile, J. Molecular imaging of biological samples: Localization of peptides and proteins using MALDI-TOF MS. *Analytical Chemistry* **69**, 4751-4760, (1997).
- 266 Schwartz, S. A., Reyzer, M. L. & Caprioli, R. M. Direct tissue analysis using matrix-assisted laser desorption/ionization mass spectrometry: practical aspects of sample preparation. *Journal of Mass Spectrometry* **38**, 699-708, (2003).
- 267 Stoeckli, M., Chaurand, P., Hallahan, D. E. & Caprioli, R. M. Imaging mass spectrometry: A new technology for the analysis of protein expression in mammalian tissues. *Nature Medicine* **7**, 493-496, (2001).
- 268 Trim, P. J., Henson, C. M., Avery, J. L., McEwen, A., Snel, M. F., Claude, E., Marshall, P. S., West, A., Princivalle, A. P. & Clench, M. R. Matrix-Assisted Laser Desorption/Ionization Mobility Separation-Mass Spectrometry Imaging of Vinblastine in Whole Body Tissue Sections. *Analytical Chemistry* **80**, 8628-8634, (2008).
- 269 Rizzi, M., Baltes, M., Theobald, U. & Reuss, M. In vivo analysis of metabolic dynamics in *Saccharomyces cerevisiae* .2. Mathematical model. *Biotechnology and Bioengineering* **55**, 592-608, (1997).
- 270 Koning, W. d. & Dam, K. v. A method for the determination of changes of glycolytic metabolites in yeast on a subsecond time scale using extraction at neutral pH. *Analytical Biochemistry* **204**, 118-123, (1992).
- 271 Ross, J. F. & Orłowski, M. Growth-Rate-Dependent Adjustment of Ribosome Function in Chemostat-Grown Cells of the Fungus *Mucor-Racemosus*. *Journal of Bacteriology* **149**, 650-653, (1982).
- 272 Nyquist, H. Certain topics in telegraph transmission theory (Reprinted from Transactions of the A. I. E. E., February, pg 617-644, 1928). *Proceedings of the Ieee* **90**, 280-305, (2002).
- 273 Shannon, C. E. Communication in the presence of noise (Reprinted from the Proceedings of the IRE, vol 37, pg 10-21, 1949). *Proceedings of the Ieee* **86**, 447-457, (1998).
- 274 Vestal, M. L. The Future of Biological Mass Spectrometry. *Journal of the American Society for Mass Spectrometry* **22**, 953-959, (2011).

- 275 Domon, B. & Aebersold, R. Review - Mass spectrometry and protein analysis. *Science* **312**, 212-217, (2006).
- 276 Rubakhin, S. S. & Sweedler, J. V. *Mass Spectrometry Imaging: Principles and Protocols*. Vol. 656 (Springer, 2010).
- 277 Kell, D. B. Metabolomics and systems biology: making sense of the soup. *Current Opinion in Microbiology* **7**, 296-307, (2004).
- 278 Kell, D. B., Brown, M., Davey, H. M., Dunn, W. B., Spasic, I. & Oliver, S. G. Metabolic footprinting and systems biology: The medium is the message. *Nature Reviews Microbiology* **3**, 557-565, (2005).
- 279 Sia, S. K. & Whitesides, G. M. Microfluidic devices fabricated in poly(dimethylsiloxane) for biological studies. *Electrophoresis* **24**, 3563-3576, (2003).
- 280 Whitesides, G. M., Ostuni, E., Takayama, S., Jiang, X. Y. & Ingber, D. E. Soft lithography in biology and biochemistry. *Annual Review of Biomedical Engineering* **3**, 335-373, (2001).
- 281 Faley, S., Seale, K., Hughey, J., Schaffer, D. K., VanCornpernelle, S., McKinney, B., Baudenbacher, F., Unutmaz, D. & Wikswow, J. P. Microfluidic platform for real-time signaling analysis of multiple single T cells in parallel. *Lab on a Chip* **8**, 1700-1712, (2008).
- 282 Whitesides, G. M. The origins and the future of microfluidics. *Nature* **442**, 368-373, (2006).
- 283 Faley, S. L., Copland, M., Wlodkowic, D., Kolch, W., Seale, K. T., Wikswow, J. P. & Cooper, J. M. Microfluidic single cell arrays to interrogate signalling dynamics of individual, patient-derived hematopoietic stem cells. *Lab on a Chip* **9**, 2659-2664, (2009).
- 284 Warnement, M. R., Faley, S. L., Wikswow, J. P. & Rosenthal, S. J. Quantum dot probes for monitoring dynamic cellular response: Reporters of T cell activation. *Ieee Transactions on Nanobioscience* **5**, 268-272, (2006).
- 285 Eklund, S. E., Cliffel, D. E., Kozlov, E., Prokop, A., Wikswow, J. & Baudenbacher, F. Modification of the Cytosensor (TM) microphysiometer to simultaneously measure extracellular acidification and oxygen consumption rates. *Analytica Chimica Acta* **496**, 93-101, (2003).
- 286 Eklund, S. E., Snider, R. M., Wikswow, J., Baudenbacher, F., Prokop, A. & Cliffel, D. E. Multianalyte microphysiometry as a tool in metabolomics and systems biology. *Journal of Electroanalytical Chemistry* **587**, 333-339, (2006).
- 287 Eklund, S. E., Thompson, R. G., Snider, R. M., Carney, C. K., Wright, D. W., Wikswow, J. & Cliffel, D. E. Metabolic Discrimination of Select List Agents by Monitoring Cellular Responses in a Multianalyte Microphysiometer. *Sensors* **9**, 2117-2133, (2009).

- 288 Prokop, A., Prokop, Z., Schaffer, D., Kozlov, E., Wikswow, J., Cliffel, D. & Baudenbacher, F. NanoLiterBioReactor: Long-term mammalian cell culture at nanofabricated scale. *Biomedical Microdevices* **6**, 325-339, (2004).
- 289 Velkovsky, M., Cliffel, D., Eklund, S., Eluvathingal, S., Stremmer, M. & Wikswow, J. Extracting metabolic fluxes from measurements with a multianalyte Microphysiometer. *Biophysical Journal* **88**, 521a-522a, (2005).
- 290 Velkovsky, M., Snider, R., Cliffel, D. E. & Wikswow, J. P. Modeling the measurements of cellular fluxes in microbioreactor devices using thin enzyme electrodes. *Journal of Mathematical Chemistry* **49**, 251-275, (2011).
- 291 Wikswow, J. P., Prokop, A., Baudenbacher, F., Cliffel, D., Csukas, B. & Velkovsky, M. Engineering challenges of BioNEMS: the integration of microfluidics, micro- and nanodevices, models and external control for systems biology. *Iee Proceedings-Nanobiotechnology* **153**, 81-101, (2006).
- 292 Werdich, A. A., Lima, E. A., Ivanov, B., Ges, I., Anderson, M. E., Wikswow, J. P. & Baudenbacher, F. J. A microfluidic device to confine a single cardiac myocyte in a sub-nanoliter volume on planar microelectrodes for extracellular potential recordings. *Lab on a Chip* **4**, 357-362, (2004).
- 293 Ges, I. A. & Baudenbacher, F. Microfluidic device to confine single cardiac myocytes in sub-nanoliter volumes for extracellular pH measurements. *Journal of Experimental Nanoscience* **3**, 63-75, (2008).
- 294 Ges, I. A. & Baudenbacher, F. Enzyme electrodes to monitor glucose consumption of single cardiac myocytes in sub-nanoliter volumes. *Biosensors & Bioelectronics* **25**, 1019-1024, (2010).
- 295 Ges, I. A., Dzhura, I. A. & Baudenbacher, F. J. On-chip acidification rate measurements from single cardiac cells confined in sub-nanoliter volumes. *Biomedical Microdevices* **10**, 347-354, (2008).
- 296 Ges, I. A., Ivanov, B. L., Schaffer, D. K., Lima, E. A., Werdich, A. A. & Baudenbacher, F. J. Thin-film IrOx pH microelectrode for microfluidic-based microsystems. *Biosensors & Bioelectronics* **21**, 248-256, (2005).
- 297 Ges, I. A., Ivanov, B. L., Werdich, A. A. & Baudenbacher, F. J. Differential pH measurements of metabolic cellular activity in nl culture volumes using microfabricated iridium oxide electrodes. *Biosensors & Bioelectronics* **22**, 1303-1310, (2007).
- 298 Enders, J. R., Goodwin, C. R., Marasco, C. C., Seale, K. T., Wikswow, J. P. & McLean, J. A. Advanced Structural Mass Spectrometry for Systems Biology: Pulling the Needles from Haystacks. *Current Trends in Mass Spectrometry* **July**, 18-23, (2011).
- 299 Giddings, J. C. Two-Dimensional Separations - Concept and Promise. *Analytical Chemistry* **56**, 1258A, (1984).

- 300 Smith, C., Want, E., O'Maille, G., Abagyan, R. & Siuzdak, G. XCMS: processing mass spectrometry data for metabolite profiling using nonlinear peak alignment, matching, and identification. *Anal Chem* **78**, 779 - 787, (2006).
- 301 Broeckling, C., Reddy, I., Duran, A., Zhao, X. & Sumner, L. MET-IDEA: data extraction tool for mass spectrometry-based metabolomics. *Anal Chem* **78**, 4334 - 4341, (2006).
- 302 Baran, R., Kochi, H., Saito, N., Suematsu, M., Soga, T., Nishioka, T., Robert, M. & Tomita, M. MathDAMP: a package for differential analysis of metabolite profiles. *BMC Bioinformatics* **7**, 530, (2006).
- 303 Sud, M., Fahy, E., Cotter, D., Brown, A., Dennis, E. A., Glass, C. K., Merrill, A. H., Murphy, R. C., Raetz, C. R. H., Russell, D. W. & Subramaniam, S. LMSD: LIPID MAPS structure database. *Nucleic Acids Research* **35**, D527-D532, (2007).
- 304 Roper, M. G., Shackman, J. G., Dahlgren, G. M. & Kennedy, R. T. Microfluidic chip for continuous monitoring of hormone secretion from live cells using an electrophoresis-based immunoassay. *Analytical Chemistry* **75**, 4711-4717, (2003).
- 305 Cellar, N. A., Burns, S. T., Meiners, J. C., Chen, H. & Kennedy, R. T. Microfluidic chip for low-flow push-pull perfusion sampling in vivo with on-line analysis of amino acids. *Analytical Chemistry* **77**, 7067-7073, (2005).
- 306 Shackman, J. G., Dahlgren, G. M., Peters, J. L. & Kennedy, R. T. Perfusion and chemical monitoring of living cells on a microfluidic chip. *Lab on a Chip* **5**, 56-63, (2005).
- 307 Cellar, N. A. & Kennedy, R. T. A capillary-PDMS hybrid chip for separations-based sensing of neurotransmitters in vivo. *Lab on a Chip* **6**, 1205-1212, (2006).
- 308 Oleschuk, R. D. & Harrison, D. J. Analytical microdevices for mass spectrometry. *Trends in Analytical Chemistry* **19**, 379-388, (2000).
- 309 Chan, J. H., Timperman, A. T., Qin, D. & Aebersold, R. Microfabricated polymer devices for automated sample delivery of peptides for analysis by electrospray ionization tandem mass spectrometry. *Analytical Chemistry* **71**, 4437-4444, (1999).
- 310 Chiou, C. H., Lee, G. B., Hsu, H. T., Chen, P. W. & Liao, P. C. Micro devices integrated with microchannels and electrospray nozzles using PDMS casting techniques. *Sensors and Actuators B-Chemical* **86**, 280-286, (2002).
- 311 Jiang, Y., Wang, P. C., Locascio, L. E. & Lee, C. S. Integrated plastic microfluidic devices with ESI-MS for drug screening and residue analysis. *Analytical Chemistry* **73**, 2048-2053, (2001).
- 312 Enders, J. R., Marasco, C. C., Kole, A., Nguyen, B., Sevugarajan, S., Seale, K. T., Wikswo, J. P. & McLean, J. A. Towards monitoring real-time cellular response using an integrated

- microfluidics-matrix assisted laser desorption ionisation/nanoelectrospray ionisation-ion mobility-mass spectrometry platform. *IET Systems Biology* **4**, 416-427, (2010).
- 313 LeDuc, P. R., Messner, W. C. & Wikswo, J. P. How Do Control-Based Approaches Enter into Biology? *Annual Review of Biomedical Engineering* **13**, in press, (2011).
- 314 Rohner, T. C., Staab, D. & Stoeckli, M. MALDI mass spectrometric imaging of biological tissue sections. *Mechanisms of Ageing and Development* **126**, 177-185, (2005).
- 315 Fabrizio, P. & Longo, V. D. The chronological life span of *Saccharomyces cerevisiae*. *Aging Cell* **2**, 73-81, (2003).
- 316 Rayleigh, L. On the Capillary Phenomena of Jets. *Proceedings of the Royal Society of London* **29**, 71-97, (1879).
- 317 Rayleigh, L. On the equilibrium of liquid conducting masses charged with electricity. *The London, Edinburgh, and Dublin Philosophical Magazine* **14**, 184-186, (1882).
- 318 Rayleigh, L. On convection currents in a horizontal layer of fluids, when the higher temperature is on the under side. *The London, Edinburgh, and Dublin Philosophical Magazine* **32**, 529-546, (1916).
- 319 Zeleny, J. The Electrical Discharge from Liquid Points, and a Hydrostatic Method of Measuring the Electric Intensity at Their Surfaces. *Physical Review* **3**, 69, (1914).
- 320 Zeleny, J. Instability of Electrified Liquid Surfaces. *Physical Review* **10**, 1, (1917).
- 321 Taylor, G. Disintegration of Water Drops in an Electric Field. *Proceedings of the Royal Society of London. Series A. Mathematical and Physical Sciences* **280**, 383-397, (1964).
- 322 Fenn, J. B., Mann, M., Meng, C. K., Wong, S. F. & Whitehouse, C. M. Electrospray Ionization for Mass-Spectrometry of Large Biomolecules. *Science* **246**, 64-71, (1989).
- 323 Dole, M., Mack, L. L. & Hines, R. L. Molecular Beams of Macroions. *Journal of Chemical Physics* **49**, 2240-&, (1968).
- 324 Rollgen, F. W., Bramerweger, E. & Butfering, L. Field-Ion Emission from Liquid Solutions - Ion Evaporation against Electrohydrodynamic Disintegration. *Journal De Physique* **48**, 253-256, (1987).
- 325 Schmelzeisenredeker, G., Butfering, L. & Rollgen, F. W. Desolvation of Ions and Molecules in Thermospray Mass-Spectrometry. *International Journal of Mass Spectrometry and Ion Processes* **90**, 139-150, (1989).
- 326 Nehring, H., Thiebes, S., Butfering, L. & Rollgen, F. W. Cluster Ion Formation in Thermospray Mass-Spectrometry of Ammonium-Salts. *International Journal of Mass Spectrometry and Ion Processes* **128**, 123-132, (1993).

- 327 Kebarle, P. & Peschke, M. On the mechanisms by which the charged droplets produced by electrospray lead to gas phase ions. *Analytica Chimica Acta* **406**, 11-35, (2000).
- 328 Iribarne, J. V. & Thomson, B. A. Evaporation of Small Ions from Charged Droplets. *Journal of Chemical Physics* **64**, 2287-2294, (1976).
- 329 Thomson, B. A. & Iribarne, J. V. Field-Induced Ion Evaporation from Liquid Surfaces At Atmospheric-Pressure. *Journal of Chemical Physics* **71**, 4451-4463, (1979).
- 330 Fenn, J. B. Electrospray wings for molecular elephants (Nobel lecture). *Angewandte Chemie-International Edition* **42**, 3871-3894, (2003).
- 331 Yamashita, M. & Fenn, J. B. Electrospray Ion-Source - Another Variation on the Free-Jet Theme. *Journal of Physical Chemistry* **88**, 4451-4459, (1984).
- 332 Fenn, J. B., Mann, M., Meng, C. K., Wong, S. F. & Whitehouse, C. M. Electrospray Ionization-Principles and Practice. *Mass Spectrometry Reviews* **9**, 37-70, (1990).
- 333 Vanberkel, G. J., Mcluckey, S. A. & Glish, G. L. Electrochemical Origin of Radical Cations Observed in Electrospray Ionization Mass-Spectra. *Analytical Chemistry* **64**, 1586-1593, (1992).
- 334 Morand, K., Talbo, G. & Mann, M. Oxidation of Peptides during Electrospray-Ionization. *Rapid Communications in Mass Spectrometry* **7**, 738-743, (1993).
- 335 Van Berkel, G. J., Quirke, J. M. E., Tigani, R. A., Dilley, A. S. & Covey, T. R. Derivatization for electrospray ionization mass spectrometry. 3. Electrochemically ionizable derivatives. *Analytical Chemistry* **70**, 1544-1554, (1998).
- 336 Speight, J. G. & Lange, N. A. *Lange's handbook of chemistry*. (McGraw-Hill Professional, 2004).
- 337 Cech, N. B. & Enke, C. G. Practical implications of some recent studies in electrospray ionization fundamentals. *Mass Spectrometry Reviews* **20**, 362-387, (2001).
- 338 Hartman, R. P. A., Brunner, D. J., Camelot, D. M. A., Marijnissen, J. C. M. & Scarlett, B. Jet Break-Up in Electrohydrodynamic Atomization in the Cone-Jet Mode. *Journal of Aerosol Science* **31**, 65-95, (2000).
- 339 Rayleigh, L. Chapter XX. in *The Theory of Sound* Vol. 2 Ch. 20, 343-375 (MacMillan and Co., Inc., 1896).
- 340 Cloupeau, M. & Prunet-Foch, B. Electrostatic spraying of liquids: Main functioning modes. *Journal of Electrostatics* **25**, 165-184, (1990).
- 341 Gomez, A. & Tang, K. Q. Charge and Fission of Droplets in Electrostatic Sprays. *Physics of Fluids* **6**, 404-414, (1994).

- 342 Duft, D., Achtzehn, T., Muller, R., Huber, B. A. & Leisner, T. Coulomb fission - Rayleigh jets from levitated microdroplets. *Nature* **421**, 128-128, (2003).
- 343 Hilger, R. T., Westphal, M. S. & Smith, L. M. Controlling charge on levitating drops. *Analytical Chemistry* **79**, 6027-6030, (2007).
- 344 Taflin, D. C., Ward, T. L. & Davis, E. J. Electrified Droplet Fission and the Rayleigh Limit. *Langmuir* **5**, 376-384, (1989).
- 345 Tang, K. Q. & Smith, R. D. Physical/chemical separations in the break-up of highly charged droplets from electrosprays. *Journal of the American Society for Mass Spectrometry* **12**, 343-347, (2001).
- 346 Tang, K. Q. & Smith, R. D. Theoretical prediction of charged droplet evaporation and fission in electrospray ionization. *International Journal of Mass Spectrometry* **187**, 97-105, (1999).
- 347 Kebarle, P. & Tang, L. From Ions in Solution to Ions in the Gas-Phase - the Mechanism of Electrospray Mass-Spectrometry. *Analytical Chemistry* **65**, A972-A986, (1993).
- 348 Bahr, U., Pfenninger, A., Karas, M. & Stahl, B. High sensitivity analysis of neutral underivatized oligosaccharides by nanoelectrospray mass spectrometry. *Analytical Chemistry* **69**, 4530-4535, (1997).
- 349 Karas, M., Bahr, U. & Dulcks, T. Nano-electrospray ionization mass spectrometry: addressing analytical problems beyond routine. *Fresenius Journal of Analytical Chemistry* **366**, 669-676, (2000).
- 350 Kebarle, P. A brief overview of the present status of the mechanisms involved in electrospray mass spectrometry. *Journal of Mass Spectrometry* **35**, 804-817, (2000).
- 351 Loscertales, I. G. & Delamora, J. F. Experiments on the Kinetics of Field Evaporation of Small Ions from Droplets. *Journal of Chemical Physics* **103**, 5041-5060, (1995).
- 352 Gamero-Castano, M. & de la Mora, J. F. Kinetics of small ion evaporation from the charge and mass distribution of multiply charged clusters in electrosprays. *Journal of Mass Spectrometry* **35**, 790-803, (2000).
- 353 Gamero-Castano, M. & de la Mora, J. F. Mechanisms of electrospray ionization of singly and multiply charged salt clusters. *Analytica Chimica Acta* **406**, 67-91, (2000).
- 354 de la Mora, J. F. Electrospray ionization of large multiply charged species proceeds via Dole's charged residue mechanism. *Analytica Chimica Acta* **406**, 93-104, (2000).
- 355 Zhou, S. L. & Cook, K. D. Protonation in electrospray mass spectrometry: Wrong-way-round or right-way-round? *Journal of the American Society for Mass Spectrometry* **11**, 961-966, (2000).

- 356 Wilm, M. & Mann, M. Analytical Properties of the Nanoelectrospray Ion Source. *Analytical Chemistry* **68**, 1-8, (1996).
- 357 Juraschek, R., Dulcks, T. & Karas, M. Nanoelectrospray - More than just a minimized-flow electrospray ionization source. *Journal of the American Society for Mass Spectrometry* **10**, 300-308, (1999).
- 358 Constantopoulos, T. L., Jackson, G. S. & Enke, C. G. Effects of salt concentration on analyte response using electrospray ionization mass spectrometry. *Journal of the American Society for Mass Spectrometry* **10**, 625-634, (1999).
- 359 King, R., Bonfiglio, R., Fernandez-Metzler, C., Miller-Stein, C. & Olah, T. Mechanistic investigation of ionization suppression in electrospray ionization. *Journal of the American Society for Mass Spectrometry* **11**, 942-950, (2000).
- 360 Annesley, T. M. Ion suppression in mass spectrometry. *Clinical Chemistry* **49**, 1041-1044, (2003).
- 361 Mallet, C. R., Lu, Z. L. & Mazzeo, J. R. A study of ion suppression effects in electrospray ionization from mobile phase additives and solid-phase extracts. *Rapid Communications in Mass Spectrometry* **18**, 49-58, (2004).
- 362 Jessome, L. L. & Volmer, D. A. Ion suppression: A major concern in mass spectrometry. *Lc Gc North America* **24**, 498-510, (2006).
- 363 Buchholz, A., Hurlebaus, J., Wandrey, C. & Takors, R. Metabolomics: quantification of intracellular metabolite dynamics. *Biomolecular Engineering* **19**, 5-15, (2002).
- 364 Maughan, R. J. Fluid and electrolyte loss and replacement in exercise*. *Journal of Sports Sciences* **9**, 117-142, (1991).
- 365 Moore, G. E., Gerner, R. E. & Franklin, H. A. Culture of Normal Human Leukocytes. *Journal of the American Medical Association* **199**, 519-&, (1967).
- 366 Mossinger, J. Invitro Cultivation of Adult Litomosoides-Carinii - Evaluation of Basic Culture Media, Gas Phases and Supplements. *Parasitology* **103**, 85-95, (1991).
- 367 Matuszewski, B. K., Constanzer, M. L. & Chavez-Eng, C. M. Strategies for the assessment of matrix effect in quantitative bioanalytical methods based on HPLC-MS/MS. *Analytical Chemistry* **75**, 3019-3030, (2003).
- 368 Cunningham, B. A., Deeney, J. T., Bliss, C. R., Corkey, B. E. & Tornheim, K. Glucose-induced oscillatory insulin secretion in perfused rat pancreatic islets and clonal beta-cells (HIT). *American Journal of Physiology-Endocrinology and Metabolism* **271**, E702-E710, (1996).

- 369 Puig, D. & Barcelo, D. Comparative-Study of Online Solid-Phase Extraction Followed by Uv and Electrochemical Detection in Liquid-Chromatography for the Determination of Priority Phenols in River Water Samples. *Analytica Chimica Acta* **311**, 63-69, (1995).
- 370 Figeys, D., Ducret, A. & Aebersold, R. Identification of proteins by capillary electrophoresis tandem mass spectrometry - Evaluation of an on-line solid-phase extraction device. *Journal of Chromatography A* **763**, 295-306, (1997).
- 371 Bjarnason, B., Chimuka, L. & Ramstrom, O. On-line solid-phase extraction of triazine herbicides using a molecularly imprinted polymer for selective sample enrichment. *Analytical Chemistry* **71**, 2152-2156, (1999).
- 372 Stoob, K., Singer, H. P., Goetz, C. W., Ruff, M. & Mueller, S. R. Fully automated online solid phase extraction coupled directly to liquid chromatography-tandem mass spectrometry - Quantification of sulfonamide antibiotics, neutral and acidic pesticides at low concentrations in surface waters. *Journal of Chromatography A* **1097**, 138-147, (2005).
- 373 Kuklenyik, Z., Needham, L. L. & Calafat, A. M. Measurement of 18 perfluorinated organic acids and amides in human serum using on-line solid-phase extraction. *Analytical Chemistry* **77**, 6085-6091, (2005).
- 374 Su, C. K., Li, T. W. & Sun, Y. C. Online in-tube solid-phase extraction using a nonfunctionalized PVC tube coupled with ICPMS for in vivo monitoring of trace metals in rat brain microdialysates. *Analytical Chemistry* **80**, 6959-6967, (2008).
- 375 Chiuminatto, U., Gosetti, F., Dossetto, P., Mazzucco, E., Zampieri, D., Robotti, E., Gennaro, M. C. & Marengo, E. Automated Online Solid Phase Extraction Ultra High Performance Liquid Chromatography Method Coupled with Tandem Mass Spectrometry for Determination of Forty-Two Therapeutic Drugs and Drugs of Abuse in Human Urine. *Analytical Chemistry* **82**, 5636-5645, (2010).
- 376 Gosetti, F., Chiuminatto, U., Zampieri, D., Mazzucco, E., Marengo, E. & Gennaro, M. C. A new on-line solid phase extraction high performance liquid chromatography tandem mass spectrometry method to study the sun light photodegradation of mono-chloroanilines in river water. *Journal of Chromatography A* **1217**, 3427-3434, (2010).
- 377 Kuklenyik, Z., Calafat, A. M., Barr, J. R. & Pirkle, J. L. Design of online solid phase extraction-liquid chromatography-tandem mass spectrometry (SPE-LC-MS/MS) hyphenated systems for quantitative analysis of small organic compounds in biological matrices. *Journal of Separation Science* **34**, 3606-3618, (2011).
- 378 Chen, Q. S., Wu, J., Zhang, Y. D. & Lin, J. M. Qualitative and Quantitative Analysis of Tumor Cell Metabolism via Stable Isotope Labeling Assisted Microfluidic Chip Electrospray Ionization Mass Spectrometry. *Analytical Chemistry* **84**, 1695-1701, (2012).
- 379 Jones, R. L., Owen, L. J., Adaway, J. E. & Keevil, B. G. Simultaneous analysis of cortisol and cortisone in saliva using XLC-MS/MS for fully automated online solid phase

- extraction. *Journal of Chromatography B-Analytical Technologies in the Biomedical and Life Sciences* **881-82**, 42-48, (2012).
- 380 Moser, C., Zoderer, D., Luef, G., Rauchenzauner, M., Wildt, L., Griesmacher, A. & Seger, C. Simultaneous online SPE-LC-MS/MS quantification of six widely used synthetic progestins in human plasma. *Analytical and Bioanalytical Chemistry* **403**, 961-972, (2012).
- 381 Su, C. K., Lin, Y. L. & Sun, Y. C. Simultaneous in vivo monitoring of multiple brain metals using an online microdialysis-in-loop solid phase extraction-inductively coupled plasma mass spectrometry system. *Journal of Analytical Atomic Spectrometry* **27**, 56-62, (2012).
- 382 Arkles, B. Tailoring Surfaces with Silanes. *Chemtech* **7**, 766-778, (1977).
- 383 Norwood, D. L., Kodo, N., Millington, D. S. & Gaskell, S. J. Application of continuous-flow liquid chromatography/fast-atom bombardment mass spectrometry to the analysis of diagnostic acylcarnitines in human urine. *Rapid Communications in Mass Spectrometry* **2**, 269-272, (1988).
- 384 Steele, K. M. & Lunte, C. E. Microdialysis Sampling Coupled to Online Microbore Liquid-Chromatography for Pharmacokinetic Studies. *Journal of Pharmaceutical and Biomedical Analysis* **13**, 149-154, (1995).
- 385 Kuban, P., Berg, M., Garcia, C. & Karlberg, B. On-line flow sample stacking in a flow injection analysis-capillary electrophoresis system: 2000-fold enhancement of detection sensitivity for priority phenol pollutants. *Journal of Chromatography A* **912**, 163-170, (2001).
- 386 Wang, S. L., Huang, X. J., Fang, Z. L. & Dasgupta, P. K. A miniaturized liquid core waveguide-capillary electrophoresis system with flow injection sample introduction and fluorometric detection using light-emitting diodes. *Analytical Chemistry* **73**, 4545-4549, (2001).
- 387 Hanrahan, G., Dahdouh, F., Clarke, K. & Gomez, F. A. Flow injection-capillary electrophoresis (FI-CE): Recent advances and applications. *Current Analytical Chemistry* **1**, 321-328, (2005).
- 388 Simpson, D. C. & Smith, R. D. Combining capillary electrophoresis with mass spectrometry for applications in proteomics. *Electrophoresis* **26**, 1291-1305, (2005).
- 389 Lutz, E. S. M. & Larsson, M. On-line microdialysis-electrospray mass spectrometry for automated desalting of small-volume peptide samples. *Chromatographia* **49**, S28-S34, (1999).
- 390 Hannis, J. C. & Muddiman, D. C. Characterization of a microdialysis approach to prepare polymerase chain reaction products for electrospray ionization mass spectrometry using on-line ultraviolet absorbance measurements and inductively coupled plasma-atomic

- emission spectroscopy. *Rapid Communications in Mass Spectrometry* **13**, 323-330, (1999).
- 391 Jakubowski, J. A., Hatcher, N. G. & Sweedler, J. V. Online microdialysis-dynamic nanoelectrospray ionization-mass spectrometry for monitoring neuropeptide secretion. *Journal of Mass Spectrometry* **40**, 924-931, (2005).
- 392 Bugamelli, F., Marcheselli, C., Barba, E. & Raggi, M. A. Determination of L-dopa, carbidopa, 3-O-methyldopa and entacapone in human plasma by HPLC-ED. *Journal of Pharmaceutical and Biomedical Analysis* **54**, 562-567, (2011).
- 393 Liu, C. L., Muddiman, D. C., Tang, K. Q. & Smith, R. D. Improving the microdialysis procedure for electrospray ionization mass spectrometry of biological samples. *Journal of Mass Spectrometry* **32**, 425-431, (1997).
- 394 Jorgenson, J. W. & Lukacs, K. D. Zone Electrophoresis in Open-Tubular Glass-Capillaries. *Analytical Chemistry* **53**, 1298-1302, (1981).
- 395 Jorgenson, J. W. & Lukacs, K. D. Capillary Zone Electrophoresis. *Science* **222**, 266-272, (1983).
- 396 Liu, Y., Lopezavila, V., Zhu, J. J., Wiederin, D. R. & Beckert, W. F. Capillary Electrophoresis Coupled Online with Inductively-Coupled Plasma-Mass Spectrometry for Elemental Speciation. *Analytical Chemistry* **67**, 2020-2025, (1995).
- 397 Sun, J., He, B., Yin, Y. G., Li, L. & Jiang, G. B. Speciation of organotin compounds in environmental samples with semi-permanent coated capillaries by capillary electrophoresis coupled with inductively coupled plasma mass spectrometry. *Analytical Methods* **2**, 2025-2031, (2010).
- 398 Sun, J., He, B., Liu, Q., Ruan, T. & Jiang, G. B. Characterization of interactions between organotin compounds and human serum albumin by capillary electrophoresis coupled with inductively coupled plasma mass spectrometry. *Talanta* **93**, 239-244, (2012).
- 399 Liu, C. L., Wu, Q. Y., Harms, A. C. & Smith, R. D. On line microdialysis sample cleanup for electrospray ionization mass-spectrometry of nucleic acid samples. *Analytical Chemistry* **68**, 3295-3299, (1996).
- 400 Wu, Q. Y., Liu, C. L. & Smith, R. D. On-line microdialysis desalting for electrospray ionization mass spectrometry of proteins and peptides. *Rapid Communications in Mass Spectrometry* **10**, 835-838, (1996).
- 401 Liu, C. L., Hofstadler, S. A., Bresson, J. A., Udseth, H. R., Tsukuda, T., Smith, R. D. & Snyder, A. P. On line dual microdialysis with ESI-MS for direct analysis of complex biological samples and microorganism lysates. *Analytical Chemistry* **70**, 1797-1801, (1998).

- 402 De Vos, R. C. H., Moco, S., Lommen, A., Keurentjes, J. J. B., Bino, R. J. & Hall, R. D. Untargeted large-scale plant metabolomics using liquid chromatography coupled to mass spectrometry. *Nature Protocols* **2**, 778-791, (2007).
- 403 Taylor, S. W., Andon, N. L., Bilakovics, J. M., Lowe, C., Hanley, M. R., Pittner, R. & Ghosh, S. S. Efficient high-throughput discovery of large peptidic hormones and biomarkers. *Journal of Proteome Research* **5**, 1776-1784, (2006).
- 404 Villas-Boas, S. G., Noel, S., Lane, G. A., Attwood, G. & Cookson, A. Extracellular metabolomics: A metabolic footprinting approach to assess fiber degradation in complex media. *Analytical Biochemistry* **349**, 297-305, (2006).
- 405 Yates, J. R. Mass spectrometry - from genomics to proteomics. *Trends in Genetics* **16**, 5-8, (2000).
- 406 Han, X. L. & Gross, R. W. Global analyses of cellular lipidomes directly from crude extracts of biological samples by ESI mass spectrometry: a bridge to lipidomics. *Journal of Lipid Research* **44**, 1071-1079, (2003).
- 407 Zaia, J. Mass spectrometry of oligosaccharides. *Mass Spectrometry Reviews* **23**, 161-227, (2004).
- 408 Bagasra, O. & Forman, L. Functional-Analysis of Lymphocytes Subpopulations in Experimental Cocaine Abuse .1. Dose-Dependent Activation of Lymphocyte Subsets. *Clinical and Experimental Immunology* **77**, 289-293, (1989).
- 409 Chao, C., Jacobson, L. P., Tashkin, D., Martinez-Maza, O., Roth, M. D., Margolick, J. B., Chmiel, J. S., Rinaldo, C., Zhang, Z. F. & Detels, R. Recreational drug use and T lymphocyte subpopulations in HIV-uninfected and HIV-infected men. *Drug and Alcohol Dependence* **94**, 165-171, (2008).
- 410 Kubera, M., Filip, M., Basta-Kaim, A., Nowak, E., Siwanowicz, J., Zajicova, A., Holan, V., Maes, M. & Lason, W. The effect of cocaine sensitization on mouse immunoreactivity. *European Journal of Pharmacology* **483**, 309-315, (2004).
- 411 Pellegrino, T. & Bayer, B. M. In vivo effects of cocaine on immune cell function. *Journal of Neuroimmunology* **83**, 139-147, (1998).
- 412 Roth, M. D., Whittaker, K. M., Choi, R., Tashkin, D. P. & Baldwin, G. C. Cocaine and sigma-1 receptors modulate HIV infection, chemokine receptors, and the HPA axis in the huPBL-SCID model. *Journal of Leukocyte Biology* **78**, 1198-1203, (2005).
- 413 Duffy, D. C., McDonald, J. C., Schueller, O. J. A. & Whitesides, G. M. Rapid prototyping of microfluidic systems in poly(dimethylsiloxane). *Analytical Chemistry* **70**, 4974-4984, (1998).

- 414 Wong, I. & Ho, C. M. Surface molecular property modifications for poly(dimethylsiloxane) (PDMS) based microfluidic devices. *Microfluidics and Nanofluidics* **7**, 291-306, (2009).
- 415 Zhou, J. W., Ellis, A. V. & Voelcker, N. H. Recent developments in PDMS surface modification for microfluidic devices. *Electrophoresis* **31**, 2-16, (2010).
- 416 Xia, Y., Wang, P. P., Bartlett, M. G., Solomon, H. M. & Busch, K. L. An LC-MS-MS method for the comprehensive analysis of cocaine and cocaine metabolites in meconium. *Analytical Chemistry* **72**, 764-771, (2000).
- 417 Fandino, A. S., Toennes, S. W. & Kauert, G. F. Studies on hydrolytic and oxidative metabolic pathways of anhydroecgonine methyl ester (methylecgonidine) using microsomal preparations from rat organs. *Chemical Research in Toxicology* **15**, 1543-1548, (2002).
- 418 Pacifici, R., Zuccaro, P., Farre, M., Pichini, S., Di Carlo, S., Roset, P. N., Palmi, I., Ortuno, J., Menoyo, E., Segura, J. & De la Torre, R. Cell-mediated immune response in MDMA users after repeated dose administration - Studies in controlled versus noncontrolled settings. *Cellular and Molecular Mechanisms of Drugs of Abuse II: Cocaine, Substituted Amphetamines, Ghb, and Opiates* **965**, 421-433, (2002).
- 419 Warner, A. & Norman, A. B. Mechanisms of cocaine hydrolysis and metabolism in vitro and in vivo: A clarification. *Therapeutic Drug Monitoring* **22**, 266-270, (2000).
- 420 King, R. D., Rowland, J., Oliver, S. G., Young, M., Aubrey, W., Byrne, E., Liakata, M., Markham, M., Pir, P., Soldatova, L. N., Sparkes, A., Whelan, K. E. & Clare, A. The Automation of Science. *Science* **324**, 85-89, (2009).
- 421 Soldatova, L. N., Clare, A., Sparkes, A. & King, R. D. An ontology for a Robot Scientist. *Bioinformatics* **22**, E464-E471, (2006).
- 422 Schmidt, M. & Lipson, H. Distilling Free-Form Natural Laws from Experimental Data. *Science* **324**, 81-85, (2009).
- 423 Bongard, J. & Lipson, H. Automated reverse engineering of nonlinear dynamical systems. *Proceedings of the National Academy of Sciences of the United States of America* **104**, 9943-9948, (2007).
- 424 Bongard, J., Zykov, V. & Lipson, H. Resilient machines through continuous self-modeling. *Science* **314**, 1118-1121, (2006).
- 425 Karas, M. & Hillenkamp, F. Laser Desorption Ionization of proteins with molecular masses exceeding 10000 Daltons. *Analytical Chemistry* **60**, 2299-2301, (1988).

Jeffrey R. Enders

Vanderbilt University Department of Chemistry
7330 Stevenson Center, Station B 351822
Nashville, TN 37235
Lab: 615-343-4563
jeffrey.r.enders@vanderbilt.edu

40 Jump Hill Rd.
Levittown, PA 19056
(215)-869-5173 (cell)
jeffenders@gmail.com

PERSONAL STATEMENT

For the past five years, while at Vanderbilt University, I have worked on technological integration and implementation involving the use of mass spectrometry and microfluidics for measuring living biological systems. I am the primary graduate student on U.S. Defense Threat Reduction Agency grant (HDTRA-09-1-0013) which received funding in 2009 and was renewed in 2012. I am the first author on a number of peer reviewed publications, as well as one patent currently under review. In my five years at Vanderbilt I have worked closely with the Searle Systems Biology and Bioengineering Undergraduate Research Experience (Searle SyBBURE, www.sybbure.org) program and have been highly involved in guiding undergraduate research projects, ultimately leading to publication in one such case ["Publications" #5].

QUALIFICATIONS

- Bioanalytical mass spectrometrist with strong analytical chemistry background
- Skilled at using the following instrumentation (listed from most experienced to least): Waters Synapt G2 (nESI, LC, ESI, ETD, MALDI, GC), Applied Biosystems Voyager STR MALDI-TOF, Thermo-Finnigan LCQ, and custom ion mobility-mass spectrometer instrumentation made by Ionwerks
- Performed proteomic and metabolomic analyses on various biological fluids including whole blood, serum, plasma, tissue homogenate, wound fluid, culture effluent, and heart perfusate
- Fabricated new means of online desalting using online solid phase extraction (patent under review)
- Familiar with cell culturing techniques having worked directly with primary islets and primary lymphocytes, as well as Jurkat cell and insulinoma Rin-m5f cell lines
- Qualified to perform clean room UV photolithography and soft lithography of PDMS-based microfluidic devices
- Designed and ran experiments to quantitate metabolite levels in tissue homogenate samples using isotope labeled standards for UPLC-MS
- Implemented ICP-OES for the quantitation of salts and protein in samples
- Adept at utilizing Waters MassLynx and MarkerLynx line of programs
- Proficient in html, php, and flash and familiar with javascript for developing and maintaining websites and online databases
- Skilled at AutoCAD (2009, 2010, 2011), and SIMION 8
- Experienced in setting up and maintaining server computers for data storage and/or website/data hosting

EDUCATION

Vanderbilt University, Nashville, TN

Ph.D., Chemistry, August, 2012

- Mentor: John A. McLean
- Concentration: Coupling real time ion mobility-mass spectrometry to online bioreactor microfluidics, solid phase extraction

Drexel University, Philadelphia, PA

B.S./M.S. Dual Degree, Chemistry, Graduated June, 2007

- Advisor: Kevin G. Owens
- Senior project: Microwave assisted strong acid digestion of proteins

EXPERIENCE

- Graduate research, Vanderbilt University, Nashville, TN
Jul 2007-Jul 2012
 - Built an integrated platform to combine cell-trapping microfluidics with ion mobility-mass spectrometry in an online fashion
 - Designed new means of online solid phase extraction (SPE) for sampling secreted materials from a cellular bioreactor
 - Fabricated PDMS microfluidic devices using photolithography and soft lithography and cultured various cell lines to be placed in these devices
- Chemist, PQ Corporation, Exploratory research department, Conshohocken, PA
Mar 2004-Sept 2005
 - Performed medium scale batch autoclave synthesis of inorganic titanium silicate zeolites using multiple autoclaves and pressure microwave reactors
 - Analyzed/interpreted products using FTIR spectroscopy analysis, DTA, particle size distribution analysis, X-ray diffraction, X-ray fluorescence spectroscopy, gas sorption, and Raman/UV spectroscopy

HONORS AND AWARDS

- Center for Nonlinear Studies Student Travel Award (2010)
- Society for Applied Spectroscopy Student Poster Award (2009)
- Federation of Analytical Chemistry and Spectroscopy Societies Student Poster Award (2009)
- David Hercules Fellowship Award, Vanderbilt University (2007)
- Anthony J. Drexel Academic Scholarship, Drexel University (2002-2007)
- Admitted into the Honors Program, Drexel University (2002)

PUBLICATIONS

1. Christina C. Marasco, **Jeffrey R. Enders**, Kevin T. Seale, John A. McLean, John P. Wikswo. Real-Time Cellular Exometabolome Analysis with a Microfluidic-Mass Spectrometry Platform. In preparation for submission to *PLoS One*.
2. **Jeffrey R. Enders**, Christina C. Marasco, John P. Wikswo, John A. McLean. A Dual-Column Solid Phase Extraction Strategy for Online Collection and Preparation of Continuously Flowing Effluent Streams for Mass Spectrometry. Submitted to *Analytical Chemistry*.

3. Kelly M. Hines, **Jeffrey R. Enders**, and John A. McLean." Multidimensional Separations by Ion Mobility-Mass Spectrometry". Invited chapter for inclusion in *Encyclopedia of Analytical Chemistry*, Robert Myers and David Muddiman, Eds., John Wiley & Sons, Ltd. In press.
4. **Jeffrey R. Enders**, Cody R. Goodwin, Christina C. Marasco, Kevin T. Seale, John P. Wikswow, and John A. McLean, Advanced structural mass spectrometry for systems biology: Pulling the needles from haystacks, *Current Trends in Mass Spectrometry*, July 2011, pgs. 18-23.
5. **Jeffrey R. Enders**, Michal Kliman, Sevugarajan Sundarapandian, John A. McLean, "Peptide and Protein Analysis using Ion Mobility-Mass Spectrometry". Invited chapter for inclusion in *Protein and Peptide Mass Spectrometry in Drug Discovery*, Michael Gross, Ben Pramanik, Guodong Chen eds. John Wiley & Sons, 2011, chapter 6.
6. **Jeffrey R. Enders**, Christina C. Marasco, Ayeeshik Kole, Bao Nguyen, Sevugarajan Sundarapandian, Kevin T. Seale, John P. Wikswow, and John A. McLean, "Towards monitoring real-time cellular response using an integrated microfluidics-MALDI/nESI-ion mobility-mass spectrometry platform", *IET Systems Biology* 2010, 4 (6):416-427.
7. John A. McLean, Larissa S. Fenn, and **Jeffrey R. Enders**. "Structurally Selective Imaging Mass Spectrometry by Imaging Ion Mobility-Mass Spectrometry". Invited chapter for inclusion in *Mass Spectrometric Imaging: History, Fundamentals and Protocols*, Methods in Molecular Biology Series, Jonathan Sweedler and Stanislav Rubakhin, eds. Humana Press, 2010, pgs.363-383.
8. **Jeffrey R. Enders**, John A. McLean, "Chiral and Structural Analysis of Biomolecules Using Mass Spectrometry and Ion Mobility-Mass Spectrometry", *Chirality* 2009, 21:S253-S264.

INVITED TALKS

- "Strategies and Challenges in Dynamic Systems Biology Analysis Using Structural Mass Spectrometry", in Ion Mobility MS Workshop on Applying Ion Mobility-Mass Spectrometry to Challenges in Proteomics and Systems Biology American Society for Mass Spectrometry Annual Conference, Vancouver, BC Canada (May 2012)
- "Microfluidic-ion mobility-mass spectrometry for assessing cellular response in real time", Quantitative Understanding in Biology (q-bio) Annual Conference, Santa Fe, NM (August 2009)
- "Development of a Platform for Online Analysis of the Metabolic Footprint", The Association for Mass Spectrometry Applications to the Clinical Lab (MSACL) Annual Conference, San Diego, CA (January 2012)

PRESENTATIONS

1. Jeffrey R. Enders; Christina Marasco; Kevin Seale; John Wikswow; John A. Mclean, Online analysis of a constant-perfusion cell culture microfluidic device for exometabolomic measurements, 60th American Society for Mass Spectrometry Annual Conference, Vancouver, BC (May 2012).

2. Jeffrey R. Enders, Christina Marasco, Cody Goodwin, Jody May, Kevin Seale, John Wikswo and John A. McLean, A Microfluidic-Ion Mobility-Mass Spectrometry Platform for Presymptomatic Diagnoses of CBW Agent Exposure, 2011 Chemical and Biological Defense Science and Technology Conference, Las Vegas, NV (November 2011)
3. Jeffrey R. Enders, Christina Marasco, Cody Goodwin, Jody May, Kevin Seale, John Wikswo and John A. McLean, Development of a Platform for Online Acquisition of Empirical Systems Biology Data, 5th Annual Conference on Cellular Information Processing (q-bio), Santa Fe, NM (August 10-14, 2011).
4. Jeffrey R. Enders, Christina Marasco, Cody Goodwin, Jody May, Kevin Seale, John Wikswo and John A. McLean, Microfluidic-Coupled Ion Mobility-Mass Spectrometry Platform for Real-Time, Temporally-Resolved Analysis of Excreted Cellular Materials, 59th American Society for Mass Spectrometry Annual Conference, Denver, Co (June 2011).
5. Jeffrey R. Enders, Cody Goodwin, Christina Marasco, Jody May, Kevin Seale, John Wikswo, John McLean. Temporal Analysis of Biological Fluid for the Analysis of Cellular Signaling and Response Using Ion Mobility-mass Spectrometry Analyses. Chemical and Biological Defense Science & Technology conference, Orlando, FL (November 2010).
6. John McLean, Jeffrey Enders, Jody May, Kevin Seale, John Wikswo. Advanced Structural Mass Spectrometry for Systems Biology – Towards Presymptomatic Diagnosis of Threat Agent Exposure . Chemical and Biological Defense Science & Technology conference, Orlando, FL (November 2010).
7. Jody May, Jeffrey R. Enders, Sevugarajan Sundarapandian, Kevin Seale, John Wikswo, and John A. McLean. Development of a Multiplexed (8-Channel) Ion Mobility-Mass Spectrometer Chemical Analyzer for Rapid Interrogation of Biochemical Response . Chemical and Biological Defense Science & Technology conference, Orlando, FL (November 2010).
8. Jeffrey R. Enders, Christina Marasco, Cody Goodwin, Kevin Seale, John Wikswo, John McLean. Characterizing the *Saccharomyces cerevisiae* respiratory oscillation exometabolome by ion mobility-mass spectrometry. Quantitative Understanding in Biology (q-bio) Annual Conference, Santa Fe, NM (August 2010).
9. Jody May, Sevugarajan Sundarapandian, Jeffrey R. Enders, Kevin T. Seale, John P. Wikswo, and John A. McLean. Development of a Multi-Channel Ion Mobility-Mass Spectrometer for High-Throughput Interrogation of Cellular Response. Quantitative Understanding in Biology (q-bio) Annual Conference, Santa Fe, NM (August 2010).
10. Christina Marasco, Jeffrey Enders, Kevin Seale, John McLean, John Wikswo. Investigating Leukocyte Dynamic Response to Stimuli in an Integrated Microfluidic-Ion Mobility-Mass Spectrometer Quantitative Understanding in Biology (q-bio) Annual Conference, Santa Fe, NM (August 2010).

11. Jody C. May; Jeffrey R. Enders; Sevugarajan Sundarapandian; Kevin T. Seale; John P. Wikswo; John A. Mclean, High-Throughput Ion Mobility-Mass Spectrometry Strategies for Monitoring Cellular Response in Real Time, 58th Annual American Society for Mass Spectrometry Annual Conference, Salt Lake City, UT (May 2010).
12. Jeffrey R. Enders, Sevugarajan Sundarapandian, Kevin Seale, John P. Wikswo, John A. McLean, Measuring real-time cellular responses to chemical and biological warfare agents using structural mass spectrometry techniques, Chemical and Biological Defense Science and Technology (CBD S&T) Conference, Dallas, TX (November 2009)
13. Jeffrey R. Enders, Sevugarajan Sundarapandian, Kevin Seale, John P. Wikswo, John A. McLean, Real time analysis of cell signaling and response using microfluidic cell trapping-ion mobility-mass spectrometry, Federation of Analytical Chemistry and Spectroscopy Societies conference, Louisville, KY (October 2009)
14. Jeffrey R. Enders, Sevugarajan Sundarapandian, Ayeeshik Kole, Bao Nguyen, Kevin Seale, John P. Wikswo, John A. McLean, Microfluidic-ion mobility-mass spectrometry for assessing cellular response in real time, Quantitative Understanding in Biology (q-bio) Annual Conference, Santa Fe, NM (August 2009)
15. Jeffrey R. Enders, Sevugarajan Sundarapandian, Kevin Seale, John P. Wikswo, John A. McLean, Combining microfluidic cell trapping with real time monitoring of biomolecular exudates by ion mobility-mass spectrometry, American Society for Mass Spectrometry Annual Conference, Philadelphia, PA (June 2009)
16. Jeffrey R. Enders, Sevugarajan Sundarapandian, Kevin Seale, John P. Wikswo, John A. McLean, Dynamic Biomolecular Measurements of Cellular Response by Ion Mobility-Mass Spectrometry: a New Strategy for Systems Biology, Southeast Regional Meeting of the American Chemical Society, Nashville, TN (November 2008)
17. Jeffrey R. Enders; Larissa S. Fenn, Michael F. Aldersley; James P. Ferris; Prakash C. Joshi; John A. Mclean; Dmitri Zagorevski, Ion Mobility Mass Spectrometry of the products of oligomerization of activated nucleotides with Montmorillonite, 4rd Annual Meeting of the Vanderbilt Institute for Chemical Biology, Nashville, TN (August 2008)
18. Jeffrey R. Enders; Larissa S. Fenn, Michael F. Aldersley; James P. Ferris; Prakash C. Joshi; John A. Mclean; Dmitri Zagorevski, Ion Mobility Mass Spectrometry of the products of oligomerization of activated nucleotides with Montmorillonite, American Society for Mass Spectrometry Annual Conference, Denver, CO (June 2008)

PROFESSIONAL MEMBERSHIPS

- The Society for Applied Spectroscopy
- The Coblenz Society
- The American Society for Mass Spectrometry
- The American Chemical Society

TEACHING EXPERIENCE

- Teaching Assistant, August 2007 – June 2008, August 2008 – December 2008, August-September 2009
Vanderbilt University, Department of Chemistry